Existence and stability of accelerating optical solitons

Margarida Facão

Doctor of Philosophy
University of Edinburgh
2003

To my husband Luís,
my son Luís
and my parents Manuel and Irene.

Abstract

Optical solitons exist, in a strict sense, in simple nonlinear models governed by the integrable nonlinear Schrödinger (NLS) equation. They also exist, in a wider sense, in more realistic models governed by non-integrable evolution equations. Accelerating soliton is the name coined to describe steady profile solutions, existing in some of those nonlinear optical models, that evolve along parabolic trajectories, in either a time-space or 2-dimensional space coordinate system.

In this thesis, we focus on three different optical models possessing accelerating solitons, namely, propagation of beams in photorefractive media with diffusion, pulse propagation in fibre links using sliding-frequency filters and pulse propagation governed by the NLS equation with intrapulse Raman scattering. In each case, an ordinary differential equation (ODE) is obtained from the partial differential equation (PDE) through a similarity variable reduction. Then, we investigate parameter ranges for which solutions exist and their normal mode stability. Integration of the PDE is also used to confirm acceleration regime and stability properties.

The three accelerating solitons have the common characteristic that the asymptotics of both the ODE and the stability eigenvalue problem involve solutions to Airy equations. This characteristic allows us to use Airy functions and their asymptotic properties in our analytic and numerical evaluations. It also implies that, in using Evans function ideas in a stability analysis, a significant modification is necessary. The asymptotics must be described in terms of appropriate recessive choices of Airy functions. This leads to a novel modification of the Evans function method, which is then applied in the search for eigenvalues, allowing the identification of unstable and internal (oscillatory) modes when they exist. The prediction of these modes is shown to agree with direct numerical integration of the PDEs.

Acknowledgements

It is my pleasure to thank my supervisor Prof. David Parker especially for the scientific support but also for the English counselling and his kindness. I would also like to thank Dr. Noel Smyth for providing his PDE-solver code and for the assistance he gave me during particular implementations. Also in this context, I thank the help of Jason Beech-Brandt. I am grateful for helpful conversations with Jitse Niesen and Dr. Adri B. Olde Dealhuis about Airy functions properties. My acknowledgement is also due to the School of Mathematics and Statistics, University of St. Andrews, in the person of Dr. Nik Ruškuc for allowing me to use their computer facilities while, for family reasons, I was living in St. Andrews. Finally, I acknowledge the financial support from the Fundação para a Ciência e a Tecnologia.

Declaration

I declare that this thesis was composed by myself and that the work contained therein is my own, except where explicitly stated otherwise in the text.

Table of Contents

Chapter 1

Introduction

Soliton is a word that entered the nonlinear physics vocabulary in 1965 through the work of Zabusky and Kruskal, where they reported the numerical discovery of a hump-like solution to the Korteweg-de Vries (KdV) equation that preserved its shape and speed when passing through other similar solutions [114]. This preservation of individuality was, at that time, completely unexpected in a nonlinear collision. The soliton then gained a major role in nonlinear wave physics and mathematics when, by the advent of the inverse scattering method [39], the soliton was shown to be a special exact solution to the initial value problem for the KdV equation. Later, many more nonlinear wave equations, e.g., the nonlinear Schrödinger (NLS) equation, the reduced Maxwell-Bloch equations and the sine-Gordon equation, were shown to admit soliton solutions and to be exactly solved by the inverse scattering method [115, 1, 68]. The observation of a KdV soliton was, however, first reported 131 years before it was named by Zabusky and Kruskal. The report was made by a Scottish naval engineer J. S. Russell. In 1834 he was appointed to study and improve the design of craft for navigation on the Union Canal in Edinburgh when he observed [91]

> *... a large solitary elevation, a rounded smooth and well defined heap of water, which continued its course along the channel apparently without change of form or diminution of speed.*

In recent decades, the soliton has reached more and more disciplines, not only through the enlargement of the set of nonlinear equations which are integrable but also through the widespread applicability of such equations in modelling nonlinear systems in diversified areas such as water waves, plasma physics, solid state physics, optics, neurophysiology, etc. Nowadays, in many areas such as nonlinear optics, which is the area where the solitons presented in this thesis occur, the term soliton is not confined to meaning a non-deforming solution to an integrable nonlinear system but has also embraced the solitary waves that propagate without change of shape in other non-integrable nonlinear systems.

The optical nonlinearity of materials leads to two different classes of solitons: temporal solitons and spatial solitons. The nonlinear response of the medium makes possible a non-distorting propagation in which nonlinearity is balanced by dispersion or diffraction, respectively for temporal or spatial solitons. The spatial confinement of beams resulting from the balance between the nonlinear self-focusing and the diffraction was early observed [51, 21] even before the discovery of solitons. Nevertheless, pulses of very short duration which, as a consequence of the balance between the nonlinear self-phase modulation and the dispersion, propagate without distortion for long distances - temporal solitons - dominated the first decade of research on optical solitons. This was due largely to the potential application of temporal solitons in the implementation of fibre-based ultrahigh-speed optical communications, but also due to the fact that those first spatial solitons were shown to be unstable in the presence of transverse disturbances.

Nowadays, the prospective pulses for ultrahigh-speed fibre links are the so-called *dispersion-managed solitons*. They are nonlinear pulses but propagating in a fibre-link composed of alternating portions of anomalous and normal dispersion. The main equation has non-constant coefficients and is no longer an integrable equation, however, the existence and stability of such pulses have been extensively investigated [36, 48, 47, 102]. During the last decade the subject of optical spatial solitons has grown due to interest in new forms of nonlinearity such as photorefractivity and quadratic nonlinearity. The saturable nature of these nonlinearities allows the stability of higher-dimensional solitons, i.e., propagating beams that are nonlinearly trapped in both transverse directions. The most attractive feature of these high-dimension solitons is the richness of their interactions which are possible in three dimensions. Moreover they are promising elements for future technologies such as reconfigurable waveguides and optical computation.

Usually the soliton is a steady profile that propagates at constant velocity. However, in this thesis, we shall treat steady profiles propagating at constant acceleration which were recently named as *accelerating solitons* [84]. Note that in the spatial soliton case, where the solitons exist within a 2-dimensional spatial system, they are better defined as steady beams having parabolic trajectories instead of the usual rectilinear trajectories. Examples of these accelerating solitons are solitons suffering intrapulse Raman scattering [37], dissipative optical solitons [110], solitons in systems with sliding-frequency filters [63] and self-bending photorefractive beams [18]. All of them occur in the optical context and correspond to non-integrable models of the NLS family. An accelerating soliton had earlier been found for one equation of the KdV family [96]. However, in that case the acceleration is not constant.

Here, we shall treat the existence and stability of self-bending photorefractive beams, pulses of the sliding-frequency filter systems and pulses suffering intrapulse Raman scattering. We first reduce the corresponding partial differential equation (PDE) to an ordinary differential equation (ODE) making use of the accelerating similarity variable. Then, we numerically seek localised solutions to the ODE and establish parameter regions of existence. The stability analysis of such accelerating solitons turns out to be rather challenging. The most accessible stability analysis of travelling waves involves the determination of the spectrum of a linear operator resulting from the linearisation of the evolution equation around the equilibrium wave. From the structure of the spectrum, spectral stability or instability is concluded. When dealing with many waves travelling at constant velocity, we arrive at an eigenvalue problem for a system of ODE's which asymptotically behaves as a constant coefficient ordinary differential system. However, in the accelerating wave cases, the asymptotics of the eigenvalue problem correspond to Airy functions. We shall see that also the linearisation of the ODE's is equivalent to the Airy equation and Airy functions are used in the numerical procedure to obtain the localised solutions. This main novel feature of the eigenvalue problem prohibits the use of standard methods applicable to constant velocity travelling solutions, such as the *Vakhitov-Kolokolov* criterion and the standard Evans function method. Hence, one of the main achievements of the work presented in this thesis is the implementation of a modified Evans function method that uses Airy function asymptotics. This method then allows the characterisation of the spectral structure of the eigenvalue problems arising for each of the three accelerating solitons under study.

The first accelerating solutions to be studied are the self-bending beams occurring in photorefractive materials. In this model, both the rectilinear and self-bending beams are treated. The rectilinear beams exist whenever the model does not include the diffusive effect and the self-bending beams occur otherwise. The stability analysis of the rectilinear solutions will serve to introduce the *Vakhitov-Kolokolov* criterion and the standard Evans function. In the first chapter devoted to the photorefractive model, we obtain an ODE using a generic accelerating similarity variable reduction. The ODE is then numerically integrated, yielding the rectilinear and self-bending profiles. These profiles have already been obtained elsewhere [22, 64, 84]. We stress our use of real Airy function asymptotics in the numerical procedure, although this has been used previously [5] in other photorefractive model supporting self-bending solitons . We shall also use Chapter 2 for introducing standard concepts of stability. Then we obtain the stability eigenvalue problem and relate the zero modes to the invariances of the evolution equation.

The zero modes are then useful for applying the well-known *Vakhitov-Kolokolov* criterion [109] to the rectilinear beams. They are also useful for applying a widely used multiscale expansion [89] to the self-bending solutions. The latter detects any change of stability due to eigenvalues moving through the origin.

The second photorefractive based chapter (Chapter 3) is mainly devoted to the Evans function method. First we introduce the standard version of the Evans function (both the versions based on the Wronskian and the version using exterior algebra) and apply it to characterise the non-diffusive stability spectrum. As in many other non-integrable models, this spectrum comprises *internal modes.* These are solutions to the eigenvalue problem corresponding to neutrally stable discrete eigenvalues. They correspond to solutions to the linearised stability equations that present oscillatory behaviour with respect to the evolution variable. The existence of internal modes is recognisable by persistent oscillations accompanying the evolution of perturbed soliton inputs. Using the Evans function method, we are able to find the internal modes existing for this model. Then the Evans function is adapted to Airy function asymptotics and applied in order to characterise the stability spectrum corresponding to the self-bending solutions. We are able to identify localised modes which are the counterpart of the previously mentioned internal modes.. This chapter also includes a brief section describing a procedure for searching for eigenvalues based on a discretisation of the eigenvalue problem and, at last, another section where the obtained results are compared with direct numerical integration of the evolution equation. Our photorefractive results, with special relevance given to the modified Evans function, have already been published [34].

Chapter 4 treats the sliding-frequency filter model. Its accelerating pulses were known from the time at which the model was suggested as a way of implementing soliton-based optical communication links [77]. They have been mainly treated under perturbation approaches [63, 17, 12]. However, the close relation of these pulses and the accelerating similarity variable was made recently [83]. In this thesis we present the similarity variable reduction and discuss existence of pulse-like solutions for a certain range of parameters. The pulse profiles are obtained by numerical integration of the ODE using Airy function asymptotics. After a short section devoted to zero modes, we use the modified Evans function to study the corresponding stability spectrum. The results are in agreement with previous stability approaches [63, 17, 12]. To our knowledge this is the first work that relates the stability properties of the sliding-frequency filter pulses with the structure of the corresponding stability spectrum. The chapter finishes with results obtained from direct numerical integration of the PDE.

In Chapter 5, we treat the accelerating pulses occurring in optical fibre systems which include intrapulse Raman scattering. The corresponding evolution equation was already reduced to an ODE using an accelerating similarity variable [37], but there the profiles were obtained using a perturbative method. Here, we obtain the profiles by numerical integration of the ODE using again Airy function asymptotics. The stability spectrum is then investigated using the modified Evans function and the results are compared with numerical integration of the full evolution equation. A final chapter summarises the conclusions of this work and points out some of the issues requiring future investigation.

Chapter 2

Photorefractive self-guiding beams

Photorefractive solitons are a type of optical spatial solitons which occur in photorefractive materials. Spatial solitons are beams which propagate without distortion through the balance between diffraction and self-focusing [92, 59, 100, 108]. Self-focusing is a nonlinear mechanism which often arises from a Kerr-type effect, though other nonlinear effects play a more important role in the context of spatial solitons. Examples are saturable nonlinearities such as quadratic nonlinearity and the photorefractive effect considered in this work.

The spatial solitons supported by the Kerr effect were the ones first observed and modelled in 1964 [51, 21], which was even earlier than the prediction of temporal solitons. However, they are stable only in planar waveguides and not in bulk materials where they undergo catastrophic self-focusing. Although experiments with 2D spatial solitons supported by a saturable nonlinearity date back to 1974 [14], the investigation of optical solitons was very much focused on the temporal solitons and their applicability to ultra-rapid telecommunications systems. Thus, it was only in the early 90's with the discovery of photorefractive solitons [94, 26] and with the experimental demonstration of quadratic solitons [107] that the investigation of spatial solitons grew. The active investigation of these solitons since then has demonstrated a rich variety of phenomena, namely soliton interaction in three dimensions, dark and vortex solitons and incoherent solitons. Photorefractive solitons have played an important role in this investigation, since they require only low power laser inputs, as small as μWs, and elementary experimental apparatus. Moreover they are attractive for practical applications such as beam steering and beam manipulation. As we explain below, the photorefractive beams become self-trapped by a mechanism which may be understood as one in which the beam induces its own waveguide. Hence, a waveguide may be formed by a photorefractively active wavelength (typically visible) and then

used to guide another much stronger non-photorefractive wavelength (typically infrared). Other waveguide applications that can be written by photorefractive solitons include beam splitters (X- and Y-junctions) [106, 90], directional couplers [69] and nonlinear frequency converters [70]. Although the rather slow response time of the photorefractive nonlinearity imposes limitations on such real time all-optical beam handling, the induced waveguides may be permanently fixed even after the removal of the inductor beam [60, 43]. Recently, waveguides written photorefractively but manipulated by an electro-optic based effect have also been shown to be very promising [24, 23].

Photorefractive materials are high-quality lightly-doped electro-optic crystals (i.e., crystals lacking inversion symmetry, also called noncentrosymmetric crystals) such as $BaTiO_3$ (barium titanate), $LiNbO_3$ (lithium niobate), SBN (strontium barium niobate). They exhibit a reversible change of refractive index induced by the spatial variation of an optical field. The effect has been known from 1966 and was first used in holography. It may be qualitatively explained as follows. The photorefractive crystal contains two different dopant atoms, the donor and acceptor atoms. When a beam is propagating in the crystal some optical radiation is absorbed exciting electrons from the donor atoms to the conduction band. There they are free to diffuse or to drift under the influence of a self-generated field or any applied field. Meanwhile the free electrons may be recaptured by ionized donors and the result is a non-uniform spatial distribution of charge which tends to be positive in the illuminated regions and negative in dark regions. In turn, the spatial distribution of charge gives rise to a space-charge field and that field produces a refractive index variation through the electro-optic mechanism. In the context of photorefractive solitons, the variation of refractive index is such that the original beam is trapped. Three types of photorefractive soliton have been identified: the *quasi-steady-state*, *photovoltaic* and *screening* solitons. The screening solitons are the ones being investigated in this work. They exist when the crystal is under an external electric field. The name *screening* results from the phenomenon of partial screening of the external field which in turn is a consequence of the space-charge field that builds up with an opposite polarity. Screening solitons were predicted by Segev *et al.* in 1994 [95] and by Christodoulides and Carvalho in 1995 [22] and experimentally observed in 1995/96 by Shih [98, 97].

2.1 The evolution equation

Here we follow Christodoulides and Carvalho, Yariv and Segev *et al.* [22, 113, 93] in deriving an evolution equation for bright screening solitons. Let us assume that the optical beam enters a photorefractive crystal parallel to the z axis and is guided in the y-direction so that the only diffraction is parallel to the x axis. The optical beam is linearly polarized in the x direction, which coincides with the optical c axis of the crystal. Moreover the external field is in the same direction. Thus the space charge field $E_{\rm sc}$ must be in the same direction. The local extraordinary refractive index that arises from the electro-optic effect is given by [113]

$$(n_{\rm e}')^2 = n_{\rm e}^2 - n_{\rm e}^4 r_{\rm eff} E_{\rm sc}, \tag{2.1}$$

where $n_{\rm e}$ is the unperturbed extraordinary index of refraction and $r_{\rm eff}$ is the effective electro-optic coefficient.

The space-charge field may be determined using the theory of photorefractivity based on the Kukhtarev-Vinetskii model [111, 65]. Let us first briefly describe the electronic structure of the crystal. It contains donor atoms and acceptor atoms whose densities are N_D and N_A, respectively. Even before the presence of the optical beam a fraction of the donor atoms is already ionised (with density denoted by $N_D^+ = N_A$); their electrons were accepted by acceptor atoms in a process that is energetically favourable. Thus $(N_D - N_D^+)$ is the density of donor atoms which are candidates for photo-excitation. We shall note that the main role of the acceptor atoms is to ensure that there exists everywhere a sufficiently large density of ionised donors which may act as traps for the free electrons. Hence the inhomogeneous charge distribution is possible since the excited electrons may be trapped away from the region where they were generated. Moreover, all the acceptor atoms are ionised (occupied by electrons) at all time.

In the presence of the optical beam, the donor ionisation rate results from a competition between thermal and light ionisation and recombination with free electron charges, a process that is described by the following rate equation

$$\frac{\partial N_D^+}{\partial t} = (\beta + s_i I)(N_D - N_D^+) - \gamma_r n N_D^+, \tag{2.2}$$

where β is the thermal generation rate (usually instead of β one uses $s_i I_d$, where I_d is the so-called dark irradiance), s_i is the photo-excitation cross section, I is the optical intensity, γ_r is the recombination rate and n is the free electron density. The second necessary equation is the Gauss law that in this case reads

$$\frac{\partial E}{\partial x} = \frac{\rho}{\epsilon_r \epsilon_0}, \tag{2.3}$$

where ϵ_0 and ϵ_r are the vacuum permittivity and static relative permittivity, respectively, and the charge density is given by $\rho = e(N_D^+ - N_A - n)$ where e is the electron charge. The last equation is the continuity equation given by

$$\frac{\partial \rho}{\partial t} + \frac{\partial J}{\partial x} = 0, \tag{2.4}$$

where the current density has a drift contribution proportional to E and a diffusive contribution proportional to $\partial n/\partial x$ and is given by $J = e\mu n E + \mu K_B T(\partial n/\partial x)$. In the last expression μ is the electron mobility, K_B is the Boltzmann constant and T is the absolute temperature.

As we are interested in the steady-state situation, we shall set the time derivatives above equal to zero. Note that the steady-state situation is approached after a finite time (typically of the order of seconds for mW beams) during which time some energy is absorbed by the crystal. First we eliminate N_D^+ between equations (2.2) and (2.3). Considering that in a typical photorefractive medium $N_D^+ >> n$, we obtain

$$n = \frac{s_i(I + I_d)}{\gamma_r}\left(\frac{N_D - N_A}{N_A} - \frac{\epsilon_0\epsilon_r}{eN_A}\frac{\partial E}{\partial x}\right)\left(1 + \frac{\epsilon_0\epsilon_r}{eN_A}\frac{\partial E}{\partial x}\right)^{-1}, \tag{2.5}$$

The expression above may be simplified if we suppose that $\epsilon_0\epsilon_r/eN_A(\partial E/\partial x)$ is negligible compared to one and to $(N_D - N_A)/N_A$ which is typically much larger than one. The last assumption is usually valid if the optical intensity $I(x, z)$ varies slowly with respect to x. Thus, equation (2.5) reads

$$n = \frac{s_i(I + I_d)(N_D - N_A)}{\gamma_r N_A}. \tag{2.6}$$

Inserting (2.6) into (2.4) we obtain

$$\frac{\partial}{\partial x}\left(eEs_i(I + I_d) + K_B T\frac{\partial I}{\partial x}\right) = 0. \tag{2.7}$$

The quantity inside the brackets being independent of x should be equal to its value at the dark regions where we assume $E = E_0$ and $I = \partial I/\partial x = 0$. Note that here we are considering only bright solitons; however, this photorefractive model also admits dark and gray solitons [22]. We are also assuming that the x-width of the crystal, W, is considerably larger than the width of the beam, so that E_0 may be treated as a constant and equal to $\pm V/W$ where V is the applied voltage. Thus we obtain the following expression for the space-charge field

$$E_{sc} = \frac{E_0 I_d}{I + I_d} - \frac{K_B T}{e(I + I_d)}\frac{\partial I}{\partial x}, \tag{2.8}$$

where the first term accounts for drift and the second for diffusion.

Considering that all the material optical response is contained in the expression for the refractive index (2.1) and that the optical field E and the space-charge field E_{sc} are both aligned in the same direction, we may consider the following scalar wave equation

$$\nabla^2 E = \frac{(n_e')^2}{c^2}\frac{\partial^2 E}{\partial t^2}. \tag{2.9}$$

If we write E in terms of a slowly varying envelope $\phi(x,z)$ as

$$E = \phi(x,z)\exp[i(kz-\omega t)],$$

where $k = \omega n_e/c$, equation (2.9) yields

$$i\phi_z + \frac{1}{2k}\phi_{xx} - \frac{k_0}{2}(n_e^3 r_{\text{eff}} E_{sc})\phi = 0, \tag{2.10}$$

where $k_0 = k/n_e$ is the vacuum wavenumber corresponding to k. The evolution equation may now be obtained by insertion of (2.8) into (2.10). In (2.8), the optical intensity may be written in terms of the envelope function ϕ in the form $I = n_e|\phi|^2/(2\eta_0)$ where $\eta_0 = (\mu_0/\epsilon_0)^{1/2}$. If we also make the following normalisation of variables

$$\tilde{z} = k_0 n_e^3 r_{\text{eff}} E_0 z/2, \qquad \tilde{x} = (k_0^2 n_e^4 r_{\text{eff}} E_0)^{-1/2} x \qquad \text{and} \qquad q = (n_e/2\eta_0 I_d)^{1/2}\phi,$$

we obtain

$$iq_z + q_{xx} - \frac{q}{1+|q|^2} + \gamma\frac{(|q|^2)_x q}{1+|q|^2} = 0, \tag{2.11}$$

where $\gamma = K_B T k_0 n_e^2 (r_{\text{eff}}/E_0)^{1/2}/e$ and we have dropped the tilde from $\tilde{z}$ and $\tilde{x}$ to simplify the notation. The above equation models the propagation of bright beams in biased photorefractive materials whenever both drift and diffusion contribute to the transport of charge. The diffusion term is usually neglected when the external voltage is high. In those conditions, there exist stable solitary wave solutions [22]. They have symmetric profiles and propagate in the planar waveguide along rectilinear trajectories. Whenever diffusion is appreciable the beam profiles become asymmetric and the trajectory is parabolic [18, 64, 54, 84]. Nevertheless their propagation is also distortionless which confers upon them the name of *self-bending* solitons. The self-bending phenomenon was first experimentally observed by Shih *et al.* [97] and is also present when I/I_d is small and the saturable nonlinearities may be described by the first term in their expansions [5].

In the remainder of this chapter, we shall obtain the two different screening photorefractive solitons, namely, the rectilinear and self-bending beams. Then, after a short section devoted to the general concepts of stability, we obtain the

linear stability equations and the corresponding eigenvalue problem. The zero modes, i.e., modes that correspond to the zero eigenvalue, are then identified in relation to the invariances of equation (2.11). They play an important role in the preliminary stability analysis undertaken in this chapter. The first will be the *Vakhitov-Kolokolov* approach [109] which is valid for the diffusionless case ($\gamma = 0$). For the diffusive case, that approach is not applicable. Instead we will use a multiscale expansion in searching for a threshold of any possible instability. Note that the main stability analysis of the photorefractive solitons will be the subject of the next chapter.

2.2 Equilibrium solutions

Consider the full evolution equation (2.11) of a beam in a biased photorefractive medium. The existence of self-bending solutions is exhibited by the existence of self-similar solutions to (2.11) having $\eta = x + az^2$ as similarity variable, as was shown by Parker *et al.* [84].

Here we generalize by taking $\eta = x - 2Vz + az^2$ as a similarity variable (with V and a constants) and then seeking a solution to (2.11) in the form $q(z,x) = \exp[i\theta(z,\eta)]F(\eta)$ with θ and F real. Inserting this *ansatz* into the evolution equation we obtain

$$F'' + [\theta_\eta(2V - 2az) - \theta_\eta^2 - \theta_z]F - \frac{F}{1+F^2} + \gamma\frac{2F^2F'}{1+F^2} + i[2(\theta_\eta - V + az)F' + \theta_{\eta\eta}F] = 0. \quad (2.12)$$

Setting the imaginary part of the above equation to zero, multiplying by F and integrating with respect to η yields

$$\theta_\eta(z,\eta) = V - az + \frac{C(z)}{F^2(\eta)},$$

for some $C(z)$. This may be integrated again to give

$$\theta(z,\eta) = (V - az)\eta + D(z) + \int \frac{C(z)}{F^2(\eta)}d\eta.$$

Using the above expression for $\theta(\eta, z)$ in the real part of equation (2.12) yields

$$F'' + \left\{(V - az)^2 + a\eta - D'(z) - \frac{C^2(z)}{F^4} - \int \frac{C'(z)}{F^2(\eta)}d\eta\right\}F - \frac{F}{1+F^2} + \gamma\frac{2F^2F'}{1+F^2} = 0.$$

Since F depends only on η, the coefficients in the above equation should not depend on z, which requires that $C(z)$ and $(V-az)^2 - D'(z)$ be constants. This produces the following form for the phase

$$\theta(z,\eta) = (V-az)\eta + \frac{1}{3}a^2z^3 - aVz^2 + (V^2-B)z + \int \frac{C}{F^2(\eta)}d\eta, \tag{2.13}$$

and an ordinary differential equation for the real function F given by

$$F'' + \left[B + a\eta - \frac{C^2}{F^4} - \frac{1}{1+F^2} + \gamma\frac{2FF'}{1+F^2}\right]F = 0, \tag{2.14}$$

where B and C are constants. A localised beam exists if solutions to (2.14) can be found with $F \to 0$ as $\eta \to \pm\infty$, which is possible only if $C = 0$. In this case the indefinite integral in (2.13) should be replaced by a constant, say C_1. The localised beams are self-bending ($a \neq 0$) only if $\gamma \neq 0$ and rectilinear ($a = 0$) in the diffusionless case. In fact, if we multiply equation (2.14) by $2F'$ we obtain

$$\frac{d}{d\eta}\left[(F')^2 + (B+a\eta)F^2 - \ln(1+F^2)\right] = -4\gamma\frac{F^2(F')^2}{1+F^2} + aF^2. \tag{2.15}$$

Integration over $(-\infty,\infty)$ and using the decay of F and F' as $\eta \to \pm\infty$ then yields

$$4\gamma\int_{-\infty}^{+\infty}\frac{F^2(F')^2}{1+F^2}d\eta - a\int_{-\infty}^{+\infty}F^2d\eta = 0. \tag{2.16}$$

Hence, $\gamma = 0$ implies $a = 0$. Also, as the integrals are both non-negative, for $\gamma \neq 0$ there corresponds to each γ a nonzero a of the same sign but with magnitude depending upon the solution $F(\eta)$ to (2.14).

2.2.1 Rectilinear beams

Let us consider first the simpler case where $\gamma = 0$ and $a = 0$. The ordinary differential equation is, in this case, the autonomous equation

$$F'' + \left[B - \frac{1}{1+F^2}\right]F = 0, \tag{2.17}$$

with a first integral given by

$$(F')^2 + BF^2 - \ln(1+F^2) = D. \tag{2.18}$$

For localised beams, the constant D must be zero, since F and F' must vanish simultaneously as $\eta \to \pm\infty$. For $D = 0$ and for each $B < 1$, there exists a family of positive solutions $F(\eta)$ with peak value μ related to B through

$$B = \frac{\ln(1+\mu^2)}{\mu^2}, \tag{2.19}$$

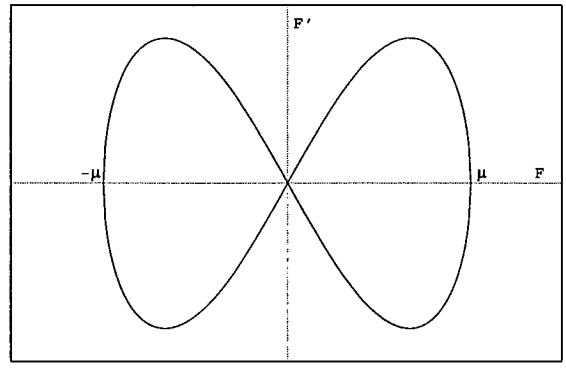

Figure 2.1: Phase plane for equation (2.18), $D = 0$ and $B < 1$ satisfying (2.19).

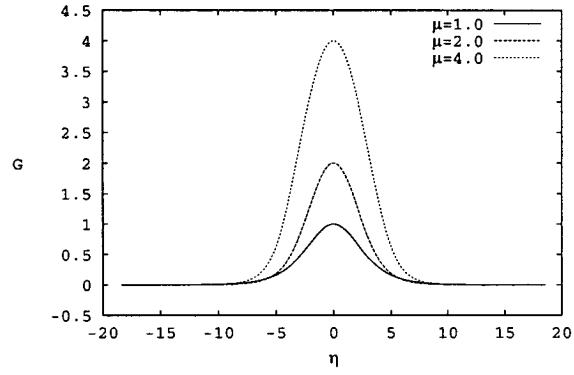

Figure 2.2: Beam profiles with peak values $\mu = 1, 2, 4$.

as is shown by the phase plane plot in Fig. 2.1. They are single-humped and symmetrical about the value of η at peak. Let us denote by $G(\eta)$ the even solution whose peak position coincides with the origin. $G(\eta)$ can be evaluated using the following definite integral

$$\eta = \pm \int_G^\mu \frac{dS}{\sqrt{\ln(1+S^2) - S^2\mu^{-2}\ln(1+\mu^2)}}, \qquad 0 < G \leq \mu.$$

The integral was evaluated numerically using the NAG routine D01AJF [79]. Fig. 2.2 shows the function $G(\eta)$ for three different peak values μ. These are the beam profiles discussed in [22].

2.2.2 Self-bending beams

As shown by equation (2.16), for $\gamma \neq 0$ the curvature parameter must be nonzero and the corresponding equation (2.14) is non-autonomous. The solutions must be calculated numerically. The strategy for finding localised solutions having a single hump is described in the following paragraphs.

The solutions for small γ may be approximated by the solutions of the autonomous ODE (2.17). Consider a solution of (2.14) whose peak is at $\eta = \eta^*$; it

may be written as an expansion in powers of γ as follows

$$F(\eta) = G(\eta - \eta^*) + \gamma F_1(\eta) + \cdots, \tag{2.20}$$

where we impose $F_1(\eta^*) = 0$ so that the first order correction contributes only to the asymmetry but not to the value $F(\eta^*)$. An analogous expansion may be written for the curvature parameter a

$$a = \gamma a_1 + \cdots. \tag{2.21}$$

Inserting the two expansions into (2.14), we recover equation (2.17) at zero order and the following non-homogeneous ODE for $F_1(\eta)$ at first order

$$F_1'' + \left[B - \frac{1}{1+G^2} + \frac{2G^2}{(1+G^2)^2}\right] F_1 = -a_1 \eta G - \frac{2G^2 G'}{1+G^2}, \tag{2.22}$$

The homogeneous part of the above equation is satisfied by $G'(\eta - \eta^*)$. Since the operator is self-adjoint, the right-hand term must be orthogonal to $G'(\eta - \eta^*)$ which is expressed by the following relation

$$a_1 \int_{\eta^*}^{+\infty} G^2(\eta - \eta^*)\, d\eta = 4 \int_{\eta^*}^{+\infty} \frac{G^2(\eta - \eta^*)[G'(\eta - \eta^*)]^2}{1 + G^2(\eta - \eta^*)}\, d\eta, \tag{2.23}$$

where we have used the property that $G(\eta - \eta^*)$ is symmetric about η^*. The above equation gives us a way of evaluating a_1 using only the solution of the diffusionless case as displayed in Fig. 2.2. Let us now insert the expansions (2.20) and (2.21) into (2.15) and integrate over (η^*, ∞). Considering $F_1(\eta^*) = 0$ and $G(0) = \mu$ we obtain

$$\begin{aligned} B\mu^2 - \ln(1-\mu^2) + \gamma a_1 \eta^* \mu^2 + \cdots \\ = \int_{\eta^*}^{+\infty} \gamma \left\{ a_1 G^2(\eta - \eta^*) - 4 \frac{G^2(\eta - \eta^*)[G'(\eta - \eta^*)]^2}{1 + G^2(\eta - \eta^*)} \right\} + \cdots d\eta \end{aligned}$$

Using the previous relation (2.23), the $O(\gamma)$ approximation implies that the peak location η^* may be approximated by zero. The equation (2.23) and the latter observation constitute the starting point for the shooting method described below.

First, we note that changing B corresponds only to a translation of the solution along the η axis. Hence it is possible to adjust the peak location by choosing B suitably (however as we see below the peak value and the value of a will change accordingly). Let us transform using $a\psi = a\eta + B$ so as to obtain an ODE without the parameter B as follows

$$F'' + \left[a\psi - \frac{1}{1+F^2} + \gamma \frac{2FF'}{1+F^2}\right] F = 0. \tag{2.24}$$

Since we are interested in localised solutions that vanish as $\eta \to \pm\infty$, the behaviour as $|F| \to 0$ is found by linearising equation (2.24) around $F = 0$ which gives us a non-standard form of the Airy equation

$$F'' + (a\psi - 1)F = 0.$$

In fact, the above equation may be transformed into a standard Airy equation given by

$$F'' - zF = 0,$$

by the change of variable $z(\psi) = a^{-2/3}(-a\psi + 1)$. For real z (real ψ) the basis solution that decays as $z \to +\infty$ ($\psi \to -\infty$) is $\mathrm{Ai}(z)$. Hence, at location ψ_1 in the left tail, F and F' may be approximated as

$$\begin{aligned} F(\psi_1) &= c_1 \mathrm{Ai}(z(\psi_1)), \\ F'(\psi_1) &= -c_1 a^{1/3} \mathrm{Ai}'(z(\psi_1)). \end{aligned}$$

In the other extremum $z \to -\infty$, both $\mathrm{Ai}(z)$ and $\mathrm{Bi}(z)$ decay algebraically, but oscillate. The reader may consult Appendix A (and references therein) concerning standard features of Airy functions. Nevertheless, preliminary numerical integration of equation (2.24) give us beam profiles with rapid decay in both sides. This behaviour occur since $a\psi < 1$ for every ψ in the numerical range and so that $z(\psi) > 0$ and small for ψ in the right tail. In this region $\mathrm{Ai}(z)$ and $\mathrm{Bi}(z)$ are both of order one and away from the algebraically decaying oscillations presented for negative z. These algebraic decay and oscillations should appear in the right tail but only when $|F(\psi)|$ is already very small.

The above considerations motivate a shooting method as follows: using (2.17) with $B = \mu^{-2}\ln(1+\mu^2)$, for a wide range of peak amplitudes μ the functions $G(\eta)$ are computed and inserted into (2.23) to determine $a_1 = a_1(\mu)$. Then, for fixed γ, a is estimated as γa_1 and a location $\bar{\psi}_1 = \bar{\eta}_1 + B/a$ is estimated such that $G(\bar{\eta}_1) = \epsilon$, where ϵ is a chosen small value (e.g. $\epsilon = 10^{-4}$). Then initial conditions for (2.24) are chosen as

$$\begin{aligned} F(\bar{\psi}_1) &= c_1 \mathrm{Ai}(z(\bar{\psi}_1)) = \epsilon, \\ F'(\bar{\psi}_1) &= -c_1 a^{1/3} \mathrm{Ai}'(z(\bar{\psi}_1)). \end{aligned}$$

Equation (2.24) is integrated in $\psi > \bar{\psi}_1$ until a first minimum of $F^2 + (F')^2$ is found. Then, the location ψ_1 is adjusted in order to decrease this minimum to ϵ^2 (or smaller). During this iterative procedure, γ and $a = \gamma a_1$ are held fixed, while the peak value $F_{\max}$ is allowed to differ from μ. Some of the computed beam profiles are shown in Fig. 2.3. The Airy function values with real argument

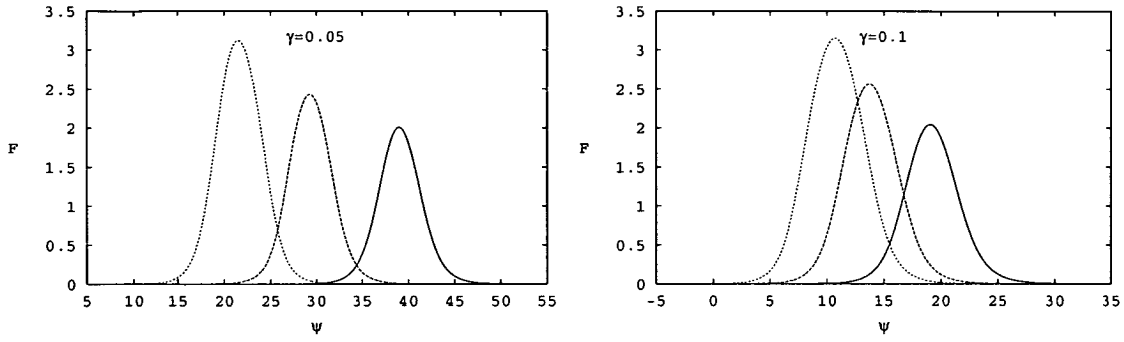

Figure 2.3: Beam profiles for $\gamma = 0.05$ and 0.1, corresponding to points marked • and ∘ in Fig. 2.4, respectively.

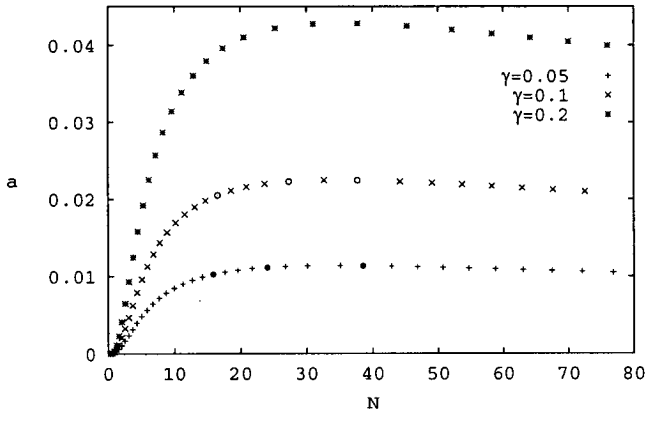

Figure 2.4: Dependence of the curvature a on the beam power N, for three values of γ.

were obtained with the NAG routine S17AGF/JF which is based on Chebyshev expansions. The integration was performed using the Runge-Kutta based routine D02PCF. The minimisation of $F^2+(F')^2$ was made with E04FCF which performs minimisation of a sum of squares using a combined Gauss-Newton and modified Newton algorithms [79]. Note that initial conditions with Airy functions were already used by Aleshkevich et al. [5] to treat the diffusive case of photorefractive solitons, but when the nonlinearity was of the Kerr type.

We were able to obtain localised solutions for γ up to 0.2. For each value of γ, as μ increases the values γa_1 arising from (2.23) increase to a maximum and then diminish slightly. A similar behaviour follows for the solutions of (2.24) computed as above. Figure 2.4 shows the dependence of curvature a on beam power $N = \int_{-\infty}^{\infty} F^2 d\psi$ [1], for $\gamma = 0.05, 0.1$ and 0.2.

[1]Note that the right tail of $F(\psi)$ behaves like the oscillatory algebraic decaying tail of the Airy functions in the negative real axis. Thus N cannot be finite. However, the real physical situation (a dielectric slab) will have finite boundaries, so that the problem (2.24) for $\psi \in \mathbb{R}$

For $\gamma = 0.3, 0.4$ and 0.5, localised solutions have also been found but only either for small beam power N or beyond the range of N presented in Fig. 2.4. For N in the range of Figure 2.4, $z(\bar{\psi}_2) < 0$ so that $G(\eta)$ is not the leading order approximation. In further stability analysis, we have restricted our attention to the ranges of γ and beam power N presented in Fig. 2.4.

2.3 Concepts of stability

Once the beam profiles are found it is important to understand their stability. In this brief section we first introduce several concepts of stability following essentially the references [52, 103].

Let us consider a dynamical system

$$\frac{\partial \mathbf{u}}{\partial t} = N\mathbf{u}, \tag{2.25}$$

where $\mathbf{u}$ is a vector function of t and x and N is a general nonlinear differential operator in x. Let $\mathbf{u_s}$ be a steady solution satisfying $N\mathbf{u_s} = 0$. To analyse its stability, regard the total solution as a sum of the steady solution $\mathbf{u_s}$ and a perturbation term $\mathbf{w}(x,t)$ in the form

$$\mathbf{u}(x,t) = \mathbf{u}_s(x) + \mathbf{w}(x,t). \tag{2.26}$$

Then, if $\mathbf{w}$ is small initially ($t = 0$), at least for some interval of time $t \in [0, T]$, the evolution of $\mathbf{w}(x,t)$ can be approximated by a solution to the linearisation of the full nonlinear governing equations, namely

$$\frac{\partial \mathbf{w}}{\partial t} = N_L(\mathbf{u}_s)\mathbf{w}, \tag{2.27}$$

where N_L is called the linearised operator and the equation is called the linear stability equation.

Definition 2.3.1 (Linearised stability) *The steady solution $\mathbf{u}_s$ is said to be linearly stable in the sense of Lyapunov with respect to the norms $\|(*)\|_I$ and $\|(*)\|_{II}$, if for every $\epsilon > 0$ there exists $\delta > 0$ such that $\|\mathbf{w}(x,0)\|_I < \delta \Rightarrow \|\mathbf{w}(x,t)\|_{II} < \epsilon$ for all $t \geq 0$, where $\mathbf{w}(x,t)$ satisfies the linear stability equation (2.27).*

---

is only an approximation of the real physical problem. Let us then assume that the effective power N is well approximated by the integral of the solution to (2.24) $F(\psi)$, but over a finite range of ψ, say $[\psi_1, \psi_2]$, many times the width at half maximum for the beam and outside which the amplitude is a minute fraction of the maximum value.

If a steady solution is linearly stable in the sense of Lyapunov, then algebraic and normal mode instabilities are absent. By algebraic instability we mean an algebraic growth of the perturbation amplitude and by normal mode instability an exponential growth. To investigate normal mode stability we assume a solution for (2.27) in the form

$$\mathbf{w}(x,t) = \mathbf{k}(x)e^{i\lambda t}. \tag{2.28}$$

Then, it follows that $\mathbf{k}(x)$ satisfies the equation

$$N_L(\mathbf{u}_s)\mathbf{k} = \lambda\mathbf{k}. \tag{2.29}$$

Normal mode stability is verified if the spectrum of $N_L(\mathbf{u}_s)$, with $|\mathbf{k}|$ bounded, has no strictly negative imaginary part.

Definition 2.3.2 (Spectral stability or normal mode stability) *The steady solution $\mathbf{u}_s$ is spectrally stable provided that the spectrum of the linearised operator has no strictly negative imaginary part.*

A special case of spectral stability is neutral stability, for which the spectrum is purely real. This corresponds to normal modes for which the time evolution is purely oscillatory. Linearised stability implies spectral stability but the converse is not generally true. For instance, multiple real eigenvalues suggest the existence of instabilities with linear growth rate.

The standard approach to treating the stability of travelling waves is to use linear stability or, more specifically, spectral stability. Spectral stability will be our stability approach also for the accelerating solutions. However, a stronger concept of stability, nonlinear stability, may be defined as:

Definition 2.3.3 (Nonlinear stability) *The steady solution $\mathbf{u}_s$ is said to be nonlinearly stable in the sense of Lyapunov with respect to the norms $\|(*)\|_I$ and $\|(*)\|_{II}$, if for every $\epsilon > 0$ there exists $\delta > 0$ such that $\|\mathbf{u}(x,0) - \mathbf{u}_s\|_I < \delta \Rightarrow \|\mathbf{u}(x,t) - \mathbf{u}_s\|_{II} < \epsilon$ for all $t \geq 0$, where $\mathbf{u}(x,t)$ satisfies the nonlinear equation (2.25).*

When linear stability is found, further efforts may be made to check whether that linear stability also implies nonlinear stability. In this thesis, however, we have limited our discussion to spectral stability supported then by tests performed using direct integration of the partial differential equation.

2.4 Linear stability equations and zero modes

Let us now consider the evolution equation (2.11) and analyse the equilibrium solutions obtained in §2.2. In order to perform linear stability analysis, we consider a total solution of the form

$$q(z,x) = \exp\left[i\theta(z,\eta)\right][F(\eta) + w(z,\eta)], \tag{2.30}$$

where $F(\eta)$ is the localised solution and $w(z,\eta)$ is a small complex perturbation term. Inserting (2.30) into (2.11), at first order, we obtain the following equation

$$iw_z + w_{\eta\eta} + \gamma\frac{F^2}{1+F^2}w_\eta + [a\eta + B + r(\eta)]w + \gamma\frac{F^2}{1+F^2}w_\eta^* + s(\eta)w^* = 0, \tag{2.31}$$

where * denotes complex conjugation and r and s are functions of η defined through F and F' as

$$r(\eta) = \frac{-1 + 3\gamma FF' + \gamma F^3F'}{(1+F^2)^2}, \qquad s(\eta) = \frac{F^2 - \gamma F^3F' + \gamma FF'}{(1+F^2)^2}.$$

Complex conjugation of (2.31) yields

$$iw_z^* - w_{\eta\eta}^* - \gamma\frac{F^2}{1+F^2}w_\eta^* - [a\eta + B + r(\eta)]w^* - \gamma\frac{F^2}{1+F^2}w_\eta - s(\eta)w = 0. \tag{2.32}$$

Adding and subtracting the two equations we obtain a coupled system for $(w + w^*)$ and $(w - w^*)$. Interpreting them as independent quantities and seeking exponential dependence on z such that $(w + w^*)(\eta, z) = U(\eta)\mathrm{e}^{i\lambda z} + U^*(\eta)\mathrm{e}^{-i\lambda^* z}$ and $(w - w^*)(\eta, z) = V(\eta)\mathrm{e}^{i\lambda z} - V^*(\eta)\mathrm{e}^{-i\lambda^* z}$, we obtain the following eigenvalue problem

$$\begin{pmatrix} 0 & L_0 \\ L_1 & 0 \end{pmatrix}\begin{pmatrix} U \\ V \end{pmatrix} = \lambda\begin{pmatrix} U \\ V \end{pmatrix}, \tag{2.33}$$

where

$$L_0 = \partial_{\eta\eta} + B + a\eta - \frac{1}{1+F^2} + \gamma\frac{2FF'}{1+F^2},$$

and

$$L_1 = \partial_{\eta\eta} + \frac{2\gamma F^2}{1+F^2}\partial_\eta + B + a\eta - \frac{1}{1+F^2} + \frac{2F^2 + 4\gamma FF'}{(1+F^2)^2}.$$

If the problem has any eigenvalue with negative imaginary part, the equilibrium solution $F(\eta)$ is unstable; and otherwise it is spectrally stable. The structure of the system (2.33) shows that if λ is an eigenvalue, so are $-\lambda$, λ^* and $-\lambda^*$. Thus the instability in this case arises whenever there exists an eigenvalue with non-zero imaginary part. Using the nomenclature introduced in the previous section, the spectral stability coincides with neutral stability.

One special eigenvalue is $\lambda = 0$, whose corresponding eigenfunctions we shall call *zero modes*. In the literature, they are also called *neutral modes* since the zero

eigenvalue is the only neutral eigenvalue occurring in integrable models. The zero modes are closely related to the invariances of the partial differential equation that governs the propagation. A close inspection of the evolution equation (2.11) shows us that it is invariant under arbitrary translations in z and in x and also under Galilean transformations and under a constant change of phase. To these four invariances correspond four arbitrary parameters and a zero stability eigenvalue with algebraic multiplicity equal to four. Although both the non-diffusive and diffusive cases admit the algebraic multiplicity four for the zero eigenvalue, its geometric multiplicity and eigenfunctions are different in the two cases. Therefore, we analyse the cases separately.

Let us first consider the non-diffusive model which admits rectilinear solutions $q(\eta, z) = \mathrm{e}^{i\theta(\eta,z)}F(\eta)$, where the phase is a simpler version of expression (2.13) given by $\theta(\eta, z) = V\eta + (V^2 - B)z + C$, $F(\eta)$ satisfies the differential equation (2.17) and $\eta = x - 2Vz + \eta_0$. The four arbitrary parameters are C, η_0, V and B. Consider one equilibrium solution corresponding to a certain choice of C, η_0, V and B. If we change any of the parameters, we still have an equilibrium solution. If the change is only infinitesimal, the first order correction to the original equilibrium solution is proportional to $\partial q/\partial C$, $\partial q/\partial \eta_0$, $\partial q/\partial V$ or $\partial q/\partial B$, respectively. Hence each of these four derivatives should satisfy the linear stability equation (2.31). These may be expressed as

$$\frac{\partial q}{\partial C} = \mathrm{e}^{i\theta}(iF), \qquad \frac{\partial q}{\partial \eta_0} = \mathrm{e}^{i\theta}(iVF + F'),$$
$$\frac{\partial q}{\partial V} = \mathrm{e}^{i\theta}(i2VzF - 2zF' + i\eta F), \qquad \frac{\partial q}{\partial B} = \mathrm{e}^{i\theta}(-izF + F_B).$$

Recall that the perturbations were defined in (2.30) as $\mathrm{e}^{i\theta}w$, hence, the solutions of the linear stability equation (2.31) are the expressions in brackets appearing above. The solutions of (2.32) are the corresponding complex conjugates. The first two derivatives have expressions inside the brackets that do not depend on z. They give us the proper eigenfunctions $y_1 = (0 \quad F)^T$ and $y_2 = (F' \quad 0)^T$ of the eigenvalue problem (2.33) (for $\gamma = 0$ and $a = 0$) corresponding to the zero eigenvalue. The other two derivatives have linear terms on z which relate them to the generalised eigenfunctions $y_3 = (0 \quad \eta F)^T$ and $y_4 = (F_B \quad 0)^T$. In fact, $Ly_3 = 2y_2$ and $Ly_4 = -y_1$, where L denotes the matrix operator of (2.33) for $\gamma = 0$ and $a = 0$. Based on the above description, we may assert that, in the non-diffusive case, the zero eigenvalue has geometric multiplicity equal to two.

The self-bending beams occurring in the presence of diffusion are given by $q(\psi, z) = \mathrm{e}^{i\theta(\psi,z)}F(\psi)$ where the phase is a version of (2.13) rewritten in terms of the new variable ψ as $\theta(\psi, z) = (V - az)\psi + 1/3a^2z^3 - aVz^2 + V^2z + \theta_0$, $F(\psi)$

satisfies the differential equation (2.24) and $\psi = x - 2Vz + az^2 + \psi_0$. It also admits four arbitrary parameters θ_0, ψ_0, V and a. Following the discussion presented for the non-diffusive case, we first obtain the expressions for the derivatives which read as

$$\begin{aligned}
\frac{\partial q}{\partial \theta_0} &= \mathrm{e}^{i\theta}(iF), \\
\frac{\partial q}{\partial \psi_0} &= \mathrm{e}^{i\theta}(iVF - iazF + F'), \\
\frac{\partial q}{\partial V} &= \mathrm{e}^{i\theta}(i2VzF - iaz^2F - 2zF' + i\psi F), \\
\frac{\partial q}{\partial a} &= \mathrm{e}^{i\theta}(-iVz^2F + \frac{i2a}{3}z^3F + z^2F' - iz\psi F + F_a).
\end{aligned}$$

The expressions inside the brackets satisfy (2.31) slightly modified, in terms of the variable ψ. In this case, the zero eigenvalue has geometric multiplicity one with one proper eigenfunction given by $y_1 = (0 \quad F)^T$. The generalised eigenfunctions are $y_2 = (F' \quad 0)^T$, $y_3 = (0 \quad \psi F)^T$ and $y_4 = (F_a \quad 0)^T$ which satisfy $L'y_2 = -ay_1$, $L'y_3 = 2y_2$ and $L'y_4 = -y_3$ (L' denotes the matrix operator rewritten in terms of ψ).

Note that the generalised eigenfunctions associated with the zero eigenvalue evolve algebraically with the propagation distance z. This algebraic growth, which is characteristic of modes associated with real eigenvalues of multiplicity greater than 1, was already pointed out in §2.3 to explain why spectral stability is not equivalent to linear stability. However, in the case of the zero modes, there is no real instability but instead an evolution corresponding to a nearby equilibrium state. To discard this false linear instability one, usually, defines linear stability in terms of the difference between perturbed and unperturbed solutions modulo symmetries of the evolution equation [103].

2.5 Vakhitov-Kolokolov criterion for the rectilinear beams

The *Vakhitov-Kolokolov* criterion was used for the first time by M. G. Vakhitov and A. A. Kolokolov in 1973 [109]. The criterion is based on the fact that the scalar operators L_0 and L_1 are Sturm-Liouville operators whose spectral properties are well known. Then, using the knowledge of their zero eigenvalue modes (closely related to the zero modes of the matrix operator L) and applying a Lagrange multiplier method, one arrives at a condition for stability that depends on the sign of the derivative of beam power with respect to the propagation constant. This criterion has been derived in more or less rigorous ways by several authors

[112, 67] and became a standard criterion for studying the stability of travelling solutions of generalised nonlinear Schrödinger equations. Recently, it has also been generalised to embrace coupled NLS equations [19, 88]. Here, we shal follow Kuznetsov and Rubenchick [67].

Taking the equilibrium solution of (2.17) as the even function $G(\eta)$, the stability operators L_0 and L_1 for $\gamma = 0$ and $a = 0$ have the form

$$L_0 = \partial_{\eta\eta} + B - \frac{1}{1+G^2},$$

and

$$L_1 = \partial_{\eta\eta} + B - \frac{1}{1+G^2} + \frac{2G^2}{(1+G^2)^2}.$$

Each of the operators L_0 and L_1 is a Sturm-Liouville operator of the Schrödinger type. Consider their respective eigenvalue problems. For L_0, the eigenvalue problem has the following form

$$\frac{\partial^2\phi}{\partial\eta^2} + \left[-\rho + B - \frac{1}{1+G^2}\right]\phi = 0, \tag{2.34}$$

where ρ is the eigenvalue parameter and ϕ is a bounded function. The potential of this Schrödinger operator is given by $U(\eta) = -B + (1+G^2)^{-1}$. The discrete spectrum that is non-degenerate must lie in $(-U_\infty, -U_{min})$, where $U_\infty = -B+1$ and $U_{min} = -B+(1+\mu^2)^{-1}$ [71]. The continuous spectrum is doubly degenerate and starts at $-U_\infty$ and extends to $-\infty$. For L_1, the eigenvalue problem is given by

$$\frac{\partial^2\psi}{\partial\eta^2} + \left[-\alpha + B - \frac{1}{1+G^2} + \frac{2G^2}{(1+G^2)^2}\right]\psi = 0, \tag{2.35}$$

where α is the eigenvalue parameter and ψ is a bounded function. In this case, the discrete spectrum is also non-degenerate and must lie between $B-1$ and $B-(1-\mu^2)/(1+\mu^2)^{-2}$. The continuous spectrum extends from $-\infty$ up to $B-1$.

G is easily recognised as the eigenfunction of the operator L_0 corresponding to the eigenvalue zero. Moreover, $G(\eta)$ is even and analysis in the phase plane shows that it has no zero. Recalling the Sturm-Liouville theory appropriate to operators of Schrödinger type, we can say that G is the fundamental eigenfunction and the operator L_0 is non-positive [71, 13]. The derivative G' of G with respect to η is an eigenfunction of the operator L_1. But since G' possesses exactly one zero, it is the second eigenfunction, not the fundamental. Thus, one positive eigenvalue must exist which corresponds to the fundamental eigenfunction.

From the system (2.33), it follows that

$$\lambda^2 U = L_0 L_1 U, \tag{2.36}$$

for all real eigenstates U of L_0L_1. On the subspace orthogonal to G the operator L_0 has an inverse, hence we can write

$$\lambda^2 = \frac{\langle U, L_1U\rangle}{\langle U, L_0^{-1}U\rangle}, \tag{2.37}$$

for any eigenfunction U of L_0L_1 satisfying $\langle U, G\rangle = 0$. In the latter expressions $\langle ., .\rangle$ denotes the standard inner product for real functions given by

$$\langle f, g\rangle = \int_{-\infty}^{\infty} f(\eta)g(\eta)d\eta.$$

On the same subspace, $\langle U, L_0^{-1}U\rangle$ is negative. For $\langle U, U\rangle = 1$, the quadratic form $\langle U, L_1U\rangle$ assumes values which cannot exceed the largest eigenvalue of L_1. To prove instability or spectral stability it is sufficient to show that the minimum eigenvalue λ^2 of (2.36) is negative or positive, respectively. The former situation occurs when $\max\langle U, L_1U\rangle > 0$ and the latter occurs when $\max\langle U, L_1U\rangle < 0$, for U on the subspace orthogonal to G. The maximisation of $\langle U, L_1U\rangle$ under the conditions $\langle U, G\rangle = 0$ and $\langle U, U\rangle = 1$ is equivalent to the maximisation of

$$H = \langle U, L_1U\rangle - 2\xi_1\langle U, G\rangle - \xi_2\langle U, U\rangle$$

which yields

$$L_1U = \xi_1G + \xi_2U, \tag{2.38}$$

where ξ_1 and ξ_2 are Lagrange multipliers and ξ_2 is the extremal value we are seeking. Let us denote the discrete eigenvalues of L_0 and L_1 by ρ_m and α_m and their corresponding eigenfunctions by ϕ_m and ψ_m, respectively. The expansions of U and G in terms of a complete orthogonal set of localised eigenfunctions $\{\psi_m\}$ of the operator L_1 are

$$U = \sum_{m=1}^{\infty} a_m\psi_m, \tag{2.39}$$

$$G = \sum_{m=1}^{\infty} b_m\psi_m. \tag{2.40}$$

Note that the second eigenfunction of L_1 is $\psi_2 = G'$ and since $\int_{-\infty}^{\infty} GG'd\eta=0$, then $\langle G, G'\rangle = 0$ and $b_2 = 0$. Substituting these expansions into (2.38) we obtain the coefficients a_m in terms of the coefficients b_m so giving U as

$$U = \xi_1\sum_{m=1}^{\infty}\frac{b_m}{\alpha_m - \xi_2}\psi_m. \tag{2.41}$$

If we substitute (2.41) into the orthogonality relation $\langle U, G\rangle = 0$, we obtain a final condition for determining ξ_2, namely

$$\xi_1\sum_{m=1}^{\infty}\frac{b_m^2}{\alpha_m - \xi_2} = \xi_1 g(\xi_2) = 0. \tag{2.42}$$

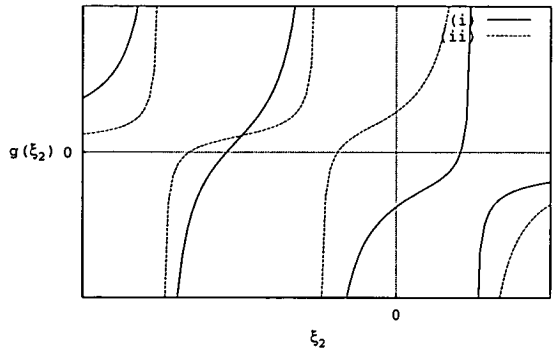

Figure 2.5: Two possibilities for the graph of $g(\xi_2)$.

The graph of $g(\xi_2)$ has asymptotes at each value $\xi_2 = \alpha_m$ (for m such that $b_m \neq 0$) and is monotonically increasing elsewhere. Since $b_2 = 0$ then $g(0)$ is finite. There are two possibilities for the largest root of equation (2.42), as can be seen in Fig. 2.5: (i) it is positive if $g(0) < 0$ or (ii) it is negative if $g(0) > 0$.

We may relate the quantity $g(0)$ to the invariant given by $N = \int_{-\infty}^{+\infty} G^2 d\eta$ which may be recognised as the beam power. First we note that $L_1^{-1}\psi_m = \psi_m/\alpha_m$ and using the expansion of G we can write $\langle G, L_1^{-1}G\rangle = g(0)$. The function G_B is a generalised eigenfunction of L_1 corresponding to the zero eigenvalue, i.e., $L_1 G_B = -G$. Since we are dealing with the subspace orthogonal to G we can write $L_1^{-1}G = -G_B$. Finally we obtain

$$g(0) = -\frac{1}{2}\frac{dN}{dB}. \tag{2.43}$$

Thus, the state G is spectrally stable if

$$dN/dB < 0$$

and it is unstable otherwise. Looking at the phase expression (2.13), we note that $(V^2 - B)$ represents the propagation constant (or more exactly, a deviation from the initially assumed propagation constant). Hence, we have arrived at the well known criterion that associates the transition to instability with a sign change of the rate of change of propagation constant with respect to power.

The above condition for stability may now be rewritten in terms of the peak value of G in the form

$$N'(\mu)/\frac{dB}{d\mu} < 0, \tag{2.44}$$

where

$$N(\mu) = \int_0^{\mu} \frac{\mu G^2 dG}{\sqrt{\mu^2 \ln(1+G^2) - \ln(1+\mu^2)G^2}}. \tag{2.45}$$

The integral $N(\mu)$ was evaluated for values of μ between 0 and 40 using the NAG routine D01AJF. In that range it is monotonically increasing. Fig. 2.6 shows the

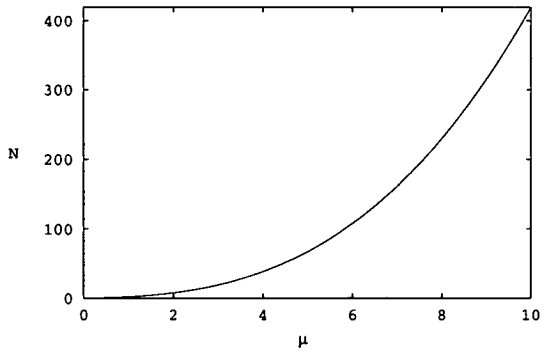

Figure 2.6: Graph of beam power $N(\mu)$ versus μ.

results for peak amplitudes up to 10. The derivative of B with respect to μ is given by

$$\frac{dB}{d\mu} = \frac{2\mu^2}{\mu^3(1+\mu^2)} - \frac{2\ln(1+\mu^2)}{\mu^3}, \tag{2.46}$$

and it is negative for all $\mu > 0$. In the range of μ analysed we can conclude that the profile $G(\eta)$ is spectrally stable.

2.6 Multiscale expansion for the self-bending beams

There is a kind of instability, usually known as *translational* instability, whose onset has been captured by a multiscale expansion, as used first by Pelinovsky *et al* [89]. In such cases, two internal modes (corresponding to real eigenvalues) collide at the origin and emerge as a pair of non-oscillatory modes (pure imaginary eigenvalues). We shall use this method to search for a possible threshold of instability for the self-bending beams.

The method is strongly dependent on the knowledge of the *zero modes*, which were found in §2.4. Let us first allow a change in the set of generalised eigenfunctions. As we know that, for many values of γ, there are two different solutions (different peak amplitude and power) with the same curvature parameter a, it is preferable to use a different parameter for describing the localised solutions to (2.14). Let us choose the beam power N and thus write $F \equiv F(\psi; \gamma, N)$. Using this representation the fourth generalised eigenfunction should now be $y_4 = (F_N \quad 0)^T$, since differentiation of (2.14) with respect to N gives $L_1 F_N = -(da/dN)\psi F$.

Let us consider the system (2.33), here rewritten as

$$L_0 V = \lambda U, \qquad L_1 U = \lambda V. \tag{2.47}$$

The main idea of the multiscale expansion is that the onset of instability occurs, if at all, for some critical value $N^{(c)}$ of N. At this critical point a pair of eigenvalues is passing through zero. Suppose that in the vicinity of this critical point, the pair of eigenvalues is of order ϵ. Following Etrich *et al* [28] and since zero has algebraic multiplicity four, then N differs from $N^{(c)}$ by only $\alpha\epsilon^4$ $(\alpha = \pm 1)$

$$N = N^{(c)} + \alpha\epsilon^4.$$

For this value of N the solution of (2.14) and the curvature parameter may be approximated by

$$\begin{aligned} F &= F^{(0)} + \alpha\epsilon^4 F^{(4)} + \cdots, \\ a &= a^{(0)} + \alpha\epsilon^4 a^{(4)} + \cdots, \end{aligned}$$

where $F^{(4)} = \dfrac{dF}{dN}(F^{(0)})$ and $a^{(4)} = \dfrac{da}{dN}(a^{(0)})$. The operators L_0 and L_1 may also be approximated by

$$\begin{aligned} L_0 &= L_0^{(0)} + \alpha\epsilon^4 L_0^{(4)} + \cdots, \\ L_1 &= L_1^{(0)} + \alpha\epsilon^4 L_1^{(4)} + \cdots. \end{aligned}$$

The fact that the number of invariances neither changes with N nor with any other parameter, suggests that at the critical point the corresponding mode should be proportional to $(U \quad V) = (0 \quad F^{(0)})$. Thus the eigenvalue λ and the eigenfunction components U and V are expanded as follows

$$\begin{aligned} \lambda &= \lambda_1\epsilon + \lambda_3\epsilon^3 + \cdots, \\ U &= U_1\epsilon + U_3\epsilon^3 + \cdots, \\ V &= F^{(0)} + V_2\epsilon^2 + V_4\epsilon^4 + \cdots. \end{aligned}$$

Substituting the above expansions into the eigenvalue problem (2.47) we obtain up to order ϵ^4:

$$\begin{aligned} O(1): &\quad L_0^{(0)} F^{(0)} = 0, \\ O(\epsilon): &\quad L_1^{(0)} U_1 = \lambda_1 F^{(0)}, \\ O(\epsilon^2): &\quad L_0^{(0)} V_2 = \lambda_1 U_1, \\ O(\epsilon^3): &\quad L_1^{(0)} U_3 = \lambda_3 F^{(0)} + \lambda_1 V_2, \\ O(\epsilon^4): &\quad L_0^{(0)} V_1 + \alpha L_0^{(4)} F^{(0)} = \lambda_3 U_1 + \lambda_1 U_3. \end{aligned} \tag{2.48}$$

The first equation is satisfied for all values of N. The solutions to the next three

inhomogeneous equations are

$$U_1 = -\lambda_1 \frac{(F^{(0)})'}{a^{(0)}}, \tag{2.49}$$

$$V_2 = -\lambda_1^2 \frac{\eta F^{(0)}}{2a^{(0)}},$$

$$U_3 = \lambda_1^3 \frac{F_N^{(0)}}{2a^{(0)}a^{(4)}} - \lambda_3 \frac{(F^{(0)})'}{a^{(0)}}. \tag{2.50}$$

Finally we apply to the fourth equation a solvability condition. First we introduce the expansions of L_0 and F into the equation $L_0 F = 0$ to obtain $L_0^{(4)} F^{(0)} = -L_0^{(0)} F^{(4)}$ at $O(\epsilon^4)$. Using the latter and the expressions (2.49) and (2.50) we may rewrite (2.48) as

$$L_0^{(0)}(V_1 - \alpha F^{(4)}) = \lambda_1^4 \frac{F_N^{(0)}}{2a^{(0)}a^{(4)}} - 2\lambda_3\lambda_1 \frac{(F^{(0)})'}{a^{(0)}}. \tag{2.51}$$

The operator L_0 and, in particular, $L_0^{(0)}$ is a self-adjoint operator. The null space of the operator $L_0^{(0)}$ is spanned by $F^{(0)}$, thus the right hand member of (2.51) should be orthogonal to $F^{(0)}$. This condition yields

$$\frac{\lambda_1^4}{2a^{(0)}a^{(4)}} \int_{-\infty}^{\infty} F^{(0)} F_N^{(0)} d\eta = 0$$

The above integral is proportional to the derivative of the power with respect to N itself which is one. Thus λ_1 must be zero, except for the case $a^{(4)} = 0$ for which the expression is not defined.

The case $a^{(4)} = 0$ corresponds to $\dfrac{da}{dN} = 0$ which we know occurs for a particular value of $a^* = a_{max}$. At this value, $F_N^* = F_N(\psi; \gamma, N^*)$ satisfies $L_1 F_N^* = 0$ and (F_N^* 0) becomes a proper eigenfunction. We believe that there is no onset of instability at N^*, but that instead $N = N^*$ is only an isolated value at which $\lambda = 0$ has geometric multiplicity two.

Although, the present method is far from a complete analysis of normal mode stability, the results obtained in this case discard any onset of instability caused by migration of real eigenvalues to the imaginary axis.

2.7 Conclusion

The self-bending beams, that were already numerically predicted and experimentally observed, were here obtained by the use of an accelerating similarity variable reduction of (2.11). In the diffusionless case, only the rectilinear propagation is possible. While the well-known *Vakhitov-Kolokolov* criterion gave stability for the rectilinear beams, a multiscale expansion did not find any translation instability

for the self-bending beams. In next chapter we continue the stability analysis of both cases using the Evans function method, a direct numerical search for eigenvalues and a direct numerical integration of the full evolution equation.

Chapter 3

Stability of photorefractive beams

The Evans function was introduced by Evans in 1972-75 [30, 31, 32, 33] while treating the stability of travelling nerve impulses. Since then the Evans function has been extensively used to study the linear stability properties of many travelling nonlinear waves. Among the published work we draw attention to the generalisations made by Alexander *et al* [6], Pego and Weinstein [87] and Swinton [104].

As mentioned in §2.3, the standard approach to stability of nonlinear waves is based on the study of the spectrum of a linear operator L which results from the linearisation of the evolution equation around the equilibrium solution. Under the standard definition, the Evans function is a function of the eigenvalue parameter λ which is analytic away from the continuous spectrum of L and is zero if and only if λ is an eigenvalue of L. Construction of an Evans function uses the fact that, in the context of waves travelling at constant velocity, the equilibrium solution $F(x)$ tends exponentially to zero or some other constant value as $x \to \pm\infty$ and so the asymptotic form of the operator L is generally a coupled system of constant coefficient differential equations having exponential-like solutions. The spectrum of L consists of both a continuous spectrum and discrete eigenvalues. The discrete eigenvalues are values of λ for which a localised solution to $L\mathbf{k} = \lambda\mathbf{k}$ exist. For a localised solution to exist the stable manifold (the manifold that is spanned by the solutions that match the exponentials decaying as $x \to +\infty$), should intersect with the unstable manifold (the manifold that is spanned by the solutions that match the exponentials decaying as $x \to -\infty$). This intersection occurs if and only if the Evans function (a Wronskian-like quantity) vanishes. Though, in general, the Evans function will not be known in closed form many stability properties may be inferred from analytical considerations of it [87, 55]. Moreover, when the Evans function is numerically evaluated along a closed path

in the λ-plane, since it is an analytic function, one may use the argument principle to identify the number of eigenvalues inside the region enclosed by such a closed path [105, 85, 11, 3, 86, 42]. The continuation of the Evans function across the continuous spectrum, using the so-called *gap lemma*, is one important development of the Evans function tool. This was implemented independently by Kapitula and Sandstede [56] and Gardner and Zumbrun [40] and is a useful tool for predicting and tracking eigenvalues that pop out from the continuous spectrum whenever an integrable model is perturbed.

A different approach to the Evans function is, however, necessary when we want to treat accelerating solutions, such as those of the diffusive photorefractive model found in the previous chapter. Though, the localised pulses have rapid decay in the close vicinity of the pulse, the decay is eventually algebraic in one direction. Moreover, the asymptotic form of L is not a system of constant coefficient differential equations but a system of Airy equations. Fortunately, there is also a vast knowledge of the Airy equation and its solutions, Airy functions, which makes possible the implementation of a modified Evans function method using Airy functions instead of exponentials [34].

This chapter is organised as follows. First we introduce and use the standard Evans function method to study the stability of the diffusionless photorefractive solutions. Then, the new Evans function method is established and used to check the stability properties of the diffusive solutions. We briefly discuss results concerning the spectrum obtained using a discretization of the operator L and, finally, we present the results of numerical simulation of the full evolution equation, confirming the results previously obtained using the modified Evans function method.

First of all, let us put the eigenvalue problem into a preferred form. For this purpose, let us treat w and w^* as independent variables and seek solutions with exponential dependence on z, such that $w(\eta, z) = u(\eta)\mathrm{e}^{i\lambda z} + v^*(\eta)\mathrm{e}^{-i\lambda^* z}$ and $w^*(\eta, z) = u^*(\eta)\mathrm{e}^{-i\lambda^* z} + v(\eta)\mathrm{e}^{i\lambda z}$. This converts (2.31) and (2.32) into a new form of eigenvalue problem, namely

$$L\begin{pmatrix} u \\ v \end{pmatrix} = \lambda \begin{pmatrix} u \\ v \end{pmatrix} \tag{3.1}$$

where the operator L is given by

$$L = \begin{pmatrix} \partial_{\eta\eta} + B + a\eta + \gamma\dfrac{F^2}{1+F^2}\partial_\eta + r(\eta) & \gamma\dfrac{F^2}{1+F^2}\partial_\eta + s(\eta) \\ -\gamma\dfrac{F^2}{1+F^2}\partial_\eta - s(\eta) & -\partial_{\eta\eta} - B - a\eta - \gamma\dfrac{F^2}{1+F^2}\partial_\eta - r(\eta) \end{pmatrix}$$

with $r(\eta)$ and $s(\eta)$ as defined after equation (2.31).

3.1 Evans function method applied to rectilinear beams

The Evans function method has two advantages relative to the *Vakhitov-Kolokolov* approach used in the previous chapter. It does not use the property of completeness of the eigenfunctions, for which a proof is beyond the scope of our work. Also it is suitable for finding all the discrete eigenvalues of the operator L, whether they are stable or unstable.

Let us consider the eigenvalue problem (3.1) applied with $F(\eta)$ chosen as the even solution of (2.17), denoted by $G(\eta)$ in section 2.2.1. It then reads as

$$\begin{pmatrix} \partial_{\eta\eta} + B + r & s \\ -s & -\partial_{\eta\eta} - B - r \end{pmatrix} \begin{pmatrix} u \\ v \end{pmatrix} = \lambda \begin{pmatrix} u \\ v \end{pmatrix}, \tag{3.2}$$

where in this case the functions r and s take the form

$$r = -\frac{1}{1+G^2} + \frac{G^2}{(1+G^2)^2},$$

and

$$s = \frac{G^2}{(1+G^2)^2}.$$

The spectrum of the above matrix differential operator consists of a discrete spectrum of isolated eigenvalues and a continuous spectrum. Since $G(\eta)$ tends to zero exponentially as $\eta \to \pm\infty$ then r tends to -1 and s to zero as $\eta \to \pm\infty$. Thus, the asymptotic form of L given by

$$L_\infty = \begin{pmatrix} \partial_{\eta\eta} - \omega & 0 \\ 0 & -\partial_{\eta\eta} + \omega \end{pmatrix}, \tag{3.3}$$

where $\omega = 1 - B$. The L_∞ operator is a constant coefficient differential operator whose continuous spectrum consists of two half-lines on the real axis given by the set

$$Q = \{\lambda \in \mathbb{R} : \ |\lambda| \geq \omega\}.$$

Following Henry [50] we may assert that Q is also the continuous spectrum of L. The isolated eigenvalues of L will be determined by the Evans function method.

First, we rewrite the stability equations as a system of four first-order differential equations using the change of variables $Y = \begin{pmatrix} u & u_\eta & v & v_\eta \end{pmatrix}^T$. This yields

$$\frac{dY}{d\eta} = A(\eta, \lambda)Y, \tag{3.4}$$

where

$$A(\eta,\lambda) = \begin{pmatrix} 0 & 1 & 0 & 0 \\ -B - r + \lambda & 0 & -s & 0 \\ 0 & 0 & 0 & 1 \\ -s & 0 & -B - r - \lambda & 0 \end{pmatrix}. \tag{3.5}$$

As $\eta \to \pm\infty$, the matrix operator takes the following constant form

$$A_\infty(\lambda) = \begin{pmatrix} 0 & 1 & 0 & 0 \\ \omega+\lambda & 0 & 0 & 0 \\ 0 & 0 & 0 & 1 \\ 0 & 0 & \omega-\lambda & 0 \end{pmatrix}. \tag{3.6}$$

The system (3.4) with $A(\eta,\lambda)$ replaced by $A_\infty(\lambda)$ will be denoted by asymptotic system. It has solutions of the form $\exp(\rho(\lambda)\eta)$ where $\rho(\lambda)$ is one of the eigenvalues of $A_\infty(\lambda)$ given by

$$\rho(\lambda) = \pm\sqrt{\omega \pm \lambda}.$$

For each λ such that $\lambda \in \Omega = \mathbb{C} \setminus Q$ there are two values of ρ with positive real part and two with negative real part. Let us denote them as suggested by the following inequalities

$$\mathrm{Re}(\rho_i) < 0 < \mathrm{Re}(\rho_j), \qquad j = 1,2 \qquad \text{and} \qquad i = 3,4;$$

and denote by Y_k^∞ the solutions to the asymptotic system which are explicitly given by

$$Y_1^\infty(\eta,\lambda) = \begin{pmatrix} 1 & \rho_1(\lambda) & 0 & 0 \end{pmatrix}^T \exp(\rho_1(\lambda)\eta) = y_1(\lambda)\exp(\rho_1(\lambda)\eta), \tag{3.7}$$

$$Y_2^\infty(\eta,\lambda) = \begin{pmatrix} 0 & 0 & 1 & \rho_2(\lambda) \end{pmatrix}^T \exp(\rho_2(\lambda)\eta) = y_2(\lambda)\exp(\rho_2(\lambda)\eta), \tag{3.8}$$

$$Y_3^\infty(\eta,\lambda) = \begin{pmatrix} 1 & \rho_3(\lambda) & 0 & 0 \end{pmatrix}^T \exp(\rho_3(\lambda)\eta) = y_3(\lambda)\exp(\rho_3(\lambda)\eta), \tag{3.9}$$

$$Y_4^\infty(\eta,\lambda) = \begin{pmatrix} 0 & 0 & 1 & \rho_4(\lambda) \end{pmatrix}^T \exp(\rho_4(\lambda)\eta) = y_4(\lambda)\exp(\rho_4(\lambda)\eta). \tag{3.10}$$

Then $|Y_j^\infty| \to 0$ $(j = 1,2)$ as $\eta \to -\infty$ with $|Y_j^\infty|$ unbounded as $\eta \to \infty$. For $Y_i^\infty(\eta,\lambda)$ $(i = 3,4)$, the situation is reversed. The full problem (3.4) has particular solutions Y_k^- for which the behaviour as $\eta \to -\infty$ satisfies

$$Y_k^-(\eta,\lambda) \sim Y_k^\infty \qquad \text{as} \qquad \eta \to -\infty, \qquad k = 1,\ldots,4$$

and has also solutions Y_k^+ for which the behaviour as $\eta \to +\infty$ satisfies:

$$Y_k^+(\eta,\lambda) \sim Y_k^\infty \qquad \text{as} \qquad \eta \to +\infty \qquad k = 1,\ldots,4.$$

Either set of solutions forms a basis for the solution space to (3.4).

The isolated eigenvalues should correspond to localised eigenfunctions. Such a function should be a linear combination of $Y_1^-(\eta,\lambda)$ and $Y_2^-(\eta,\lambda)$ (they span the unstable manifold), because these are decaying as $\eta \to -\infty$, and simultaneously a linear combination of $Y_3^+(\eta,\lambda)$ and $Y_4^+(\eta,\lambda)$ (they span the stable manifold) because these are decaying in the other limit. That is, if λ^* is an eigenvalue then

$$a_1(\lambda^*)Y_1^-(\eta,\lambda^*) + a_2(\lambda^*)Y_2^-(\eta,\lambda^*) = a_3(\lambda^*)Y_3^+(\eta,\lambda^*) + a_4(\lambda^*)Y_4^+(\eta,\lambda^*). \tag{3.11}$$

In its simpler version, the Evans function is given by the Wronskian of these four vectors, namely,

$$D_s(\lambda) = \begin{vmatrix} Y_{11}^-(\eta,\lambda) & Y_{21}^-(\eta,\lambda) & Y_{31}^+(\eta,\lambda) & Y_{41}^+(\eta,\lambda) \\ Y_{12}^-(\eta,\lambda) & Y_{22}^-(\eta,\lambda) & Y_{32}^+(\eta,\lambda) & Y_{42}^+(\eta,\lambda) \\ Y_{13}^-(\eta,\lambda) & Y_{23}^-(\eta,\lambda) & Y_{33}^+(\eta,\lambda) & Y_{43}^+(\eta,\lambda) \\ Y_{14}^-(\eta,\lambda) & Y_{24}^-(\eta,\lambda) & Y_{34}^+(\eta,\lambda) & Y_{44}^+(\eta,\lambda) \end{vmatrix}, \tag{3.12}$$

where $Y_{ij}^{\pm}$ is the j-component of $Y_i^{\pm}$. Note that since $\mathrm{Tr}(A(\eta,\lambda)) = 0$, Abel's formula says that the above Wronskian is independent of η. Moreover $D_s(\lambda)$ vanishes if and only if (3.11) is satisfied. However, this definition has two main drawbacks. Although (Y_1^-, Y_2^-) and (Y_3^+, Y_4^+) are linearly independent solutions to (3.4), in solving this system numerically, solutions corresponding to all initial conditions will be attracted to the solution associated to the largest growth rate. This is a typical symptom of *stiffness*. In the case of system (3.4), this problem may be overcome as explained in page 44. The second drawback is related to the analyticity of $D_s(\lambda)$ which is only proved for those λ for which the eigenvalues ρ_i $(i = 1, \cdots, 4)$ are distinct. This requirement is imposed when proving that the solutions Y_1^-, Y_2^-, Y_3^+ and Y_4^+ depend analytically on analytic initial data [104]. In our case, this requirement excludes the case $\lambda = 0$.

The definition of the Evans function introduced by Alexander *et al* [6] avoids the lack of analyticity at values λ where the eigenvalues of $A(\lambda)$ coalesce, by posing the eigenvalue problem on the exterior algebra of $\mathbb{C}^n$. The numerical procedure associated with this approach is also suitable for overcoming the *stiffness*. This was first used by Alexander and Sachs [7] and well explained in [3, 16] but a similar method called the compound matrix method was originally used by Ng and Reid [80, 81] to solve numerically unstable linear systems of ordinary differential equations. The relationship between the two methods was discussed in [8].

Let us first introduce elementary notions of exterior algebras [20] so as to define a different Evans function. Consider the vector space $\mathbb{C}^n$ and let $\xi_1, \cdots, \xi_k$ be any k vectors of $\mathbb{C}^n$. The element $\xi_1 \wedge \cdots \wedge \xi_k$ is called a *k-vector*. The operation denoted by $\wedge$ and called *exterior product* or *wedge product* is a k-linear and totally antisymmetric operation such that

$$\xi_1 \wedge \cdots \wedge \xi_{i-1} \wedge \xi_i \wedge \cdots \wedge \xi_k = -\xi_1 \wedge \cdots \wedge \xi_i \wedge \xi_{i-1} \wedge \cdots \wedge \xi_k.$$

From those properties it follows that the k-form vanishes if it involves any repeated vector or any number of linearly dependent vectors. Furthermore, if the order of the terms is changed by a permutation $\pi \in S_k$ then the resulting k-form is unchanged if π is an even permutation and merely changed in sign otherwise. All the k-forms create a vector space of dimension $d = \binom{n}{k}$ called the *exterior space*

of $\mathbb{C}^n$ and denoted by $\Lambda^k(\mathbb{C}^n)$. The formal sum

$$\Lambda(\mathbb{C}^n) = \sum_{k=0}^{n} \Lambda^k(\mathbb{C}^n),$$

with the wedge product is an associative algebra called *exterior algebra* or *Grassman algebra*. Let $\mathbf{e}_1, \cdots, \mathbf{e}_n$ be the standard orthonormal basis, then a natural basis for $\Lambda^k(\mathbb{C}^n)$ is given by

$$\{\mathbf{e}_{i_1} \wedge \cdots \wedge \mathbf{e}_{i_k}, 1 \leq i_1 < \cdots < i_k \leq n\}.$$

Furthermore, if $\xi_1, \cdots, \xi_k$ span a k-dimensional space, then the single k-form $\xi_1 \wedge \cdots \wedge \xi_k$ represents this k-dimensional space. For this reason the use of exterior vectors is advantageous in solving eigenvalue problems like system (3.4).

The set of solutions to system (3.4) forms a vector space of dimension 4 which is isomorphic to $\mathbb{C}^4$. Since the subspaces of interest are the two-dimensional stable and unstable subspaces, we consider the 2-forms belonging to the exterior space $\Lambda^2(\mathbb{C}^4)$. Let us consider two independent solutions to (3.4) Y and $\tilde{Y}$ whose expansions in the standard orthonormal basis of $\mathbb{C}^4$ are

$$Y = \sum_{i=1}^{4} Y_i \mathbf{e}_i, \qquad \tilde{Y} = \sum_{i=1}^{4} \tilde{Y}_i \mathbf{e}_i.$$

The 2-form $Y \wedge \tilde{Y}$ is a six-dimensional vector which may be expanded as follows

$$\begin{aligned} U = Y \wedge \tilde{Y} &= \sum_{j=1}^{4} \sum_{k>j}^{4} (Y_j \tilde{Y}_k - Y_k \tilde{Y}_j) \mathbf{e}_j \wedge \mathbf{e}_k \\ &= \sum_{l=1}^{6} U_l \boldsymbol{\omega}_l. \end{aligned}$$

Here the base vectors $\boldsymbol{\omega}_l$ $(l = 1, \cdots, 6)$ correspond to $\mathbf{e}_j \wedge \mathbf{e}_k$ as follows

$$\begin{array}{lll} \boldsymbol{\omega}_1 = \mathbf{e}_1 \wedge \mathbf{e}_2, & \boldsymbol{\omega}_2 = \mathbf{e}_1 \wedge \mathbf{e}_3, & \boldsymbol{\omega}_3 = \mathbf{e}_1 \wedge \mathbf{e}_4, \\ \boldsymbol{\omega}_4 = \mathbf{e}_2 \wedge \mathbf{e}_3, & \boldsymbol{\omega}_5 = \mathbf{e}_2 \wedge \mathbf{e}_4, & \boldsymbol{\omega}_6 = \mathbf{e}_3 \wedge \mathbf{e}_4. \end{array} \tag{3.13}$$

The vector U (strictly the column vector $(U_1 \quad U_2 \quad U_3 \quad U_4 \quad U_5 \quad U_6)^T$) satisfies the so-called *exterior system*, given by

$$\frac{dU}{d\eta} = A^{(2)}(\eta, \lambda) U, \tag{3.14}$$

where $A^{(2)}$ may be obtained by direct calculation and reads as

$$A^{(2)}(\eta, \lambda) = \begin{pmatrix} 0 & -s & 0 & 0 & 0 & 0 \\ 0 & 0 & 1 & 1 & 0 & 0 \\ 0 & -B - r - \lambda & 0 & 0 & 1 & 0 \\ 0 & -B - r + \lambda & 0 & 0 & 1 & 0 \\ s & 0 & -B - r + \lambda & -B - r - \lambda & 0 & -s \\ 0 & s & 0 & 0 & 0 & 0 \end{pmatrix}. \tag{3.15}$$

As for the previous matrix operator $A(\eta,\lambda)$, it is possible to define the 6×6 constant matrix $A^{(2)}_{\infty}(\lambda)=\lim_{|\eta|\to\infty}A^{(2)}(\eta,\lambda)$ for which the eigenvalues are the sum of any two distinct eigenvalues of $A_{\infty}(\lambda)$. Since $A_{\infty}(\lambda)$ has 2 eigenvalues with positive real part and 2 with negative real part, therefore $A^{(2)}_{\infty}(\lambda)$ has one of largest real part and one of smallest real part and both are simple. Denote them by $\sigma_+=\sqrt{\omega+\lambda}+\sqrt{\omega-\lambda}$ and $\sigma_-=-\sqrt{\omega+\lambda}-\sqrt{\omega-\lambda}$. Corresponding to these eigenvalues of $A^{(2)}_{\infty}(\lambda)$, the differential system (3.14) has solutions given by

$$U^-(\eta,\lambda)=Y_1^-(\eta,\lambda)\wedge Y_2^-(\eta,\lambda),$$

and

$$U^+(\eta,\lambda)=Y_3^+(\eta,\lambda)\wedge Y_4^+(\eta,\lambda).$$

They correspond to the largest exponential growths; σ_+ as we integrate forward and σ_- if we integrate backward with respect to η, respectively. They also represent the previously discussed unstable and stable subspaces for this new differential system (3.14). Similarly, for this system, we may assign an asymptotic behaviour to U^- and U^+ given by

$$U^{\pm}(\eta,\lambda)\sim U^{\pm}_{\infty}\equiv u^{\pm}(\lambda)\exp(\sigma_{\mp}\eta)\qquad\text{as}\qquad\eta\to\pm\infty,$$

where $u^{\pm}(\lambda)$ is a 6-component vector that when written in terms of the basis $\boldsymbol{\omega}_1,\cdots,\boldsymbol{\omega}_6$ reads as

$$u^{\pm}(\lambda)=\left(0\quad 1\quad\left(\tfrac{\sigma_{\mp}}{2}-\tfrac{\lambda}{\sigma_{\mp}}\right)\quad\left(\tfrac{\sigma_{\mp}}{2}+\tfrac{\lambda}{\sigma_{\mp}}\right)\quad\left(\tfrac{\sigma_{\mp}^2}{2}-\omega\right)\quad 0\right)^T.$$

In this new formulation, λ is an eigenvalue if and only if the 2-forms $U^-(\lambda,\eta)$ and $U^+(\lambda,\eta)$ are linearly dependent, i.e., $U^-(\lambda,\eta)\wedge U^+(\lambda,\eta)=0$. The quantity

$$\tilde{D}(\lambda,\eta)=U^-(\lambda,\eta)\wedge U^+(\lambda,\eta)$$

lies in the one-dimensional space $\Lambda^4(\mathbb{C}^4)$ and satisfies

$$\frac{d\tilde{D}}{d\eta}=A^{(4)}(\lambda,\eta)\tilde{D}.$$

The natural basis for $\Lambda^4(\mathbb{C}^4)$ is $\mathbf{e}_1\wedge\mathbf{e}_2\wedge\mathbf{e}_3\wedge\mathbf{e}_4$, where $A^{(4)}(\lambda,\eta)=\mathrm{Tr}A(\lambda,\eta)$. In this particular case $\mathrm{Tr}A(\lambda,\eta)=0$, so that $\tilde{D}(\lambda,\eta)$ is independent of η; $\tilde{D}(\lambda,\eta)\equiv\tilde{D}(\lambda)$. Moreover, using the expansions of $U^-(\lambda,\eta)$ and $U^+(\lambda,\eta)$ in the basis (3.13) as follows

$$U^-(\lambda,\eta)=\sum_{i=1}^{6}U_i^-\boldsymbol{\omega}_i,\qquad U^+(\lambda,\eta)=\sum_{i=1}^{6}U_i^+\boldsymbol{\omega}_i,$$

we arrive at

$$\tilde{D}(\lambda)=D(\lambda)\mathbf{e}_1\wedge\mathbf{e}_2\wedge\mathbf{e}_3\wedge\mathbf{e}_4$$

where $D(\lambda)$ is the new definition of the Evans function given by

$$D(\lambda) = (U_1^- U_6^+ - U_2^- U_5^+ + U_3^- U_4^+ + U_4^- U_3^+ - U_5^- U_2^+ + U_6^- U_1^+). \tag{3.16}$$

Note that for the exterior system (3.14), σ^+ and σ^- are simple eigenvalues, thus based on the discussion in page 35 we can guarantee that $U^-(\lambda, \eta)$ and $U^+(\lambda, \eta)$ depend analytically on their initial conditions for every $\lambda \in \Omega$. This feature guarantees us the global analyticity of the Evans function (3.16) for $\lambda \in \Omega$.

The computational algorithm consists of solving (3.14) as an initial value problem. First we integrate forward to $\eta = 0$ from a certain $\eta_- < 0$, for which in (3.2) $G(\eta_-) = \epsilon \ll 1$, using $U(\eta_-) = U_\infty^-(\eta_-)$. Similarly, we integrate backward to $\eta = 0$ from η_+ where $G(\eta_+) = \epsilon$, with $U(\eta_+) = U_\infty^+(\eta_+)$. Using the computed components of $U^-(0)$ and $U^+(0)$ we may determine $D(\lambda)$ from expression (3.16). To avoid complications due to exponentially growing terms we introduce new variables in each integration. Hence, in the forward integration we make the following change of variables

$$\psi(\eta, \lambda) = \exp(-\sigma_+ \eta) U.$$

This new variable satisfies the initial value problem given by

$$\frac{d\psi}{d\eta} = \left[A^{(2)} - \sigma_+ I_6\right] \psi,$$

$$\psi(\eta_-, \lambda) = u^-(\lambda). \tag{3.17}$$

Similarly, we define a new variable for the backward integration given by

$$\phi(\eta, \lambda) = \exp(-\sigma_- \eta) U,$$

satisfying the following initial value problem

$$\frac{d\phi}{d\eta} = \left[A^{(2)} - \sigma_- I_6\right] \phi,$$

$$\phi(\eta_+, \lambda) = u^+(\lambda), \tag{3.18}$$

where I_6 is the 6×6 identity matrix.

We solve simultaneously system (3.17) and equation (2.17) using a forward integration from $\eta = \eta_-$ to $\eta = 0$. Then we solve (3.18) and (2.17) using backward integration from $\eta = \eta_+$ to $\eta = 0$. The integration is performed using the NAG routine D02PCF. In terms of these new variables the numerical value of the Evans function is given by

$$D(\lambda) = (\psi_1 \phi_6 - \psi_2 \phi_5 + \psi_3 \phi_4 + \psi_4 \phi_3 - \psi_5 \phi_2 + \psi_6 \phi_1),$$

where ψ_i and ϕ_i $(i = 1, \cdots, 6)$ are the components of $\psi(0, \lambda)$ and $\phi(0, \lambda)$, respectively.

Let us discuss the value of $D(\lambda)$ for large $|\lambda|$. When $|\lambda|$ is large the η-dependence of $A^{(2)}(\eta, \lambda)$ is negligible and the system (3.14) is well approximated by the asymptotic system ($A^{(2)}(\eta, \lambda)$ replaced by $A^{(2)}_{\infty}(\lambda)$). The same is true for systems (3.17) and (3.18). Since $u^-(\lambda)$ and $u^+(\lambda)$ are the eigenvectors of $A^{(2)}_{\infty}(\lambda)$ corresponding to the eigenvalues σ_+ and σ^-, respectively, the integration of systems (3.17) and (3.18) will preserve them unchanged. Hence, for large $|\lambda|$

$$\psi(0, \lambda) \sim \psi(\eta^-, \lambda) \qquad \text{and} \qquad \phi(0, \lambda) \sim \phi(\eta^-, \lambda)$$

which gives

$$D(\lambda) \to -4\sqrt{\omega^2 - \lambda^2} \qquad \text{as} \qquad |\lambda| \to \infty.$$

Defining a normalised version of the Evans function as

$$E(\lambda) = \frac{D(\lambda)}{-4\sqrt{\omega^2 - \lambda^2}}, \tag{3.19}$$

we then obtain $E(\lambda) \to 1$ as $|\lambda| \to \infty$. Note that $E(\lambda)$ has $-\omega$ and ω as branch points but, if we take as branch cuts the portions of the real axis that constitute the continuous spectrum S and perform the evaluations of $\sqrt{\omega^2 - \lambda^2}$ using the same branch everywhere, then $E(\lambda)$ is analytic on Ω.

3.1.1 Numerical results

The search for zeros of $D(\lambda)$ or $E(\lambda)$ may be simplified if we use the argument principle. The argument principle results from applying the residue theorem to $f'(z)/f(z)$. Let $f(z)$ be an analytic function on a bounded domain D of the complex z-plane, with analytic extension onto the boundary ∂D such that $f(z) \neq 0$ on ∂D. Then the increase in the argument of $f(z)$ around the boundary of D is 2π times the number of zeros of $f(z)$ within D;

$$\int_{\partial D} d \arg f(z) = 2\pi n,$$

where n is the number of zeros of $f(z)$ in D [38]. Graphically, if a function is analytic within a closed curve and has no zeros on that curve, then the number of zeros within that curve equals the number of times the image graph wraps around the origin as the original curve is traversed. We may use this principle within the set Ω where $D(\lambda)$ and $E(\lambda)$ were shown to be analytic. Thus the number of zeros of $E(\lambda)$ in the negative imaginary half-plane (equal to the number of unstable modes) may be determined as the number of times $E(\lambda)$ wraps around the origin

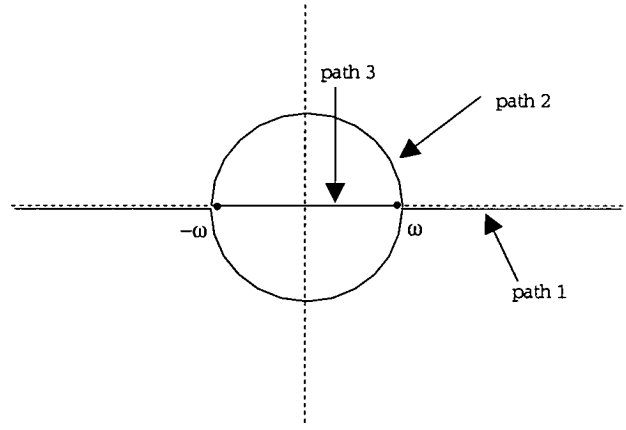

Figure 3.1: Paths of evaluation of $E(\lambda)$

while $E(\lambda)$ is evaluated with λ at points on a path in the complex λ-plane parallel to the real axis and infinitesimally close to it, i.e., $\{\lambda : \lambda = t + i0^{-}, t \in \mathbb{R}\}$. In fact, if we evaluate $E(\lambda)$ along such a path parallel to the real axis, we obtain a very complicated figure for $E(\lambda)$, due to the behaviour near $\lambda = 0$. Hence, instead we use path 1 (see Fig. 3.1) parallel and very close to the real axis for $|\lambda| > \omega$, but completed by semicircles in the lower half-plane centred at $\lambda = 0$ and of radii ω and R ($>> \omega$). To complement the analysis we use also two more paths: a circle (path 2) with centre at $\lambda = 0$ and radius $\omega - \epsilon$ ($\epsilon \sim 10^{-4}$) and an open path (path 3) consisting of the segment of the real axis between $-\omega + \epsilon$ and $\omega - \epsilon$.

As might be anticipated from the Vakhitov-Kolokolov stability analysis, using the Evans function method we found that the solutions of (2.17) are stable under the evolution equation (2.11) for $\gamma = 0$. We have analysed profiles up to the amplitude $\mu = 6.0$. For all those amplitudes, all the eigenvalues lie on the real axis. For small amplitudes, only the eigenvalue $\lambda = 0$ exists, with algebraic multiplicity of four. Between $\mu = 1.2$ and $\mu = 1.3$ two more eigenvalues appear within $(-\omega, \omega)$. They lie symmetrically on the real axis and an increase in amplitude makes them move towards the origin. For higher amplitudes, new pairs of real eigenvalues were observed. For instance, for $\mu = 4.0$ there are two nonzero pairs and for $\mu = 6.0$ there are three nonzero pairs. This suggests that these pairs emerge from the continuous spectrum and move towards the origin without ever reaching it. Hence, they never appear on the imaginary axis which would mean instability.

In Figure 3.2, the Evans function $E(\lambda)$ is plotted as λ moves along the path 1 for a solution of amplitude $\mu = 1.0$. The point $E = 1$ corresponds to large values of $|\lambda|$. Following the curve we note that the net change of the argument of $E(\lambda)$ is zero which means that there are no eigenvalues in the lower half-plane outside

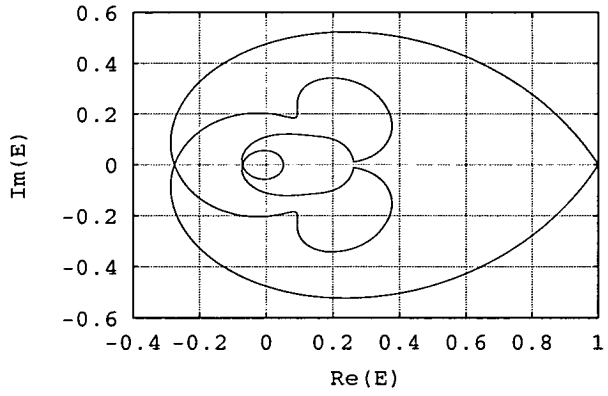

Figure 3.2: Image of the path 1 for a solution of amplitude $\mu = 1.0$.

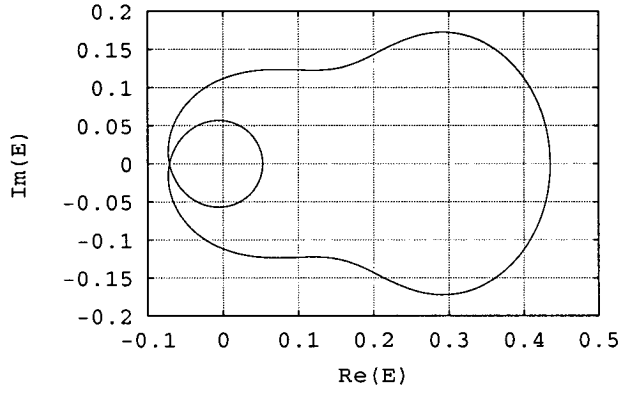

Figure 3.3: Image of the path 2 for a solution of amplitude $\mu = 1.0$.

the semicircle. Figure 3.3 corresponds to the path 2 for the same amplitude μ. The figure shows that the origin is enclosed twice, but in fact the curve shown was traversed twice and the argument of E has changed by 8π. The repetition occurs because $E(\lambda)$ has a symmetry which gives $E(\lambda) = E(-\lambda)$. Hence, the circle that constitutes the path 2, encloses 4 eigenvalues. Evaluating $E(\lambda)$ along smaller circles centred at $\lambda = 0$ shows us that the four eigenvalues correspond to the algebraic multiplicity of the eigenvalue $\lambda = 0$.

Repeating the calculations for a solution of amplitude $\mu = 2.0$, we have the same kind of result for path 1. The image of path 2 under the function $E(\lambda)$ is shown in Fig. 3.4 and once again the displayed curve was traversed twice. Therefore, the argument of E changes by 12π which means that there exist 6 eigenvalues inside the circle of radius $\omega - \epsilon$. At this stage, we do not know if the two extra eigenvalues are real or pure imaginary. In Figure 3.5 we show $E(\lambda)$ for λ moving along the segment $(-\omega + \epsilon, \omega - \epsilon)$ (path 3). In this case $E(\lambda)$ is real, hence, we have plotted $\mathrm{Re}(E)$ versus λ. $E(\lambda)$ is zero at $\lambda = 0$ and also at two other symmetrically placed values. These results clarify that the extra two

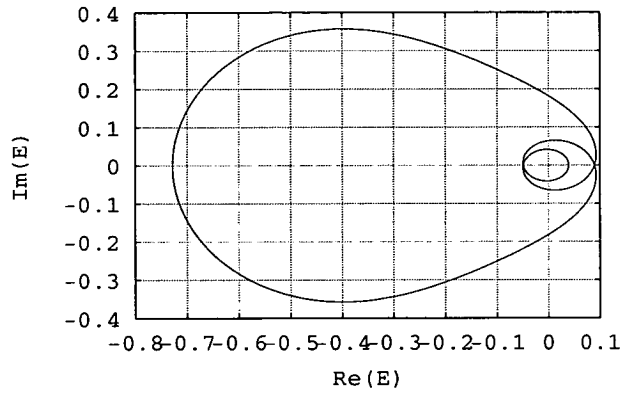

Figure 3.4: Image of the path 2 for a solution of amplitude $\mu = 2.0$.

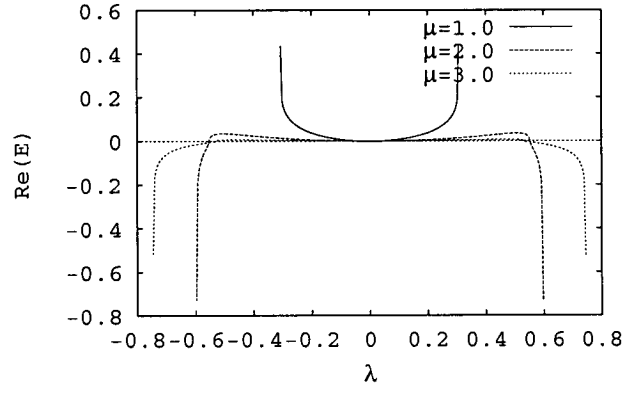

Figure 3.5: Re(E) for λ moving along path 3 for solutions of amplitude $\mu = 1.0, 2.0, 3.0$.

eigenvalues are in fact real ones. In the same figure, we show also $E(\lambda)$ evaluated along the same path, but for amplitude $\mu = 3.0$. The graph is similar, it has the same number of zeros and we may observe that the nonzero eigenvalues have moved towards the origin.

Since we have determined the eigenvalues, it should be possible to determine the corresponding eigenfunctions. Using only the data obtained by the algorithm described, this is not possible. We should recall that we have not determined explicitly the Y_1^-, Y_2^-, Y_3^+ and Y_4^+ with which we may reconstruct the eigenfunction as a linear combination. Instead we determined U^- and U^+. Using a method found in the context of the compound matrix approach [81] it is possible to recover the functions Y_1^-, Y_2^-, Y_3^+ and Y_4^+ from U^- and U^+ whenever the latter do not vanish in the range of integration. In our case they vanish, which makes it difficult to obtain the full profile of the eigenfunctions. To overcome this difficulty we have used the Wronskian definition of the Evans function (3.12). As mentioned earlier we cannot prove the analyticity at $\lambda = 0$ of this version of the

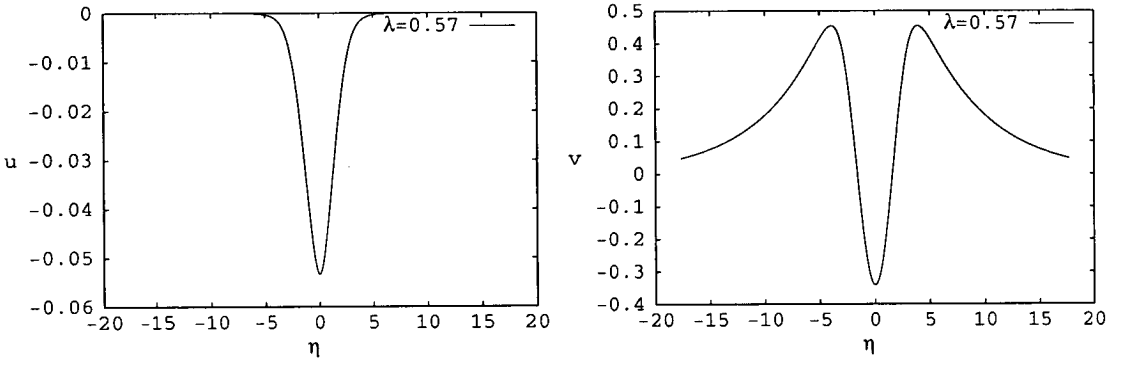

(a)

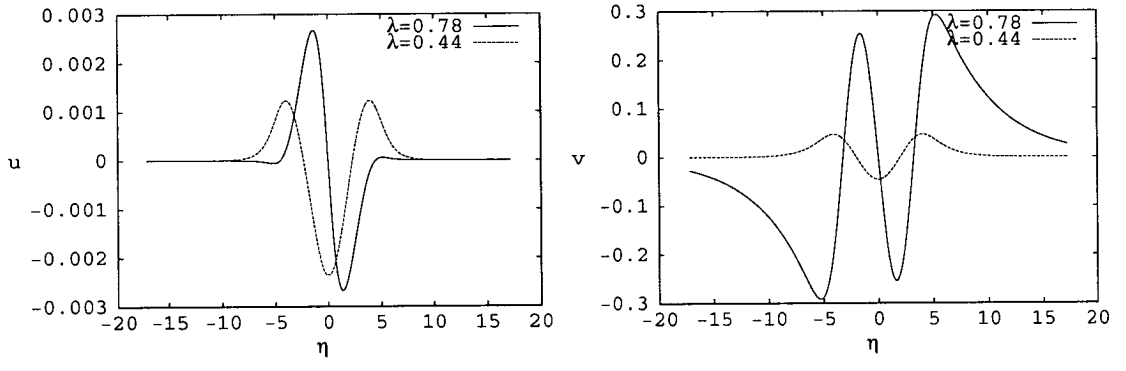

(b)

Figure 3.6: Perturbations u and v that constitute the eigenfunction corresponding to (a) $\lambda = \pm 0.57$ for a solution of amplitude $\mu = 2.0$, (b) $\lambda = \pm 0.44, \pm 0.78$ for a solution of amplitude $\mu = 4.0$.

Evans function but we know that the function vanishes at λ, if λ is an eigenvalue. The *stiffness* problem associate with this version of the Evans function is eliminated by the following change of variable:

$$\phi(\eta,\lambda) = \begin{pmatrix} \exp(-\rho_k\eta)I_2 & 0 \\ 0 & \exp(-\rho_l\eta)I_2 \end{pmatrix} Y, \tag{3.20}$$

where $k = 1, 3$, $l = 2, 4$ and I_2 is the 2×2 identity matrix. For $\phi(\eta,\lambda)$, we introduce the following initial value problems

$$\frac{d\phi}{d\eta} = \left\{ A - \begin{pmatrix} \rho_k I_2 & 0 \\ 0 & \rho_l I_2 \end{pmatrix} \right\} \phi,$$

$$\phi(\eta^-,\lambda) = y_i, \qquad i = 1,2 \qquad \text{and} \qquad \phi(\eta^+,\lambda) = y_j, \qquad j = 3,4, \tag{3.21}$$

where y_m $(m = 1, \cdots, 4)$ are defined in expressions (3.7)-(3.10). While in the forward integration we use $k = 1$ and $l = 2$, in the backward integration we use $k = 3$ and $l = 4$. After the four integration stages we have the data corresponding to $\phi_1^-(\eta)$ and $\phi_2^-(\eta,\lambda)$ in the range $[\eta^-, 0]$ and the data corresponding to $\phi_3^+(\eta)$ and $\phi_4^+(\eta,\lambda)$ in the range $[0, \eta^+]$. The vectors Y_1^-, Y_2^-, Y_3^+ and Y_4^+ in the appropriate ranges may be easily recovered by the use of (3.20). At an eigenvalue λ^*, the four vectors are linearly dependent, i.e., they satisfy (3.11)

$$a_1(\lambda^*)Y_1^-(\eta,\lambda^*) + a_2(\lambda^*)Y_2^-(\eta,\lambda^*) = a_3(\lambda^*)Y_3^+(\eta,\lambda^*) + a_4(\lambda^*)Y_4^+(\eta,\lambda^*).$$

The vector $a(\lambda^*) = \begin{pmatrix} a_1 & a_2 & -a_3 & -a_4 \end{pmatrix}^T_{\lambda^*}$ is the solution to

$$\mathcal{D}(\eta,\lambda^*)a = 0, \tag{3.22}$$

where $\mathcal{D}(\eta,\lambda^*)$ is the 4×4 matrix having $Y_1^-(\eta,\lambda^*)$, $Y_2^-(\eta,\lambda^*)$, $Y_3^+(\eta,\lambda^*)$ and $Y_4^+(\eta,\lambda^*)$ as columns. For practical purposes this matrix will be evaluated at $\eta = 0$. The eigenfunction components $u(\eta)$ and $v(\eta)$ corresponding to λ^* may be evaluated from the 1st and 3rd components of the above vectors as follows

$$\begin{aligned} u(\eta) &= a_1(\lambda^*)Y_{11}^-(\eta,\lambda^*) + a_2(\lambda^*)Y_{21}^-(\eta,\lambda^*), \\ v(\eta) &= a_1(\lambda^*)Y_{13}^-(\eta,\lambda^*) + a_2(\lambda^*)Y_{23}^-(\eta,\lambda^*) \qquad \text{for} \qquad \eta \in [\eta^-, 0], \end{aligned}$$

and

$$\begin{aligned} u(\eta) &= a_3(\lambda^*)Y_{31}^+(\eta,\lambda^*) + a_4(\lambda^*)Y_{41}^+(\eta,\lambda^*), \\ v(\eta) &= a_3(\lambda^*)Y_{33}^-(\eta,\lambda^*) + a_4(\lambda^*)Y_{43}^+(\eta,\lambda^*) \qquad \text{for} \qquad \eta \in [0, \eta^+]. \end{aligned}$$

To determine the vector $a(\lambda^*)$ we have used a singular value decomposition of $\mathcal{D}(0,\lambda^*)$, in which the matrix is factorised as

$$\mathcal{D} = QSP^H$$

where Q and P are 4×4 unitary matrices and S is a diagonal matrix with real non-negative diagonal elements which are called the singular values of $\mathcal{D}$. The superscript ^{H} stands for Hermitian transpose. Whenever λ^* is a simple eigenvalue, the matrix $\mathcal{D}(0, \lambda^*)$ has rank 3 with zero as one of its singular values. In practice this singular value is numerically negligible. In this case the solution to (3.22) is given by [72]

$$a = \alpha p_4,$$

where α is an arbitrary complex constant and p_4 is the column of P corresponding to the negligible element of S.

Following the above procedure and using the NAG routine F02XEF [79] to perform the singular value decomposition, we are able to find the eigenfunction components $u(\eta)$ and $v(\eta)$. Figure 3.6(a) shows the eigenfunction corresponding to the pair of eigenvalues $\lambda = \pm 0.57$ belonging to the spectrum of the stability equations for G with amplitude $\mu = 2.0$. Figure 3.6(b) shows the two eigenfunctions corresponding to the two pairs of nonzero eigenvalues within $(-\omega, \omega)$ for a solution of amplitude $\mu = 4.0$.

3.2 Evans function method applied to self-bending beams

The standard Evans function approach which we have used for the diffusionless photorefractive model cannot be applied when diffusion is present and the beam solutions propagate along curved paths. In the latter, the asymptotic forms of the stability equations are not second order constant coefficient differential equations. Nevertheless, by a suitable change of variables we may recognise a pair of Airy equations as the asymptotic system.

Let us first rewrite the operator L in terms of a new independent variable $\psi = \eta + B/a$, so that $F(\psi)$ is a solution of (2.24), so giving the following form

$$L = \begin{pmatrix} \partial_{\psi\psi} + a\psi + \gamma \dfrac{F^2}{1+F^2}\partial_\psi + r(\psi) & \gamma \dfrac{F^2}{1+F^2}\partial_\psi + s(\psi) \\ -\gamma \dfrac{F^2}{1+F^2}\partial_\psi - s(\psi) & -\partial_{\psi\psi} - a\psi - \gamma \dfrac{F^2}{1+F^2}\partial_\psi - r(\psi) \end{pmatrix}, \tag{3.23}$$

where $r(\psi)$ and $s(\psi)$ are defined through $F(\psi)$ and $F'(\psi)$ as in §2.4. As was discussed in §2.2.2 the solution $F(\psi)$ and its first derivative $F'(\psi)$ have rapid decay to zero in both directions away from the beam centre, then the asymptotic form of the operator L is given by

$$L_\infty = \begin{pmatrix} \partial_{\psi\psi} + a\psi - 1 & 0 \\ 0 & -\partial_{\psi\psi} - a\psi + 1 \end{pmatrix}.$$

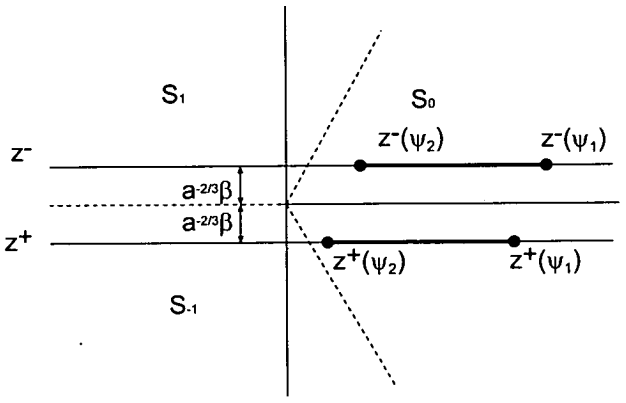

Figure 3.7: $z^{\pm}$ lines and profile domains $[z^{\pm}(\psi_2), z^{\pm}(\psi_1)]$ for $\lambda = \alpha - \beta i$, $\beta > 0$.

By performing the two following changes of independent variables:

$$z^+ = a^{-2/3}(-a\psi + 1 + \lambda),$$

$$z^- = a^{-2/3}(-a\psi + 1 - \lambda),$$

the asymptotic system transforms to the two Airy equations:

$$(\partial_{z^+z^+} - z^+)u = 0,$$

$$(\partial_{z^-z^-} - z^-)v = 0. \tag{3.24}$$

Before we proceed, it is useful to make some observations about how our search for eigenvalues of (3.23) should relate to the solutions of the pair of Airy equations (3.24). We note that the domain of ψ is $\mathbb{R}$, and the numerical integration range is only a real interval. This corresponds to horizontal lines (or segments of horizontal lines) in the complex plane which is the domain of z^+ and z^-. Changing the parameter λ corresponds to translating these two lines within the complex plane as sketched in Fig. 3.7.

For all real λ, the two lines lie within the real axis. The portions corresponding to $[z^{\pm}(\psi_2), z^{\pm}(\psi_1)]$ will be called the profile domains. The profile domains coincide for $\lambda = 0$ and are on the positive semi-axis but, as the modulus of λ increases, they move apart in opposite directions. We define two important sets of real λ:

(i). $Q_1 = \{\lambda \in \mathbb{R} : 0 \leq |\lambda| < \lambda_1\}$

For $\lambda \in Q_1$, the profile domains for z^+ and z^- are as sketched in Fig. 3.8(a), i.e., they remain on the positive semi-axis. Q_1 is the real interval of λ for which localised solutions to (3.23) are possible. They should match to the behaviour of Ai(z) to the left ($\psi - \psi^* < 0$, where ψ^* is the peak position) and to the behaviour of Bi(z) to the right ($\psi - \psi^* > 0$). Note that, although Ai(z) is also a bounded function (with algebraic decay) as $z \to -\infty$ ($\psi \to +\infty$), within and

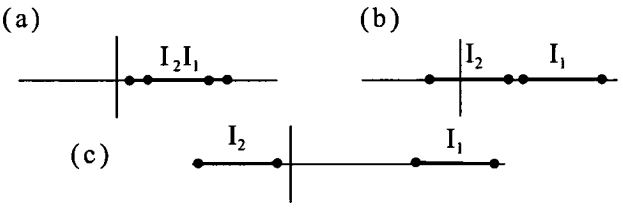

Figure 3.8: Location of profile domains for real λ

near the profile location it still grows to the left. The localised modes are then the intersection of the two-dimensional space (spanned by $\mathrm{Ai}(z^+)$ and $\mathrm{Ai}(z^-)$) at the left-hand side and the two-dimensional space (spanned by $\mathrm{Bi}(z^+)$ and $\mathrm{Bi}(z^-)$) at the right-hand side. Thus, the localised modes occur at discrete values of $\lambda \in Q_1$. One trivial example of a localised mode is $F(\psi)$ which corresponds to $\lambda = 0$. Moreover, as γ tends to zero, Q_1 should tend to the gap $(-\omega, \omega)$ of the diffusionless case. For sufficiently small γ, we show in a subsequent section that there are localised solutions of (3.23) within Q_1. They are the counterpart of the internal modes of the diffusionless case.

(ii). $Q_2 = \{\lambda \in \mathbb{R} : |\lambda| > \lambda_2 > 0, \lambda_2 \geq \lambda_1\}$

For $\lambda \in Q_2$, the profile domains lie as sketched in Fig. 3.8(c), i.e, one of the profile domains lies on the positive semi-axis and the other one lies on the negative semi-axis. Here, the bounded solution to (3.23) should match the exponential decay of $\mathrm{Ai}(z)$ at the left-hand side (as $\psi \to -\infty$) and the oscillatory algebraic decay at the right-hand side (as $\psi \to +\infty$). As these solutions have oscillatory behaviour at one hand side, they are analogous to the solutions in the continuous spectrum of the non-diffusive case and of other similar systems; that is, they are similar to radiation modes . Moreover, these solutions are the intersection of the two-dimensional space (spanned by $\mathrm{Ai}(z^+)$ and $\mathrm{Ai}(z^-)$) at the left-hand side and the three-dimensional space (spanned by $\mathrm{Bi}(z^+)$, $\mathrm{Bi}(z^-)$ and $\mathrm{Ai}(z^+)$ or $\mathrm{Ai}(z^-)$) at the right hand side. Thus, they exist for every $\lambda \in Q_2$.

For real λ such that $\lambda_1 < |\lambda| < \lambda_2$, the profile domains lie as sketched in Fig. 3.8(b). There, the solutions to (3.23) should be neither localised nor radiation-like solutions. Despite having distinguished two subsets of the real λ-domain by the properties of solutions existing in each of them, it is not yet clear to whether the whole real domain constitutes the continuous spectrum of the full problem (3.23), since for the asymptotic system $L_\infty(u \;\; v)^T = \lambda(u \;\; v)^T$, it constitutes the continuous spectrum.

For λ complex, the asymptotic behaviour of the solutions of (3.1) with L given by (3.23) matches the Airy functions away from the real axis. Those functions are briefly considered in Appendix A. We say that $\lambda \in \mathbb{C} \setminus \mathbb{R}$ is an eigenvalue

if, for that value, the system (3.1) with L given by (3.23) has a bounded and localised solution whose asymptotic behaviour as $|\psi| \to \infty$ matches the appropriate *recessive* Airy function of $|z^{\pm}| \to \infty$.

The recessive Airy function is different in different sectors of the z-plane (see Appendix A). Nevertheless there are regions of the λ-plane for which the extreme values of z^+ and z^- remain in a fixed sector as λ varies. When the calculations are made within such regions of the λ-plane, the appropriate recessive Airy functions are fixed. One of such region is the lower half-plane. The corresponding lines in the $z^{\pm}$-plane were illustrated in Fig. 3.7. As $\psi \to +\infty$ ($z^{\pm} \to -\infty$) Ai_{-1} is the appropriate asymptotic condition for u and Ai_1 for v. In the other extremum ($\psi \to -\infty$) both z^+ and z^- are in the S_0 sector and both u and v should match multiples of Ai_0.

Let us write the eigenvalue problem for the operator (3.23) as a first order system and follow an approach similar to that in §3.1 in order to obtain a definition of the Evans function. Using the change of variables $Y = \begin{pmatrix} u & u_\psi & v & v_\psi \end{pmatrix}^T$ we obtain

$$\frac{dY}{d\psi} = A(\psi, \lambda)Y, \tag{3.25}$$

where

$$A(\psi,\lambda) = \begin{pmatrix} 0 & 1 & 0 & 0 \\ -a\psi - r + \lambda & -\gamma F^2/(1+F^2) & -s & -\gamma F^2/(1+F^2) \\ 0 & 0 & 0 & 1 \\ -s & -\gamma F^2/(1+F^2) & -a\psi - r - \lambda & -\gamma F^2/(1+F^2) \end{pmatrix}. \tag{3.26}$$

This has the following asymptotic form

$$A_\infty(\psi,\lambda) = \begin{pmatrix} 0 & 1 & 0 & 0 \\ -a\psi + 1 + \lambda & 0 & 0 & 0 \\ 0 & 0 & 0 & 1 \\ 0 & 0 & -a\psi + 1 - \lambda & 0 \end{pmatrix}. \tag{3.27}$$

For $\lambda \in \{\lambda : \lambda = \alpha + \beta i, \beta < 0\}$, the asymptotic system has the following solutions:

$$\begin{aligned} Y_1^\infty(\psi,\lambda) &= \begin{pmatrix} \mathrm{Ai}_0(z^+) & -a^{1/3}\mathrm{Ai}_0'(z^+) & 0 & 0 \end{pmatrix}^T, \\ Y_2^\infty(\psi,\lambda) &= \begin{pmatrix} 0 & 0 & \mathrm{Ai}_0(z^-) & -a^{1/3}\mathrm{Ai}_0'(z^-) \end{pmatrix}^T, \\ Y_3^\infty(\psi,\lambda) &= \begin{pmatrix} \mathrm{Ai}_{-1}(z^+) & -a^{1/3}\mathrm{Ai}_{-1}'(z^+) & 0 & 0 \end{pmatrix}^T, \\ Y_4^\infty(\psi,\lambda) &= \begin{pmatrix} 0 & 0 & \mathrm{Ai}_1(z^-) & -a^{1/3}\mathrm{Ai}_1'(z^-) \end{pmatrix}^T. \end{aligned} \tag{3.28}$$

Much as in §3.1, we construct two bases to solutions of the full problem, say $\{Y_k^+\}$ and $\{Y_k^-\}$, for which the behaviours at $+\infty$ and $-\infty$ satisfy

$$Y_k^+(\psi,\lambda) \sim Y_k^\infty \qquad \text{as} \qquad \psi \to +\infty$$

and

$$Y_k^-(\psi,\lambda) \sim Y_k^\infty \qquad \text{as} \qquad \psi \to -\infty.$$

The required bounded solution which corresponds to the eigenvalue λ^* should be a linear combination of Y_1^- and Y_2^- and simultaneously a linear combination of Y_3^+ and Y_4^+. Hence, if λ^* is an eigenvalue then the identity

$$a_1(\lambda^*)Y_1^-(\psi,\lambda^*)+a_2(\lambda^*)Y_2^-(\psi,\lambda^*) = a_3(\lambda^*)Y_3^+(\psi,\lambda^*)+a_4(\lambda^*)Y_4^+(\psi,\lambda^*) \quad (3.29)$$

must be satisfied. The Wronskian of those four solutions given by

$$\tilde{D}(\psi,\lambda) = \begin{vmatrix} Y_{11}^-(\psi,\lambda) & Y_{21}^-(\psi,\lambda) & Y_{31}^+(\psi,\lambda) & Y_{41}^+(\psi,\lambda) \\ Y_{12}^-(\psi,\lambda) & Y_{22}^-(\psi,\lambda) & Y_{32}^+(\psi,\lambda) & Y_{42}^+(\psi,\lambda) \\ Y_{13}^-(\psi,\lambda) & Y_{23}^-(\psi,\lambda) & Y_{33}^+(\psi,\lambda) & Y_{43}^+(\psi,\lambda) \\ Y_{14}^-(\psi,\lambda) & Y_{24}^-(\psi,\lambda) & Y_{34}^+(\psi,\lambda) & Y_{44}^+(\psi,\lambda) \end{vmatrix} \quad (3.30)$$

should vanish at every ψ when (3.29) is satisfied. Note that for system (3.25), $\mathrm{Tr}(A(\psi,\lambda)) = -2\gamma F^2/(1+F^2)$ and thus $\tilde{D}(\psi,\lambda)$ is not independent of ψ. However, if the solutions are linearly dependent $\tilde{D}(\psi,\lambda)$ will vanish at every ψ. Let us define our modified Evans function as

$$D_{\mathrm{ai}}(\lambda) = \tilde{D}(\psi^*,\lambda), \quad (3.31)$$

where ψ^* denotes the peak location. In order that $D_{\mathrm{ai}}(\lambda)$ may be used as in §3.1, it must be an analytic function of λ. Then the work in searching for eigenvalues will be reduced by the use of the argument principle. The Airy functions are entire functions, i.e., functions that are analytic everywhere in $\mathbb{C}$, and the variables $z^\pm$ are analytic functions of λ. Hence, the initial conditions Y_k^∞ are analytic functions of λ. Moreover, we assume without proof that the solutions Y_i^+ $(i=1,2)$ and Y_j^- $(j=3,4)$ depend analytically on their initial conditions. The determinant is an algebraic operation, therefore $D_{\mathrm{ai}}(\lambda)$ is analytic in λ.

The main problem of this approach is restricting attention to a region of the λ-plane where the boundary conditions considered do have the required rapid decay. We have chosen the lower half-plane, but a similar approach could be used in the upper half-plane. We should only replace Ai_1 by Ai_{-1} and vice versa. However, we cannot cross the real axis in the λ-plane because the left-hand end of the lines in the $z^\pm$-plane would fall into a different sector and the boundary conditions would use a dominant Airy function instead of the recessive one.

3.2.1 Numerical results

Normal mode stability of the self-bending beams given by $F(\psi)$ means that the operator (3.23) has no eigenvalues with negative imaginary part, which, because

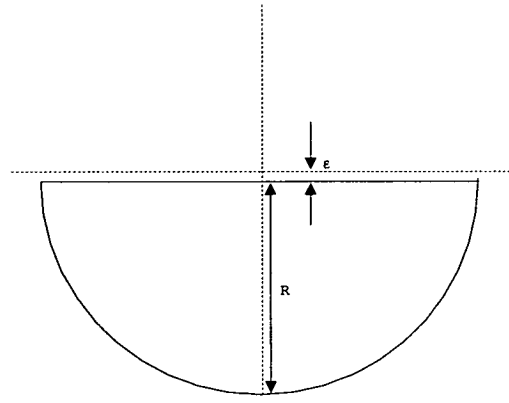

Figure 3.9: Path of evaluation of $D_{\rm ai}(\lambda)$

of the symmetry of the problem, is equivalent to saying that it has no complex eigenvalue. Our goal is to evaluate $D_{\rm ai}(\lambda)$ along a closed path that encloses all the lower half-plane of λ; however, numerically this is not reasonable. First, there are zeros of $D_{\rm ai}(\lambda)$ on the real axis, thus the evaluation path cannot coincide with the real axis but instead should be very close. The second difficulty is the chaotic behaviour presented by numerical approximation to $D_{\rm ai}(\lambda)$ for $|\lambda|$ large. Hence, we have performed calculations of $D_{\rm ai}(\lambda)$ along a semi-circle as in Fig. 3.9, where $\epsilon \sim 5 \times 10^{-5}$ and R (typically ~ 10) was chosen in order to avoid the mentioned chaotic behaviour.

The practical evaluation of $D_{\rm ai}(\lambda)$ implies the simultaneous integration (using NAG routine D02PCF) of (3.25) and (2.24) twice forward from ψ_1 to ψ^* and twice backward from ψ_2 to ψ^* ($\psi_1 < \psi_2$). The initial conditions for (2.24) were the ones obtained by the shooting method described in §2.2.2 and for (3.25) were Y_1^∞ and Y_2^∞ at $\psi = \psi_2$ for the backward integration and Y_3^∞ and Y_4^∞ at $\psi = \psi_1$ for the forward integration. The solutions obtained at ψ^* were used to evaluate the determinant (3.30). The determinant was found using the NAG routine F03ADF which applies a LU factorisation with partial pivoting [79]. The evaluation of the Airy functions at the specified point was done by the NAG routine S17DGF [79] which is based on the relations between the Airy functions and the modified Bessel function. As we performed calculations for relatively large $|\lambda|$, the quantities $\mathrm{Re}(z^{\pm})$ also are large and we necessarily used an option that returns the Airy values scaled by the factor $\mathrm{e}^{2z\sqrt{z}/3}$.

We have determined $D_{\rm ai}(\lambda)$ along the semi-circle for $\gamma = 0.05, 0.1, 0.15$ and 0.2 and for peak amplitudes $F_{\max} = 0.5, 1.0, 2.0$ and 4.0. In order to count the number of zeros we constructed a continuous function for the argument of $D_{\rm ai}(\lambda)$

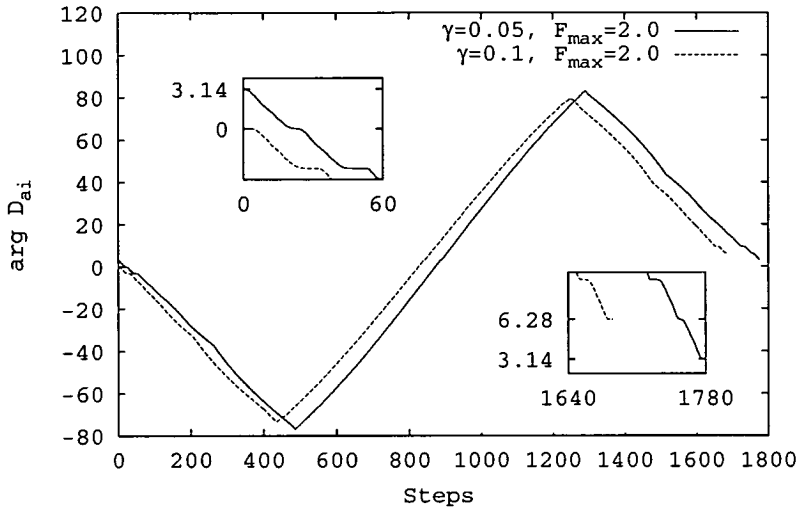

Figure 3.10: Argument of $D_{\rm ai}$ versus number of steps when λ takes values along the semi-circle of Fig. 3.9 with $R = 10.0$ and $\epsilon = 1.0 \times 10^{-5}$. The insets show the initial and final values of $\arg D_{\rm ai}$.

that is updated at each step of λ. The number of zeros is given by

$$n = \left| \frac{\arg D_{\rm ai}(\lambda_i) - \arg D_{\rm ai}(\lambda_f)}{2\pi} \right|,$$

where λ_i and λ_f are the initial and final λ-values, respectively. In a closed path as the semi-circle, λ_i coincides with λ_f.

In Fig. 3.10 the $\arg D_{\rm ai}$ is plotted against the number of steps obtained along the semi-circle of Fig. 3.9 for two solutions. For $\gamma = 0.05$ the change in $\arg D_{\rm ai}$ is zero, but for $\gamma = 0.1$ the change is 2π, corresponding to zero and one eigenvalues inside the semi-circle, respectively. In fact, our calculations showed three different situations: one pure imaginary, two complex or no zeros of $D_{\rm ai}(\lambda)$ inside the semi-circle. They were always near $\lambda = 0$ and the following results and considerations should assign them as numerical approximations to the zero eigenvalue.

In §2.6 we asserted that the eigenvalue $\lambda = 0$ has multiplicity four. Considering that $D_{\rm ai}$ recovers the multiplicity of an eigenvalue, it should be approximated by $D_{\rm ai}(\lambda) \sim a_4\lambda^4$ near $\lambda = 0$. The analysis of the behaviour of $D_{\rm ai}$ confirms this approximation. Fig. 3.11 show us that behaviour for $\gamma = 0.1$ and $F_{\rm max} = 2.0$ when λ takes values on real and imaginary segments including the origin. In those segments $D_{\rm ai}$ is real and the main characteristic of the curves coincides with that of λ^4 allowing for the fact that it has zeros not exactly at zero, but nearby. In this particular case, $D_{\rm ai}(\lambda)$ passes through zero at $\lambda = \pm 0.032$ and $\lambda = \pm 0.015i$ but as they fall in the region of λ^4-behaviour they should be taken as numerical deviations from the zero eigenvalue. The existence of two, one or no zeros of $D_{\rm ai}$ inside the semi-circle of Fig. 3.9 relates to the position of these numerical

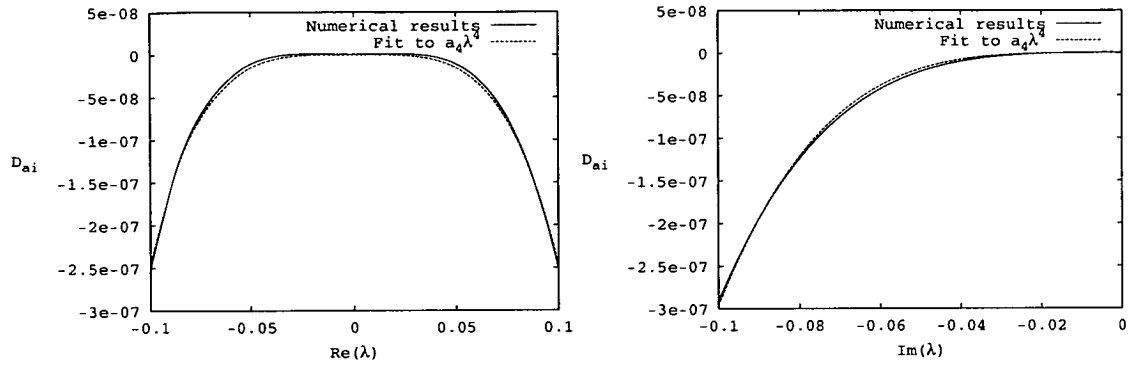

Figure 3.11: D_{ai} and its fitting to $a_4\lambda^4$ for $\gamma = 0.1$ and $F_{\max} = 2.0$ (a) real $\lambda \in (-0.1, 0.1)$ and (b) imaginary $\lambda \in (0, 0.1i)$.

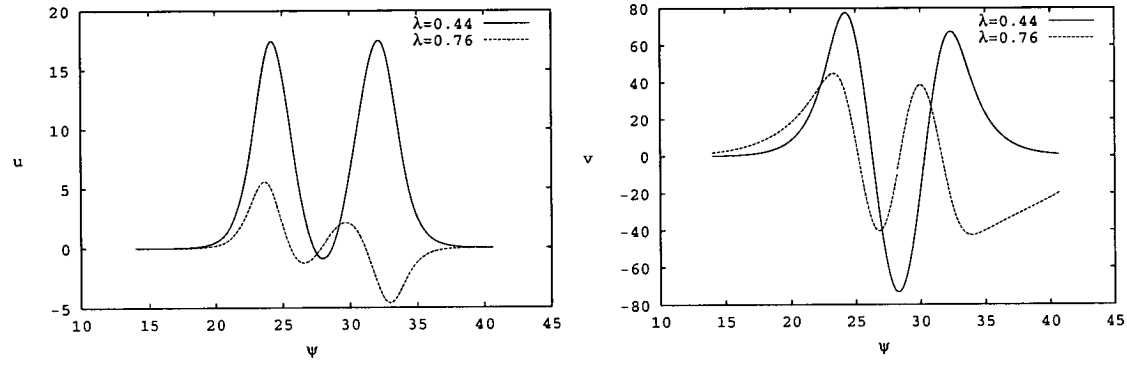

Figure 3.12: Eigenfunctions corresponding to $\lambda = \pm 0.76$ and $\lambda = \pm 0.44$ for a beam profile with amplitude $F_{\max} = 4.0$ and $\gamma = 0.03$.

deviations of the zero eigenvalue, respectively, a set of four complex ones, at least one imaginary pair or only a real pair.

In view of the observations on page 47, we have searched the real axis for possible localised modes. In fact, whenever they exist they correspond to $\lambda \in Q_1$. For γ small those solutions do exist for peak amplitudes greater than ~ 1.3 as in the diffusionless case. As γ increases and the peak amplitude is maintained, solutions similar to those localised solutions cease to exist. The explanation is that Q_1 narrows as γ increases. Let us take ψ_2 as our reference value in the right tail of $F(\psi)$. Note that $z^{\pm}(\psi_2)$ are the left-hand reference points in the $z^{\pm}$ profile domains. We may estimate λ_1 by $\lambda_1 \sim -a\psi_2 + 1$, where the latter was obtained by imposing $z^{\pm}(\psi_2) = 0$. The numerical estimates for λ_1 confirm that Q_1 is narrower for larger γ. An analytical confirmation reads as follows: ψ_2 is approximated by $\bar{\psi}_2 = \bar{\eta}_2 + B/a$ then $-a\psi_2 + 1 \sim -a\bar{\eta}_2 - B + 1$. As B is approximately constant for profiles of the same amplitude and a increases with γ, thus λ_1 should decrease with γ. As was also expected, λ_1 tends to the gap limit of the diffusionless case, $\omega = -B + 1$, as γ tends to zero.

Fig. 3.12 shows the localised eigenfunctions found for a beam profile with $F_{\max} = 4.0$ and $\gamma = 0.03$. They are similar to the ones presented in Fig. 3.6(b) for the rectilinear beams but with noticeable asymmetry. When γ is increased while $F_{\max}$ is maintained, these localised eigenfunctions cease to exist. For $\gamma = 0.1$, the only localised solution to (3.25) for λ nonzero occurs at $\lambda = \pm 0.43$ and, for $\gamma = 0.2$, there are no localised solutions to (3.25) apart from F at $\lambda = 0$. For even larger γ, we were unable to find a solution to the ODE defining F, suggesting that there is no localised solution.

3.3 Discretisation of the eigenvalue problem

This section describes experience with a straightforward numerical search for eigenvalues using a discretisation of the eigenvalue problem (3.1) on a truncated domain. We have used this procedure to search for eigenvalues for both kind of solutions (rectilinear for $\gamma = 0$ and self-bending for $\gamma \neq 0$). The eigenvalue problem (3.1) was first discretised using second-order finite differences and taking the boundary conditions at the ends of the truncated domain to be zero. We observe that the correct boundary conditions are the ones mentioned in sections §3.1 and §3.2, but those contain the eigenvalue that we are seeking, so that the problem is implicit. Although we were aware of the inaccuracy resulting from using the boundary conditions $u = v = 0$ at the ends of the numerical integration range, this was a first approach to searching for eigenvalues and is a complementary technique which is useful in the diffusive model for which the Evans function technique is not well defined for large $|\lambda|$. Our discretisation yields an algebraic matrix of dimension around 800×800. The eigenvalues of the matrix were obtained using a *Hessenberg QR* algorithm provided by the F02EBF routine of the NAG library [79] and confirmed by the *Implicitly Restarted Arnoldi* method provided by the ARPACK routines [73].

Let us first discuss the results for the rectilinear beams. The algorithm receives the algebraic matrix that results from the discretisation of (3.1) and gives a large set of eigenvalues (as large as the row-dimension of the matrix). Four of them are small in magnitude, around 100 times smaller than those next in order of magnitude. Those four consist of two purely real and two purely imaginary. Initially, we expected four eigenvalues numerically equal to zero, which would be consistent with the multiplicity four of $\lambda = 0$. The corresponding eigenfunctions are $(F \quad -F)^T$ and $(F' \quad F')^T$. Inspection of the eigenfunctions associated with the eigenvalues of smallest magnitude confirm that they are numerical deviations from the zero eigenvalue. To the pair of small real eigenvalues corresponds $(F \quad -F)^T$

and to the pair of small imaginary eigenvalues corresponds $(F' \quad F')^T$ plus a small imaginary contribution.

All the others eigenvalues occur as real symmetric pairs. They are easily recognised as internal modes if they are inside the gap $(-\omega, \omega)$ since their eigenfunctions are localised. The internal modes were also found in the same number and for approximately the same peak amplitudes as were found using the Evans function method. Apart from the four eigenvalues of small amplitude and apart from those corresponding to localised eigenfunctions, whenever they exist, the remaining eigenvalues were selected pairs of symmetric real values belonging to the continuous spectrum. They were selected by our choice of zero boundary conditions and by the numerical discretisation.

For the self-bending beams the results were similar. For all the solutions of (2.24) used, we have also found four eigenvalues of magnitude around 100 times smaller than those next in order of magnitude which were interpreted as numerical approximations to the four zero eigenvalues. For beams $F(\psi)$ having small amplitude, these four numerically determined eigenvalues form one pair of purely imaginary eigenvalues and one pair of purely real ones. For solutions of larger amplitude, they are instead a set of four complex eigenvalues (λ,$-\lambda$, λ^* and $-\lambda^*$). The transition occurs near, but not always exactly at, the maximum value of a (see Fig. 2.4).

All the other eigenvalues occur as real symmetric pairs. An inspection of the eigenvalues shows that the *internal modes* predicted by the Evans function method were also picked by this method. Hence, for approximately the same solutions $F(\psi; \gamma, N)$ as in the Evans function method, one or more nonzero eigenvalues (the next to $\lambda = 0$ approximations in order of magnitude) have corresponding eigenfunctions which are localised. All the others are non-localised.

The numerical evaluation of the stability eigenvalues also points to normal mode stability of the self-bending beams in the range of parameters studied (for $\gamma = 0.05 - 0.2$ and beam powers N up to ~ 75).

3.4 Direct numerical integration

Finally, to complete our stability analysis we used the obtained beam profiles as initial conditions for the evolution equation (2.11). We have used a pseudospectral method based on Fornberg and Whitham [35] which we describe briefly in Appendix B.

Let us first discuss the results concerning the rectilinear beams. Fig. 3.13 shows the propagation of $G(\eta)$ with peak amplitude $\mu = 1.0$ and $V \neq 0$. The

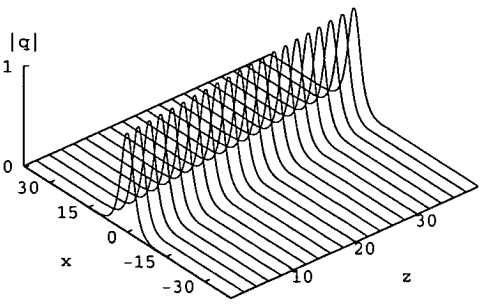

Figure 3.13: Numerical simulation of equation (2.11) with initial condition $q(0,x) = G(x)e^{i0.1x}$ for a peak amplitude $\mu = 1.0$.

propagation is steady and the peak position follows $x^p = x_0^p + 2Vz$ as was expected (x_0^p denotes initial peak position).

To confirm their stability we used as initial conditions the obtained beam profiles with additional small perturbations. We have used perturbations such as: sinusoidal disturbances, scaling of the beam profile or addition of a small multiple of its first derivative. Sinusoidal disturbances diffract rapidly so that the final output is the clean beam. Other perturbations cause readjustment of the beam shape and emission of radiation. However the consequent propagation is rather dependent on the existence of, or absence of internal modes. Thus, if we propagate a slightly perturbed beam profile for which the stability equations possess an internal mode, the amplitude oscillates along the propagation distance in a persistent way. If instead we perturb an equilibrium profile without internal modes and use it as initial condition the beam only adjusts to a nearby stationary shape, while emitting some radiation. This process is also accompanied by some amplitude oscillations, but these decay rapidly.

Fig. 3.14(a) shows the peak amplitude evolution when the input was an equilibrium profile with peak amplitude equal to 2.0 and scaled by 10%. The amplitude first decays corresponding to the initial shape adjustment of the beam and then oscillates steadily about a fixed value. The oscillation period is about 11.2 which is consistent with $2\pi/\lambda_i$ where λ_i is the eigenvalue of the internal mode for the average beam. These persistent oscillations are a common feature of the evolution of solitary solutions in nonintegrable generalised NLS's. The phenomenon is not observable in integrable models, whose only discrete eigenvalue is zero. They were observed in numerical simulations [99, 89] even before they were attributed to the excitation of internal modes [29, 2].

A qualitatively different evolution of the peak amplitude is illustrated in

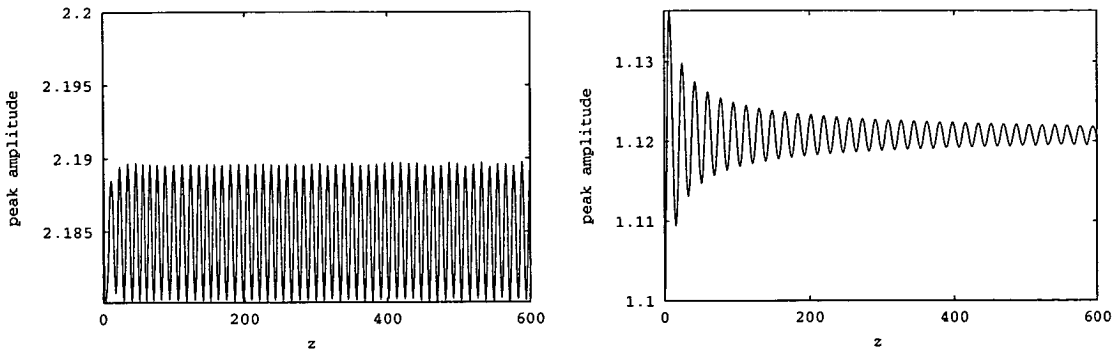

(a) (b)

Figure 3.14: Peak amplitude evolution when the input was $1.1 \times G(x)$ for (a) $\mu = 2.0$ and (b) $\mu = 1.0$.

Fig. 3.14(b). The initial beam was a solution of (2.17) with peak amplitude equal to 1.0 scaled by 10%. First the beam shape readjusts reaching a larger peak amplitude. Then the peak amplitude exhibits also an oscillation. However, in this case the oscillations are clearly being damped. The damping is confirmed as $\propto z^{-1/2}$ as happens for the NLS [66]. The oscillation period approaches the value 17.8 which is consistent with $2\pi/\lambda_{ce}$ where λ_{ce} is the eigenvalue of the edge of the continuous spectrum of the average beam, as also occurs for the NLS model [66].

The numerical simulations of the full evolution equation (2.11) also confirmed the stability of the self-bending beams. We have used the corresponding beam profiles as initial conditions in a way that spans the studied ranges of γ and peak amplitude. In all cases, we have observed steady propagation along the predicted parabolic trajectory. Fig. 3.4 shows the propagation for $\gamma = 0.1$ and $F_{max} = 1.0$. In Fig. 3.4 we note the exact coincidence between the peak trajectory and the curve $x_0^p - az^2$. Moreover, initial conditions composed of the beam profiles plus small perturbations, as used in the diffusionless case, produce stable propagation. Fig. 3.16 shows the propagation of an input beam perturbed by a sinusoidal disturbance up to a distance where the beam is already clean.

As for the diffusionless case, the propagation of perturbed beams reveals the existence or absence of localised modes in the stability spectrum. Thus, we may observe large persistent oscillations in the propagation of beams whose spectrum admits localised modes and smaller decaying oscillations otherwise. The frequency of the decaying oscillations is, in this case, coincident with the limit λ_2 of Q_2. This set was introduced on page 47 as the set of real λ for which the

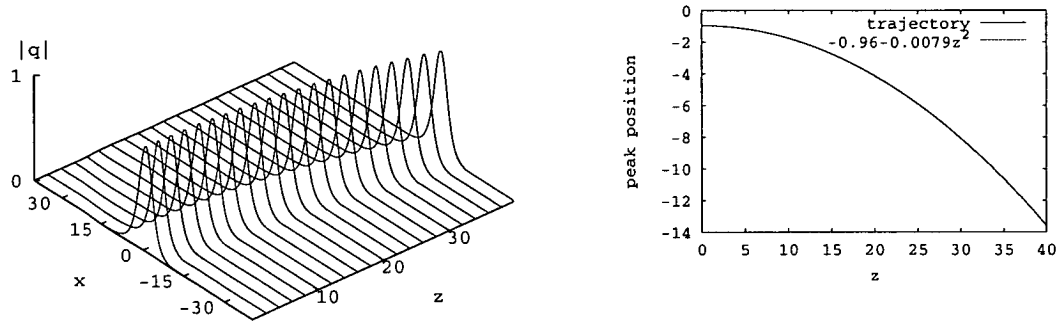

Figure 3.15: Beam propagation for $\gamma = 0.1$ and $F_{\max} = 1.0$. Trajectory of the peak position is coincident with the parabolic curve $-0.96 - 0.0079z^2$.

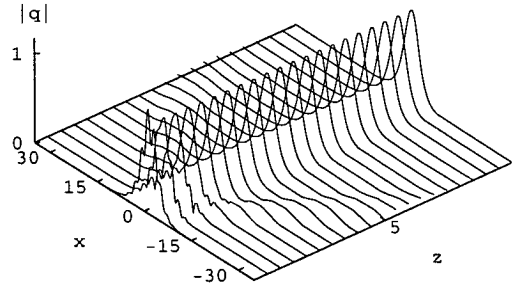

Figure 3.16: Propagation of $F(x) \times (1.0 + 0.2\cos(3x))$ for $F_{\max} = 1.0$ and $\gamma = 0.1$.

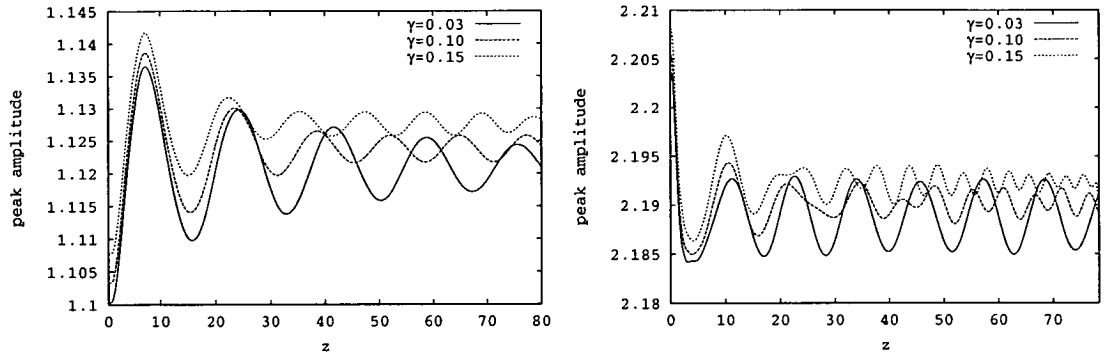

(a) (b)

Figure 3.17: Peak amplitude evolution for beams scaled by 10% concerning $\gamma = 0.03, 0.10, 0.15$ when (a) $F_{\max} \sim 1.0$ and (b) $F_{\max} \sim 2.0$.

solutions of (3.23) have more similarity with the solutions of the continuous spectrum in the diffusionless case. In that perspective, also the self-bending beams without *internal modes* relax, when perturbed, with amplitude oscillations whose frequency is equal to the lowest frequency of their radiation-like modes. Figure 3.17(a) shows the peak amplitude evolution for beams with $F_{\max} \sim 1.0$ scaled by 10% and with various values of γ. We recall that these profiles have no localised modes except the one corresponding to $\lambda = 0$. The frequency of the amplitude oscillations increases with increasing γ, as happens with λ_2. The limit λ_2 was estimated by $\lambda_2 \sim -a\psi_1 + 1$ (ψ_1 is in the left tail of the profile) following similar arguments as used to estimate λ_1. Furthermore, λ_2 tends also to ω as γ tends to zero. Fig. 3.17(a) shows also a noticeable decrease in the amplitude of the oscillation with increasing γ. The case $\gamma = 0.03$ of Fig. 3.17(b) shows long-lived oscillations whose frequency coincides with the eigenvalue of the localised mode. However, beams of similar peak amplitude but corresponding to larger diffusion parameter evolve accompanied by decaying oscillations. We have confirmed that the average beams of those latter cases have no localised modes other than the zero eigenmode. The frequency of the oscillations again increases with γ.

3.5 Conclusion

The two kinds of photorefractive soliton treated in this thesis were shown to be stable by the Evans function method, by a discretisation of the eigenvalue problem and by direct integration of the evolution equation. The Evans function method has permitted us to find internal modes that exist for both solutions above a threshold of peak amplitude. The existence of internal modes is well revealed by

direct integration of the full equation since perturbed self-similar profiles used as initial conditions evolve with persistent oscillations whose frequency is equal to the frequency of the internal mode. Note that although the self-bending solitons also admit internal modes above a threshold of amplitude, this threshold is usually higher for larger values of γ. Thus, any practical application for which these persistent oscillations are prejudicial yet larger curvature is not an impediment may benefit from larger values of diffusion.

We should stress that in the photorefractive case the change from the rectilinear regime to the parabolic regime does not affect the stability. Moreover, although the asymptotics of the stability eigenmodes change from exponential to Airy functions the general characteristics of the spectrum are preserved. In both situations we have radiation-like modes, zero modes and, in some cases, internal modes. However, the presence of diffusion and curvature changes some detailed characteristics, such as limit frequency of the radiation-like modes and amplitude threshold for internal modes.

Chapter 4

Sliding-frequency filter systems

Sliding-frequency filters were extensively studied in the early 90's as one of the techniques for implementing feasible soliton-based optical communications. The active research on such soliton based systems started with the successful experimental demonstration of soliton propagation in fibres in 1980 by Mollenauer *et al* [78]. This experiment was performed 7 years after the theoretical work of Hasegawa and Tappert [49] which demonstrated that the propagation of pulses in dispersive and weakly nonlinear fibres is modelled by the nonlinear Schrödinger equation plus higher order terms. Attenuation was the most important of those terms, making necessary the installation of amplifiers. Continuous amplification was first proposed using co-propagating radiation that would supply the necessary energy to the pulse stream in a process mediated by the medium through the Raman effect [44, 25]. However, erbium-doped fibre amplifiers (EDFA) regularly spaced along the fibre have been shown to be much more efficient. Even for this type of discrete amplification, it was proved that the NLS equation describes well the average pulse whenever the amplifier spacing is short compared to the dispersion length. This demonstration introduced a new concept of soliton, usually called the *guiding-centre soliton* [45, 46]. Unfortunately, amplification introduces spontaneous emission noise which in these nonlinear systems is particularly prejudicial. In fact, due to the nonlinearity, this noise changes the amplitude and frequency of the soliton. The change in frequency causes temporal displacements of the pulse in a mechanism called the *Gordon-Haus effect* [41]. To combat the Gordon-Haus effect, researchers proposed the use of frequency filters after each amplification stage [75]. The first systems used filters of fixed peak frequency but, only one year later sliding frequency filter systems were already preferred [77]. In the latter, the peak frequency was slightly shifted from one filter to the next along the fibre link. Systems using filters of fixed peak frequency require gain sufficient to overcome side-band losses experienced by the pulse. The excess gain, in turn, amplifies the unwanted noise. This process is avoided by using the

sliding-frequency filters which have been shown to guide the soliton but not the noise. Moreover, these systems have been shown to be efficient in suppressing the interaction between neighbouring solitons in a pulse stream which encodes the digital information [63].

4.1 The governing equation

As mentioned above, Hasegawa and Tappert derived the evolution equation for pulses travelling in a monomode fibre with dispersion and weak nonlinearity and, in the leading order approximation, arrived at the NLS equation. After the experimental demonstration in 1980 and subsequent intensive research on this topic, several authors have contributed to the derivation of governing equations that included higher order effects and control techniques. Here, following the approach of Agrawal and of Kodama and Hasegawa [4, 62], we present a rather simplified derivation of the governing equation of a system with amplification and sliding frequency filters.

The optical electric field $\mathbf{E}$ propagates along the fibre in accordance with the following wave equation

$$\nabla^2\mathbf{E} - \frac{1}{c^2}\frac{\partial^2\mathbf{E}}{\partial t^2} = \mu_0\frac{\partial^2\mathbf{P}}{\partial t^2}, \tag{4.1}$$

where $\mathbf{P}$ is the induced polarisation vector, c is the vacuum light speed and μ_0 is the vacuum permeability. This wave equation is valid under the assumption that the spatial dependence of the index of refraction is small. Whenever the optical frequency is away from any medium resonance, the induced polarisation may be expressed as a power series expansion in the electric field. Thus, up to third order, the j-component of the induced polarisation is related to the components of the electric field by

$$\begin{aligned} P_j(\mathbf{r},t) = \epsilon_0 \int_{-\infty}^{\infty} \chi^{(1)}_{jk}(t-\tau)E_k(\tau)d\tau + \\ + \epsilon_0 \int_{-\infty}^{\infty} \chi^{(3)}_{jklm}(t-\tau_1, t-\tau_2, t-\tau_3)E_k(\tau_1)E_l(\tau_2)E_m(\tau_3)d\tau_1 d\tau_2 d\tau_3, \end{aligned} \tag{4.2}$$

where summation convention over repeated indices is implied. In this expression, ϵ_0 is the vacuum permittivity and $\chi^{(1)}_{jk}$ and $\chi^{(3)}_{jklm}$ are the components of the first and third order susceptibility tensors, respectively. The second order susceptibility, $\chi^{(2)}$, was not considered since this is identically zero in centrosymmetric and isotropic media such as the fibre material. The first term is linear in $\mathbf{E}$ and the second is nonlinear. They will be denoted by P^L_j and P^{NL}_j respectively. We will treat the nonlinear term as a small perturbation to the linear term. The nonlinear

response is often considered instantaneous, which is valid for pulse widths larger than 1ps, consequently, the time dependence of $\chi^{(3)}_{jklm}$ is given by the product of three delta functions of the form $\delta(t-\tau)$. Thus, the nonlinear part of P_j is given by

$$P_j^{NL} = \epsilon_0 \chi^{(3)}_{jklm} E_k E_l E_m.$$

In making the last approximation we are removing the intrapulse Raman scattering from the model.

Two other main assumptions are considered: the optical field is assumed to maintain its polarisation, which permits a scalar approach, and is assumed to be quasi-monochromatic, i.e, its spectral width is much smaller than the carrier frequency. Let us then consider an optical field linearly polarised in the x-direction, written under the slowly varying envelope approximation, as

$$\mathbf{E}(\mathbf{r},t) = \frac{1}{2}\hat{\mathbf{x}}\left[E(\mathbf{r},t)\exp(ik_0 z - i\omega_0 t) + \text{c.c.}\right], \tag{4.3}$$

where $\hat{\mathbf{x}}$ is a unit vector along Ox, $E(\mathbf{r},t)$ is a slowly varying function of time and z, ω_0 is the carrier frequency, k_0 is the wavenumber at $\omega = \omega_0$ and c.c. denotes the complex conjugate. Introducing (4.3) into (4.2), we obtain the following expression for the linear part of the induced polarisation (4.2)

$$\mathbf{P}^{\text{L}}(\mathbf{r},t) = \frac{\epsilon_0}{2}\hat{\mathbf{x}}\int_{-\infty}^{\infty}\chi^{(1)}_{11}(t-\tau)\left[E(\mathbf{r},\tau)\exp(ik_0 z - i\omega_0\tau) + \text{c.c.}\right]d\tau,$$

and two terms for the nonlinear part of the polarisation; one oscillating at ω_0 and the other oscillating at the third harmonic $3\omega_0$. Unless special care is taken to permit phase-matching, the latter term may be neglected. Hence, generically, the nonlinear polarisation is approximated by

$$\mathbf{P}^{\text{NL}}(\mathbf{r},t) = \frac{\epsilon_0}{2}\hat{\mathbf{x}}\epsilon_{\text{NL}}\left[E(\mathbf{r},t)\exp(ik_0 z - i\omega_0 t) + \text{c.c.}\right], \tag{4.4}$$

where $\epsilon_{\text{NL}} = \frac{3}{4}\chi^{(3)}_{1111}|E(\mathbf{r},t)|^2$. Temporarily, we consider ϵ_{NL} as independent of z and t. Under this assumption, the wave equation is linear and may be treated in the Fourier domain where it takes the following form

$$2ik_0\frac{\partial\tilde{E}}{\partial z} - k_0^2\tilde{E} + \nabla^2\tilde{E}(\mathbf{r},\omega-\omega_0) + \frac{\omega^2}{c^2}\epsilon(\omega,x,y)\tilde{E}(\mathbf{r},\omega-\omega_0) = 0, \tag{4.5}$$

where the dielectric constant is given by $\epsilon(\omega,|E|^2) = 1 + \tilde{\chi}^{(1)}_{11}(\omega) + \epsilon_{\text{NL}}$, and is temporarily assumed to vary only with frequency and transverse coordinates x and y, i.e., $\epsilon(\omega,|E|^2) \equiv \epsilon(\omega,x,y)$. $\tilde{E}(\mathbf{r},\omega-\omega_0)$ and $\tilde{\chi}^{(1)}_{11}(\omega)$ are the Fourier transforms of $E(\mathbf{r},t)$ around ω_0 and $\chi^{(1)}_{11}$ around $\omega = 0$, respectively. They are given by

$$\tilde{E}(\mathbf{r},\omega-\omega_0) = \int_{-\infty}^{\infty}E(\mathbf{r},t)\exp[i(\omega-\omega_0)t]dt,$$

$$\tilde{\chi}_{11}^{(1)}(\omega) = \int_{-\infty}^{\infty} \chi_{11}^{(1)}(t) \exp(i\omega t) dt.$$

Let us regard the field $\tilde{E}$ as composed of a transverse modal distribution $F(x, y)$ modulated by a complex amplitude function $\tilde{A}(z, \omega - \omega_0)$, i.e,

$$\tilde{E}(\mathbf{r}, \omega - \omega_0) = F(x, y)\tilde{A}(z, \omega - \omega_0).$$

Introducing the above *ansatz* into (4.5), we obtain an equation for $F(x, y)$:

$$\frac{\partial^2 F}{\partial x^2} + \frac{\partial^2 F}{\partial y^2} + \left[\epsilon(\omega, x, y)\frac{\omega^2}{c^2} - k^2\right] F = 0, \tag{4.6}$$

and an equation for the envelope function $\tilde{A}$ which, under the assumption of slow modulation so that the second derivative of $\tilde{A}$ with respect to z is negligibly small, may be written as

$$2ik_0\frac{\partial \tilde{A}}{\partial z} + (k^2 - k_0^2)\tilde{A} = 0. \tag{4.7}$$

Equation (4.6) with suitable boundary conditions for the fibre geometry is an eigenvalue problem with k^2 as the eigenvalue.

Let us now re-introduce the full dependence of the dielectric constant. This may be written as a sum of three terms

$$\epsilon(\omega, |E|^2) = \left(1 + \mathrm{Re}[\tilde{\chi}_{11}^{(1)}(\omega)]\right) + i\mathrm{Im}[\tilde{\chi}_{11}^{(1)}] + \frac{3}{4}\tilde{\chi}_{1111}^{(3)}|E|^2.$$

which may be then related to the macroscopic quantities, namely, linear refractive index $n(\omega)$, absorption coefficient α, and nonlinear index coefficient n_2 (also known as the Kerr coefficient), using

$$\epsilon(\omega, |E|^2) = \left(n(\omega) + \frac{i\alpha c}{2\omega_0} + n_2|E|^2\right)^2 \simeq n^2(\omega) + 2n(\omega)\left(\frac{i\alpha c}{2\omega_0} + n_2|E|^2\right).$$

In the last approximation, we have assumed that the absorption and nonlinear terms are small compared with the linear refractive index. The imaginary part of $\tilde{\chi}_{1111}^{(3)}$ is usually negligible, so we have

$$n(\omega) = \sqrt{1 + \mathrm{Re}[\tilde{\chi}_{11}^{(1)}(\omega)]}, \qquad \alpha = \frac{\omega_0}{nc}\mathrm{Im}[\tilde{\chi}_{11}^{(1)}(\omega_0)], \qquad n_2 = \frac{3}{8n}\tilde{\chi}_{1111}^{(3)}$$

where the frequency dependence of $\mathrm{Im}[\tilde{\chi}_{11}^{(1)}]$ is also neglected.

The equation (4.6) may be solved iteratively, first replacing $\epsilon(\omega, |E|^2)$ by $n^2(\omega)$ and then introducing the absorption and the nonlinear terms. After iteration, the eigenvalue k will be found as a function of the frequency ω and of the envelope intensity $|A|^2$;

$$k \equiv k_r(\omega, |A|^2) + ik_i$$

with the contribution from the modal distribution $F(x,y)$ buried inside the function $k_r(\omega,|A|^2)$. Remembering the assumption of quasi-monochromaticity and of small nonlinear effect, we write k_r in a Taylor expansion around the carrier frequency ω_0 and zero amplitude, yielding

$$k = k_0 + (\omega-\omega_0)k'_{r0} + \frac{1}{2}(\omega-\omega_0)^2 k''_{r0} + \cdots + \frac{\partial k_r}{\partial|A|^2}|A|^2 + \cdots + ik_i, \qquad (4.8)$$

where k'_{r0} and k''_{r0} are the first and second derivatives of $k_r(\omega,|A|^2)$ with respect to ω evaluated at ω_0. They depend on the material dispersion but also on the modal distribution. The other coefficients in the expansion may be shown to relate to macroscopic quantities in such a way that [4]

$$\frac{\partial k_r}{\partial|A|^2} = \frac{\omega_0 n_2}{cA_{\text{eff}}}, \qquad k_i = \frac{\alpha}{2},$$

where A_{eff} is known as the effective core area of the fibre and is given by

$$A_{\text{eff}} = \frac{\left(\int|F(x,y)|^2dxdy\right)^2}{\int|F(x,y)|^4dxdy}. \qquad (4.9)$$

Using the approximation $k^2-k_0^2 \simeq 2k_0(k-k_0)$, equation (4.7) reads as

$$\frac{\partial\tilde{A}}{\partial z} = i[k-k_0]\tilde{A}. \qquad (4.10)$$

Then, introducing the expansion (4.8) and definitions (4.9) into (4.10) yields

$$\frac{\partial\tilde{A}}{\partial z} = i\left[(\omega-\omega_0)k'_{r0} + \frac{1}{2}(\omega-\omega_0)^2k''_{r0} + i\frac{\alpha}{2} + \frac{\omega_0 n_2}{cA_{\text{eff}}}|A|^2\right]\tilde{A}. \qquad (4.11)$$

This equation, when inverted, yields the NLS equation plus an absorption term. The effects of amplifiers and filters have yet to be included. The gain provided by the discrete amplifiers is treated by introducing an average gain g and the distributed spectral response of a Fabry-Perot filter is taken as [63]

$$h(\omega-\omega_f) = -\ln\left(1+\frac{2i(\omega-\omega_f)}{B}\right) \simeq -\frac{2i}{B}(\omega-\omega_f) - \frac{2}{B^2}(\omega-\omega_f)^2,$$

where B is the filter bandwidth and ω_f is its peak frequency. Allowing ω_f to depend on z in the form $\omega_f \equiv \omega_f(z) = \omega_0 + \Omega(z) = \omega_0 + \Omega' z$ with Ω' constant, including these two terms acting on $\tilde{A}$ into equation (4.11) and taking the inverse Fourier transform, we obtain the following equation for the the envelope function $A(z,t)$;

$$\frac{\partial A}{\partial z} + \left(k'_{r0} - \frac{2}{B}\right)\frac{\partial A}{\partial t} + i\frac{k''_{r0}}{2}\frac{\partial^2 A}{\partial t^2} - i\frac{\omega_0 n_2}{cA_{\text{eff}}}|A|^2A = \\ -\frac{\alpha}{2}A + gA + i\frac{2\Omega}{B}A + \frac{2}{B^2}\left(\frac{\partial}{\partial t} + i\Omega(z)\right)^2 A.$$

The term $\partial A/\partial t$ may be removed by the Galilean transformation $\tau = t - (k'_{r0} - 2/B)z$, which yields

$$\frac{\partial A}{\partial z} + i\frac{k''_{r0}}{2}\frac{\partial^2 A}{\partial \tau^2} - i\frac{\omega_0 n_2}{cA_{\text{eff}}}|A|^2 A = -\frac{\alpha}{2}A + gA + i\frac{2\Omega}{B}A + \frac{2}{B^2}\left(\frac{\partial}{\partial \tau} + i\Omega(z)\right)^2 A.$$

After the normalisation

$$A = \sqrt{\frac{cA_{\text{eff}}}{\omega_0 n_2 z_0}}\exp(i\frac{\Omega' z_0 z^2}{B})q, \qquad Z = \frac{z}{z_0}, \qquad T = \frac{\tau}{\tau_0},$$

where $z_0 = \tau_0^2/|k''_{r0}|$ and τ_0 is the pulse width, the equation takes the final form

$$iq_Z + \frac{1}{2}q_{TT} + |q|^2 q = i\delta q + i\beta\left\{\partial_T + i\sigma Z\right\}^2 q, \tag{4.12}$$

where $\delta = (g - \alpha/2)z_0$ is the excess gain, $\beta = 2/(B^2|k''_0|)$ and $\sigma = \tau_0^3\Omega'/|k''_0|$. We have assumed that k''_0 is negative, the situation for which the NLS equation admits bright solitons. Note that, as was mentioned in the introduction, the amplification and filtering occur at discrete locations but the *guiding centre* theory predicts that the average pulse satisfies equation (4.12), with the coefficients g and β resulting from averaging the physical parameters over the amplifier spacing [63].

Pulse propagation governed by equation (4.12) has been mostly studied using perturbation methods. Several perturbation approaches have been developed to study soliton propagation governed by perturbed NLS equations [58, 57, 9, 61]. In some of them, the shape of the NLS soliton is assumed to remain constant while the soliton parameters evolve with propagation distance. Let us, briefly, show the results of one of these perturbation methods, the adiabatic approach of the perturbed inverse scattering method [57], applied to the sliding frequency filter model. Consider first the new variable

$$u(Z,\xi) = q(Z,T)\exp\left(i\sigma ZT + i\frac{\sigma^2 Z^3}{3}\right),$$

with $\xi = T + \sigma Z^2/2$, which satisfies the equation

$$u_Z - \frac{i}{2}u_{\xi\xi} - i|u|^2 u = -i\sigma\xi u + \delta u + \beta u_{\xi\xi}.$$

The left-hand side of the equation is the NLS equation. Considering the terms on the right-hand side as small perturbations to the NLS equation, the adiabatic approximation for u is written as a one-soliton solution with parameters allowed to depend on Z and given by

$$u(Z,\xi) = \mu(Z)\text{sech}[\mu(Z)(\xi - \xi_0(Z))]\exp[-i\kappa(Z)\xi + i\phi_0(Z)],$$

where $\mu(Z)$, $\kappa(Z)$, $\xi_0(Z)$ and $\phi_0(Z)$ are the amplitude, frequency or velocity, peak position and phase, respectively. The perturbation approach gives the following differential equations for the four parameters

$$\frac{d\mu}{dZ} = 2\delta\mu - 2\beta\mu\left(\frac{\mu^2}{3} + \kappa^2\right), \tag{4.13}$$

$$\frac{d\kappa}{dZ} = -\sigma - \frac{4}{3}\beta\mu^2\kappa, \tag{4.14}$$

$$\frac{d\xi_0}{dZ} = -\kappa, \tag{4.15}$$

$$\frac{d\phi_0}{dZ} = \frac{1}{2}(\mu^2 - \kappa^2) + \xi_0\frac{d\kappa}{dZ} - \sigma\xi_0. \tag{4.16}$$

Setting equations (4.13) and (4.14) equal to zero, we found that the equilibrium states with $\mu \neq 0$ have frequencies, κ, given by the negative solutions to the following cubic equation

$$4\beta\kappa^3 - 4\delta\kappa - \sigma = 0. \tag{4.17}$$

The amplitudes are related to the frequencies by $\mu^2 = -3\sigma/4\beta\kappa$. These negative roots exist below a critical sliding rate given by

$$\sigma_c = \frac{8\delta}{3}\sqrt{\frac{\delta}{3\beta}}.$$

Thus, if $|\sigma| < \sigma_c$ there are two equilibrium states, if $|\sigma| = \sigma_c$ there is one and if $|\sigma| > \sigma_c$ there are none. Further stability analysis shows that, for the case $|\sigma| < \sigma_c$, the equilibrium state of larger amplitude and smaller absolute frequency is stable while the other is unstable [63, 17] . Let us denote the equilibrium amplitude and velocity by μ_e and κ_e, respectively. In an equilibrium situation, the peak position and phase may be deduced by integration of equations (4.15) and (4.16) and are given by

$$\xi_0 = -\kappa_e Z + \xi_{0i}, \qquad \phi_0 = \frac{1}{2}(\mu_e^2 - \kappa_e^2)Z - \frac{1}{2}\sigma\kappa_e Z^2 + \sigma\xi_{0i}Z + \phi_{0i},$$

where ξ_{0i} and ϕ_{0i} are the respective initial values. Thus the perturbation approach predicts a steady pulse of the form

$$\begin{aligned} q(Z,T) = {} & \mu_e \mathrm{sech}[\mu_e(T + \kappa_e Z - \tfrac{1}{2}\sigma Z^2 - \xi_{0i})] \times \\ & \exp[-i\kappa_e T - i\sigma ZT + \tfrac{i}{2}(\mu_e^2 - \kappa^2 - 2\sigma\xi_{0i})Z - i\sigma\kappa_e Z^2 - \tfrac{i}{3}\sigma^2 Z^3 + i\phi_{0i}]. \end{aligned} \tag{4.18}$$

The results of this perturbation technique suggests that equation (4.12) admits self-similar accelerating solutions, as will be investigated in the next section. After the accelerating solutions are found, we will treat their stability eigenvalue problem by making use of an Evans function similar to that defined for the self-bending photorefractive solutions. Finally, the stability results will be verified by direct integration of the evolution equation.

4.2 Equilibrium solutions

Following the pattern of §2.2 and the previous section, we seek the accelerating pulse solutions for (4.12) by introducing the *ansatz* given by

$$q(Z,T) = F(\zeta)\mathrm{e}^{i\theta(Z,\zeta)}, \tag{4.19}$$

where the similarity variable is $\zeta = T + aZ^2 + bZ$ (with a and b constants) and $F(\zeta)$ is a real function [83]. Inserting (4.19) into (4.12) yields

$$\frac{1}{2}F'' + (2\beta\theta_\zeta + 2\beta\sigma Z)F' + \left\{-\theta_Z - \theta_\zeta(2aZ+b) - \frac{\theta_\zeta^2}{2} + \beta\theta_{\zeta\zeta} + F^2\right\}F + i\left\{-\beta F'' + (2aZ + b + \theta_\zeta)F' + \left(\frac{\theta_{\zeta\zeta}}{2} + \beta\theta_\zeta^2 + 2\beta\sigma Z\theta_\zeta + \beta\sigma^2Z^2 - \delta\right)F\right\} = 0. \tag{4.20}$$

The real and imaginary coefficients of the ordinary differential equation for F should be independent of Z. Imposing the above condition on the real and imaginary coefficients of F' we obtain $a = \sigma/2$ and a primordial form for the phase given by

$$\theta(Z,\zeta) = -\sigma Z\zeta + Y(\zeta) + X(Z).$$

Inserting the derivatives $\theta_Z = -\sigma\zeta + X'(Z)$, $\theta_\zeta = -\sigma Z + Y'(\zeta)$ and $\theta_{\zeta\zeta} = Y''(\zeta)$ into the coefficient of F, we obtain an imaginary part independent of Z and, imposing the same condition on the real part yields the following form for $X(Z)$;

$$X(Z) = \sigma^2\frac{Z^3}{6} + b\sigma\frac{Z^2}{2} + c_0Z + c_1. \tag{4.21}$$

The function $Y(\zeta)$ remains undefined, which motivates that we, instead, search for a complex function $W(\zeta) = F(\zeta)\mathrm{e}^{iY(\zeta)}$. In fact the equation (4.20) may be now rewritten as

$$(1+4\beta^2)\left\{F'' + i(Y''F + 2Y'F') - (Y')^2F\right\} + 2(1+2i\beta)\left\{ib(F' + iY'F) + (\sigma\zeta - c_0 - i\delta + F^2)F\right\} = 0, \tag{4.22}$$

which is easily recognised as an ODE for the function $W(\zeta)$. Therefore, let us refine our *ansatz* as

$$q(Z,T) = \mathrm{e}^{i\Theta(Z,\zeta)}[\sigma^2(1+4\beta^2)]^{1/6}w(y), \tag{4.23}$$

where $\Theta(Z,\zeta)$ is the known part of the phase θ, namely

$$\Theta(Z,\zeta) = (c_0 - \sigma\zeta)Z + b\sigma\frac{Z^2}{2} + \sigma^2\frac{Z^3}{6} + c_1. \tag{4.24}$$

The function $w(y)$ is a rescaled version of the complex function $W(\zeta)$, given by $w(y) = [\sigma^2(1+4\beta^2)]^{-1/6}W(\zeta)$ and y results from the transformation $(\sigma\zeta - c_0) = [\sigma^2(1+4\beta^2)]^{1/3}y$. The ordinary differential equation for $w(y)$ is easily obtained using (4.22) and reads as

$$w'' + 2(1+2i\beta)\left\{iBw' + (y - i\Delta + |w|^2)w\right\} = 0, \tag{4.25}$$

where $B = [\sigma^{1/2}(1+4\beta^2)]^{-2/3}b$ and $\Delta = [\sigma^2(1+4\beta^2)]^{-1/3}\delta$. We should note that we have reduced the number of real parameters in the ODE from three occurring in the evolution equation to two occurring in (4.25), which was possible because σ and δ appear only in the form $\sigma^{-2/3}\delta$.

For the accelerating pulses (4.23) to exist, equation (4.25) should admit solutions for which w and w' tend to zero in both directions (i.e., $y \to \pm\infty$). The numerical algorithm to find such solutions is based on a perturbation around the NLS solution and uses initial conditions based on the Airy function asymptotics of (4.25) as $|w| \to 0$. Let us first find estimates for the velocity parameter B and the location of the peak $y = y_p$ using a perturbation around a sech function. Introducing the substitutions $w = \mathrm{e}^{-iBy}\chi(\xi)$ and $\xi = y - y_p$ into the equation (4.25), we obtain

$$\chi'' - \Gamma^2\chi + 2|\chi|^2\chi = \mathcal{F}(\chi, \chi^*, \chi', \xi), \tag{4.26}$$

where

$$\mathcal{F}(\chi, \chi^*, \chi', \xi) = 4\beta B\chi' - 2i(2\beta B^2 + 2\beta y_p - \Delta)\chi - 2(1+2i\beta)\xi\chi - 4i\beta|\chi|^2\chi,$$

and

$$\Gamma^2 = -B^2 - 2y_p. \tag{4.27}$$

When β and Δ are small and 2ξ is small compared to Γ^2 the right-hand side of equation (4.26) may be neglected and the solution should be approximately equal to $\chi(\xi) = \Gamma\mathrm{sech}(\Gamma\xi)$. Let $\bar{y_p}$, $\bar{B}$ and $\bar{\Gamma}$ be the first estimates for y_p, B and amplitude Γ, respectively. Following [83], it is possible to use integral equalities satisfied by the solutions $\chi(\xi)$ that, up to first order in β and Δ, give us the following equations

$$\frac{4}{3}\bar{B}\bar{\Gamma}^2\beta + 1 = 0 \qquad \text{and} \qquad \bar{B}^2 + \frac{1}{3}\bar{\Gamma}^2 = \beta^{-1}\Delta. \tag{4.28}$$

The first equation implies that, for positive filtering strength β, the velocity $\bar{B}$ should be negative. Finally, the above equations give a cubic equation for $\bar{B}$:

$$4\beta\bar{B}^3 - 4\Delta\bar{B} - 1 = 0. \tag{4.29}$$

We should note that this cubic equation for $\bar{B}$ is similar to the cubic equation for κ obtained in page 66 using the perturbation technique. Thus, similarly, this

equation has negative roots only for $\Delta\beta^{-1/3} \geq \frac{3}{4}$; one when the equality is satisfied and two in the general case. Once we have found the two possible estimates $\bar{B}_i$ $(i = 1, 2)$, we may obtain an estimate for the amplitude $\bar{\Gamma}$ using (4.28) and an estimate for the peak location y_p using (4.27).

As for the photorefractive model, the appropriate boundary conditions may be given by Airy functions. In fact, linearisation of equation (4.25) gives

$$w'' + 2(1 + 2i\beta)\{iBw' + (y - i\Delta)w\} = 0 \tag{4.30}$$

to which we may apply a dependent variable transformation given by

$$w(y) = \mathcal{W}(y)\exp[-iB(1 + 2i\beta)y], \tag{4.31}$$

so obtaining a differential equation for $\mathcal{W}(y)$ without the first derivative, namely

$$\mathcal{W}'' + \left\{(1 + 2i\beta)^2B^2 + 2(1 + 2i\beta)(y - i\Delta)\right\}\mathcal{W} = 0. \tag{4.32}$$

This equation may, now, be transformed to an Airy equation $\mathcal{W}'' - z\mathcal{W} = 0$ by the change of variable

$$z(y) = (2 + 4i\beta)^{1/3}\left\{-y + i\Delta - (1 + 2i\beta)\frac{B^2}{2}\right\}. \tag{4.33}$$

The transformation (4.33) maps the real independent variable y to the complex-valued variable z. It consists of a translation and a rotation of $\phi = [\arg(2+4i\beta)]/3$, if we consider the principal branch of the cubic root appearing in expression (4.33). Therefore, the real domain for y is mapped into an oblique line in the complex z-plane. This line crosses the real axis at $(4 + 16\beta^2)^{1/6}(\Delta - \beta B^2)/\sin\phi$ and its slope is ϕ (which is small compared to $\pi/3$), hence, the large positive and negative values of y correspond to lines in the sectors S_{-1} and S_0 of the z-plane (see Appendix A). The suitable initial conditions for a pulse-like solution to equation (4.32) are multiples of the values of $\mathrm{Ai}_0(z)$ and $\mathrm{Ai}_{-1}(z)$ at the appropriate z values. Recall that both Ai_0 and Ai_{-1} are recessive solutions of the Airy equation in the corresponding sector, hence, eventually $\mathrm{Ai}_0(z)$ and $\mathrm{Ai}_{-1}(z)$ must decay exponentially as $y \to -\infty$ and $y \to +\infty$, respectively. Note that $w(y)$ is obtained from $\mathcal{W}(y)$ by multiplying by a factor whose modulus is $\exp(2B\beta y)$ (with $B < 0$ and $\beta > 0$). However, the rapid decay of $\mathcal{W}(y)$ as $y \to -\infty$ is also shared by $w(y)$ in the same limit, since the rate of the exponential decay of $\mathrm{Ai}_0(z)$ for large $z \in S_0$ is proportional to $y^{3/2}$ which is larger than the linear rate of growth represented by transformation (4.31).

The existence of localised solutions should not be expected if Δ, β and y are such that $z(y)$ is close to any of the three sector borders, namely $\arg(z) = \pm\pi/3, \pi$

(see Appendix A) where the Airy functions exhibit algebraic decay. Since we expect ϕ to be small, the proximity of the oblique line $z(y)$ to those three semi-axes is very evident for the negative real semi-axis $\arg(z) = \pi$. Thus, the major problems should occur whenever the line $z(y)$ intersects the semi-axis $\arg(z) = \pi$.

The numerical search for localised solutions was planned as follows. First we fix β and Δ, then the two possible values for $\bar{B}$ are found by solving the cubic equation (4.29) (making use of NAG routine C02AGF which uses a modified Laguerre method). For each one, we try to obtain a one-hump pulse. Hence, using the approximation $w(y) \sim \bar{\Gamma}\mathrm{sech}[\bar{\Gamma}(y - \bar{y_p})]$ (where $\bar{\Gamma}$ and $\bar{y_p}$ were obtained as explained above) we may estimate a location y_1 on the left tail ($y_1 < \bar{y_p}$) by $\bar{y_1} = \bar{y_p} - \ln(2\bar{\Gamma}/\epsilon)/\bar{\Gamma}$ at which $w \sim \epsilon$.

The shooting method starts at $\bar{y_1}$ where the solution $w(\bar{y_1})$ should be well described by $\mathrm{Ai}_0(z(\bar{y_1}))$ through the auxiliary function $\mathcal{W}$. Hence, we start the integration of (2.31) at $\bar{y_1}$ with the following initial conditions:

$$w(\bar{y_1}) = c_1 \mathrm{Ai}_0(z(\bar{y_1}))\exp[-i\bar{B}(1+2i\beta)\bar{y_1}] = \epsilon,$$

$$w'(\bar{y_1}) = -c_1\left\{(2+4i\beta)^{1/3}\mathrm{Ai}_0'(z(\bar{y_1})) + i\bar{B}(1+2i\beta)\mathrm{Ai}_0(z(\bar{y_1}))\right\}\times \exp[-i\bar{B}(1+2i\beta)\bar{y_1}],$$

and integrate forward passing through a maximum of $|w|$ and stopping when it reaches a minimum of $|w|^2 + |w'|^2$. Then y_1 and B are improved in order to minimize $|w|^2 + |w'|^2$ down to ϵ^2 or smaller. In fact, the minimisation algorithm showed better convergence rate if we minimize $|w|^2 + 10^{-2}|w'|^2$. A similar shooting method could start at y_2 which is located on the right tail. In this case, the initial conditions should use the appropriate recessive Airy function at $z(y_2)$ which is $\mathrm{Ai}_{-1}(z)$. Generally, the forward integration starting at y_1 showed more ability to find localised single-humped solutions than the backward integration starting at y_2. However, there are some controversial results that will be discussed in the next section. The integration was performed with D02PCF and the minimisation with E04FCF, as previously for the shooting applied to the photorefractive model.

4.2.1 Numerical results

We have searched, throughout the region of the parameter space (β, Δ) covering β from 0.001 to 0.23 and Δ from $\frac{3}{4}\beta^{1/3}$ to 3.5, for pulse profiles containing a single peak. The lower boundary, $\Delta \geq \frac{3}{4}\beta^{1/3}$, is required for the cubic equation in B to have the required negative solutions. When the above inequality is satisfied there are two of these solutions. Let us denote the smaller in modulus by B_s and the other one by B_l. The solutions corresponding to B_s are larger in amplitude and,

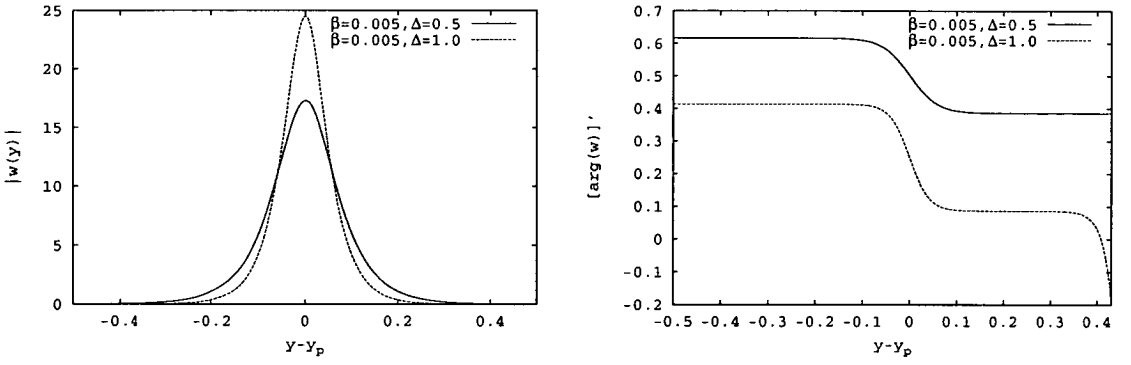

(a) (b)

Figure 4.1: Pulse profile (a) and chirp (b) for two B_s solutions with $\beta = 0.005$ and $\Delta = 0.5, 1.0$. Velocities are $B = -0.50$ and $B = -0.25$, respectively.

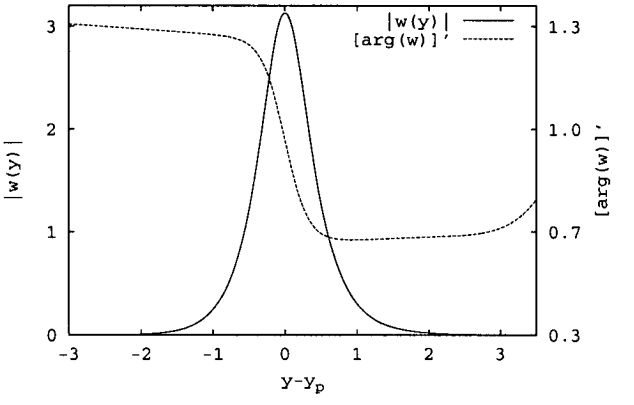

Figure 4.2: Pulse profile and chirp for the B_s solution with $\beta = 0.08$ and $\Delta = 0.33$. Velocity is $B = -0.96$.

according to the perturbation theory in §4.1, are the stable ones. The existence of a single-hump solution of (4.25) is rather dependent on the choice of B.

Let us first consider the results concerning B_s. Using the forward integration, we found pulse solutions almost everywhere in the parameter region under investigation. However, for large Δ and small β the estimates of y_1 and y_2 are such that $|z(y_i)|$ for $i = 1, 2$ are very large and consequently the computation of $\mathrm{Ai}(z)$ using the NAG routine is not possible.

For fixed β, the absolute value of the velocity B decreases with increasing Δ and the profile peak amplitude increases with Δ. The pulse profiles are very close to sech-profiles, however the phase has chirp which is close to a tanh behaviour. Fig. 4.1 shows the profile and chirp for fixed β and two values of Δ. Let us remember the results, presented in expression (4.18), obtained with the adiabatic approximation of the perturbed inverse scattering. Comparing the phase expression

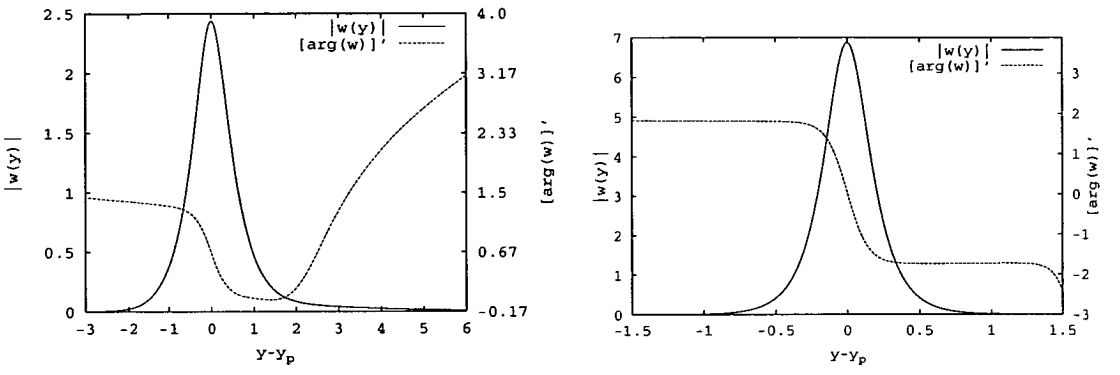

(a) (b)

Figure 4.3: Pulse profile and chirp for two B_s solutions with $\beta = 0.2$, (a) $\Delta = 0.44$ and $B = -0.64$ (b) $\Delta = 3.0$ and $B = -0.08$.

in (4.18) with the phase (4.24), we conclude that, for our approach to agree with the perturbation results, the argument of $w(y)$ should have a linear dependence upon y. Nevertheless, a NLS model with amplification and filtering but without sliding ($\sigma = 0$) has an exact stationary solution possessing a tanh-type chirp. The solution is given by $q(Z,T) = A \text{ sech } k(\zeta - \zeta_0) \exp\{i\Theta(Z,\zeta) + ic \ln[\text{sech } k(\zeta - \zeta_0)]\}$. The form of ζ is the same as assumed above but with $b = 0$, the function $\Theta(Z,\zeta)$ was defined in §4.2 and the parameters A, c and k must satisfy some relations involving the parameters c_0, β and δ [77, 83].

There are however some deviations from the sech profile and the tanh chirp which occur for large β ($\beta \sim 0.2$) and small Δ. Fig. 4.3(a) shows one of these more asymmetric profiles whose corresponding chirp also deviates from the tanh type. The asymmetry arises from the fact that the right tail crosses the negative semi-axis in the z-plane, where $\text{Ai}_{-1}(z)$ is more slowly decreasing. Remember that the z location of the pulse in the complex plane is on a line of slope ϕ. Furthermore, $\bar{y_2}$, the estimate of y_2, already yields $z(\bar{y_2})$ lying in the bottom of the second quadrant. An interesting observation was that in some cases the backward integration using $\text{Ai}_{-1}(z)$ at the vicinity of $z(\bar{y_2})$ produces solutions which better preserve their shape during numerical integration of the full equation (4.12). In such cases, the profiles produced by backward integration are more asymmetric. An explanation could be that forward integration is not discarding the $\text{Ai}_1(z)$ behaviour at the right tail. Since integration stops when z is very close to the negative real semi-axis, where $\text{Ai}_1(z)$ and $\text{Ai}_{-1}(z)$ have very similar behaviour, the integration could be wrongly including an $\text{Ai}_1(z)$ contribution. This reasoning indicates that a backward integration should be always preferable, since it starts

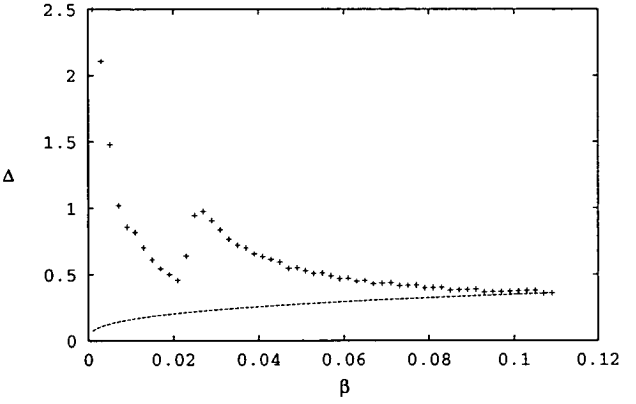

Figure 4.4: The region of existence of single peak solutions with velocity B_l is between the lower curve $\Delta = \frac{3}{4}\beta^{1/3}$ and the upper roughly determined curve.

with the correct form of tail in the right and at the left the integration terminates in a region of z where the only decaying solution is $\mathrm{Ai}_0(z)$. However, for a reason not yet clear, the backward integration does not produce localised solutions for a large number of pairs (β, Δ).

Whenever considering B_l, the existence scenario is different. It seems that in addition to the lower boundary imposed by $\Delta \geq \frac{3}{4}\beta^{1/3}$, an upper boundary in Δ also exists (see Fig. 4.4). The values marked + in Fig. 4.4 roughly determine this upper boundary and have been found as the values of Δ above which the shooting method, using forward integration, does not produce a localised profile. The shooting procedure using backward integration agrees reasonably with that pattern of existence. Apart from the part around $\beta = 0.025$, the slope of this curve is negative. Thus, for typical β, solutions exist for a range of values of Δ, but above $\beta \sim 0.11$ no solutions were found. Hence, for B_l the region of (β, Δ) for which a single peak solution exists is much smaller than for B_s. An exception occurred at $\beta = 0.23$ and $\Delta = 3.7$ where we have found a very asymmetric solution. This has motivated a search that found a region around $\beta = 0.28$ and $\Delta = 4.5$ where very asymmetric solutions exist. One example is shown in Fig. 4.5. Note that they exist for B close to $\bar{B}$ but they are much narrower than those predicted using (4.28). Apart from these asymmetric solutions, the other B_l profiles are quite symmetric. Similarly to the case of B_s, for small β they are all very close to the sech shape and to the tanh chirp and for large β and small Δ (remember that in this case there are no solutions for large β and large Δ rather than the very asymmetric ones) they deviate slightly from those shape and chirp types. In the B_l case, contrarily to the B_s case, for a given β the modulus of B increases with increasing Δ and the peak amplitude decreases.

Investigation of the locations of $z(\bar{y}_{1,2})$ brings some light to the above existence

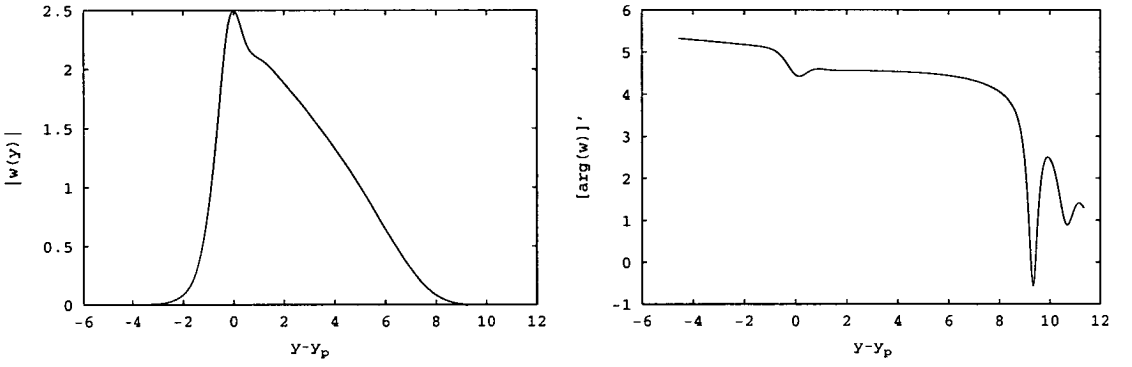

(a) (b)

Figure 4.5: Pulse profile (a) and chirp (b) for the B_l solution with $\beta = 0.27$, $\Delta = 4.5$ and $B = -4.05$.

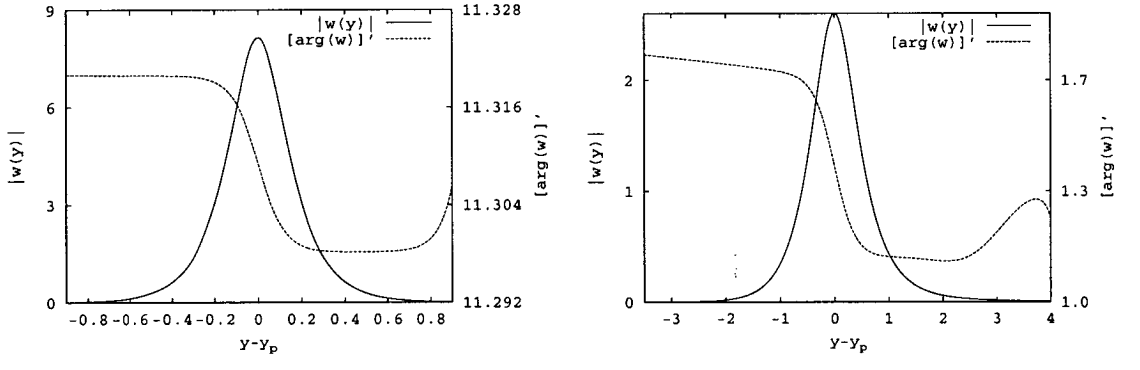

(a) (b)

Figure 4.6: Pulse profile and chirp for two B_l solutions (a) $\beta = 0.001$, $\Delta = 0.15$ and $B = -11.3$ and (b) $\beta = 0.08$, $\Delta = 0.33$ and $B = -1.40$.

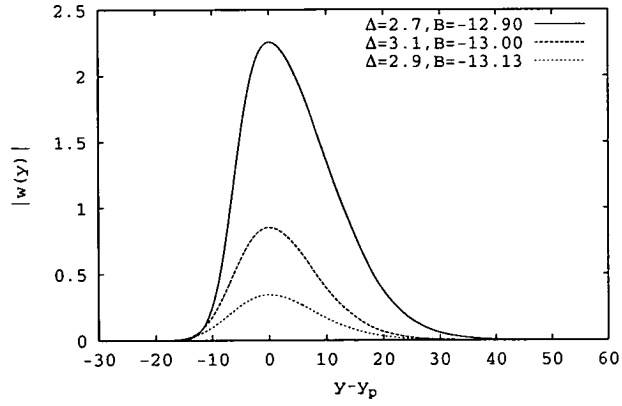

Figure 4.7: Asymmetric pulse profiles for $\beta = 0.08$ and various values of Δ and B.

pattern. In fact, increasing β from 0.001 towards 0.11 causes $z(\bar{y}_2)$ to leave the first quadrant and enter the second and eventually the third quadrants. For a given β, this movement of $z(\bar{y}_2)$ is achieved also by increasing Δ. Thus, the region in (β, Δ) for which a B_l solution was found is linked with the z-location of the pulse being in the first quadrant. The proximity of the estimated pulse z-location to $z = 0$ and the lack of success of the shooting method suggests that this region, being the intersection point of the Airy sector boundaries, is a region where the asymptotic decaying behaviour of the Airy functions is not well defined. Therefore, either our shooting procedure is not well designed for finding solutions in such situations or no single pulse solutions exist for B_l in those parameter ranges. The asymmetric solution of Fig. 4.5, although being unstable as observed by numerical simulation of the full equation, is an example of a solution that is not located in the position estimated by the approximate theory.

Experiments with the ODE (4.25) using other estimates for B and y_1, show localised solutions that differ significantly from the sech shape. One example is illustrated in Fig. 4.7. In that parameter region, there are solutions for B whose modulus is larger than the modulus of the two negative roots of (4.29). There, the peak amplitude is strongly dependent upon B rather than upon Δ. For the same β and Δ we may find solutions with different peak amplitude each one corresponding to a different value of B. Nevertheless, the different values of B do not differ from each other by much more than 10%.

The above presented results suggest that the ODE (4.25) has a rich set of solutions. In fact, the solutions may be very symmetric and close to the sech shape as was predicted by the perturbation theory [63, 17], however there are also very asymmetric ones. We should note that apart from the single-hump profiles, we have also found multi-hump profiles in our experiments. The major

question, that we discuss in the following sections, is whether they are stable or unstable pulse profiles, when evolving under the propagation equation (4.12).

4.3 Linear stability equations and zero modes

The linear stability equations are obtained by introducing a total solution of the form

$$q(Z,T) = \exp(i\Theta)[\sigma^2(1+\beta^2)]^{1/6}[w(y) + r(Z,y)] \tag{4.34}$$

into the evolution equation (4.12). This total solution consists of the equilibrium solution $w(y)$ plus a small complex perturbation $r(Z,y)$. At zero order, we obtain the ODE (4.25) and, to linear approximation in r, this yields

$$i\Delta r_{Z'} + \frac{r_{yy}}{2(1+2i\beta)} + iBr_y + (y - i\Delta)r + w^2 r^* + 2|w|^2 r = 0, \tag{4.35}$$

where we have scaled the propagation variable as $Z' = \delta Z$. Complex conjugation of the above equation gives

$$-i\Delta r^*_{Z'} + \frac{r^*_{yy}}{2(1-2i\beta)} - iBr^*_y + (y + i\Delta)r^* + (w^*)^2 r + 2|w|^2 r^* = 0. \tag{4.36}$$

In order to obtain the stability eigenvalue problem, we seek r and r^* depending exponentially on Z' in the form $r(Z',y) = u(y)\mathrm{e}^{i\lambda Z'} + v^*(y)\mathrm{e}^{-i\lambda^* Z'}$ and $r^*(Z',y) = u^*(y)\mathrm{e}^{-i\lambda^* Z'} + v(y)\mathrm{e}^{i\lambda Z'}$. Then, we arrive at the following eigenvalue problem

$$L\begin{pmatrix} u \\ v \end{pmatrix} = \lambda\Delta\begin{pmatrix} u \\ v \end{pmatrix}, \tag{4.37}$$

(together with its complex conjugate) where L is given by

$$\begin{pmatrix} \dfrac{\partial_{yy}}{2(1+2i\beta)} + iB\partial_y + y - i\Delta + 2|w|^2 & w^2 \\ -(w^*)^2 & -\dfrac{\partial_{yy}}{2(1-2i\beta)} + iB\partial_y - y - i\Delta - 2|w|^2 \end{pmatrix}.$$

As usual, the normal mode stability is verified if this eigenvalue problem has no eigenvalues with negative imaginary part.

Our first approach to the eigenvalue problem (4.37) is the identification of the zero modes. Following the procedure in §2.4, we search for zero modes by identifying the invariances of the evolution equation (4.12) and the arbitrary parameters present in the equilibrium solution. At a first inspection we recognise the parameters c_1, c_0 and b. The parameter c_1 appears in the phase expression (4.24) and c_0 in (4.21). The latter was removed by the change of variables from ζ to y. They are easily recognised as consequences of invariances under constant change

of phase and under translations in T. The velocity b relates to the invariance under the following transformation:

$$T' = T - \sigma\nu Z, \qquad Z' = \sigma + Z,$$
$$q'(Z',T') = q(Z,T)\exp\left[i\left(\tfrac{1}{2}\sigma^2\nu^2 Z - \sigma\nu T\right)\right],$$

where ν is an arbitrary constant.

According to what has been discussed in §2.4, the zero modes of L may be identified using the first derivatives of $q(Z,T)$ with respect to the arbitrary parameters which are

$$\frac{\partial q}{\partial c_1} = \mathrm{e}^{i\Theta}[\sigma^2(1+4\beta^2)]^{1/6}(iw),$$
$$\frac{\partial q}{\partial c_0} = \mathrm{e}^{i\Theta}[\sigma^2(1+4\beta^2)]^{-1/6}\left(\frac{iZ}{\Delta}w - w'\right), \tag{4.38}$$
$$\frac{\partial q}{\partial b} = \mathrm{e}^{i\Theta}(1+4\beta^2)^{-1/2}\left(\frac{iZ^2}{2\Delta}w + \frac{Z}{\Delta}w' + w_B\right).$$

The expressions in brackets in each equation above consist of a solution of the linear stability equation (4.35). Furthermore, in conjunction with their complex conjugate, they constitute the proper and generalised eigenfunctions of the zero eigenvalue of (4.37). However, if the solution w of the stability equation is the localised single-humped profile that we found, the parameter b (or B) is not arbitrary but may only take one or two values. This suggests that if we consider general solutions of (4.25) (possibly non localised) for which B may be taken arbitrarily, the zero eigenvalue could have multiplicity equal to three. However, in our case the derivative w_B is not defined and we expect to obtain results consistent with only two eigenfunctions corresponding to the zero eigenvalue. They are a proper eigenfunction given by $(w \quad -w^*)^T$ and a generalised one given by $(w' \quad (w^*)')^T$.

4.4 Evans function method

The equivalence between the linearisation of the ODE for w and the Airy equation anticipates the possibility of using the modified Evans function method introduced in the previous chapter for studying the stability of these accelerating solutions. In fact, the pulse profiles obtained in §4.2 are rapidly decaying functions in both directions. Thus the asymptotic form of the stability operator L is given by

$$L_\infty = \begin{pmatrix} \dfrac{\partial_{yy}}{2(1+2i\beta)} + iB\partial_y + y - i\Delta & 0 \\ 0 & \dfrac{-\partial_{yy}}{2(1-2i\beta)} + iB\partial_y - y - i\Delta \end{pmatrix}.$$

If we introduce the new variables $\mathcal{U}$ and $\mathcal{V}$ given by

$$u(y) = \mathcal{U}(y)\exp[-iB(1+2i\beta)y], \tag{4.39}$$

$$v(y) = \mathcal{V}(y)\exp[iB(1-2i\beta)y], \tag{4.40}$$

the asymptotic eigenvalue problem may be rewritten in the following form

$$\mathcal{U}'' + (1+2i\beta)\{B^2 + 2i\beta B^2 + 2y - 2i\Delta - 2\lambda\Delta\}\mathcal{U} = 0,$$

$$\mathcal{V}'' + (1-2i\beta)\{B^2 - 2i\beta B^2 + 2y + 2i\Delta + 2\lambda\Delta\}\mathcal{V} = 0,$$

which in turn may be transformed to a system of Airy equations

$$\mathcal{U}'' - z^+\mathcal{U} = 0 \qquad \mathcal{V}'' - z^-\mathcal{V} = 0$$

if we perform the following two changes of variable:

$$z^{\pm}(y) = (2 \pm 4i\beta)^{1/3}\{-y \pm i\Delta \pm \lambda\Delta - \frac{B^2}{2} \mp i\beta B^2\}. \tag{4.41}$$

Our search for eigenvalues is equivalent to a search for localised solutions. The philosophy of the Evans function method, as already explained, is based on the detection of the λ values for which the right- and left-decaying solutions of (4.37) at large $|y-y_p|$ have non-empty intersection. Here, we use again the recessive Airy functions to estimate the proper decaying solutions. To correctly choose them, first we need to understand the location of z^+ and z^- when y take values in the real domain. Fig. 4.8 shows corresponding typical locations of $z^{\pm}$ for fixed λ. They are lines of inclination $\pm\phi$, where the angle ϕ is the same as presented in §4.2 given by $\phi = [\arg(2+4i\beta)]/3$. The two lines move to parallel positions whenever the imaginary part of λ is changed. Changing the real part of λ only moves $z^{\pm}$ along the respective line. The portions of these lines $[z^{\pm}(y_2), z^{\pm}(y_1)]$ corresponding to the numerical integration range we shall call *profile domains*. They move along the same line if $\mathrm{Re}(\lambda)$ is changed and move to a parallel location if, otherwise, $\mathrm{Im}(\lambda)$ is changed. Note that the intercepts of the $z^{\pm}$ lines with the real line coincide, but depend upon the imaginary part of λ and do not necessarily arise on the negative semi-axis as in the example shown in Figure 4.8. As $y \to -\infty$, z^- and z^+ lie in S_0. As $y \to +\infty$, z^- lies in S_1 and z^+ in S_{-1}. The respective recessive Airy functions are $\mathrm{Ai}_0(z)$, $\mathrm{Ai}_1(z)$ and $\mathrm{Ai}_{-1}(z)$.

Following the treatment used for the photorefractive model, we use the variable $Y = (u \quad u_y \quad v \quad v_y)^T$ to rewrite the eigenvalue problem (4.37) as the following first order system

$$\frac{dY}{dy} = A(y,\lambda)Y, \tag{4.42}$$

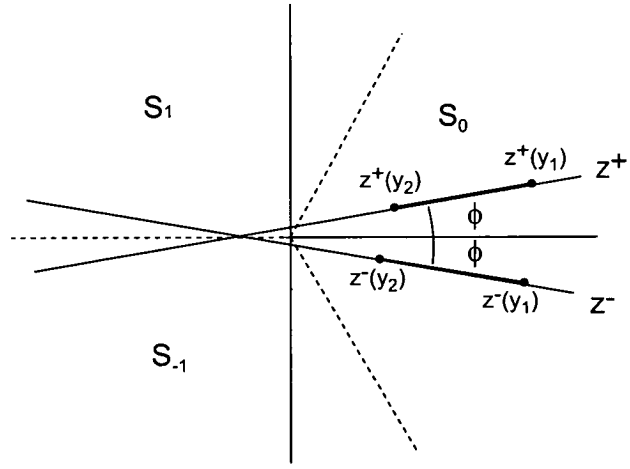

Figure 4.8: $z^{\pm}$ lines and profile domains $[z^{\pm}(y_2), z^{\pm}(y_1)]$ for fixed λ.

where $A(y,\lambda)$ is given by

$$\begin{pmatrix} 0 & 1 & 0 & 0 \\ \sigma^+(-y+\Delta(i+\lambda)-2|w|^2) & -iB\sigma^+ & -\sigma^+ w^2 & 0 \\ 0 & 0 & 0 & 1 \\ -\sigma^-(w^*)^2 & 0 & \sigma^-(-y-\Delta(i+\lambda)-2|w|^2) & iB\sigma^- \end{pmatrix}, \tag{4.43}$$

with $\sigma^{\pm} = (2 \pm 4i\beta)$.

We use the definition of the Evans function given in §3.2, which we reproduce here, with the appropriate variables

$$D_{ai}(\lambda) = \begin{vmatrix} Y_{11}^-(y_p,\lambda) & Y_{21}^-(y_p,\lambda) & Y_{31}^+(y_p,\lambda) & Y_{41}^+(y_p,\lambda) \\ Y_{12}^-(y_p,\lambda) & Y_{22}^-(y_p,\lambda) & Y_{32}^+(y_p,\lambda) & Y_{42}^+(y_p,\lambda) \\ Y_{13}^-(y_p,\lambda) & Y_{23}^-(y_p,\lambda) & Y_{33}^+(y_p,\lambda) & Y_{43}^+(y_p,\lambda) \\ Y_{14}^-(y_p,\lambda) & Y_{24}^-(y_p,\lambda) & Y_{34}^+(y_p,\lambda) & Y_{44}^+(y_p,\lambda) \end{vmatrix}, \tag{4.44}$$

where $Y_{ij}^{\pm}$ $(i,j = 1,\cdots,4)$ is the j component of $Y_i^{\pm}$. The solutions $Y_1^-(y,\lambda)$ and $Y_2^-(y,\lambda)$ are the ones decaying as $y \to -\infty$. As mentioned above, at that limit $z^{\pm}$ lie in S_0 so initial data $Y_1^-(y_1,\lambda)$ and $Y_2^-(y_1,\lambda)$ should be taken from $\mathrm{Ai}_0(z_1^{\pm})$ as follows

$$\begin{aligned} Y_1^-(y_1,\lambda) =& \mathrm{e}^{-iB\sigma^+ y_1/2}\left(\mathrm{Ai}_0(z_1^+) \quad -(\sigma^+)^{1/3}\mathrm{Ai}_0'(z_1^+) - iB\sigma_+\mathrm{Ai}_0(z_1^+) \quad 0 \quad 0\right)^T, \\ Y_2^-(y_1,\lambda) =& \mathrm{e}^{iB\sigma^- y_1/2}\left(0 \quad 0 \quad \mathrm{Ai}_0(z_1^-) \quad -(\sigma^-)^{1/3}\mathrm{Ai}_0'(z_1^-) + iB\sigma^-\mathrm{Ai}_0(z_1^-)\right)^T, \end{aligned}$$

where $z_1^{\pm}$ stands for $z^{\pm}(y)$ evaluated at $y = y_1$. At the other limit $(y \to +\infty)$, $Y_3^+(y,\lambda)$ and $Y_4^+(y,\lambda)$ are the decaying solutions. There, z^+ lies in S_{-1} so the initial data $Y_3^+(y_2,\lambda)$ is based on $\mathrm{Ai}_{-1}(z_2^+)$; but z^- lies in S_1 so $Y_4^+(y_2,\lambda)$ is based on $\mathrm{Ai}_1(z_2^-)$:

$$\begin{aligned} Y_3^+(y_2,\lambda) =& \mathrm{e}^{-iB\sigma^+ y_2/2}\left(\mathrm{Ai}_{-1}(z_2^+) \quad -(\sigma^+)^{1/3}\mathrm{Ai}_{-1}'(z_2^+) - iB\sigma^+\mathrm{Ai}_{-1}(z_2^+) \quad 0 \quad 0\right)^T, \\ Y_4^+(y_2,\lambda) =& \mathrm{e}^{iB\sigma^- y_2/2}\left(0 \quad 0 \quad \mathrm{Ai}_1(z_2^-) \quad -(\sigma^-)^{1/3}\mathrm{Ai}_1'(z_2^-) + iB\sigma^-\mathrm{Ai}_1(z_2^-)\right)^T, \end{aligned}$$

where $z_2^{\pm}$ stands for $z^{\pm}(y)$ evaluated at the $y = y_2$. Note that $Y_1^-(y,\lambda)$ and $Y_3^+(y,\lambda)$ relate with Airy functions through relation (4.39) and $z^+(y)$ given by (4.41). $Y_2^-(y,\lambda)$ and $Y_4^+(y,\lambda)$ relate with Airy functions through relation (4.40) and $z^+(y)$ also given by (4.41). A comment similar to that in page 69 applies here to guarantee that $u(y)$ and $v(y)$ have rapid decay as $y \to -\infty$ though they are related to $\mathrm{Ai}_0(z^{\pm})$ for large $z^{\pm} \in S_0$ through transformations (4.39) and (4.40).

4.4.1 Numerical results

Let us first record that we could not apply the method to the more asymmetric solutions of the type shown by the examples in Fig. 4.5 and Fig. 4.7. The application of this method involves forward and backward integrations, however, in such cases, one of the integration directions was not numerically feasible. Full numerical integration of the evolution equation (4.12) using those asymmetric solutions as initial conditions shows severe instability.

As happened in the full photorefractive case, our search for eigenvalues was limited to the neighborhood of zero. However, in some cases we were able to evaluate the Evans function for values of λ as large as 10^3. Some of the numerical problems for large $|\lambda|$ arise from lack of accuracy in evaluating the Airy function values for large $|z^{\pm}|$. These problems are reported by the NAG routine and may be overcome if the routine is asked to return the value scaled by $\mathrm{e}^{2z\sqrt{z}/3}$. Note that for some profiles, even for $\lambda = 0$, the modulus of $z^{\pm}$ is already too large to use the unscaled option. Although the scaled option overcomes the difficulties in evaluating the Airy function values, the scaled Airy function is no longer an analytic function in the whole complex plane. In fact, the scaled Airy function returned by the routine has a branch cut along the negative real axis. This implies the existence of branch cuts at $\arg(z) = \pi/3$, $\arg(z) = \pi$ and $\arg(z) = -\pi/3$, respectively for $\mathrm{Ai}_{-1}(z)$, $\mathrm{Ai}_0(z)$ and $\mathrm{Ai}_1(z)$. Thus our choice of closed paths during a search for eigenvalues using the argument principle should account for this lack of analyticity. Moreover, even with the scaled option active and away from the mentioned branch cuts, usually there is a larger value of $|\lambda|$ from which $D_{\mathrm{ai}}(\lambda)$ starts to behave erratically. We shall present numerical procedures and results, separately, by topics.

1. Multiplicity of the zero eigenvalue

Evaluation of the Evans function as λ moves around a circle of small radius centred on $\lambda = 0$ shows a change in its argument by 4π. This result is compatible with a zero eigenvalue of multiplicity equal to two, in agreement with discussion in the section devoted to the zero modes.

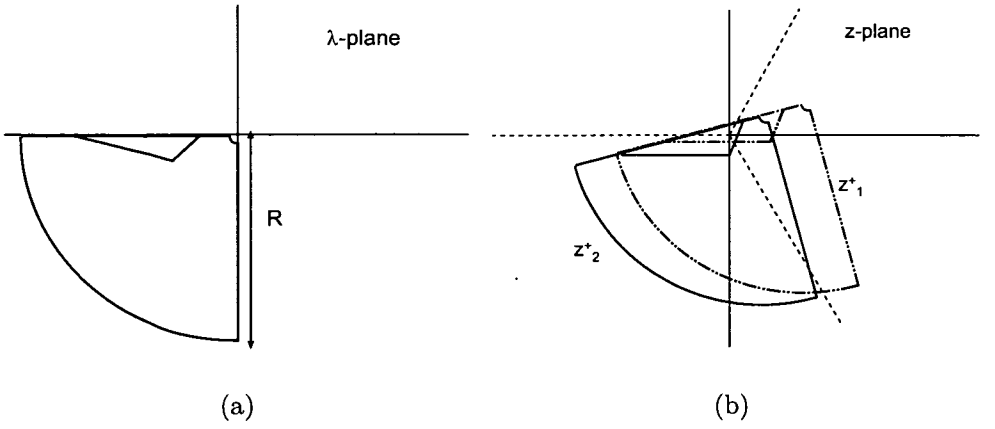

Figure 4.9: Paths on the lower λ-plane and corresponding paths of z_2^+ and z_1^+.

2. Spectrum for solutions corresponding to B_s

The stability spectrum for solutions corresponding to B_s always has several eigenvalues in the upper half-plane. They constitute the stable eigenvalues and they move in the λ-plane, as β or Δ changes. Among these movements we highlight two important ones.

For fixed β, as Δ decreases toward the boundary $\Delta = \frac{3}{4}\beta^{1/3}$, the pure imaginary eigenvalue of lowest absolute value moves toward the origin. The actual boundary is the value of Δ for which $B_s = B_l$, which is found to be very close to $\Delta = \frac{3}{4}\beta^{1/3}$. At the actual boundary, the above eigenvalue coincides with the repeated zero eigenvalue.

The other important movement of eigenvalues happens when, as Δ increases for fixed β, some stable complex eigenvalues cross the real axis and move into the lower half-plane, implying the loss of stability. Thus, there the system undergoes a Hopf bifurcation. The Evans function method permitted us to follow this movement of eigenvalues and to obtain the boundary in the (β, Δ) plane between the stable and unstable regions (line of the Hopf bifurcation), as shown in Fig. 4.10. The numerical procedure used to obtain this threshold of stability followed from the strategy used to seek unstable eigenvalues. The symmetry of the eigenvalue problem guarantees that all eigenvalues occur in pairs such as $(\lambda, -\lambda^*)$. Thus, using the argument principle, we searched for eigenvalues in the quarter disk shown in Fig 4.9(a), where R is chosen as large as is numerically possible. A small quarter disk was excluded from the closed region, to avoid the zero of $D_{\mathrm{ai}}(\lambda)$ at $\lambda = 0$. In order to maximize R, or in cases such that $|z^{\pm}(y_{1,2})|$ is large even for $\lambda = 0$, some of the required values of the Airy functions may only be obtained in the scaled version. As λ moves along the path of Fig. 4.9(a), $z^+(y_1)$ and $z^+(y_2)$ move along the paths illustrated in Fig. 4.9(b). Note that we require $\mathrm{Ai}_0(z_1^+)$

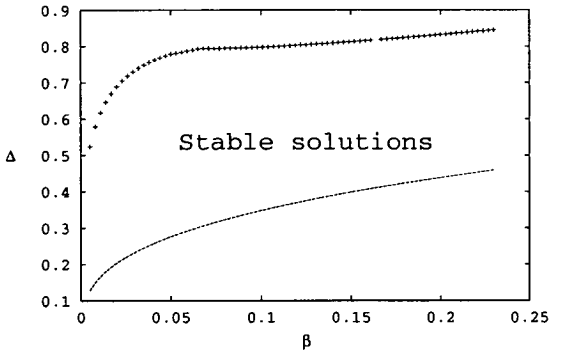

Figure 4.10: Boundaries of existence and stability in the (β, Δ) plane for B_s solutions. Lower limit of $\Delta = \frac{3}{4}\beta^{1/3}$ and upper limit of stability $\Delta_{\text{lim}}(\beta)$ obtained by the Evans function method.

and $\text{Ai}_{-1}(z_2^+)$, however $z^+(y_1)$ and $z^+(y_2)$ usually cross the branch cuts of the scaled versions of $\text{Ai}_0(z)$ and $\text{Ai}_{-1}(z)$ which are $\arg(z) = \pi$ and $\arg(z) = \pi/3$, respectively. Note that in all our cases, the $z^-(y_1)$ and $z^-(y_2)$ do not cross the respective branch cuts, i.e, $\arg(z) = \pi$ for $\text{Ai}_0(z)$ and $\arg(z) = -\pi/3$ for $\text{Ai}_1(z)$. To overcome this difficulty, we divided the path into two parts as also is shown in Fig. 4.9(a). The triangle contains all the values of λ for which $z^+(y_1)$ and $z^+(y_2)$ cross the aforementioned branch cuts. The computation of the Evans function $D_{\text{ai}}(\lambda)$ on the triangle used the unscaled Airy function values at $z^+(y_1)$ and $z^+(y_2)$ and the scaled values at $z^-(y_1)$ and $z^-(y_2)$. All the Airy function values used in the computation of $D_{\text{ai}}(\lambda)$ on the complementary path were scaled.

The number of zeros of $D_{\text{ai}}(\lambda)$ within the regions enclosed by the paths of Fig. 4.9(a) was counted by the argument principle using the procedure described on page 51 for the photorefractive model. The final result of such a search procedure is the line $\Delta_{\text{lim}}(\beta)$ in the (β, Δ) plane that separates the regions of stability and instability (Fig. 4.10). The transition occurs whenever one pair of complex eigenvalues (λ and $-\lambda^*$) enters the lower half-plane. In all the investigated cases, as we reach $\Delta_{\text{lim}}(\beta)$ from below the numerical procedure detects the first unstable eigenvalue always in the region delimited by the triangle of Fig. 4.9(a). Increasing Δ from the threshold value $\Delta_{\text{lim}}(\beta)$, results in increasing the number of unstable eigenvalues. Moreover, the eigenvalues enter deeper into the lower half-plane which implies larger exponential growth of the corresponding unstable modes.

The eigenfunctions are of two main types, depending on whether they are localised or non-localised within the profile domain. Apart from the eigenfunction belonging to $\lambda = 0$ which coincides with $w(y)$, we generally found two more localised eigenfunctions belonging to the two lowest pure imaginary (positive imaginary) eigenvalues. These two eigenfunctions for $\beta = 0.08$ and $\Delta = 0.33, 0.79$ are

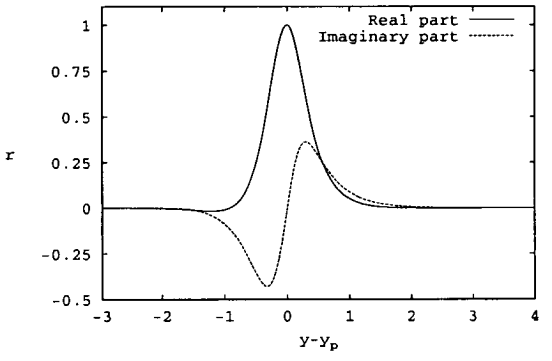

(a) $\lambda = 0.815i$

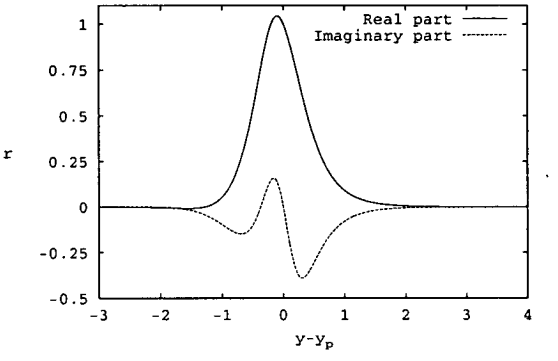

(b) $\lambda = 5.322i$

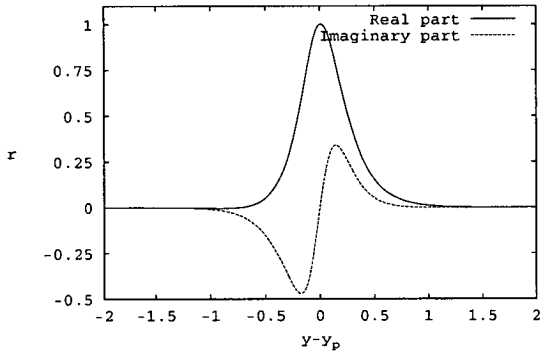

(c) $\lambda = 3.427i$

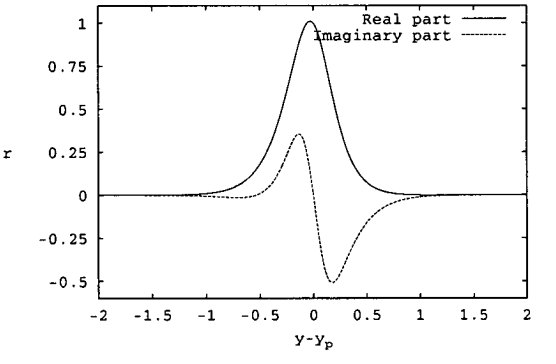

(d) $\lambda = 4.513i$

Figure 4.11: Perturbation $r(0, y)$ built from the eigenfunction $(u \;\; v)^T$ corresponding to two different eigenvalues for B_s solutions with $\beta = 0.08$; (a)-(b) $\Delta = 0.33$ and (c)-(d) $\Delta = 0.79$.

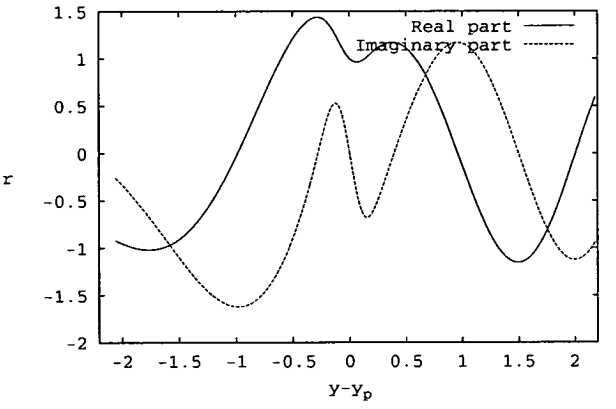

Figure 4.12: Perturbation $r(0, y)$ built from the eigenfunction $(u \;\; v)^T$ corresponding to $\lambda = \pm 21.36 - \epsilon i$ for a B_s solution with $\beta = 0.08$ and $\Delta = 0.7947$.

shown in Fig. 4.11. However, the eigenfunctions belonging to the group of complex eigenvalues responsible for the loss of stability at the upper curve of Fig. 4.10 are not localised within the profile domain. One example of such eigenfunctions is shown in Fig. 4.12. This corresponds to the first eigenvalue crossing the real axis. Note, that, although these functions are not localised within the profile domain they are not unbounded, since away from this domain they behave as the recessive Airy function of the corresponding sector.

The upper limit of stability that we found using the Evans function method should correspond to the limit found experimentally and numerically in 1994 by Mamyshev and Mollenauer [74]. They described this as an upper energy limit above which non-soliton components are not completely removed by the sliding filtering. The stability boundary found here is an upper limit for Δ. However, for fixed β, as Δ increases the peak amplitude and energy also both increase, which confirms the correspondence between our boundary shown in Fig. 4.10 and the Mamyshev limit. Meanwhile, the same stability limit was analytically estimated using two different perturbation techniques [17, 12]. Both works attributed the loss of stability to the growth of dispersive radiation and estimated this growth, in order to predict the stability threshold. Likewise, the Evans function method here applied predicts the loss of stability whenever a non-localised mode (radiation like mode) crosses the real axis and become unstable.

3. Spectrum for solutions corresponding to B_l

The solutions corresponding to B_l were classified as unstable solutions by the perturbation techniques (see page 66). The Evans function method, confirming that classification, found one pure negative imaginary eigenvalue for all solutions corresponding to B_l. The unstable eigenvalue λ_u was found confined to a portion of the negative imaginary axis, i.e., $\lambda_u = -\rho i$ with $0 \leq \rho \lesssim 1.47$. The eigenvalue

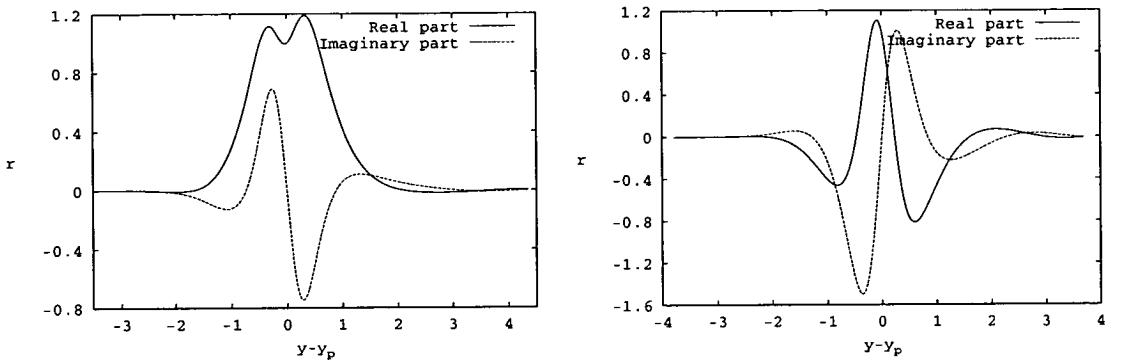

(a) $\lambda = -0.717i$ (b) $\lambda = -1.378i$

Figure 4.13: Perturbation $r(0, y)$ built from the eigenfunction $(u\ v)^T$ corresponding to the pure negative imaginary eigenvalue for B_l solutions with $\beta = 0.08$; (a) $\Delta = 0.33$ and (b) $\Delta = 0.39$.

takes the limit value $\lambda_u = 0$ at the boundary where $B_l = B_s$ and, as Δ is increased and β fixed, it moves toward $-1.47i$. For values of β for which solutions were found for a wider range of Δ (see Fig. 4.4), the eigenvalue reaches $\lambda_u = -1.47i$ and reverses its direction if Δ is further increased. Nevertheless, the upper Δ-limit is always reached before λ_u comes close to zero again. The eigenfunctions belonging to this eigenvalue are shown in Fig. 4.13 for two different solutions. A rough inspection of other eigenvalues reveals a pure positive imaginary eigenvalue and other complex eigenvalues with nonzero real part. In some cases we detected the movement of those later complex eigenvalues from the upper half-plane to the lower half-plane. In this case of $B = B_l$, this transition does not affect the stability properties since all the solutions are unstable due to the negative imaginary eigenvalue.

4.5 Direct numerical integration

The numerical simulation of the evolution equation (4.12) using the localised pulses as initial conditions was used to confirm the acceleration regime and the stability results. Whenever the propagation is stable, which has been confirmed for pulses with velocity B_s within the region of (β, Δ) in Fig. 4.10, the trajectory is in good agreement with the predicted curve $T^p = T_0^p - bZ - \sigma Z^2/2$. Fig. 4.14(a) shows the actual and predicted trajectories being coincident, when $\beta = 0.2$, $\Delta = 0.44$ and $\sigma = 0.1$. Typically, the peak amplitude evolves as shown in Fig. 4.14(b), i.e., it suffers a slight decrease and then readjusts to a value very close to the initial value. This evolution could be a symptom of a difference between the

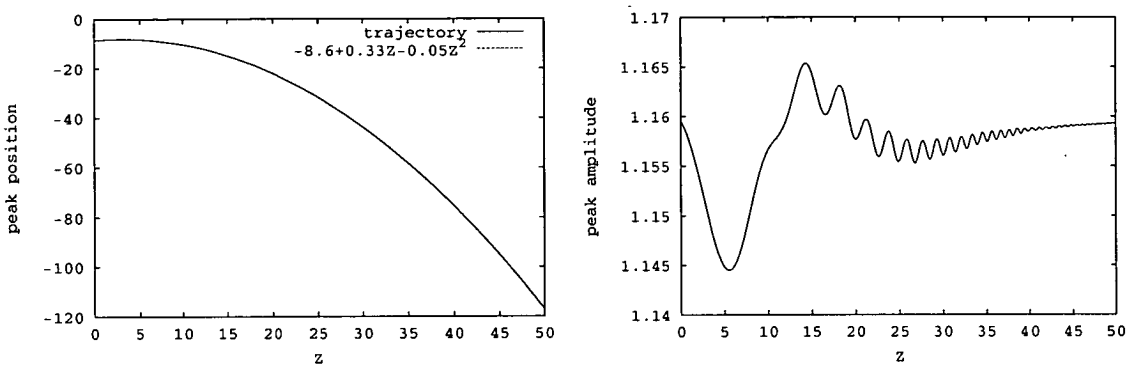

(a) (b)

Figure 4.14: Peak amplitude and position during propagation of a initial pulse corresponding to $\beta = 0.2$, $\Delta = 0.44$, $\sigma = 0.1$ and $B = B_s$. The trajectory of the peak position is in coincidence with the predicted parabola.

initial condition obtained numerically as a solution to the ODE (4.25) and the actual equilibrium pulse. In general, a visual comparison of the initial and final profiles reveals a close similarity, even though a possible difference in the tails can occur. There was another observation, made with the numerical simulation of (4.12), that supports the existence of some inaccuracy in the computation of the right tail using the shooting method described in §4.2. The more asymmetric solutions obtained using forward integration were not so well preserved during propagation as the solutions for the same β and Δ but obtained using backward integration. A discussion on this topic was already presented in §4.2.1.

The numerical integration of equation (4.12) also confirmed the upper stability-boundary in the (β, Δ) plane. For Δ values in the vicinity of the boundary, the peak amplitude undergoes oscillations whose period is in agreement with the eigenvalue that crosses the real axis at this boundary. For example, the period of oscillation shown in the inset of Fig. 4.15(a) is $T \simeq 1.7$ and the crossing eigenvalue for these values of β and Δ is $\lambda = \pm 21.4$, confirming the predicted relation $T = 2\pi/\lambda\delta$ (note that $\sigma = 0.1$ and consequently $\delta = 0.17$). These oscillations are decaying if Δ is slightly below the boundary (Fig. 4.15(a)) and growing otherwise (Fig. 4.15(b)).

As was pointed out in the Evans function treatment, this instability arising for Δ values above the upper boundary is related to growing radiation modes. They produce these amplitude oscillations and eventually may cause a second soliton to break off. The formation of a second soliton or even more solitons was experimentally observed early by Mamyshev [74]. Fig. 4.16 shows the profiles for a sector of propagation distance where the second soliton starts to be noticeable.

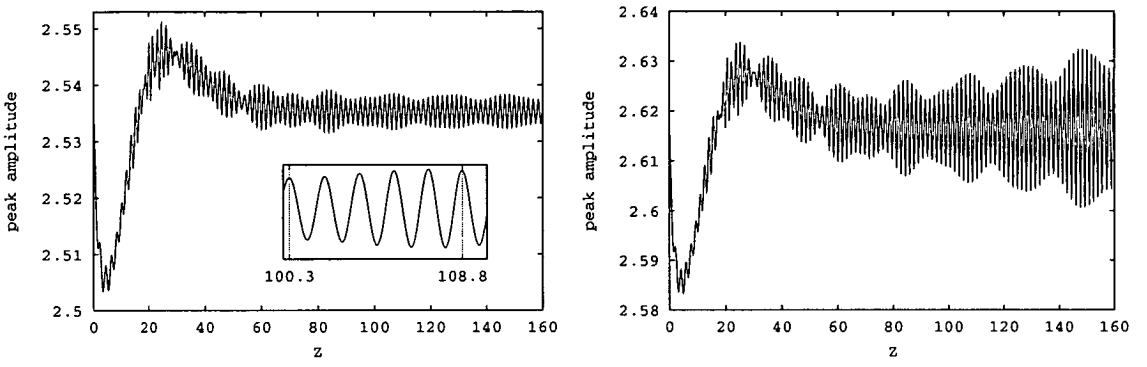

(a) (b)

Figure 4.15: Peak amplitude evolution of a initial pulse corresponding to $\beta = 0.08$, $\sigma = 0.1$, $B = B_s$ and (a) $\Delta = 0.79$, (b) $\Delta = 0.84$. Inset in (a) shows the period of oscillation.

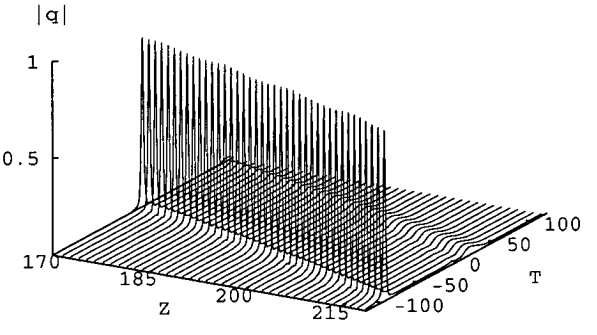

Figure 4.16: Formation of the second soliton for $\beta = 0.2$, $\Delta = 1.0$, $\sigma = 0.01$ and $B = B_s$.

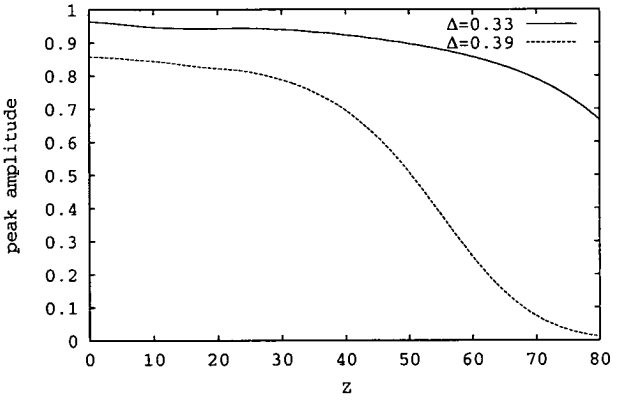

Figure 4.17: Evolution of peak amplitude for two B_l solutions with $\beta = 0.2$, $\Delta = 0.33, 0.39$ and $\sigma = 0.05$.

The pulses corresponding to velocity B_l were found to be unstable, confirming the results of the Evans function method. This unstable family of solutions has been known from the early stages of research on the sliding frequency filter model. Fig. 4.17 shows peak amplitude evolution for two B_l solutions where the typical decaying behaviour is present. Note that the solution corresponding to larger Δ has a more rapid decay. The estimated growth rate of the unstable modes is $\delta\lambda$, which gives 0.032 for the $\Delta = 0.33$ solution and 0.073 for the $\Delta = 0.39$ solution.

4.6 Conclusion

The two family of accelerating solitons (corresponding to B_s and B_l) of equation (4.12), already treated in the literature by perturbation techniques around the NLS model, were here found by a similarity variable reduction. This procedure reveals that only two combinations of the three original parameters in the PDE are significant. Here, we chose β and $\Delta \equiv \Delta(\delta, \beta, \sigma)$ The numerical integration of the resulting ODE shows pulses close to sech-profiles but slightly asymmetric and with a tanh-like chirp rather than the predicted linear chirp.

The Evans function method involving Airy asymptotics was used to study their stability. The B_l family was confirmed unstable by the presence of one unstable purely imaginary eigenvalue. The B_s family is stable within a region of (β, Δ) between the lower boundary of existence $\Delta \simeq \frac{3}{4}\beta^{1/3}$ and the curve $\Delta = \Delta_{\text{lim}}(\beta)$, where the solution loses its stability via a Hopf bifurcation.

The direct integration of the evolution equation confirmed the stability characteristics shown by the Evans function method.

Chapter 5

Pulse propagation with intrapulse Raman scattering

Intrapulse Raman scattering is a nonlinear phenomenon usually neglected when nonlinear pulse propagation in fibres is modelled. The Raman phenomenon occurs whenever one incident photon is annihilated and a new photon of different frequency is created. The process involves transfer of energy between the medium and the optical field. Thus, the medium is left in a different energy state. Usually, there is one incident radiation called a *pump* wave and one emitted radiation called a *Stokes* or an *anti-Stokes* wave. *Stokes* scattering denotes the case of frequency down-shifting and excitation of the medium. On the other hand, one uses the term *anti-Stokes* scattering whenever the frequency is up-shifted and the medium passes to the ground state. This is possible if the medium is already in an excited state which may have occurred by thermal excitation. Spontaneous Raman scattering is dominated by the *Stokes* emission since, at room temperature, this type has typically larger probability than the anti-Stokes type.

In the intrapulse Raman scattering only one carrier frequency is present, however the spectral width is sufficiently large so that the spectral Raman gain which characterises the material allows energy transfer from the high frequency components to the low frequency components. The consequence of this phenomenon for the propagation of solitons in fibers is a continuous down-shift of the mean frequency of subpicosecond soliton pulses. The effect was first observed in 1986 by Mitschke and Mollenauer [76] and named as *soliton self-frequency shift.* The effect was attributed to Raman scattering and, as demonstrated by Gordon [41], may be theoretically explained as a delayed Kerr response. The basic steps for the introduction of intrapulse Raman scattering into the governing equation will be given in the next section.

The Raman gain coefficient, denoted by $g_{\mathrm{R}}(\Omega)$ (with Ω equal to the difference in frequency between the pump and the Stokes waves), describes the gain

experienced by radiation of frequency $f_s = f_p - \Omega$ when it co-propagates with a pump radiation of frequency f_p through a Raman medium. Furthermore, $g_{\rm R}(\Omega)$ is related to the imaginary part of the third-order susceptibility. In silica fibers, the Raman gain extends over a large frequency range (up to 40 THz) with a broad peak located near 13 THz. Note that the energetic states of the silica involved in the Raman scattering belong to the molecular vibrational modes. Due to the amorphous nature of the material, the vibrational modes spread over energy bands instead of being well-defined lines.

5.1 Governing equation

To account for intrapulse Raman scattering in solitons propagating in fibres, a nonlinear term of the type $q|q|_t^2$ is usually included in the NLS equation. This result was demonstrated by Gordon [41] and is here shown in outline, following [15, 4]. Instead of the nonlinear relation between the polarisation and the optical field given by (4.4) in §4.1, let us assume a causal and time dependent relation acting only on the optical field intensity given by

$$\mathbf{P}^{\rm NL}(\mathbf{r},t) = \frac{\epsilon_0}{2}\hat{\mathbf{x}}\frac{3}{4}\chi^{(3)}\left[E(\mathbf{r},t)\exp(ik_0 z - i\omega_0 t) + \text{c.c.}\right]\int_{-\infty}^{\infty} f(t_1)|E(\mathbf{r},t-t_1)|^2 dt_1, \tag{5.1}$$

where the response function $f(t_1)$ is zero for $t_1 < 0$ (to guarantee causality) and is normalised so that $\int_{-\infty}^{\infty} f(t)dt = 1$. The response function should include both electronic and vibrational contributions. On a femtosecond time scale, the former is instantaneous and will be represented by a delta function. This corresponds to the Kerr effect already present in the NLS model. The latter is much slower and will be here represented by the Raman response function $h_{\rm R}(t)$. Thus, the total response function is given by

$$f(t) = (1 - f_{\rm R})\delta(t) + f_{\rm R}h_{\rm R}(t), \tag{5.2}$$

where $f_{\rm R}$ represents the relative strength of the Raman contribution which is estimated as about 0.18. The Raman response function $h_{\rm R}$ may be obtained from measured Raman gain spectrum. The typical response function for pure silica core fibers consists of a damped oscillation with initial period ~ 75 fs, corresponding to the peak of the Raman gain $g_{\rm R}$ being about 13 THz [101].

A simplification of expression (5.1) may be achieved using a Taylor series expansion of $|E(\mathbf{r},t-t_1)|^2$ around time t such that

$$|E(\mathbf{r},t-t_1)|^2 \simeq |E(\mathbf{r},t)|^2 - t_1\left(|E(\mathbf{r},t)|^2\right)_t + \cdots. \tag{5.3}$$

Inserting (5.2) and (5.3) into (5.1) yields

$$\mathbf{P}^{\mathrm{NL}}(\mathbf{r},t)=\frac{\epsilon_0}{2}\hat{\mathbf{x}}\frac{3}{4}\chi^{(3)}\left[|E(\mathbf{r},t)|^2-t_{\mathrm{R}}\left(|E(\mathbf{r},t)|^2\right)_t\right]\left[E(\mathbf{r},t)\exp(ik_0z-i\omega_0)+\text{c.c.}\right],$$

where

$$t_{\mathrm{R}}=f_{\mathrm{R}}\int_{-\infty}^{\infty}t_1h_{\mathrm{R}}(t_1)dt_1$$

is called the Raman parameter. Assuming that the Raman gain spectrum varies linearly with frequency in the vicinity of the carrier frequency, the numerical value of the Raman parameter could be deduced from experimental data as $t_{\mathrm{R}}=3$ fs at $\lambda\sim 1.55$ μm [10].

Following the approach presented in §4.1 for the derivation of the governing equation of the sliding frequency filter model, the effective dielectric constant is here given by

$$\epsilon\left(\omega,|E|^2,\left(|E|^2\right)_t\right)\simeq n^2(\omega)+2n\left[\frac{i\alpha c}{2\omega_0}+n_2|E|^2-n_2t_{\mathrm{R}}\left(|E(\mathbf{r},t)|^2\right)_t\right].$$

In this case, the eigenvalue k is also a function of $(|A|^2)_t$ so that its Taylor expansion reads as

$$k=k_0+(\omega-\omega_0)k'_{r0}+\frac{1}{2}(\omega-\omega_0)^2k''_{r0}+\cdots+\frac{\partial k_r}{\partial|A|^2}|A|^2+\cdots+\frac{\partial k_r}{\partial(|A|^2)_t}(|A|^2)_t+\cdots+ik_i,$$

where the coefficient of the extra term relates with t_{R} by [4]

$$\frac{\partial k_r}{\partial(|A|^2)_t}=-\frac{\omega_0n_2t_{\mathrm{R}}}{cA_{\mathrm{eff}}}.$$

Thus, the equation for the envelope function $A(z,\tau)$, where $\tau=t-k'_{r0}z$, is given by

$$\frac{\partial A}{\partial z}+i\frac{k''_{r0}}{2}\frac{\partial^2A}{\partial\tau^2}-i\frac{\omega_0n_2}{cA_{\mathrm{eff}}}\left\{|A|^2-t_{\mathrm{R}}(|A|^2)_\tau\right\}A=0,$$

where fibre loss was neglected by setting $\alpha=0$. A non-dimensionalisation as in §4.1, namely

$$A(z,\tau)=\sqrt{\frac{cA_{\mathrm{eff}}}{\omega_0n_2z_0}}q(Z,T),\qquad Z=\frac{z}{z_0}\qquad\text{and}\qquad T=\frac{\tau}{\tau_0}$$

yields

$$iq_Z+\frac{1}{2}q_{TT}+|q|^2q=T_{\mathrm{R}}(|q|^2)_Tq,\tag{5.4}$$

where $T_{\mathrm{R}}=t_{\mathrm{R}}/\tau_0$. This same governing equation was proposed by Gordon [41] in the first attempt to explain soliton self-frequency shift.

Straightforward application of an adiabatic perturbation technique to the above perturbed NLS equation yields a frequency shift in accordance with the

experimental observations. Let us consider that T_R is small, thus the adiabatic approximation for the solution to (5.4) is

$$q(Z,T) = \mu \mathrm{sech}[\mu(T - T_0(Z))] \exp[-i\kappa(Z)T + i\phi_0(Z)],$$

where the amplitude μ is constant, and the frequency $\kappa(Z)$, the peak position $T_0(Z)$, and the phase $\phi(Z)$, evolve as

$$\kappa(Z) = -\frac{8}{15} T_R \mu^4 Z + \kappa_i, \tag{5.5}$$

$$T_0(Z) = \frac{4}{15} T_R \mu^4 Z^2 - \kappa_i Z + T_{0i}, \tag{5.6}$$

$$\phi_0(Z) = \left(\frac{\mu^2 - \kappa_i^2}{2} - \frac{8}{15} T_R \mu^4 T_{0i} \right) Z + \frac{8}{15} T_R \mu^4 \kappa_i Z^2 - \frac{64}{675} T_R^2 \mu^8 Z^3 + \phi_{0i}, \tag{5.7}$$

where κ_i, T_{0i} and ϕ_{0i} are the initial values of frequency, peak position and phase, respectively. For an amplitude $\mu = 1$ (which implies a full width at half maximum in power of $1.76\tau_0$), the frequency shift $(\kappa(Z) - \kappa_i)$ may be transformed to physical units, yielding

$$\Delta\omega_0(z) = \frac{8|k_0''|t_R}{15\tau_0^4} z,$$

which is in satisfactorily agreement with the experimentally observed self-frequency shift. The factor τ_0^{-4} shows that the effect can be very large for pulse widths of a few tens of femtoseconds, however, it becomes negligible for pulse widths of several tens of picoseconds. As the group-velocity is frequency-dependent, this frequency shift also changes the soliton velocity from its original value. This effect produces a temporal displacement predicted by the perturbation method as (5.6) and indicating that self-similar accelerating pulses might exist.

5.2 Equilibrium solutions

The procedure for obtaining the ordinary differential equation which governs the accelerating pulses of equation (5.4) is very similar to the one used for the photorefractive model and described in §2.2. Defining a new variable $\eta = T - \frac{a}{4}Z^2 + bZ$ (with a and b constants) and inserting the *ansatz* $q(Z,T) = \exp[i\theta(Z,\eta)]F(\eta)$ into the equation (5.4), we obtain

$$\frac{1}{2}F'' + \left\{ -\theta_Z + \theta_\eta \left(\frac{a}{2}Z - b \right) - \frac{1}{2}\theta_\eta^2 \right\} F + F^3 - 2T_R F^2 F' + \\ + i \left\{ \frac{1}{2}\theta_{\eta\eta} F - \left(\frac{a}{2}Z - b \right) F' + \theta_\eta F' \right\} = 0. \tag{5.8}$$

Multiplying the imaginary part of the above equation by $2F$ and integrating with respect to η, we obtain

$$\theta_\eta(Z,\eta) = \frac{a}{2}Z - b + \frac{C(Z)}{F^2(\eta)}.$$

However, as pointed out for the photorefractive model, the existence of localised solutions $F(\eta)$ is only possible if we assert that $C(Z) = 0$. Another integration with respect to η yields

$$\theta(Z,\eta) = \left(\frac{a}{2}Z - b\right)\eta + B(Z).$$

Inserting the above expressions for the phase and its derivative with respect to η into the real part of equation (5.8) we obtain

$$\frac{1}{2}F'' + \left\{-\frac{a}{2}\eta - B'(Z) + \frac{1}{2}\left(\frac{a}{2}Z - b\right)^2\right\}F + F^3 - 2T_R F^2 F' = 0.$$

For F to be a function of η only, $-B'(Z) + \frac{1}{2}(\frac{a}{2}Z - b)^2$ must be constant, denoted by $-D/2$, say. Hence, we may obtain a final form for the phase

$$\theta(Z,\eta) = \left(\frac{a}{2}Z - b\right)\eta + \frac{1}{2}(D + b^2)Z - \frac{1}{4}baZ^2 + \frac{1}{24}a^2Z^3 + E, \qquad (5.9)$$

where E is an arbitrary constant. The ordinary differential equation for $F(\eta)$ then becomes

$$F'' + \left(-a\eta - D + 2F^2 - 4T_R F F'\right)F = 0. \qquad (5.10)$$

The above equation admits accelerating solutions ($a \neq 0$) only for $T_R \neq 0$. Furthermore, the two parameters a and T_R may be replaced by a single parameter. Hence defining new variables

$$F(\eta) = \frac{\gamma}{4T_\mathrm{R}}P(\zeta), \qquad \zeta = \frac{\gamma}{4T_\mathrm{R}}\eta, \qquad \gamma = a^{1/4}(4T_\mathrm{R})^{3/4}, \qquad (5.11)$$

we obtain the following ODE

$$P'' + (-C - \gamma\zeta + 2P^2 - \gamma P P')P = 0, \qquad (5.12)$$

where $C = (4T_\mathrm{R}/a)^{1/2}D$. Note that a perturbation method applied to ODE (5.10) shows a linear relation between T_R and a in the vicinity of $a = 0$ and $T_\mathrm{R} = 0$. Therefore, C is well defined and not necessarily zero at $a = 0$ and $T_\mathrm{R} = 0$. The new parameter γ may also be written in terms of C and the original parameters by $\gamma = 4T_\mathrm{R}(D/C)^{1/2}$. Note that T_R arises in the evolution equation (5.4) while the adjustable parameter D occurs in the phase expression (5.9). The transformation (5.11) may also be written as

$$F(\eta) = \left(\frac{D}{C}\right)^{1/2}P(\zeta), \qquad \zeta = \left(\frac{D}{C}\right)^{1/2}\eta. \qquad (5.13)$$

For $\gamma = 0$, the above equation reduces to

$$P'' - CP + 2P^3 = 0,$$

which admits the solution $P(\zeta) = G(\zeta - \zeta_0) \equiv \sqrt{C}\mathrm{sech}[\sqrt{C}(\zeta - \zeta_0)]$, with $\zeta = \zeta_0$ being the peak position. This sech solution was already expected since the case $T_R = 0$ and $a = 0$ reduces the evolution equation (5.4) to the NLS equation and our *ansatz* to its travelling solution.

The solutions to the full ODE (5.12) must be evaluated numerically. For this purpose, let us consider γ small and approximate the solution $P(\zeta)$ whose peak is located at ζ_0 by the first terms in the expansion

$$P(\zeta) = G(\zeta - \zeta_0) + \gamma P_1(\zeta) + \cdots . \tag{5.14}$$

Inserting the above expansion into equation (5.12), the $O(\gamma)$ approximation yields the following differential equation for $P_1(\zeta)$;

$$P_1'' + (-C + 6G^2)P_1 = \zeta G + G^2 G', \tag{5.15}$$

for which the related homogeneous equation is satisfied by G'. Hence, the solvability condition $\int_{-\infty}^{\infty}(\zeta G + G^2 G')G' d\zeta = 0$ for (5.15) gives

$$C = \frac{\sqrt{15}}{2}. \tag{5.16}$$

Requiring that $P_1(\zeta_0) = 0$ implies that, up to order $O(\gamma^2)$, the pulse peak location coincides with $\zeta = 0$. In fact, multiplying equation (5.12) by $2P'$ and integrating over $(-\infty, \zeta_0)$ yields

$$-(C + \gamma\zeta_0)P^2(\zeta_0) + P^4(\zeta_0) = -\gamma \int_{-\infty}^{\zeta_0} P^2 d\zeta + 2\gamma \int_{-\infty}^{\zeta_0} P^2 (P')^2 d\zeta.$$

Using the expansion (5.14) in the above equation, the approximation at order $O(\gamma)$ reads as

$$-\zeta_0 C = -\int_{-\infty}^{\zeta_0} G^2 d\zeta + 2\int_{-\infty}^{\zeta_0} G^2 (G')^2 d\zeta,$$

which, considering $C = \sqrt{15}/2$ as in (5.16), gives $\zeta_0 = 0$. Based on the above perturbation approach we expect that for $4T_R \ll (C/D)^{1/2}$ ($\gamma \ll 1$) there exists an accelerating pulse $P(\zeta)$ of amplitude close to $A = \sqrt{C} = (15/4)^{1/4}$.

The ODE for $P(\zeta)$ may be further simplified if we define a new variable ψ by $\gamma\psi = \gamma\zeta + C$. The differential equation for $P(\psi)$ is then given by

$$P'' + \left(-\gamma\psi + 2P^2 - \gamma PP'\right) P = 0. \tag{5.17}$$

The linearisation of the above ODE is equivalent to the Airy equation. This property has been observed for all the ODEs presented in this thesis as describing accelerating pulses and bending beams. Therefore, after the change of variable $z(\psi) = \gamma^{1/3}\psi$ we obtain the standard Airy equation. We expect the localised solutions $P(\psi)$ to behave like $\mathrm{Ai}(z)$ and $\mathrm{Bi}(z)$ at the right and left tails, respectively, in such a way that

$$\begin{aligned} P(\psi_1) =& c_1 \mathrm{Bi}[z(\psi_1)], \\ P'(\psi_1) =& c_1 \gamma^{1/3} \mathrm{Bi}'[z(\psi_1)], \\ P(\psi_2) =& c_2 \mathrm{Ai}[z(\psi_2)], \\ P'(\psi_2) =& c_2 \gamma^{1/3} \mathrm{Ai}'[z(\psi_2)]. \end{aligned}$$

The foregoing discussion suggests a shooting method as described below. We choose a small value for γ and expect a solution similar to a sech-profile with amplitude close to $A = (15/4)^{1/4}$. Therefore, we may use a first estimate for ψ_2 in the right tail as $\bar{\psi}_2 = \bar{\zeta}_2 + A^2/\gamma$ such that $\bar{\zeta}_2 = \ln(2A/\epsilon)/A$ (with ϵ small). We, then, integrate (5.17) backward from $\bar{\psi}_2$ with the following initial conditions;

$$P(\bar{\psi}_2) = c_2 \mathrm{Ai}[z(\bar{\psi}_2)] = \epsilon,$$

$$P'(\bar{\psi}_2) = c_2 \gamma^{1/3} \mathrm{Ai}'[z(\bar{\psi}_2)],$$

until we find a minimum for $P^2 + (P')^2$. Then ψ_2 is improved in order to minimize $P^2 + (P')^2$ until it becomes as small as ϵ^2.

Following the described shooting procedure we found single-humped localised solutions, denoted by $P(\psi;\gamma)$, for γ up to ~ 0.25. For small γ, the peak amplitude is very close to $C^{1/2} = (15/4)^{1/4}$ and the profile is also very close to the sech shape. However, as γ increases the asymmetry grows and the peak amplitude starts to deviate from that value (see Fig. 5.1). This growing asymmetry relates to the fact that the z-location of the pulse is also becoming closer to $z = 0$. This proximity to $z = 0$, where $\mathrm{Bi}(z)$ loses its exponential behaviour, imposes on the left tail a rather slow decay. A further increase in γ from ~ 0.25 forces the estimates of $z(\psi_1)$ and $z(\psi_2)$ to enter the negative axis, so not allowing any localised solution to exist.

Let us discuss the implications of such results in terms of the original variables. The pulses $P(\psi,\gamma)$ found, so far, are reasonably close in shape and in peak amplitude for all γ up to ~ 0.25. However, for each value T_R, corresponding to each of the pulse profiles $P(\psi;\gamma)$ we may construct a pulse profile $F(\eta) = (\gamma/4T_\mathrm{R})P(\psi;\gamma)$ of different amplitude. Its peak amplitude should be close to $\gamma C^{1/2}/4T_\mathrm{R}$ and it will evolve with Z with acceleration $a/4 = (\gamma/4)^4/T_\mathrm{R}^3$. Note that

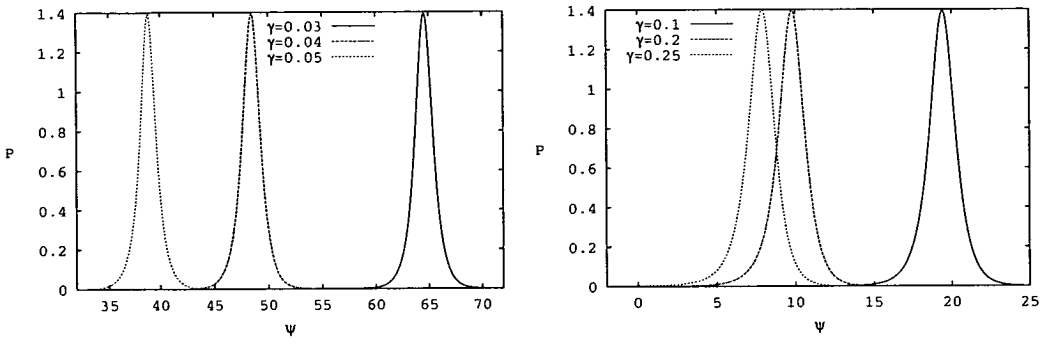

Figure 5.1: Pulse profiles for $\gamma = 0.03, 0.04, 0.05, 0.1, 0.2$ and 0.25.

$\gamma C^{1/2}/4T_{\mathrm{R}} \equiv D^{1/2}$ thus, for fixed T_{R} the different solutions may be parameterised by D which is approximately equal to the squared peak amplitude. The existence boundary $\gamma \sim 0.25$ implies that for each T_{R} there is a maximum of the permitted peak amplitude, approximately given by $\max(F_{\max}) \sim 0.25C^{1/2}/4T_{\mathrm{R}}$, which is inversely proportional to T_{R}. The growing asymmetry occurring for larger values of γ is, in the original variables, occurring for larger peak amplitude if T_{R} is fixed.

5.3 Linear stability equations and zero modes

Following the stability procedure used in the photorefractive and sliding filter models, we consider a solution composed of the equilibrium profile, $P(\psi)$, plus a small complex perturbation $w(Z,\psi)$; given by

$$q(Z,T) = \frac{\gamma}{4T_{\mathrm{R}}} \exp[i\theta(Z,\psi)][P(\psi) + w(Z,\psi)].$$

Introducing this solution into the evolution equation (5.4), and linearising, we obtain

$$2iw_{Z'} + w_{\psi\psi} - \frac{\gamma}{2}P^2(w_\psi + w_\psi^*) - (\gamma\psi - 4P^2 + \frac{3\gamma}{2}PP')w + (P^2 - \frac{\gamma}{2}PP')w^* = 0. \quad (5.18)$$

where we have used $Z = (4T_{\mathrm{R}}/\gamma)^2 Z'$. Complex conjugation of the above equation, yields

$$2iw^{*\prime}{}_Z - w^*_{\psi\psi} + \frac{\gamma}{2}P^2(w^*_\psi + w_\psi) + (\gamma\psi - 4P^2 + \frac{3\gamma}{2}PP')w^* - (P^2 - \frac{\gamma}{2}PP')w = 0. \quad (5.19)$$

Finally, the stability eigenvalue problem is obtained from (5.18) and (5.19) by considering that w depends exponentially upon Z' by the form $w(Z',\psi) = u(\psi)\mathrm{e}^{i\lambda Z'} +$

$v^*(\psi)\mathrm{e}^{-i\lambda^* Z'}$. Then, the eigenvalue problem reads

$$L\begin{pmatrix} u \\ v \end{pmatrix} = \lambda \begin{pmatrix} u \\ v \end{pmatrix}, \tag{5.20}$$

where the operator L is given by

$$\begin{pmatrix} \frac{1}{2}\partial_{\psi\psi} - \frac{\gamma}{2}\psi + 2P^2 - \frac{3\gamma}{4}PP' - \frac{\gamma}{4}P^2\partial_\psi & P^2 - \frac{\gamma}{4}PP' - \frac{\gamma}{4}P^2\partial_\psi \\ -P^2 + \frac{\gamma}{4}PP' + \frac{\gamma}{4}P^2\partial_\psi & -\frac{1}{2}\partial_{\psi\psi} + \frac{\gamma}{2}\psi - 2P^2 + \frac{3\gamma}{4}PP' + \frac{\gamma}{4}P^2\partial_\psi \end{pmatrix}$$

The spectrum of L will be investigated in §5.4 using the modified Evans function method. As in the other chapters, we first present the zero modes of L. The evolution equation (5.4) has four invariances, namely, invariances under translation in Z and in T, under change of phase and under Galilean transformations. Associated with those invariances, there are four arbitrary parameters in the equilibrium solution. The equilibrium solution written in terms of the variable ψ reads

$$q(Z,T) = \frac{\gamma}{4T_{\mathrm{R}}}\mathrm{e}^{i\theta(Z,\psi)}P(\psi),$$

with

$$\theta(Z,\psi) = \frac{4T_R}{\gamma}\left(\frac{\gamma^4}{2(4T_{\mathrm{R}})^3}Z - b\right)\psi + \frac{V^2}{2}Z - \frac{\gamma^4 b}{4(4T_{\mathrm{R}})^3}Z^2 + \frac{\gamma^8}{24(4T_{\mathrm{R}})^6}Z^3 + \theta_0$$

and

$$\psi = \frac{\gamma}{4T_{\mathrm{R}}}\left(T + bZ - \frac{\gamma^4}{4(4T_{\mathrm{R}})^3}Z^2\right) + \psi_0.$$

Note that the arbitrary temporal position of the pulse, expressed here by ψ_0, was omitted in §5.2. The derivatives of $q(Z,T)$ with respect to the four arbitrary parameters θ_0, ψ_0, b and γ are given by

$$\begin{aligned}
\frac{\partial q}{\partial \theta_0} &= \frac{\gamma}{4T_{\mathrm{R}}}\mathrm{e}^{i\theta}\{iP\} \\
\frac{\partial q}{\partial \psi_0} &= \frac{\gamma}{4T_{\mathrm{R}}}\mathrm{e}^{i\theta}\left\{\frac{i4T_R}{\gamma}\left(\frac{\gamma^4}{2(4T_{\mathrm{R}})^3}Z - b\right)P + P'\right\}, \\
\frac{\partial q}{\partial b} &= \frac{\gamma}{4T_{\mathrm{R}}}\mathrm{e}^{i\theta}\left\{\frac{i\gamma^4}{4(4T_{\mathrm{R}})^3}Z^2P + \frac{\gamma}{4T_{\mathrm{R}}}ZP' - \frac{i4T_{\mathrm{R}}}{\gamma}\psi P\right\}, \\
\frac{\partial q}{\partial \gamma} &= \frac{\gamma}{4T_{\mathrm{R}}}\mathrm{e}^{i\theta}\left\{i\left(\frac{4T_{\mathrm{R}}b\psi_0}{\gamma^2} - \frac{\gamma^2\psi_0}{2(4T_{\mathrm{R}})^2}Z - \frac{\gamma^7}{6(4T_{\mathrm{R}})^6}Z^3\right)P - \right. \\
&\quad \left. - \left(\frac{\psi_0}{\gamma} + \frac{\gamma^4}{(4T_{\mathrm{R}})^4}Z^2\right)P' + i\frac{2\gamma^2}{(4T_{\mathrm{R}})^2}Z\psi P + \frac{P + \psi P'}{\gamma} + P_\gamma\right\}.
\end{aligned}$$

Recalling the discussion in §2.4, we recognise the expressions in brackets as one proper eigenfunction and three generalised eigenfunctions corresponding to the zero eigenvalue. The proper eigenfunction is $y_1 = (P \quad -P)^T$ and the generalised eigenfunctions are

$$y_2 = (P' \quad P')^T, \qquad y_3 = (\psi P \quad -\psi P)^T,$$

$$y_4 = \left(\frac{P+\psi P'}{\gamma} + P_\gamma \quad \frac{P+\psi P'}{\gamma} + P_\gamma \right)^T.$$

In fact, $Ly_1 = 0$, $Ly_2 = \gamma y_1$, $Ly_3 = 2y_2$ and $Ly_4 = 4y_3$. Thus, $\lambda = 0$ is an eigenvalue of (5.20) with geometric multiplicity equal to one and algebraic multiplicity equal to four.

5.4 Evans function method

A brief inspection of the eigenvalue problem (5.20) shows that for ψ in the tails of the pulse solutions, where $P(\psi) \simeq 0$, the eigenvalue problem is equivalent to a decoupled pair of Airy equations. In other words, the asymptotic problem is described by the following operator

$$L_\infty = \begin{pmatrix} \frac{1}{2}(\partial_{\psi\psi} - \gamma\psi) & 0 \\ 0 & -\frac{1}{2}(\partial_{\psi\psi} - \gamma\psi) \end{pmatrix},$$

and with the suitable change of variables $z^\pm = \gamma^{-2/3}(\gamma\psi \pm 2\lambda)$ transforms to two standard Airy equations, namely

$$(\partial_{z^+z^+} - z^+)u = 0, \qquad (\partial_{z^-z^-} - z^-)v = 0.$$

The real domain of ψ transforms to horizontal lines in the $z^\pm$ complex planes. The lines coincide with each other and with the real axis whenever λ is real. As in §3.2, similar subsets should be defined, namely, $Q_1 = \{|\lambda| < \lambda_1\}$ and $Q_2 = \{|\lambda| > \lambda_2\}$. In Q_1, discrete localised modes are possible solutions to (5.20), i.e., solutions that match to $\mathrm{Ai}(z)$ to the right and to $\mathrm{Bi}(z)$ to the left. Whenever existing, they should manifest themselves as *internal modes*. The trivial example is $\lambda = 0$. For every $\lambda \in Q_2$ there exist a bounded solution to (5.20) that is similar to radiation modes. Note that λ_1 may be approximately estimated as the value $\lambda > 0$ for which $z^-(\psi_1) = 0$. Similarly, λ_2 is estimated by the positive λ that makes $z^-(\psi_1) = 0$.

Let us first comment on the limiting case $\gamma = 0$ for which the model reduces to the NLS model. The stability eigenvalue problem for the sech soliton has a single discrete eigenvalue at $\lambda = 0$, with algebraic multiplicity equal to four, inside the gap of the continuous spectrum. Considering the ODE (5.12) with $\gamma = 0$ and its solution $\sqrt{C}\mathrm{sech}(\sqrt{C}(\zeta - \zeta_0))$, we readily arrive at the typical continuous spectrum given by $Q = \{\lambda \in \mathbb{R} : |\lambda| \geq C/2\}$. In the original variables, we should consider the ODE (5.10) which for $\gamma = 0$ possesses the solution $G(\zeta) = \sqrt{D}\mathrm{sech}(\sqrt{D}(\eta - \eta_0))$. The continuous spectrum is, in this case, given by $Q_o = \{\lambda \in \mathbb{R} : |\lambda| \geq D/2 = G_{\max}^2/2\}$.

For $\gamma \neq 0$, the estimates of λ_1 and λ_2 imply that Q_1 is narrower than the gap $(-C/2, C/2)$ in Q and that Q_2 has a wider gap than Q. As γ tends to zero, Q_1 tends to the gap $(-C/2, C/2)$ and Q_2 tends to Q.

After these preliminary observations about the spectrum in the real axis, let us define the Evans function which will permit us to search for complex eigenvalues. The situation is again very similar to the photorefractive case, therefore, here the Evans function method will follow closely the procedure applied in the photorefractive case. The eigenvalue problem (5.20) is first rewritten as a first order system using the vector $Y = \begin{pmatrix} u & u_\psi & v & v_\psi \end{pmatrix}^T$. This yields

$$\frac{dY}{d\psi} = A(\psi, \lambda)Y, \tag{5.21}$$

where $A(\psi, \lambda)$ is given by

$$\begin{pmatrix} 0 & 1 & 0 & 0 \\ \gamma\psi - 4P^2 + \frac{3\gamma}{2}PP' + 2\lambda & \frac{\gamma}{2}P^2 & -2P^2 + \frac{\gamma}{2}PP' & \frac{\gamma}{2}P^2 \\ 0 & 0 & 0 & 1 \\ -2P^2 + \frac{\gamma}{2}PP' & \frac{\gamma}{2}P^2 & \gamma\psi - 4P^2 + \frac{3\gamma}{2}PP' - 2\lambda & \frac{\gamma}{2}P^2 \end{pmatrix}.$$

The unstable eigenvalues are such that their imaginary part is negative. However, due to the symmetry of the eigenvalue problem, to any pair of eigenvalues in the lower half-plane $(\lambda, -\lambda^*)$ there corresponds a pair in the upper half-plane $(-\lambda, \lambda^*)$. Therefore, we may search for unstable eigenvalues in either of the two half-planes. Let us, arbitrarily, choose the lower half-plane. For $\lambda \in \{\lambda : \lambda = \alpha + \beta i, \beta < 0\}$ to be an eigenvalue, the solution to (5.21) should be a linear combination of $Y_1^-(\psi, \lambda)$ and $Y_2^-(\psi, \lambda)$ and also a linear combination of $Y_3^+(\psi, \lambda)$ and $Y_4^+(\psi, \lambda)$, where these functions are solutions to (5.21) having decay behaviour as follows

$$\begin{aligned}
Y_1^-(\psi, \lambda) &\to \begin{pmatrix} \mathrm{Ai}_{-1}(z^+) & \gamma^{1/3}\mathrm{Ai}'_{-1}(z^+) & 0 & 0 \end{pmatrix}^T \quad \text{as} \quad \psi \to -\infty, \\
Y_2^-(\psi, \lambda) &\to \begin{pmatrix} 0 & 0 & \mathrm{Ai}_1(z^-) & \gamma^{1/3}\mathrm{Ai}'_1(z^-) \end{pmatrix}^T \quad \text{as} \quad \psi \to -\infty, \\
Y_3^+(\psi, \lambda) &\to \begin{pmatrix} \mathrm{Ai}_0(z^+) & \gamma^{1/3}\mathrm{Ai}'_0(z^+) & 0 & 0 \end{pmatrix}^T \quad \text{as} \quad \psi \to +\infty, \\
Y_4^+(\psi, \lambda) &\to \begin{pmatrix} 0 & 0 & \mathrm{Ai}_0(z^-) & \gamma^{1/3}\mathrm{Ai}'_0(z^-) \end{pmatrix}^T \quad \text{as} \quad \psi \to +\infty.
\end{aligned}$$

The intersection of those subspaces of solutions, namely, the subspace spanned by $\{Y_1^-, Y_2^-\}$ and the subspace spanned by $\{Y_3^+, Y_4^+\}$, is then recognised as the zeros of the Evans function defined by

$$D_{\mathrm{ai}}(\lambda) = \begin{vmatrix} Y_{11}^-(\psi^*, \lambda) & Y_{21}^-(\psi^*, \lambda) & Y_{31}^+(\psi^*, \lambda) & Y_{41}^+(\psi^*, \lambda) \\ Y_{12}^-(\psi^*, \lambda) & Y_{22}^-(\psi^*, \lambda) & Y_{32}^+(\psi^*, \lambda) & Y_{42}^+(\psi^*, \lambda) \\ Y_{13}^-(\psi^*, \lambda) & Y_{23}^-(\psi^*, \lambda) & Y_{33}^+(\psi^*, \lambda) & Y_{43}^+(\psi^*, \lambda) \\ Y_{14}^-(\psi^*, \lambda) & Y_{24}^-(\psi^*, \lambda) & Y_{34}^+(\psi^*, \lambda) & Y_{44}^+(\psi^*, \lambda) \end{vmatrix}, \tag{5.22}$$

where ψ^* is the peak position of $P(\psi)$.

The procedure used to search for unstable eigenvalues consist of the evaluation of the Evans function along a path in the lower half λ-plane. The chosen path is a semicircle as shown in §3.2, Fig. 3.9. The distance to the real axis was also chosen to be $\epsilon = 5\times10^{-5}$ and, due to the chaotic behaviour produced by numerical evaluation of $D_{\rm ai}(\lambda)$ for large λ, R must be restricted to a value around 15. The argument principle is then used to count the number of zeros inside the semicircle. Apart from the numerical approximations to the zero eigenvalue occurring close to $\lambda = 0$, no other zeros of $D_{\rm ai}(\lambda)$ were found. These numerical approximations of the zero eigenvalue arise, in the lower half-plane, as one imaginary value or as a pair of complex values falling in the region where $D_{\rm ai}(\lambda)$ behaves like λ^4 in such a way as explained in the photorefractive context (§3.2, Fig. 3.11).

The Evans function method was also used to seek possible internal modes, i.e, eigenvalues in the real set Q_1. For this purpose, we replaced $\mathrm{Ai}_{-1}(z)$ and $\mathrm{Ai}_1(z)$ by $\mathrm{Bi}(z)$ in the functions $Y_1^-(\psi,\lambda)$ and $Y_2^-(\psi,\lambda)$. We have evaluated the Evans function for λ in the estimated Q_1 and, apart from the $\lambda = 0$, no other eigenvalues were found.

In conclusion, the Evans function method applied to the accelerating solutions of the NLS with intrapulse Raman scattering indicates stability and absence of internal modes.

5.5 Direct numerical integration

The integration of the evolution equation (5.4) produces results in agreement with the acceleration regime and with the stability properties presented in the previous section. Fig. 5.2 shows the parabolic trajectory of the peak pulse in complete agreement with $T^p = T_0^p + 4D^2T_{\rm R}/15Z^2$ for an initial condition $q(Z,T) = (4/15)^{1/4}D^{1/2}P(\psi;\gamma)$ with $T = (15/4)^{1/4}/D^{1/2}\psi$, $T_{\rm R} = 0.03$ and $D = 1.345$ ($\gamma = 0.1$).

Their stability was also tested using initial conditions that differ from the profiles $P(\psi;\gamma)$ by small perturbations (sinusoidal disturbances or small multiples of $P(\psi;\gamma)$ or of $P'(\psi;\gamma)$). In each case, the initial condition evolves to a nearby equilibrium profile which then propagates steadily, with constant acceleration. In that relaxation, we observe decaying amplitude oscillations. They are never persistent, non-decaying oscillations so confirming the absence of internal modes. The frequency of such amplitude oscillations is also in agreement with the discussion in §5.4 of characteristics of the real spectrum. For pulses of equal peak amplitude (D approximately equal), as $T_{\rm R}$ increases (γ increases) the oscillation

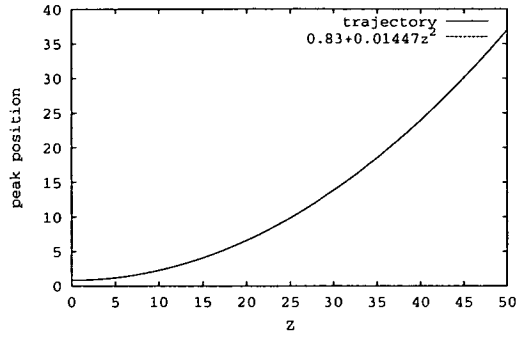

Figure 5.2: Peak position in coincidence with the predicted parabola for an initial condition obtained from $P(\psi;\gamma)$ with $T_R = 0.03$ and $D = 1.345$ ($\gamma = 0.1$).

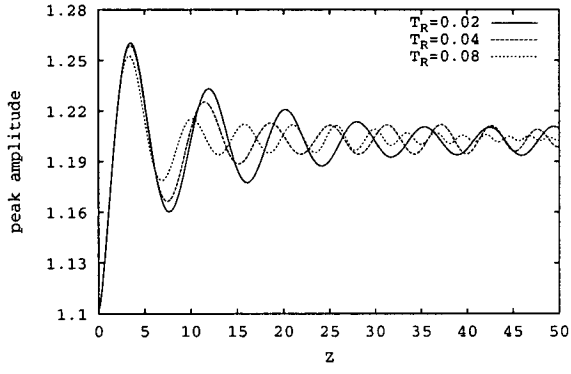

Figure 5.3: Peak amplitude for initial conditions obtained from $P(\psi;\gamma)$ and scaled by 10%. Three different values of $T_{\rm R}$ and γ chosen as $\gamma = 4T_{\rm R}C^{-1/2}$ to obtain approximately equal peak amplitudes (equal value of D).

frequency also increases. Remember that we expect that this frequency coincides with the lower frequency of the radiation-like modes [66]. Using the nomenclature of §5.4, we expect that this frequency coincides with the limit of Q_2 (appropriately scaled by $(4/15)^{1/2}D$ to conform with the original variables), whose gap was estimated to increase with γ. Fig. 5.3 shows the amplitude oscillations obtained for three initial conditions obtained from the self-similar profiles multiplying by the factor 1.1. The value of γ was chosen to obtain approximately the same peak amplitude. Moreover, simulations performed with smaller values of $T_{\rm R}$ confirm that this relaxation frequency approaches the characteristic frequency of the NLS sech soliton $|q|^2_{\rm max}/2$ as $T_{\rm R}$ tends to zero.

5.6 Conclusion

As suggested by the temporal displacement, proportional to Z^2, presented by pulses suffering intrapulse Raman scattering, the evolution equation admits self-

similar accelerating solutions. The accelerating profiles are parameterised by a single parameter γ. In the original variables, each profile characterised by γ maps a family of different peak amplitude (and different acceleration) solutions distinguished by T_{R}. For fixed T_{R}, the typical asymmetry of the accelerating profiles increases with increasing amplitude.

The Evans function method was used and revealed that the pulses are stable for all γ, with complete absence of internal modes. These stability results were then confirmed by the direct integration of the evolution equation.

Note that the general characteristics of the spectrum of the NLS soliton (such as stability, absence of internal modes, gap in the frequency of radiation-like modes) are preserved by the introduction of intrapulse Raman scattering ever though the consequent soliton accelerates.

Chapter 6

Conclusion

The main achievement of this work consists of the modification of the Evans function to deal with the stability of the accelerating solitons. This has required an adaption of the Evans function to cope with Airy function asymptotics. The resulting generalisation has successfully revealed many spectral features of the stability eigenvalue problems associated with some accelerating solitons known in nonlinear optics. We shall however point out some aspects which remain yet for discussion. While the basic idea of the Evans function is quite intuitive, the validity of the method is guaranteed only by rigorous demonstration of several fundamental details. Examples are: the demonstration that the solutions to the full eigenvalue problem asymptotically tend to the solutions of the asymptotic problem and the demonstration that those solutions depend analytically on their initial data. For the standard Evans function, these issues are treated by the Levinson theorem [27] and its generalisations. However, our implementation of the new version of the Evans function has not included rigorous mathematical demonstrations such as those mentioned above. Nevertheless, our Evans function results were confirmed by direct numerical simulation, which without being a proof, supports the validity of our approach.

Another issue that was not rigorously discussed is the structure of the continuous spectrum. While we know of theoretical results that predict the continuous spectrum of the operator L from the knowledge of the continuous spectrum of L_∞ whenever L_∞ corresponds to a system of constant coefficient differential equations [50], we do not know of any similar result applicable to our non-autonomous system. The asymptotic eigenvalue problem for the accelerating solutions has been found to be a system of Airy equations defined in the complex plane. If we mean by continuous spectrum a set of λ so that for every λ within the set there is a bounded solution, then P is the continuous spectrum if for every $\lambda \in P$ the lines $z^+(x,\lambda)$ and $z^-(x,\lambda)$ (where $x \in \mathbb{R}$ is the original spatial coordinate) coincide with any of the Airy sector boundaries. In the photorefractive and intrapulse

Raman scattering cases, this P is the entire real line, but in the sliding-frequency filter case such a set does not exist. However, the possibility that the real line is the continuous spectrum of the full eigenvalue problems for the photorefractive case and for intrapulse Raman scattering has not been investigated. In these cases, our discussion about solutions to the eigenvalue problem for real λ only includes the identification of two subsets where localised modes are possible and radiation-like modes exist. The latter was mainly motivated by results obtained with the Evans function method and through direct numerical integration.

Let us also mention that recently other work has been reported in which the Evans function has been adjusted to modified Bessel functions asymptotics [86]. With more than 30 years of history, the Evans function is continually proving to be a powerful tool to investigate the stability of nonlinear waves. The predictions in this thesis have useful implications for nonlinear optics. The methodology developed for coping with Airy function asymptotics of the eigenvalue problem also raises a number of issues worthy of closer analytic study.

Appendix A

Airy functions

The Airy functions are special functions which are solutions to the linear second-order ordinary differential equation (Airy's equation) given by

$$\frac{d^2w}{dx^2} = xw. \tag{A.1}$$

For real x, the Airy functions $\mathrm{Ai}(x)$ and $\mathrm{Bi}(x)$ are two real linearly independent solutions to (A.1). These solutions are distinguished by their behaviour as $x \to +\infty$. While $\mathrm{Ai}(x)$ tends exponentially to zero as $x \to +\infty$, $\mathrm{Bi}(x)$ grows exponentially. As $x \to -\infty$, they both have algebraically decaying oscillations. The oscillations have the same amplitude but differ in phase by $\pi/2$.

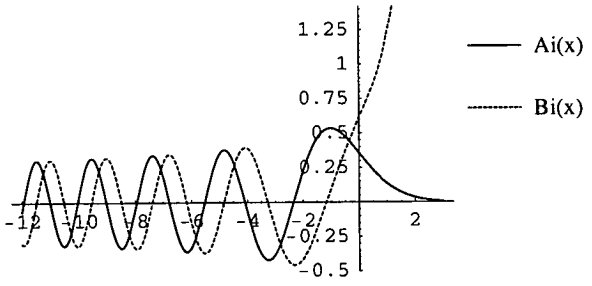

Figure A.1: Graph of the Airy functions $\mathrm{Ai}(x)$ and $\mathrm{Bi}(x)$ for real argument.

Whenever the Airy equation is defined in the complex plane, it is usual to replace x by z, namely

$$\frac{d^2w}{dz^2} = zw. \tag{A.2}$$

In the complex case, $\mathrm{Ai}(z)$ and $\mathrm{Bi}(z)$ denote also two linearly independent solutions. These are analytic continuations of $\mathrm{Ai}(x)$ and $\mathrm{Bi}(x)$ into the complex plane. One of the possible representations for the Airy functions uses the Bessel functions. The NAG routine, used to evaluate the Airy functions in our work, uses that representation. We reproduce here the relations between the Airy functions

and the modified Bessel functions I_ν of order ν:

$$\mathrm{Ai}(z) = \frac{1}{3}\sqrt{z}\left(I_{-1/3}(\zeta) - I_{1/3}(\zeta)\right),$$
$$\mathrm{Bi}(z) = \sqrt{\frac{z}{3}}\left(I_{1/3}(\zeta) + I_{-1/3}(\zeta)\right),$$

where $\zeta = \frac{2}{3}z^{3/2}$. Others solutions to (A.2) include $\mathrm{Ai}(ze^{\pm 2\pi i/3})$ and $\mathrm{Bi}(ze^{\pm 2\pi i/3})$. Note that all the solutions to the Airy equation are entire functions, i.e., analytic functions in the whole complex domain $\mathbb{C}$. Note also that no more than two solutions can be linearly independent.

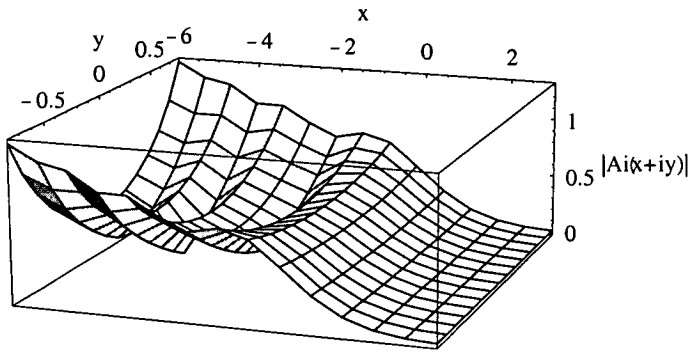

Figure A.2: Graph of the magnitude of $\mathrm{Ai}(x + iy)$.

Standard asymptotic theory [82] of the Airy solutions involves $\mathrm{Ai}(z)$ and $\mathrm{Ai}(ze^{\pm 2\pi i/3})$. Furthermore, it is usual to use the following notation

$$\mathrm{Ai}_0(z) = \mathrm{Ai}(z), \qquad \mathrm{Ai}_1(z) = \mathrm{Ai}(ze^{-2\pi i/3}), \qquad \mathrm{Ai}_{-1}(z) = \mathrm{Ai}(ze^{2\pi i/3}).$$

Thus, while the function values of $\mathrm{Ai}_1(z)$ are obtained from those of $\mathrm{Ai}_0(z)$ by rotation anti-clockwise through $\pi/3$ in the z-plane, the function values of $\mathrm{Ai}_{-1}(z)$ are obtained from those of $\mathrm{Ai}_0(z)$ by rotation clockwise through $\pi/3$. This has motivated the division of the complex plane into three $2\pi/3$ sectors, namely, S_0, S_1 and S_{-1}. These correspond to $|\arg(z)| \leq \pi/3$, $\pi/3 \leq \arg(z) \leq \pi$ and $-\pi \leq \arg(z) \leq -\pi/3$, respectively.

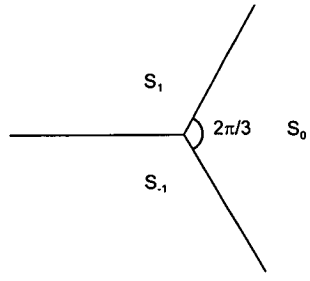

The asymptotic behaviour of the three functions in the neighborhood of infinity arises from the corresponding asymptotic expansion of $\mathrm{Ai}(z)$, given by

$$\mathrm{Ai}(z) \sim \frac{e^{-\zeta}}{2\sqrt{\pi} z^{1/4}} \sum_{s=0}^{\infty} (-1)^s \frac{u_s}{\zeta^s} \qquad |\arg(z)| < \pi,$$

$$\mathrm{Ai}(-z) \sim \frac{1}{\sqrt{\pi} z^{1/4}} \left(\cos(\zeta - \tfrac{\pi}{4}) \sum_{s=0}^{\infty} (-1)^s \frac{u_{2s}}{\zeta^{2s}} + \sin(\zeta - \tfrac{\pi}{4}) \sum_{s=0}^{\infty} (-1)^s \frac{u_{2s+1}}{\zeta^{2s+1}} \right) \qquad |\arg(z)| < \tfrac{2}{3}\pi,$$

where $u_0 = 1$ and

$$u_s = \frac{(2s+1)(2s+3)(2s+5)\cdots(6s-1)}{(216)^s s!}.$$

The asymptotic expansion of its first derivative is given by

$$\mathrm{Ai}'(z) \sim -\frac{z^{1/4} e^{-\zeta}}{2\sqrt{\pi}} \sum_{s=0}^{\infty} (-1)^s \frac{v_s}{\zeta^s} \qquad |\arg(z)| < \pi,$$

$$\mathrm{Ai}'(-z) \sim \frac{z^{1/4}}{\sqrt{\pi}} \left(\sin(\zeta - \tfrac{\pi}{4}) \sum_{s=0}^{\infty} (-1)^s \frac{v_{2s}}{\zeta^{2s}} - \cos(\zeta - \tfrac{\pi}{4}) \sum_{s=0}^{\infty} (-1)^s \frac{v_{2s+1}}{\zeta^{2s+1}} \right) \qquad |\arg(z)| < \tfrac{2}{3}\pi,$$

where $v_0 = 1$ and

$$v_s = -\frac{6s+1}{6s-1} u_s.$$

Clearly, $\mathrm{Ai}_0(z)$ is exponentially decaying within S_0 and exponentially growing within S_1 and S_{-1}. Similarly, $\mathrm{Ai}_j(z)$ $(j = 1, -1)$ is exponentially decaying within S_j and exponentially growing within the other two sectors. Each of the three functions has algebraic decay as $|z| \to \infty$ on all three of the sector borders, namely, $\arg(z) = \pi$ and $\arg(z) = \pm\pi/3$. Furthermore, the algebraic decay is accompanied by oscillations on one of these sector borders. Thus, $\mathrm{Ai}_0(z)$ exhibits such oscillations for z on the negative real axis, $\arg(z) = \pi$, and, accordingly to their definition, $\mathrm{Ai}_1(z)$ and $\mathrm{Ai}_{-1}(z)$ have the same behaviour for z on the radial lines $\arg(z) = -\pi/3$ and $\arg(z) = \pi/3$, respectively.

From the standard theory of asymptotic estimation of solutions of linear ordinary differential equations [82], $\mathrm{Ai}_j(z)$ $(j = -1, 0, 1)$ is called a *recessive* solution at infinity within S_j and a *dominant* solution at infinity within the other two sectors. The *recessive* and *dominant* characters are tied to a particular singularity of the ODE. The *recessive* solution is the smaller solution as the singularity is

approached. Any solution which is linearly independent of the *recessive* solution is said to be *dominant*. The ratio of magnitudes of the dominant/recessive solutions tends to infinity as the singularity is approached. For the Airy equation, the only singularity is an irregular singularity at infinity. The *recessive* solution at infinity changes as we move in the complex plane by a rotation of $2\pi/3$, as was discussed above. Another notion related to recession and dominance is the *numerically satisfactory* pair. The *numerically satisfactory* pair of solutions in the neighbourhood of a singularity should be composed of the recessive and one of the dominant solutions.

Appendix B

Pseudospectral method to solve the partial differential equation

Here we briefly describe the pseudospectral method used in this thesis to solve the partial differential equations. The method is based on Fornberg and Whitham [35]. As an example, let us consider the evolution equation for the photorefractive model given by

$$q_z - iq_{xx} = -i\frac{q}{1+|q|^2} + i\gamma\frac{(|q|^2)_x q}{1+|q|^2} = v(z,x), \tag{B.1}$$

and apply a Fourier transform to the x variable, yielding an equation in the Fourier k-space

$$\hat{q}_z(z,k) - i(ik)^2\hat{q}(z,k) = \hat{v}(z,k), \tag{B.2}$$

where the $\hat{}$ stands for Fourier transform given by

$$\hat{h}(k) = \mathcal{F}(h(x)) = \int_{-\infty}^{\infty} h(x)\, \mathrm{e}^{ikx} dx.$$

Note that the nonlinear part $v(z,x)$ has been transformed as one entity. Multiplying (B.2) by e^{ik^2z} we obtain

$$\frac{d}{dz}(\mathrm{e}^{ik^2z}\hat{q}) = \mathrm{e}^{ik^2z}\hat{v},$$

which may be interpreted as an ordinary differential equation for $X(z,k) = \mathrm{e}^{ik^2z}\hat{q}(z,k)$ as follows

$$X_z = F(X,z), \tag{B.3}$$

which will be integrated using a Runge-Kutta method.

The Fourier transform plays an important role in the method and will be evaluated numerically. Let us introduce the definition of the discrete Fourier transform of a numerically defined function $h(x)$. Suppose that we have $h(x)$ defined by N values at N equidistant points spaced by Δx

$$h_j \equiv h(x_j), \qquad x_j = j\Delta x, \qquad j = 0,1,2,\ldots,N-1.$$

The Fourier transform $\hat{h}(k) = \mathcal{F}(h(x))$ may also be defined numerically by

$$\hat{h}_n \equiv h(k_n) = \sum_{j=0}^{N-1} h_j e^{ik_n x_j}, \qquad k_n = \frac{2\pi n}{N\Delta x}, \qquad n = -\frac{N}{2}, \ldots, \frac{N}{2}.$$

The inverse formula that permit us to recover the h_j's from the $\hat{h}_n$'s is given by

$$h_j = \mathcal{F}^{-1}(\hat{h}_n) = \frac{1}{N} \sum_{n=-N/2}^{N/2} \hat{h}_n e^{-ik_n x_j}.$$

These transforms may be performed in an efficient way using the fast Fourier transform (FFT) which we shall use in our algorithm.

The algorithm to solve the partial differential equation (B.1) comprises the following steps:

- Transformation of $q(z_0, x_j)$, $j = 0, 1, \ldots, N-1$ to the Fourier space, yielding $\hat{q}(z_0, k_n)$, $n = -N/2, \ldots, N/2$,
- Evaluation of the first derivative in the Fourier space as

$$\hat{q_x}(z_0, k_n) = ik_n \hat{q}(z_0, k_n),$$

- Obtaining the first derivative in the physical space by performing an inverse Fourier transform

$$q_x(z_0, x_j) = \mathcal{F}^{-1}(\hat{q_x}(z_0, k_n)),$$

- Evaluation of the nonlinear term $v(z_0, x_j)$ using $q(z_0, x_j)$ and $q_x(z_0, x_j)$,
- Transformation of $v(z_0, x_j)$ to the Fourier space, giving $\hat{v}(z_0, k_n)$,
- Determination of the initial data for (B.3)

$$X_0(z_0, k_n) = e^{ik_n^2 z_0} \hat{q}(z_0, k_n),$$

$$F(X_0, z_0) = e^{ik_n^2 z_0} \hat{v}(z_0, k_n),$$

- Integration of (B.3) by a fourth-order Runge-Kutta method. We note that, within the Runge-Kutta procedure, it is necessary to return to the physical space three times in order to evaluate the appropriate v. However, all the propagation steps in z are made in the Fourier space.
- Return to the original variable

$$\hat{q}(z_0 + \Delta z, k_n) = e^{-ik_n^2 (z_0 + \Delta z)} X_f(z_0 + \Delta z, k_n),$$

- Return to the physical space

$$q(z_0 + \Delta z, x_j) = \mathcal{F}^{-1}(\hat{q}(z_0 + \Delta z, k_n)).$$

The method requires the use of absorbing boundaries [53]. This is accomplished introducing a damping term $-\Gamma(x)$ in the nonlinear term v. The damping term is only nonzero in the boundaries of the numerical x-domain and it works by absorbing outgoing radiation.

Bibliography

[1] M. J. Ablowitz, D. J. Kaup, A. C. Newell, and H. Segur. Method for solving the sine-Gordon equation. *Physical Reviews Letters*, 30:1262–1264, 1973.

[2] V. V. Afanasjev, P. L. Chu, and Y. S. Kivshar. Breathing spatial solitons in non-Kerr media. *Opt. Lett.*, 22(18):1388–1390, 1997.

[3] A. L. Afendikov and T. J. Bridges. Instability of the Hocking-Stewartson pulse and its applications for three-dimensional Poiseuille flow. *Proc. R. Soc. Lond. A*, 457:257–272, 2000.

[4] G. P. Agrawal. *Nonlinear fiber optics.* Academic Press, 2001.

[5] V. Aleshkevich, Y. Kartashov, and V. Vysloukh. Self-bending of the coupled spatial soliton pairs in a photorefractive medium with drift and diffusion nonlinearity. *Phys. Rev. E*, 63:16603, 2000.

[6] J. Alexander, R. Gardner, and C. Jones. A topological invariant arising in the stability analysis of travelling waves. *J. Reine Angew. Math.*, 410:167–212, 1990.

[7] J. C. Alexander and R. Sachs. Linear instability of solitary waves of a Boussinesq-type equation: a computer assisted computation. *Nonlin. World*, 2:471–507, 1995.

[8] L. Allen and T. J. Bridges. Numerical exterior algebra and the compound matrix method. *Numer. Math.*, 92:197–232, 2001.

[9] D. Anderson. Variational approach to nonlinear pulse propagation in optical fibers. *Phys. Rev. A*, 27(6):3135–3145, 1983.

[10] A. K. Atieh, P. Myslinski, J. Chrostowski, and P. Galko. Measuring the Raman time constant (T_R) for soliton pulses in standard single-mode fiber. *J. Lightwave Technol.*, 17(2):216–221, 1999.

[11] N. J. Balmforth, R. V. Craster, and S. J. A. Malham. Unsteady fronts in an autocatalytic system. *Proc. R. Soc. Lond. A*, 455(1984):1401–1433, 1999.

[12] J. J. Beech-Brandt and N. F. Smyth. Pulse evolution in nonlinear optical fibers with sliding-frequency filters. *Phys. Rev. E*, 63:56604, 2001.

[13] G. Birkhoff and G-C. Rota. *Ordinary differential equations.* John Wiley & Sons, 1989.

[14] J. E. Bjorkhol and A. Ashkin. cw self-focusing and self-traping of light in sodium vapour. *Phys. Rev. Lett.*, 32:129–132, 1974.

[15] K. J. Blow and D. Wood. Theoretical description of transient stimulated Raman scattering in optical fibers. *IEEE J. Quant. Elect.*, 25(12):2665–2673, 1989.

[16] T. J. Bridges, G. Derks, and G. Gottwald. Stability and instability of solitary waves of the fifth-order KdV equation: a numerical framework. *Physica D*, 172:190–216, 2002.

[17] S. Burtsev and D. J. Kaup. Effective control of a soliton by sliding-frequency guiding filters. *J. Opt. Soc. Am. B*, 14(3):627–635, 1997.

[18] M. I. Carvalho, S. R. Singh, and D. N. Christodoulides. Self-deflection of steady-state bright spatial solitons in biased photorefractive crystals. *Opt. Commun.*, 120:311–315, 1995.

[19] Y. Chen. Stability criterion of coupled soliton states. *Phys. Rev. E*, 57(3):3542–3550, 1998.

[20] S. S. Chern, W. H. Chen, and K. S. Lam. *Lectures on differential geometry.* World Scientific, Singapore, 1999.

[21] R. Y. Chiao, E. Garmire, and C. H. Townes. Self-trapping of optical beams. *Phys. Rev. Lett.*, 13:479, 1964.

[22] D. N. Christodoulides and M. I. Carvalho. Bright, dark and gray spatial soliton states in photorefractive media. *J. Opt. Soc. Am. B*, 12(9):1628–1633, 1995.

[23] E. DelRe, B. Crosignani, P. DiPorto, E. Palange, and A. J. Agranat. Electro-optic beam manipulation through photorefractive needles. *Opt. Lett.*, 27:2188–2190, 2002.

[24] E. DelRe, M. Tamburrini, and A. J. Agranat. Soliton electro-optic effects in paraelectrics. *Opt. Lett.*, 25:963–965, 2000.

[25] E. M. Dianov, Z. S. Nikonova, A. M. Prokhorov, and V. N. Serkin. Nonlinear dynamics of the soliton enhancement of stimulated Raman-scattering in fiber-optical communication lines. *Dokl. Akad. Nauk. SSSR*, 283:1342–1346, 1985.

[26] G. Duree, J. L. Shultz, G. Salamo, M. Segev, A. Yariv, B. Crosignani, P. DiPorto, E. Sharp, and R. R. Neurgaonkar. Observing of self-trapping of an optical beam due to the photorefractive effect. *Phys. Rev. Lett.*, 71:533, 1993.

[27] M. S. P. Eastham. *The asymptotic solution of linear differential systems: applications of the Levinson theorem.* Clarendon Press, Oxford, 1989.

[28] C. Etrich, U. Peschel, F. Lederer, and B. A. Malomed. Stability of temporal chirped solitary waves in quadratically nonlinear media. *Phys. Rev. E*, 55(5):6155–6161, 1997.

[29] C. Etrich, U. Peschel, F. Lederer, B. A. Malomed, and Y. S. Kivshar. Origin of the persistent oscillations of solitary waves in nonlinear quadratic media. *Phys. Rev. E*, 54(4):4321–4324, 1996.

[30] J. W. Evans. Nerve axon equations: I. Linear approximations. *Indiana U. Math. J.*, 21:877–885, 1972.

[31] J. W. Evans. Nerve axon equations: II. Stability at rest. *Indiana U. Math. J.*, 22:75–90, 1972.

[32] J. W. Evans. Nerve axon equations: III. Stability of the nerve impulse. *Indiana U. Math. J.*, 22:577–593, 1972.

[33] J. W. Evans. Nerve axon equations: IV. The stable and unstable impulse. *Indiana U. Math. J.*, 24:1169–1190, 1975.

[34] M. Facão and D. F. Parker. Stability of screening solitons in photorefractive media. *Phys. Rev. E*, 68(1):16610, 2003.

[35] B. Fornberg and G. B. Whitham. A numerical and theoretical study of certain nonlinear wave phenomena. *Phil. Trans. R. Soc. Lond. A*, 289(1361):373–404, 1978.

[36] W. Forysiak, F. M. Knox, and N. J. Doran. Average soliton propagation in periodically amplified systems with stepwise dispersion-profiled fiber. *Opt. Lett.*, 19:174, 1994.

[37] L. Gagnon and P. A. Bélanger. Soliton self-frequency shift versus Galilean-like symmetry. *Opt. Lett.*, 15(9):466–468, 1990.

[38] T. W. Gamelin. *Complex Analysis.* Springer-Verlag, New York, 2001.

[39] C. S. Gardner, J. M. Greene, M. D. Kruskal, and R. M. Miura. Method for solving the Korteweg-deVries equation. *Phys. Rev. Lett.*, 19(19):1095–1097, 1967.

[40] R. A. Gardner and K. Zumbrun. The gap lemma and geometric criteria for instability of viscous shock profiles. *Comm. Pure Appl. Math.*, 51:797–855, 1998.

[41] J. P. Gordon. Theory of the soliton self-frequency shift. *Opt. Lett.*, 11(10):662–664, 1986.

[42] V. Gubernov, G. N. Mercer, H. S. Sidhu, and R. O. Weber. Evans function stability of combustion waves. *SIAM J. Appl. Math.*, 63(4):1259–1275, 2003.

[43] A. Guo, M. Henry, G. J. Salamo, M. Segev, and G. L. Wood. Fixing multiple waveguides induced by photorefractive solitons: directional couplers and beam splitters. *Opt. Lett.*, 26:1274–1276, 2001.

[44] A. Hasegawa. Amplification and reshaping of optical solitons in a glass-fiber: (IV). Use of the stimulated raman process. *Opt. Lett.*, 8:650–652, 1983.

[45] A. Hasegawa and Y. Kodama. Guiding-center soliton in optical fibers. *Opt. Lett.*, 15(24):1443–1445, 1990.

[46] A. Hasegawa and Y. Kodama. Guiding-center soliton. *Phys. Rev. Lett.*, 66(2):161–164, 1991.

[47] A. Hasegawa, Y. Kodama, and A. Maruta. Recent progress in dispersion-managed soliton transmission technologies. *Opt. Fiber Technol*, 3(3):197–213, 1997.

[48] A. Hasegawa, S. Kumar, and Y. Kodama. Reduction of collision-induced time jitters in dispersion-managed soliton transmission systems. *Opt. Lett.*, 21:39, 1996.

[49] A. Hasegawa and F. Tappert. Transmission of stationary nonlinear optical pulses in dispersive dielectric fibers. I. Anomalous dispersion. *Appl. Phys. Lett.*, 23:142–144, 1973.

[50] D. Henry. *Geometric theory of semilinear parabolic equations*, volume 840 of *Lecture Notes in Mathematics*. Springer-Verlag, Berlin, 3rd edition, 1993.

[51] M. Hercher. Laser-induced damage in transparent media. *J. Opt. Soc. Am.*, 1964.

[52] D. D. Holm, J. E. Marsden, T. Ratiu, and A. Weinstein. Nonlinear stability of fluid and plasma equilibria. *Phys. Rep.*, 123:1–116, 1985.

[53] F. If, P. Berg, P. L. Christiansen, and O. Skovgaard. Split-step spectral method for nonlinear Schrödinger equation with absorbing boundaries. *J. Comput. Phys.*, 72:501–503, 1987.

[54] L. Jinsong and L. Keqing. Screening-photovoltaic spatial solitons in biased photovoltaic-photorefractive crystals and their self-deflection. *J. Opt. Soc. Am. B*, 16(4):550–555, 1999.

[55] T. Kapitula. The Evans function and generalized Melnikov integrals. *SIAM J. Math. Anal.*, 30(2):273–297, 1998.

[56] T. Kapitula and B. Sandstede. Stability of bright solitary-wave solutions to perturbed nonlinear Schrödinger equations. *Physica D*, 124:58–103, 1998.

[57] V. I. Karpman and E. M. Maslov. Perturbation theory for solitons. *Sov. Phys. JETP*, 46(2):281–291, 1978.

[58] D. J. Kaup. A perturbation expansion for the Zakharov-Shabat inverse scattering transform. *SIAM J. Appl. Math.*, 31:121–133, 1976.

[59] Y. S. Kivshar. Bright and dark spatial solitons in non-Kerr media. *Opt. Quant. Electron.*, 30:571–614, 1998.

[60] M. Klotz, H. Meng, G. J. Salamo, M. Segev, and G. L. Wood. Fixing the photorefractive soliton. *Opt. Lett.*, 24:77–79, 1999.

[61] Y. Kodama. Normal form for weakly dispersive wave equations. *Phys. Lett. A*, 122:193–196, 1985.

[62] Y. Kodama and A. Hasegawa. Nonlinear pulse propagation in a monomode dielectric guide. *IEEE J. Quantum Elect.*, 23(5):510–524, 1987.

[63] Y. Kodama and S. Wabnitz. Analysis of soliton stability and interactions with sliding filters. *Opt. Lett.*, 19(3):162–164, 1994.

[64] W. Królikowski, N. Akhmediev, B. Luther-Davies, and M. Cronin-Golomb. Self-bending photorefractive solitons. *Phys. Rev. E*, 54(5):5761–5765, 1996.

[65] N. Kukhtarev, V. B. Markov, S. G. Odulov, M. S. Soskin, and V. L. Vinetskii. Holographic storage in electro-optic crystals: (I). Steady state. *Ferroelectrics*, 22, 1979.

[66] E. A. Kuznetsov, A. V. Mikhailov, and I. A. Shimokhin. Nonlinear interaction of solitons and radiation. *Physica D*, 87:201–215, 1995.

[67] E. A. Kuznetsov, A. M. Rubenchick, and V. E. Zakharov. Soliton stability in plasmas and hydrodynamics. *Phys. Rep.*, 142(3):103–165, 1986.

[68] G. L. Lamb Jr. Coherent-optical-pulse propagation as an inverse problem. *Phys. Rev. A*, 9:422–430, 1974.

[69] S. Lan, E. DelRe, Z. Chen, M. Shih, and M. Segev. Directional coupler using soliton-induced waveguides. *Opt. Lett.*, 24:475–477, 1999.

[70] S. Lan, M. Shih, G. Mizell, J. A. Giordmaine, Z. Chen, C. Anastossiou, J. Martin, and M. Segev. Second harmonic generation in waveguides induced by photorefractive spatial solitons. *Opt. Lett.*, 24:1145–1147, 1999.

[71] L. Landau and E. Lifshitz. *Quantum Mechanics.* Pregamon, 1977.

[72] C. L. Lawson and R. J. Hanson. *Solving least squares problems.* SIAM, Philadelphia, 1995.

[73] R. B. Lehoucq, D. C. Sorensen, and C. Yang. *ARPACK Users' Guide: Solution of Large Scale Eigenvalue Problems with Implicitly Restarted Arnoldi Methods.* University of Leeds, 1997.

[74] P. V. Mamyshev and L. F. Mollenauer. Stability of soliton propagation with sliding-frequency guiding filters. *Opt. Lett.*, 19(24):2083–2085, 1994.

[75] A. Mecozzi, J. D. Mooresa, H. A. Haus, and Y. Lai. Soliton transmission control. *Opt. Lett.*, 16:1841–1843, 1991.

[76] F. M. Mitschke and L. F. Mollenauer. Discovery of the soliton self-frequency shift. *Opt. Lett.*, 11(10):659–661, 1986.

[77] L. F. Mollenauer, J. P. Gordon, and S. G. Evangelides. The sliding-frequency guiding filter: an improved form of soliton jitter control. *Opt. Lett.*, 17(22):1575–1577, 1992.

[78] L. F. Mollenauer, R. H. Stolen, and J. P. Gordon. Experimental observation of picosecond pulse narrowing and solitons in optical fibers. *Phys. Rev. Lett.*, 45:1095–1098, 1980.

[79] NAG. *The NAG Fortran Library Manual, Mark 19.* The Numerical Algorithms Group Ltd, 1999.

[80] B. S. Ng and W. H. Reid. A initial-value method for eigenvalue problems using compound matrices. *J. Comput. Phys.*, 30:125–136, 1979.

[81] B. S. Ng and W. H. Reid. The compound matrix method for ordinary differential systems. *J. Comput. Phys.*, 58:209–228, 1985.

[82] F. W. J. Olver. *Asymptotics and special functions.* Academic Press, 1974.

[83] D. F. Parker, Ch. Radha, and M. Facão. Accelerating solutions for sliding frequency filter systems. *Phys. Rev. E*, 65:66615, 2002.

[84] D. F. Parker, C. Sophocleous, and Ch. Radha. Photorefractive accelerating pulses. *J. Phys. A-Math. Gen.*, 35:1283–1295, 2002.

[85] R. L. Pego, P. Smereka, and M. I. Weinstein. Oscillatory instability of travelling waves for a KdV-Burgers equation. *Physica D*, 67:45–65, 1993.

[86] R. L. Pego and H. A. Warchall. Spectrally stable encapsulated vortices for nonlinear Schrödinger equations. *J. Nonlinear Sci.*, 12(4):347–394, 2002.

[87] R. L. Pego and M. I. Weinstein. Eigenvalues, and instabilities of solitary waves. *Philos. T. Roy. Soc. A*, 340:47–94, 1992.

[88] D. E. Pelinovsky. Matrix stability theory for incoherent optical solitons. *SIAM J. Math. Anal.* Submitted.

[89] D. E. Pelinovsky, A. V. Buryak, and Y. S. Kivshar. Instability of solitons governed by quadratic nonlinearities. *Phys. Rev. Lett.*, 75:591–595, 1995.

[90] J. Petter and C. Denz. Guiding and dividing waves with photorefractive solitons. *Opt. Commun.*, 188:55–61, 2001.

[91] J. S. Russell. *Report on Waves.* British Association Reports, 1844.

[92] M. Segev. Optical spatial solitons. *Opt. Quant. Electron.*, 30:503–533, 1998.

[93] M. Segev, B. Crosignani, P. DiPorto, M. Shih, Z. Chen, M. Mitchell, and G. Salamo. *Beam shaping and control with nonlinear optics*, volume 369 of *NATO ASI*, chapter Photorefractive spatial solitons. Plenum Press, New York, 1998.

[94] M. Segev, B. Crosignani, A. Yariv, and B. Fisher. Spatial solitons in photorefractive media. *Phys. Rev. Lett.*, 68:923, 1992.

[95] M. Segev, G. C. Valley, B. Crosignani, P. DiPorto, and A. Yariv. Steady-state spatial screening solitons in photorefractive materials with external applied field. *Phys. Rev. Lett.*, 73(24):3211–3214, 1994.

[96] G. K. Sen and D. K. Sinha. Accelerating Korteweg-de Vries solitons. *Int. J. Theor. Phys*, 28(4):481–486, 1989.

[97] M. Shih, P. Leach, M. Segev, G. Salamo, M. H. Garret, and G. C. Valley. Two-dimensional steady-state photorefractive screening solitons. *Opt. Lett.*, 21(5):324–326, 1996.

[98] M. Shih, M. Segev, G. C. Valley, G. Salamo, B. Crosignani, and P. DiPorto. Observation of two-dimensional steady-state photorefractive screening solitons. *Electron. Lett.*, 31:826, 1995.

[99] A. W. Snyder, S. J. Hewlett, and D. J. Mitchell. Periodic solitons in optics. *Phys. Rev. E*, 51(6):6297–6302, 1995.

[100] G. I. A. Stegeman, D. N. Christodoulides, and M. Segev. Optical spatial solitons: historical perspectives. *IEEE J. Sel. Top. Quant.*, 6(6):1419–1427, 2000.

[101] R. H. Stolen, J. P. Gordon, W. J. Tomlinson, and H. A. Haus. Raman response function of silica-core fibers. *J. Opt. Soc. Am. B*, 6(6):1159–1165, 1989.

[102] M. Suzuki and N. Edagawa. Dispersion-managed high-capacity ultra-long-haul transmission. *J. Lightwave Technol.*, 21(4):916–929, 2003.

[103] G. Swaters. *Introduction to Hamiltonian fluid dynamics and stability theory.* Chapman & Hall, 2000.

[104] J. Swinton. The stability of homoclinic pulses: a generalisation of Evans's method. *Phys. Lett. A*, 163(1,2):57–62, 1992.

[105] J. Swinton and J. Elgin. Stability of travelling pulse solutions to a laser equation. *Phys. Lett. A*, 145(8,9):428–433, 1990.

[106] M. Taya, M. C. Bashaw, M. M. Fejer, M. Segev, and G. Valley. Y-junctions arising from dark-soliton propagation in photovoltaic media. *Opt. Lett.*, 21:943–945, 1996.

[107] W. E. Torruellas, Z. Wang, D. J. Hagan, E. W. VanStryland, G. I. Stegeman, L. Torner, and C. R. Menyuk. Observation of 2-dimensional spatial solitary waves in a quadratic medium. *Phys. Rev. Lett.*, 74(25):5036–5039, 1995.

[108] S. Trillo and W. Torruellas, editors. *Spatial solitons.* Springer-Verlag, 2001.

[109] M. G. Vakhitov and A. A. Kolokolov. Stationary solutions of the wave equation in a medium with nonlinearity saturation. *Radiophysics and Quantum Electronics*, 16:783, 1973.

[110] E. V. Vanin, A. I. Korytin, A. M. Sergeev, D. Anderson, M. Lisak, and L. Vázquez. Dissipative optical solitons. *Phys. Rev. A*, 49(4):2806–2811, 1994.

[111] V. L. Vinetskii and N. V. Kukhtarev. Theory of the conductivity induced by recording holographic gratings in nonmetallic crystals. *Sov. Phys. Solid State*, 16(12):2414–2415, 1975.

[112] M. I. Weinstein. Lyapunov stability of ground states of nonlinear dispersive evolution equations. *Commun. Pur. Appl. Math.*, 39:51–68, 1986.

[113] A. Yariv. *Optical Electronics in Modern Communications.* Oxford University Press, 1997.

[114] N. J. Zabusky and M. D. Kruskal. Interaction of "solitons" in a collisionless plasma and the recurrence of initial states. *Phys. Rev. Lett.*, 15:140–243, 1965.

[115] V. E. Zakharov and A. B. Shabat. Exact theory of two-dimensional self-focusing and one-dimensional self-modulation of waves in nonlinear media. *Sov. Phys. - JETP*, 34:62–69, 1972.

ACCELERATING SOLITONS AND PHOTOREFRACTIVITY

D.F. Parker and M. Facão
Dept. of Mathematics and Statistics, University of Edinburgh,
The King's Buildings, Edinburgh, EH9 3JZ, U.K.
D.F.Parker@ed.ac.uk, margarida@maths.ed.ac.uk

Ch. Radha
Dept. of Mathematics, Visvesvaraya Regional College of Engineering,
Nagpur 440011, India
rarahda@USA.NET

Abstract Many evolution equations of nonlinear optics permit localized self-similar pulses having constant acceleration, or beams localized around a parabolic path. Examples include *dissipative solitons* in active media and pulses in sliding frequency filter systems. In the absence of diffusion, photorefractive beams propagate rectilinearly, but the presence of transverse diffusion causes beam curvature. Beam profiles are described exactly as self-similar solutions with an *accelerating* similarity variable. Computation of a nonlinear eigenvalue problem yields the dependence of beam curvature upon power. A perturbation analysis predicts this well.

Keywords: nonlinear optics, evolution equations, dissipative solitons, acceleration, sliding frequency, photorefractive beams, similarity variable, curvature, stability.

1. THE ACCELERATING SIMILARITY VARIABLE

Many of the evolution equations and systems familiar in nonlinear optics allow travelling wave solutions, often known as solitons or vector solitons. These have pulse, or beam, profiles governed by (ordinary) differential equations obtained by similarity reductions of the full equations. However, many of the systems possess similarity variables other than the travelling wave coordinate $x - 2Vz$. For example, the similarity variables $xz^{-1/2}$, $(x - 2Vz)z^{-1/2}$ and $x - \kappa z^2$ all arise [1] from Lie group

F. Abdullaev et al. (eds.), Nonlinearity and Disorder: Theory and Applications, 435–441.

analysis of the system

$$iu_z + u_{xx} + \left(|u|^2 + \sigma\,|v|^2\right) u = 0\,,\ iv_z + v_{xx} + \left(\sigma\,|u|^2 + |v|^2\right) v = 0$$

arising from the symmetric 'cross-phase modulation' in an optical waveguide. If z is interpreted as time, while x is 'distance' through the pulse, the paths $x - \kappa z^2 =$ constant have constant acceleration. Localized solutions having this as similarity variable will be called *accelerating solitons* and are the subject of this paper.

A practical example was discussed in (1994) by Vanin *et al.* [2], who treated ultra-short laser-generated pulses in an active medium by studying complex amplitudes $A(x,z)$ satisfying

$$-iA_z + A_{xx} + |A|^2 A + iA\left\{1 - \int_{-\infty}^{x} |A|^2\,dx'\right\} = 0\,. \tag{1}$$

Since rewriting as $A = F\mathrm{e}^{i\theta}$, in terms of the (real) modulus F and argument θ, yields

$$F_{xx} + \{\theta_z - (\theta_x)^2\}F + F^3 = 0\quad, \tag{2}$$

$$-F_z + 2\theta_x F_x + \theta_{xx} F + (1-C)\,F = 0\ , \tag{3}$$

$$C_x = F^2\quad,\qquad C(-\infty, z) = 0\,, \tag{4}$$

while equation (3) has the first integral $2\theta_x F^2 - C_z - C^2 + 2C =$ const., it is clear that solutions exist with F, θ_x, θ_z and C depending only upon $x - 2Vz$. However, in [2] it is argued that corresponding solitons cannot be stable, but that *dissipative solitons* of the form

$$A = \mathrm{e}^{i\theta(z,\eta)} F(\eta)\quad,\qquad C = C(\eta)\quad,\qquad \eta \equiv x - \kappa z^2$$

can exist. Actually, we can readily show, by using the *similarity variable*

$$\eta = x - 2Vz - \kappa z^2 \tag{5}$$

and again writing $A = \mathrm{e}^{i\theta(z,\eta)}F(\eta)$, $C = C(\eta)$, that the system (2)-(4) leads to the *phase* having the form

$$\theta = -(V + \kappa z)\eta + z(\Gamma - V^2 - \kappa V z - \tfrac{1}{3}\kappa^2 z^2) + \Theta(\eta) \tag{6}$$

together with the system of ordinary differential equations (ODEs)

$$F''(\eta) + \{\Gamma - \kappa\eta - (\Theta')^2\}F + F^3 = 0\,,\quad F^2\Theta'(\eta) = \tfrac{1}{2}C^2 - C \tag{7}$$

with $C'(\eta) = F^2$ and with localized pulses satisfying also

$$F \to 0 \quad \text{as} \quad \eta \to \pm\infty\,,\quad C(-\infty) = 0\,,\quad C(\infty) = 2\,.$$

[N.B. In (7), V does not appear. For $\kappa \neq 0$, the parameter V determines only a shift in the origin for η and a corresponding frequency shift in (6). The parameter κ multiplies the non-autonomous term in (7) and appears as an eigenvalue related to the peak amplitude of $F(\eta)$.]

Also in (1994), Kodama and Wabnitz [3] found accelerating pulses by applying Lagrangian averaging to the sliding-frequency filter equation

$$iu_z + \tfrac{1}{2}u_{xx} + |u|^2 u = i\delta u + i\beta(\partial_x - i\alpha_0 z)^2 u \tag{8}$$

which provides a smoothed model for long-distance propagation in a system with averaged excess gain δ, with filter strength β and filter-frequency sliding rate α_0 (see also Hasegawa and Kodama [4]). Equation (8), like (1), possesses solutions [5] with $|u| = F(\eta)$ with η given by (5), with phase $\theta(z,\eta)$ as in (6) and with κ appearing as a crucial parameter in an ODE for the complex quantity $F(\eta)e^{i\Theta(\eta)} \equiv w(\eta)$. Identifying those values κ which allow solutions with $|w| \to 0$ as $\eta \to \pm\infty$, and identifying corresponding pulse maxima F_{max} and locations η_m at which $F(\eta_m) = F_{max}$, provides a fourth-order *connection problem* for ODEs.

For self-guiding beams in photorefractive media, various equations and systems have recently been proposed and studied. Christodoulides *et al.* [6] show that the system

$$\begin{aligned} i\alpha u_z + u_{xx} - \beta_1 u\{1 + |u|^2 + |v|^2\}^{-1} = 0\,, \\ iv_z + v_{xx} - \beta_2 v\{1 + |u|^2 + |v|^2\}^{-1} = 0\,. \end{aligned} \tag{9}$$

studied by Singh *et al.* [7] to describe the interaction of two orthogonal field components may, for appropriate choices of the parameters α, β_1 and β_2, possess either bright-bright or bright-dark stable vector solitons. The system (9) contains a saturating nonlinearity in each mode, but omits effects due to transverse diffusion of space charge. A single-mode equation incorporating this effect is

$$iu_z + u_{xx} - \beta\frac{u}{1+|u|^2} + \gamma\frac{(|u|_x^2)u}{1+|u|^2} = 0\,, \tag{10}$$

in which γ is a non-dimensional diffusivity. Using an averaged Lagrangian procedure, Carvalho *et al.* [8] showed that the centre of a localized beam follows a path along which $x \propto z^2$. However, as for (1) and (8), we show that for *any* system

$$i\partial_z u_n + D_n\,\partial_x^2 u_n + F_n\left(|u_1|^2, ..., |u_N|^2; \left(|u_1|^2\right)_x, ..., \left(|u_N|^2\right)_x\right) u_n = 0\,, \tag{11}$$

with coefficients D_n and functions F_n which are real (for $n = 1, 2, ..., N$), there exist solutions of the form

$$u_n = e^{i\theta_n(z,\eta)} U_n(\eta) \quad , \qquad \eta = x - 2Vz - \kappa z^2\,. \tag{12}$$

In particular, for the single-mode photorefractive beam governed by (10), it is shown that, whenever $\gamma \neq 0$, the acceleration (or beam curvature) parameter κ *must* be non-zero. Such self-bending beams are treated also in [9].

2. PHOTOREFRACTIVE ACCELERATING SOLITONS

For the system (11), substituting the *ansatz* (12) gives

$$\begin{aligned} i\{2(D_n\partial_\eta\theta_n - V - \kappa z)U_n{}' + D_n(\partial_\eta^2\theta_n)U_n\} + D_nU_n{}'' \\ +\{2(V+\kappa z)\partial_\eta\theta_n - D_n(\partial_\eta\theta_n)^2 - \partial_z\theta_n\}U_n \\ +F_n(U_1^2,...,U_N^2;2U_1U_1{}',...,2U_NU_N{}')U_n = 0. \end{aligned} \tag{13}$$

The vanishing of the imaginary part requires that

$$\partial_\eta\theta_n = \frac{V+\kappa z}{D_n} + \frac{C_n}{U_n^2(\eta)}\,, \qquad n = 1,2,...,N,$$

for some choice of constants C_n. Integrating this to give

$$\theta_n(z,\eta) = D_n^{-1}(V+\kappa z)\eta + \Theta_n(z) + \int C_nU_n^{-2}(\eta)\,d\eta \tag{14}$$

and inserting the expression $\partial_z\theta_n = \kappa D_n^{-1}\eta + \Theta_n{}'(z)$ into the real part of (13) makes the coefficient of U_n independent of z only if

$$\Theta_n{}'(z) = D_n^{-1}(V+\kappa z)^2 + \text{ constant}\,.$$

In consequence, the *only* choices of $\theta_n(z,\eta)$ consistent with (12) are

$$\theta_n(z,\eta) = D_n^{-1}\{(V+\kappa z)\eta + \tfrac{1}{3}\kappa^2z^3 + V\kappa z^2\} + \Gamma_nz + \int C_nU_n^{-2}(\eta)\,d\eta\,.$$

They lead to the non-autonomous system of ODEs for $U_n(\eta)$

$$\begin{aligned} D_nU_n{}''(\eta) - \{\Gamma_n + D_n^{-1}(\kappa\eta - V^2) + D_nC_n^2U_n^{-4}(\eta) \\ -F_n(U_1^2,...,U_N^2;2U_1U_1{}',...,2U_NU_N{}')\}U_n = 0, \end{aligned} \tag{15}$$

with simplification arising ($C_n = 0$) if any (or all) of the amplitudes U_n asymptotes to zero as $\eta \to \pm\infty$.

For solitary solutions $u = \mathrm{e}^{i\theta}F(\eta)$ to equation (10), the phase is $\theta = (V+\kappa z)\eta + \frac{1}{3}\kappa^2z^3 + V\kappa z^2 + (V^2-B)z + \theta_0$ and the single ODE analogous to (15) is

$$F''(\eta) + (B-\kappa\eta)F - \frac{(\beta - 2\gamma FF')F}{1+F^2} = 0\,. \tag{16}$$

Re-writing in terms of $\zeta \equiv \beta^{1/2}\eta$, with $\delta \equiv 2\gamma\beta^{-1/2}$ as in [10] yields

$$\frac{\mathrm{d}}{\mathrm{d}\zeta}\left\{[F'(\zeta)]^2 + M(\zeta)F^2 - \ln(1+F^2)\right\} = -2\delta\frac{F^2(F')^2}{1+F^2} + aF^2\,,$$

where $M(\zeta) \equiv (B - \kappa\eta)/\beta = \beta^{-1}B + a\zeta$, $a \equiv -\kappa/\beta^{3/2}$. Clearly, for $\delta \neq 0$ (i.e. $\gamma \neq 0$), solutions can have $F \to 0$ as $\zeta \to \pm\infty$ only if $a\delta > 0$, with

$$a\int_{-\infty}^{\infty} F^2(\zeta)\mathrm{d}\zeta = 2\delta\int_{-\infty}^{\infty}\frac{F^2[F'(\zeta)]^2}{1+F^2}\mathrm{d}\zeta\,. \tag{17}$$

Hence, transverse diffusion necessarily *causes* beam curvature ($a \neq 0$).

For small (even moderate) values of δ (and hence of $a = M'(\zeta)$), solutions to (17) may be constructed as perturbations about the profiles $G(\xi;\mu)$ satisfying

$$G_{\xi\xi} + M^*G = \frac{G}{1+G^2}\,; \quad G(0,\mu) \equiv \mu\,, \quad G_\xi(0,\mu) = 0\,; \quad \xi \equiv \zeta - \zeta^*\,.$$

These describe diffusionless profiles which are symmetric about the location $\zeta = \zeta^*$ at which the peak value is specified as μ and with $M^* = \mu^{-2}\ln(1+\mu^2)$. Indeed, after writing (16) as

$$\frac{\mathrm{d}^2F}{\mathrm{d}\xi^2} + (a\xi + \alpha - 1)F = \frac{-F^3}{1+F^2} - \delta\frac{F^2F'}{1+F^2}$$

with $\alpha \equiv M(\zeta^*) = a\zeta^* + B/\beta = M^* + \delta\alpha_1 + \delta^2\alpha_2 + \ldots$, solutions may be sought in powers of δ as

$$F(\zeta) = G(\xi;\mu) + \delta F_1(\xi;\mu) + \delta^2F_2(\xi;\mu) + \ldots\,, \qquad a = \delta a_1 + \delta^2 a_2 + \ldots\,.$$

With $F = \mu$, $F' = 0$ at $\zeta = \zeta^*$ (i.e. at $\xi = 0$), this requires that $F_1(\xi;\mu)$ satisfies

$$\frac{\mathrm{d}^2F_1}{\mathrm{d}\xi^2} + M^*F_1 + \frac{G^2-1}{(1+G^2)^2}F_1 = -(\alpha_1 + a_1\xi)G - \frac{G^2G_\xi}{1+G^2}$$

and $F_1(0,\mu) = 0$, $F_{1,\xi}(0,\mu) = 0$ and $F_1 \to 0$ as $\xi \to \pm\infty$. This, in turn, makes $\alpha_1 = 0$ and makes F_1 *odd* in ξ. Also it yields the identity

$$a_1\int_{-\infty}^{\infty} G^2(\xi;\mu)\mathrm{d}\xi = 2\int_{-\infty}^{\infty}\frac{G^2(\xi;\mu)(G_\xi(\xi;\mu))^2}{1+G^2(\xi;\mu)}\,\mathrm{d}\xi\,. \tag{18}$$

Equation (18) estimates the beam curvature parameter as $a = \alpha_1\delta + O(\delta^2)$, with $a_1 = a_1(\mu)$. Moreover the odd function F_1 is determined explicitly by repeated integration of the equation

$$\frac{\mathrm{d}}{\mathrm{d}\xi}\left\{(G_\xi)^2\frac{\mathrm{d}}{\mathrm{d}\xi}\left(\frac{F_1}{G_\xi}\right)\right\} = \tfrac{1}{2}a_1\left\{G^2 - \frac{\mathrm{d}}{\mathrm{d}\xi}(\xi G^2)\right\} - \frac{G^2(G_\xi)^2}{1+G^2}\,.$$

Then, with error $O(\delta^2)$, the beam has the profile

$$F(\zeta) \approx G(\xi;\mu) + \delta F_1(\xi;\mu)\,, \tag{19}$$

while, since $\alpha = M^* + O(\delta^2)$, the path ($\xi = 0$) along which the peak of amplitude $|u|_{\max} = F_{\max} = \mu$ travels is

$$x - 2Vz + 2\gamma\beta a_1 z^2 \approx \eta = \beta^{-1/2}\xi^* \approx (M^* - B/\beta)(2\gamma a_1)^{-1}\,. \tag{20}$$

3. NUMERICAL PROCEDURE AND RESULTS

Equation (16) is written in terms of the independent variable ζ as

$$F_{\zeta\zeta} + (a\zeta + b)F = (F + \delta F_\zeta)F^2/(1+F^2) \quad , \qquad b \equiv B\beta^{-1} - 1\,. \tag{21}$$

The choices $F(\zeta^*) = \mu$, $F_\zeta(\zeta^*) = 0$ then relate ζ^* to μ through

$$\zeta^* + \frac{B}{a\beta} = \frac{M^*(\mu)}{a} + \frac{1}{\mu^2}\int_{-\infty}^{\zeta^*} F^2 \mathrm{d}\zeta + \frac{2\delta}{a\mu^2}\int_{-\infty}^{\zeta^*} \frac{(FF_\zeta)^2}{1+F^2}\mathrm{d}\zeta\,. \tag{22}$$

Using estimates of ζ^* obtained from the perturbation analysis and using the estimates $F_\zeta = \mp(1 - B\beta^{-1} - a\zeta)^{1/2}F$ obtained from linearized analysis of (21) in the fringes ($\zeta - \zeta^* \gtrless 0$, respectively) of the beam (with $|\zeta - \zeta^*|$ suitably large, but ensuring that $1 - B\beta^{-1} - a\zeta > 6a$, say), a shooting method allows $F(\zeta;\mu)$ and ζ^* to be found. Note that a and δ are specified, rather than μ and δ as in the perturbation method.

Typical results [10] show that the perturbative expressions (19) and (20) are good for $\delta = 0.01$, 0.1 over a wide range of μ (or equivalently of beam power $P \equiv \int_{-\infty}^{\infty} F^2(s)\,\mathrm{d}s$). For $\delta = 0.2$ and 0.3, the prediction of beam profile deteriorates as the profiles become markedly asymmetric, though the estimate $a \approx a_1\delta$ for the curvature remains good.

In the diffusionless case ($\gamma = 0$), equation (10) is the special case $N(F^2) = -\beta(1+F^2)^{-1}$ of $iu_z + u_{xx} + N(|u|^2)u = 0$, for which solutions $u = \mathrm{e}^{i\theta}F(\eta)$ have $F''(\eta) - \{C - N(F^2)\}F = 0$, with $C = \mu^{-2}\int_0^{\mu^2} N(s)\,\mathrm{d}s$ and $\kappa = 0$. Applying stability analysis [11] to solutions of the form $u = \mathrm{e}^{i\theta}\{F(\eta) + \epsilon w(z,\eta)\}$ leads to the deduction that no relevant eigenvalues for w have positive real part if $P'(C) > 0$, where P is the beam power $P(\mu) \equiv \int_{-\infty}^{\infty} F^2(\eta)\,\mathrm{d}\eta$. For $N = -\beta(1+F^2)^{-1}$, it is found that $P(\mu)$ and $C(\mu)$ are monotonically increasing functions, so that stability for all peak amplitudes μ follows.

For $\beta \neq 0$ ($\delta \neq 0$), typical choices of (a, b, δ) correspond to isolated solutions to (21) (with associated values for μ and ζ^*). Solutions for $\delta = 0$ all are stable (with $a = 0$). The stability boundary, on which

$w + w^*$ and $w - w^*$ possess eigenfunctions $ue^{i\lambda z}$ and $ve^{i\lambda z}$ with $\lambda \approx 0$ are currently being sought following [12].

References

[1] Parker, D.F. (1988) "Coupled cubic Schrödinger equations for axially symmetric waveguides", in A. Donato and S. Giambo (eds.) *Proc. 4th Meeting on Waves and Stability in Continuous Media*, Cosenza: Editel, 261–280.

[2] Vanin, E.V., Korytin, A.I., Sergeev, A.M., Anderson, D., Lisak, M. and Vázquez, L. (1994) *Phys. Rev. A* **49**, 2806–2811.

[3] Kodama, Y. and Wabnitz, S. (1994) *Opt. Lett.* **19** 162–164.

[4] Hasegawa, A. and Kodama, Y.(1995) *Solitons in Optical Communications*, Oxford: Clarendon Press.

[5] Parker, D.F. and Radha, Ch. (2001) "Accelerating solitons for sliding frequency filter systems", under revision.

[6] Christodoulides, D.N., Singh, S.R., Carvalho, M.I. and Segev, M. (1996) *Appl. Phys. Lett.* **68** 1763–1765.

[7] Singh, S.R., Carvalho, M.I. and Christodoulides, D.N. (1995) *Opt. Lett.* **21** 2177–2179.

[8] Carvalho, M.I., Singh, S.R. and Christodoulides, D.N. (1995) *Opt. Commun.* **120** 311–315.

[9] Królikowski, W., Akhmediev, N., Luther-Davies, B. and Cronin-Golomb, M. (1996) *Phys. Rev. E* **54** 5761–5765.

[10] Parker, D.F., Sophocleous, C. and Radha, Ch. (2001) "Photorefractive accelerating pulses", submitted for publication.

[11] Kuznetsov, E.A., Rubenchik, A.M. and Zakharov, V.E. (1986) *Phys. Reports* **142** 104–165.

[12] Michalalche, D., Mazilu, D. and Crasovan, L-C. (1999) *Phys. Rev. E* 60 7504–7510.

Accelerating solitons for sliding-frequency filter systems

D. F. Parker, Ch. Radha,* and Margarida Facão
Department of Mathematics and Statistics, University of Edinburgh, The King's Buildings, Edinburgh EH9 3JZ, United Kingdom
(Received 8 November 2001; published 24 June 2002)

The sliding-frequency filter equation is shown to have similarity solutions which travel with steady profile but with *constant acceleration*. Over a wide range of the gain, filter strength and sliding-rate parameters, the pulse envelope is very well approximated by a sech profile. However, when the sliding rate is large, the chirp differs greatly from the usually assumed linear variation of frequency through the pulse. The amplitude and chirp are found for small and moderate sliding rate by a perturbation analysis and, for larger sliding rates, by solving a nonlinear eigenvalue problem for a nonautonomous differential equation.

DOI: 10.1103/PhysRevE.65.066615 PACS number(s): 42.65.Tg, 42.65.Wi, 42.81.Dp

I. INTRODUCTION

Ultralong distance fiber-optic transmission using solitons has been demonstrated [1] using periodically spaced erbium-doped amplifiers to counterbalance fiber loss. To suppress amplification of unwanted noise, filters are introduced at each amplifier, allowing passage of signals only in a narrow band centered at the central frequency of the soliton. Even this allows degradation by noise, unless the soliton frequency is incrementally shifted at each amplifier. The soliton is able gradually to adapt to this frequency shift, but low-amplitude noise, being governed by linear equations, cannot. This is the principle of sliding-frequency filter (SFF) transmission [2]. In the limit for which amplifier spacing is short compared to the dispersion length, an appropriate evolution equation [3] is

$$\mathcal{N}u \equiv iu_Z + \tfrac{1}{2}u_{TT} + |u|^2 u = i\delta u + i\beta(\partial_T + i\hat{\alpha}Z)^2 u, \quad (1)$$

where δ is the (averaged) excess gain, β is the filter strength, $-\hat{\alpha}$ is the (constant) frequency-sliding rate, Z is the (scaled) propagation distance, and T a retarded time.

It is widely known that the undamped nonlinear Schrödinger (NLS) equation $\mathcal{N}u=0$ possesses sech-envelope solutions at all carrier frequencies, viz.

$$u = A\exp i\{\Omega_1 T + \tfrac{1}{2}(A^2+\Omega_1^2)Z\}\operatorname{sech} A(T-\Omega_1 Z). \quad (2)$$

These show that the perturbation Ω_1 in soliton speed is proportional to the shift in carrier frequency (with associated shift in wavelength being quadratic in both Ω_1 and the soliton amplitude A).

When an SFF system is designed to transmit pulses with frequency shift $-\hat{\alpha}Z$ which is linear in the transmission "distance" Z, it is self-consistent to seek solutions to Eq. (1) having similarity variable

$$\zeta = T + aZ^2 + bZ. \quad (3)$$

These are "accelerating solutions"—recently shown to exist in a number of optical systems [4–6], such as dissipative media with nonlinear saturable gain and photorefractive beams and existing also [3] for a related integrable equation in which the right-hand side of Eq. (1) is replaced by $i\hat{\alpha}Zu$.

In Sec. II, the reduction of Eq. (1) to an ordinary differential Eq. (10) for a complex amplitude W, consistent with the similarity variable (3) is obtained. The "acceleration" is $a=\hat{\alpha}/2$ while, in the equation, δ and $\hat{\alpha}$ appear only in the combination $\hat{\alpha}/\delta^{3/2} \equiv \nu$ [see Eq. (10)]. In Sec. III, a perturbation method valid for any given β but for $|\nu| \ll 1$ (i.e., $|\hat{\alpha}| \ll \delta^{3/2}$) yields a criterion determining the parameter b and the initial conditions which allow Eq. (10) to possess isolated pulse solutions. Section IV extends analysis allowing estimation of the parameters and initial conditions in Eq. (10) which yield isolated pulse solutions for larger values of ν constrained only by the relation

$$27\nu^2\beta(1+4\beta^2) \lesssim 64.$$

The numerical and analytic results presented in Sec. V concerning Eq. (10) for general values of β and for both small and large values of $|\nu|$ show that a profile of $|u|$ always exists which is remarkably close to a sech curve. The expressions for b and for the pulse amplitude and width predicted in Sec. III are confirmed as good approximations for moderate values of $|\nu|$ (not just for $|\nu| \ll 1$). Also, the frequency within the pulse is found to have chirp which is *very well* approximated by a tanh curve, rather than the linear ramp usually assumed. The tanh dependence is predicted by the perturbation analysis of Sec. III, as is the relation between pulse half-width and amplitude.

II. ACCELERATING SELF-SIMILAR SOLUTIONS

We seek a solution to Eq. (1) in the form

$$u(T,Z) = e^{i\theta(\zeta,Z)}F(\zeta) \quad (4)$$

with ζ given by Eq. (3) and with a, b, θ, and F real.

Insertion of Eq. (4) into Eq. (1) and multiplication by $2+4i\beta$ yields

*Permanent address: Department of Mathematics, Visvesvaraya Regional College of Engineering, Nagpur 440011, India.

$$(1+4\beta^2)F''(\zeta)+2\{2\beta[(\hat{\alpha}-2a)Z-b]$$
$$+i[(1+4\beta^2)\theta_\zeta+(2a+4\beta^2\hat{\alpha})Z+b]\}F'(\zeta)$$
$$-\{(1+4\beta^2)(\theta_\zeta)^2+2(2aZ+b+4\beta^2\hat{\alpha}Z)\theta_\zeta$$
$$+2\theta_Z+4\beta^2\hat{\alpha}^2Z^2-4\beta\delta-i[(1+4\beta^2)\theta_{\zeta\zeta}$$
$$+4\beta(\hat{\alpha}Z-2aZ-b)\theta_\zeta-4\beta\theta_Z+2\beta\hat{\alpha}^2Z^2-2\delta]\}F(\zeta)$$
$$+2(1+2i\beta)[F(\zeta)]^3=0. \quad (5)$$

The ansatz (4) is self-consistent only if both the real and imaginary parts of the coefficients in Eq. (5) depend on ζ alone. From the coefficient of $F'(\zeta)$, we deduce immediately that $2a=\hat{\alpha}$ and that

$$\theta(\zeta,Z)=-\hat{\alpha}\zeta Z+\Theta(\zeta)+\Phi(Z),$$

so yielding the results $\theta_{\zeta\zeta}=\Theta''(\zeta)$, $\theta_\zeta+\hat{\alpha}Z=\Theta'(\zeta)$, and $\theta_Z=-\hat{\alpha}\zeta+\Phi'(Z)$. In order that the real part of the coefficient of $F(\zeta)$ is independent of Z, it is necessary that

$$\Phi'(Z)=\tfrac{1}{2}\hat{\alpha}^2Z^2+\hat{\alpha}bZ+c_0$$

for some constant c_0. This yields the expression

$$\theta(\zeta,Z)=\Theta(\zeta)-(\hat{\alpha}\zeta-c_0)Z+\tfrac{1}{6}\hat{\alpha}^2Z^3+\tfrac{1}{2}\hat{\alpha}bZ^2+c_1, \quad (6)$$

so that Eq. (5) reduces to

$$(1+4\beta^2)\{F''(\zeta)+i[\Theta''(\zeta)F+2\Theta'(\zeta)F'(\zeta)]$$
$$-[\Theta'(\zeta)]^2F\}+2(1+2i\beta)\{ib[F'(\zeta)+i\Theta'(\zeta)F]$$
$$+(\hat{\alpha}\zeta-c_0-i\delta)F+F^3\}$$
$$=0. \quad (7)$$

It is observed in [2] that Eq. (1), for $\hat{\alpha}\equiv 0$, possesses special solutions in which

$$F=A\ \mathrm{sech}\,T, \quad \theta=KZ+C\ \ln(\mathrm{sech}\,T),$$

which correspond to $b=0$, $c_0=K$. However, since these solutions impose four relations upon A, C, K, β, and δ, they apply only for special combinations of β and δ. Fortunately, there is a generalization

$$F=A\ \mathrm{sech}\,\kappa(\zeta-\zeta_0), \quad \Theta=C\ \ln[\mathrm{sech}\,\kappa(\zeta-\zeta_0)], \quad (8)$$

which satisfies Eq. (7) for $\hat{\alpha}=0$, $b=0$ provided that

$$C=\frac{8\beta}{3+\sqrt{9+32\beta^2}}=\frac{\sqrt{9+32\beta^2}-3}{4\beta},$$

$$A^2=\frac{3\delta}{4\beta}(1+\sqrt{9+32\beta^2}),$$

$$\kappa^2=\frac{8\beta\delta}{3+8\beta^2-\sqrt{9+32\beta^2}}, \quad c_0=\frac{\delta}{2\beta}\sqrt{9+32\beta^2}. \quad (9)$$

This defines a solution $F(\zeta)$ and $\theta(\zeta,Z)$ to Eq. (7) with $\hat{\alpha}=0$, $b=0$ for *all* choices of δ and β, with ζ_0 arbitrary.

Observe that expressions (8) become singular as $\beta\to 0$. Since they describe isolated pulses in which $\hat{\alpha}=0$, $b=0$, it is natural to rearrange Eq. (7) as

$$(1+4\beta^2)W''(Y)+2(1+2i\beta)\{\mu_0-i+|W|^2\}W$$
$$=-2(1+2i\beta)\{iBW'(Y)+\nu YW\}, \quad (10)$$

where

$$\mu_0\equiv\frac{\hat{\alpha}\zeta_0-c_0}{\delta}, \quad Y\equiv\delta^{1/2}(\zeta-\zeta_0),$$

$$B\equiv\delta^{-1/2}b, \quad \nu\equiv\delta^{-3/2}\hat{\alpha},$$

and

$$F(\zeta)e^{i\Theta(\zeta)}\equiv\delta^{1/2}W(Y). \quad (11)$$

III. PERTURBATION ANALYSIS

Solutions to Eq. (10) may be sought by expanding in ν as

$$W(Y)=\hat{W}(Y)+\nu V(Y)+\cdots, \quad B=\nu B_1+\cdots, \quad (12)$$

with $\hat{W}(Y)=\hat{A}\ \mathrm{sech}\,\hat{\kappa}Ye^{i\hat{\Theta}(Y)}$, $\hat{\Theta}(Y)=C\ \ln(\mathrm{sech}\,\hat{\kappa}Y)$, with $\hat{\kappa}=\delta^{-1/2}\kappa$, $\hat{A}=\delta^{-1/2}A$, and with A, C, and κ given by Eq. (9), provided that β is not too small. Then, inserting into Eq. (10) and taking $O(\nu)$ terms gives the linear differential equation for *complex* $V(Y)$:

$$\mathcal{L}V\equiv(1+4\beta^2)V''(Y)+2(1+2i\beta)$$
$$\times\{(\mu_0-i)V+\hat{A}^2(\mathrm{sech}^2\,\hat{\kappa}Y)(2V+e^{2i\hat{\Theta}}V^*)\}$$
$$=-2(1+2i\beta)\{\hat{\kappa}B_1(C-i)\tanh\hat{\kappa}Y+Y\}\hat{A}\,\mathrm{sech}\,\hat{\kappa}Y. \quad (13)$$

For Eq. (13), the four-dimensional space of complementary functions has a two-dimensional subspace composed of functions *even* in Y and a two-dimensional subspace of functions *odd* in Y. Moreover, $i\hat{W}(Y)$ belongs to the first subspace and $\hat{W}'(Y)$ belongs to the second. Since, as $Y\to\infty$ and as $Y\to-\infty$ there exist two-parameter families of unbounded solutions, the *only* bounded contributions to the complementary function have the form $ic_1\hat{W}(Y)+c_2\hat{W}'(Y)$, with c_1, c_2 real.

Since the right-hand side of Eq. (13) is an odd function of Y, it is sufficient to seek odd, bounded solutions $V(Y)$ [adding to V the even contribution $ic_1\hat{W}(Y)$ corresponds merely to a constant perturbation νc_1 to the phase $\hat{\Theta}(Y)$]. Moreover, it is permissible to set $V'(0)=id_1$ (d_1 real), since inclusion

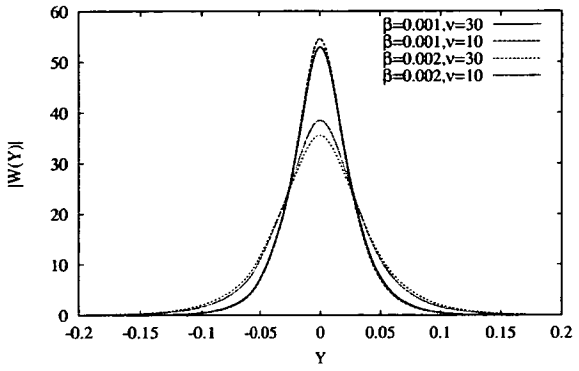

FIG. 1. Pulse envelopes $|W(Y)|$ governed by Eq. (10) for $\beta=0.001$ and 0.002, and for $\nu=10$ and $\nu=30$.

of $c_2\hat{W}'(Y)$ in $V(Y)$ merely corresponds to a perturbation in ζ_0. Thus, by solving numerically the three initial-value problems

$$\mathcal{L}V_1=0, \quad V_1(0)=0, \quad V_1'(0)=i,$$

$$\mathcal{L}V_2=-2(1+2i\beta)\kappa\hat{A}(C-i)\tanh\hat{\kappa}Y\ \mathrm{sech}\,\hat{\kappa}Y,$$

$$V_2(0)=V_2'(0)=0,$$

$$\mathcal{L}V_3=-2(1+2i\beta)\hat{A}Y\ \mathrm{sech}\,\hat{\kappa}Y, \quad V_3(0)=V_3'(0)=0,$$

to yield unbounded, odd functions, it is possible to select d_1 and B_1 so that the combination

$$V(Y)=d_1V_1(Y)+B_1V_2(Y)+V_3(Y)$$

remains bounded. The corresponding approximation $W\approx\hat{W}(Y)+\nu V(Y)$ then has $W(0)=\hat{A}+O(\nu^2)$, $W'(0)=i\nu d_1+O(\nu^2)$, so that, correct to $O(\nu)$, the maximum of $|W|$ occurs at $Y=0$.

These calculations show that, for specified excess gain δ, there exist isolated pulses which accelerate uniformly (with $a=\frac{1}{2}\hat{\alpha}$) and for which $|W(Y)|$ is very close to the familiar sech profile $\hat{A}\ \mathrm{sech}\,\hat{\kappa}Y=\hat{A}\ \mathrm{sech}\,\kappa(\zeta-\zeta_0)$. In these, the phase has *chirp* given by $\Theta'(\zeta)\approx-\kappa C\tanh\hat{\kappa}Y=-\kappa C\tanh\kappa(\zeta-\zeta_0)$ and the parameter b in Eq. (3) is given by $b\approx\nu\delta^{1/2}B_1=\hat{\alpha}\delta^{-1}B_1$. These profiles and chirp are found (see Figs. 1 and 2) to give good approximations for a wide range of values of β not only for small sliding rate $\nu\equiv\hat{\alpha}/\delta^{3/2}\ll1$, but also for $\nu=O(1)$. Moreover, the predicted value of b gives a very useful approximation for the parameter B required in the computations in Sec. IV.

IV. GENERAL TREATMENT

Equation (10) may be put into the canonical form

$$w''(y)+2(1+2i\beta)\{i\bar{B}w'(y)+(y-i\Delta+|w|^2)w\}=0, \tag{14}$$

through use of the substitutions

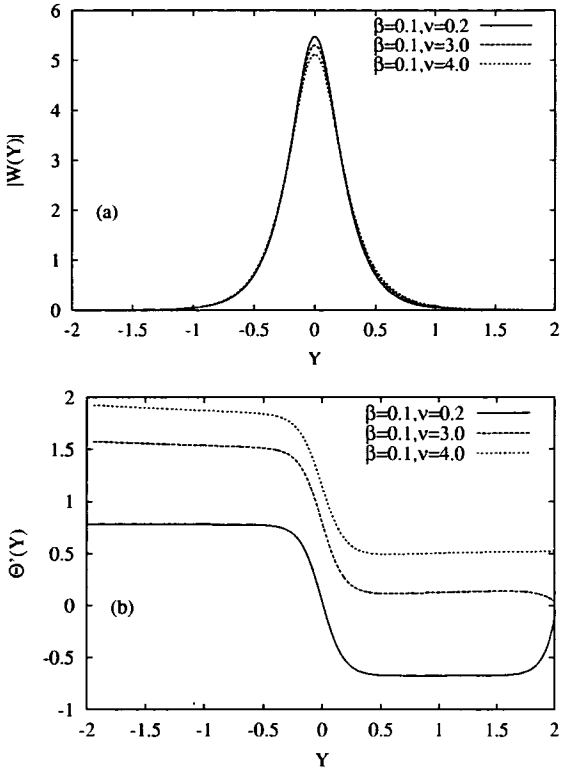

FIG. 2. (a) Some pulse envelopes $|W(Y)|$ for $\beta=0.1$; (b) the corresponding chirp $\Theta'(Y)$.

$$W(Y)=\nu^{1/3}(1+4\beta^2)^{1/6}w(y),$$

$$\nu Y+\mu_0=\nu^{2/3}(1+4\beta^2)^{1/3}y\equiv y/\Delta,$$

$$\bar{B}=\frac{B}{\nu^{1/3}(1+4\beta^2)^{2/3}}, \quad \Delta=\frac{1}{\nu^{2/3}(1+4\beta^2)^{1/3}}. \tag{15}$$

Here, β and Δ (or ν) are parameters determined by the original Eq. (1), while $\bar{B}$ is adjustable. Our goal is to find pulse-like solutions to Eq. (14) for which $w\to0$, $w'\to0$ as $y\to\pm\infty$. For specified β and Δ, solutions may be expected to exist only for selected values of $\bar{B}$, with corresponding peak amplitude $|w|=|w|_{\max}$ at some location $y=y_0\equiv\Delta\mu_0$. Then, the corresponding parameters ν, B, δ, and b follow from Eq. (11) when $\hat{\alpha}$ is specified, while the pulse is centered on the path

$$T+\tfrac{1}{2}\hat{\alpha}Z+\delta^2BZ^2=\zeta=(c_0/\hat{\alpha})+(1+4\beta^2)^{1/3}\nu^{-1/3}\delta^{-1/2}y_0\equiv\zeta_0.$$

Since c_0 and c_1 correspond merely to a shift in reference phase and in the T origin, they are set to zero without loss of generality.

In seeking solutions with $|w|$ small except near $\zeta=\zeta_0$, it is appropriate to analyze the linearization

$$w'(y)=v(y),$$

$$v'=-2(1+2i\beta)(y-i\Delta)w-2i\bar{B}(1+2i\beta)v, \tag{16}$$

which may be put into the matrix form $(w' \; v')^T = A(y)(w \; v)^T$, where the eigenvalues of A are

$$\lambda \equiv \alpha + i\gamma = -i(1+2i\beta) \times \{\bar{B} \pm \sqrt{\bar{B}^2 + 2(1+2i\beta)^{-1}(y - i\Delta)}\}. \quad (17)$$

The real parts $\alpha_\pm$ and imaginary parts $\gamma_\pm$ of these two eigenvalues of A are found from the identity

$$(\alpha - 2\bar{B}\beta) + i(\gamma + \bar{B}) = \mp i(1+2i\beta) \times \sqrt{\bar{B}^2 + 2(1+2i\beta)^{-1}(y - i\Delta)},$$

so yielding the compact representation

$$\lambda = \lambda_\pm = \alpha_\pm + i\gamma_\pm = -i\bar{B}(1+2i\beta) \pm \frac{\rho(y) + |\rho(y)|}{\{\mathrm{Re}\,\rho(y) + |\rho(y)|\}^{1/2}}, \quad (18)$$

where

$$\rho(y) \equiv -(1+2i\beta)\{y + \tfrac{1}{2}\bar{B}^2 + i(\beta\bar{B}^2 - \Delta)\}.$$

Since $\mathrm{Re}\,\rho(y) + |\rho(y)| > 0$ for all y, the eigenvalues $\lambda_\pm$ satisfy $\mathrm{Re}\,\lambda_+ \equiv \alpha_+ > \alpha_- \equiv \mathrm{Re}\,\lambda_-$. Moreover, except in some vicinity of the location $y = \bar{y} \equiv -\frac{1}{2}\bar{B}^2 + 2\beta(\beta\bar{B}^2 - \Delta)$ at which $\mathrm{Re}\,\rho(\bar{y}) = 0$, the eigenvalues have $\alpha_+ > 0$ and $\alpha_- < 0$. Thus, outside this restricted portion of the y axis, there exists an *unstable manifold* of solutions which, near $|w| = 0$, has $(w' \; v')^T \approx \lambda_+ (w \; v)^T$. Along these solutions, $|w|$ *decreases* as y decreases, with $v \approx \lambda_+ w$. Also, there is a *stable manifold* on which $v \approx \lambda_- w$ (and $|w|$ decreases as y increases). Each of these manifolds is two dimensional [since the system (16) is invariant under all mappings $\{w, v\} \mapsto \{we^{is}, ve^{is}\}$ for s real]. For chosen $\{\Delta, \beta\}$, the required pulselike solution to Eq. (14) is described by a *connection* between these two manifolds. However, since $\mathrm{Re}\,\rho = -y - \frac{1}{2}\bar{B}^2 + 2\beta(\beta\bar{B}^2 - \Delta)$, it is clear that $|\alpha_+|$ and $|\alpha_-|$ remain small for $y > \bar{y}$, but grow as y decreases below the value $\bar{y}$. This suggests that the pulse center $y = y_0$ lies in $y < \bar{y}$.

To confirm this conjecture, we consider the limiting equation ($\beta \to 0, \; \Delta \to 0$)

$$w''(y) + 2i\bar{B}w'(y) + 2yw + 2|w|^2 w = 0$$

and make the substitution $w = e^{-i\bar{B}y}\chi(y)$ to yield

$$\chi''(y) - \Gamma^2\chi + 2|\chi|^2\chi = -(\Gamma^2 + \bar{B}^2 + 2y)\chi. \quad (19)$$

When the right-hand side is neglected, Eq. (19) is the NLS equation having the familiar pulse solutions [cf. Eq. (2)]

$$\chi = \Gamma \,\mathrm{sech}\,\Gamma(y - y_0),$$

with center at $y = y_0$, with amplitude Γ, and with half-width Γ^{-1}. Neglect of the right-hand side is a good approximation provided that

$$|\Gamma^2 + \bar{B}^2 + 2y| \ll \Gamma^2 \quad \text{for} \quad \Gamma|y - y_0| < 4,$$

which is possible provided that $y_0 \approx -\frac{1}{2}(\bar{B}^2 + \Gamma^2)$, with $\Gamma^3 \geq 8$.

For chosen $\{\Delta, \beta\}$, a search procedure for y_0 and $\bar{B}$ is used, starting from the values y_1 and $\bar{B}_1$ (see Appendix). Then, motivated by the approximation $\chi \approx \Gamma_1 \,\mathrm{sech}\,\Gamma_1(y - y_1)$, where $\Gamma_1 \equiv \{-\bar{B}_1^2 - 2y_1\}^{1/2}$, a location at which $|\chi| \approx \varepsilon$ is estimated as $y_- = y_1 - \Gamma_1^{-1}\ln(2\Gamma_1/\varepsilon)$, for some chosen $\varepsilon \ll 1$. Equation (14) is then integrated numerically from y_- with initial conditions $w(y_-) = \varepsilon$, $w'(y_-) = \varepsilon\lambda_+(y_-)$ (and with β and Δ moderately small) so yielding a maximum of $|w|$ near to $y = y_1$, followed by a minimum of $|w|$ near to $y = 2y_1 - y_-$. The parameters y_- and $\bar{B}$ are then adjusted to reduce to $o(\varepsilon^2)$ the minimum of $|w|^2 + K|w'|^2$ occurring on a solution curve $w(y)$ for $y > y_-$ (with $K \approx |\lambda_-|^{-2}$). Once y_- and $\bar{B}$ are identified yielding an acceptably small value for this minimum, the corresponding pulse center y_0 is determined by locating the maximum of $|w|^2$.

V. NUMERICAL RESULTS AND DISCUSSION

For small β and δ (large ν), Eq. (A5) shows the significance of the parameter $\Delta\beta^{-1/3}$. Indeed, the initial approximation $\bar{B}_1$ exists only for $\Delta\beta^{-1/3} \geq \frac{3}{4}$, which corresponds to the threshold value for excess gain δ as a function of frequency sliding-rate $\hat{\alpha}$ predicted by Kodama and Wabnitz [7] (namely, $\hat{\alpha}^2\beta(1+4\beta^2) \leq \frac{64}{27}\delta^3$). Figure 1 shows some pulses $|W(Y)| = \delta^{-1/2}|u|$ for $\beta = 0.001$ and $\beta = 0.002$. For these values of ν ($= 10, 30$), the associated frequency perturbations $\Theta'(Y)$ are almost constant, though with a small-amplitude tanh profile of chirp [even though ν is not small, c.f. Eq. (8) and Sec. III]. Other calculations for $\beta = 0.001$ confirm the existence of similar pulses for $\Delta\beta^{-1/3} = 0.75$, but show that the boundary for the nonexistence of pulses is remarkably close to $\Delta = \frac{3}{4}\beta^{1/3}$ throughout $\beta < 0.04$. In fact, when pulses exist, two families exist [corresponding to the two negative roots of Eq. (A5)]. Pulses of the second family have smaller peak amplitude, but are unstable according to variational theory [7,8].

For larger filter strength $\beta = 0.1$ and smaller $\nu = \hat{\alpha}/\delta^{3/2}$, similar narrow pulses close in shape to a sech profile exist (see Fig. 2). As ν increases for fixed filter strength β, the peak value of $|W|$ decreases gradually and the pulse broadens. The pulses become more noticeably asymmetric for larger ν and the tanh-profile chirp $\Theta'(Y)$ [$= \delta^{-1/2}(\theta_\zeta + \hat{\alpha}Z)$] becomes prominent [see Fig. 2(b)]. Indeed, expressions (8) remain remarkably accurate even for $\nu = 3.0$, so that the perturbation analysis of Sec. III is a useful description of

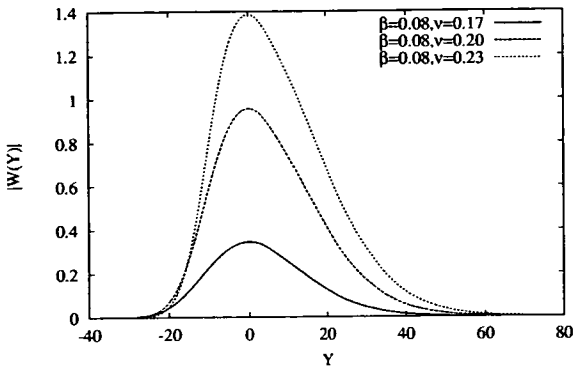

FIG. 3. $|W(Y)|$ for broad, asymmetric pulses existing for $\beta=0.08$ when ν takes moderate values.

these pulses far beyond its expected region of validity $\nu \ll 1$.

However, for $\beta \approx 0.08$ and $\nu \approx 0.20$ a second family of smaller amplitude decidedly asymmetric, broad pulses have been found by numerical search, as shown in Fig. 3. These pulses, with moderate filter strength and with sliding-rate $\hat{\alpha}$ and excess gain δ comparably important, have parameter b of much larger modulus than the narrow pulses. Also, the chirp $\Theta'(Y)$ for these pulses is much closer to the commonly assumed linear ramp than to the tanh profiles shown in Fig. 2(b). Moreover, a stability analysis currently being undertaken shows that these pulses are stable in this parameter range.

In summary, for a remarkably wide range of the parameters β, δ, and $\hat{\alpha}$, there are pulses which are exactly nondistorting and which accelerate uniformly. Typically, their profile is remarkably close to a sech curve, even though the frequency increases linearly with Z and has a pronounced chirp through the pulse.

ACKNOWLEDGMENTS

Ch.R. would like to thank the Department of Science and Technology, Government of India, for financial support. M.F. acknowledges support from the Sub-Programa Ciência e Tecnologia do 2° Quadro Comunitário de Apoio (Grant No. PRAXIS XXI/BD/21642/99).

APPENDIX

By introducing into Eq. (14) the substitutions $w=e^{-i\bar{B}y}\chi(\eta)$, $\eta=y-y_0$, we obtain

$$\chi''+(2\chi\chi^*-\Gamma^2)\chi=F(\chi,\chi^*,\chi',\eta), \tag{A1}$$

where

$$F(\chi,\chi^*,\chi',\eta)=4\beta\bar{B}\chi'-4i\beta\bar{B}^2\chi-4i\beta\chi^2\chi^* -2\{\eta+2\beta\Delta+2i\beta(y_0+\eta)-i\Delta\}\chi \tag{A2}$$

and where * denotes a complex conjugate.

From Eq. (A1) and its complex conjugate, we find the two identities

$$\frac{d}{d\eta}(\chi^{*'}\chi'+\chi^2\chi^{*2}-\Gamma^2\chi\chi^*)=\chi^{*'}F+\chi'F^*,$$

$$\frac{d}{d\eta}(\chi^*\chi'-\chi\chi^{*'})=\chi^*\chi''-\chi\chi^{*''}=\chi^*F-\chi F^*.$$

Hence, for pulses with $|\chi|\to 0$ as $\eta\to\pm\infty$, two integral conditions arise

$$\int_{-\infty}^{\infty}(\chi^{*'}F+\chi'F^*)d\eta=0, \quad \int_{-\infty}^{\infty}(\chi^*F-\chi F^*)d\eta=0.$$

Introducing into these the representations $\chi=\rho e^{i\phi}$, $\chi^*=\rho e^{-i\phi}$ yields

$$\int_{-\infty}^{\infty}\rho^2 d\eta+4\beta\bar{B}\int_{-\infty}^{\infty}(\rho')^2 d\eta -2(2\beta\bar{B}^2-\Delta+2\beta y_0)\int_{-\infty}^{\infty}\rho^2\phi' d\eta +4\beta\bar{B}\int_{-\infty}^{\infty}\rho^2(\phi')^2 d\eta -4\beta\int_{-\infty}^{\infty}\eta\rho^2\phi' d\eta-4\beta\int_{-\infty}^{\infty}\rho^4\phi' d\eta=0 \tag{A3}$$

and

$$(2\beta\bar{B}^2+2\beta y_0-\Delta)\int_{-\infty}^{\infty}\rho^2 d\eta+2\beta\int_{-\infty}^{\infty}\rho^4 d\eta +2\beta\int_{-\infty}^{\infty}\eta\rho^2 d\eta-2\beta\bar{B}\int_{-\infty}^{\infty}\rho^2\phi' d\eta=0. \tag{A4}$$

To leading order in β and Δ, we have $\rho=\Gamma_1\,\mathrm{sech}\,\Gamma_1\eta$ with $\phi'=O(\beta,\Delta)$, so that by approximating $\bar{B}$ and y_0 by $\bar{B}_1$ and by $y_1=-\frac{1}{2}(\Gamma_1^2+\bar{B}_1^2)$ we obtain the leading-order approximations

$$\Gamma_1^2\int_{-\infty}^{\infty}\mathrm{sech}^2\,\Gamma_1\eta d\eta +4\beta\bar{B}_1\Gamma_1^4\int_{-\infty}^{\infty}\mathrm{sech}^2\,\Gamma_1\eta\tanh^2\Gamma_1\eta d\eta=0$$

and

$$(2\beta\bar{B}_1^2+2\beta y_1-\Delta)\Gamma_1^2\int_{-\infty}^{\infty}\mathrm{sech}^2\,\Gamma_1\eta d\eta +2\beta\Gamma_1^4\int_{-\infty}^{\infty}\mathrm{sech}^4\,\Gamma_1\eta d\eta=0.$$

These yield the equations

$$\tfrac{4}{3}\bar{B}_1\Gamma_1^2\beta+1=0, \quad \bar{B}_1^2+\tfrac{1}{3}\Gamma_1^2=\beta^{-1}\Delta,$$

which are just the equations for the equilibrium points of the Kodama and Wabnitz [7] analysis. The resulting cubic equation for $\bar{B}_1$,

$$4\beta\bar{B}_1^3-4\Delta\bar{B}_1-1=0, \tag{A5}$$

has (two) roots with $\beta\bar{B}_1<0$ only for $\Delta\beta^{-1/3}\geqslant\frac{3}{4}$, then giving $y_1=(4\delta-\bar{B}_1^{-1})/8\beta$ and $\Gamma_1=(-4\beta\bar{B}_1/3)^{-1/2}$.

[1] L. F. Mollenauer, E. Lichtman, G. T. Harvey, M. J. Neubelt, and B. M. Nyman, Electron. Lett. **29**, 792 (1992).

[2] L. F. Mollenauer, J. P. Gordon, and S. G. Evangelides, Opt. Lett. **17**, 1575 (1992).

[3] A. Hasegawa and Y. Kodama, *Solitons in Optical Communications* (Clarendon, Oxford, 1995).

[4] E. V. Vanin, A. I. Korytin, A. M. Sergeev, D. Anderson, M. Lisak, and L. Vázquez, Phys. Rev. A **49**, 2806 (1994).

[5] M. I. Carvalho, S. R. Singh, and D. N. Christodoulides, Opt. Commun. **120**, 311 (1995).

[6] D. F. Parker, C. Sophocleous, and Ch. Radha, J. Phys. A: Math. Gen. **35**, 1283 (2002).

[7] Y. Kodama and S. Wabnitz, Opt. Lett. **19**, 162 (1994).

[8] S. Burtsev and D. J. Kaup, J. Opt. Soc. Am. B **14**, 627 (1997).

Stability of screening solitons in photorefractive media

M. Facão* and D. F. Parker†
School of Mathematics and Statistics, University of Edinburgh, The King's Buildings, Edinburgh EH9 3JZ, United Kingdom
(Received 28 February 2003; published 18 July 2003)

Normal mode stability of both rectilinear and self-bending photorefractive screening solitons is considered. In each case, the Evans function procedure is used to investigate stability and to search for internal modes. For the rectilinear case, a standard Evans function procedure is applied. However, in the self-bending case the asymptotic form of the eigenvalue problem is a system of Airy equations, instead of the usual system of constant coefficient differential equations. To overcome this difference, a modified version of the Evans function method, using Airy functions rather than exponentials, is implemented and applied. The results confirm stability and give an internal mode pattern in good agreement with full numerical integration.

DOI: 10.1103/PhysRevE.68.016610 PACS number(s): 42.65.Tg, 42.65.Sf, 42.70.Nq

I. INTRODUCTION

Photorefractive solitons were predicted in 1992 [1] and were demonstrated one year later [2]. They are distinct amongst optical solitons in requiring only low power lasers, as small as μWs, and elementary experimental apparatus. Photorefractive materials are doped electro-optic crystals that have electronic energy levels within the forbidden gap. The photorefractive effect consists of a reversible change of the refractive index induced by a spatial variation of an optical field, which is accomplished in two steps: creation of free charge by light absorption and charge migration by drift and diffusion. A photorefractive soliton is a beam that becomes self-trapped through the above mechanism, which may be interpreted as though the beam were inducing its own waveguide. Several mechanisms are possible, each one leading to a different kind of photorefractive soliton. Here we focus on the so-called *screening* photorefractive solitons. In this type, the photorefractive crystal is subjected to an external voltage orthogonal to the light propagation. The final charge distribution in the illuminated region produces a space-charge electric field E_{sc} with polarity opposite to the external field. The change in the refractive index that results from the electro-optic effect is given by $\Delta n = n^3 r_{\text{eff}} E_{sc}$, where n is the unperturbed refractive index and r_{eff} is an effective electro-optic coefficient. In turn, the space-charge field depends only on the beam power whenever only the drift produced by the external field is important, but depends also on the transverse spatial derivative of the beam power whenever the diffusion mechanism is appreciable. The first case produces symmetric beams propagating along rectilinear trajectories and occurs for high external voltage and narrow beams [3,4]. The latter produces slightly asymmetric beams propagating along a parabolic trajectory, usually known as *self-bending* solitons, and occurs for broader beams [5–7]. The only reported stability analysis of the *self-bending* solitons was based on simulations of the full evolution equation [5,6]. In this work we investigate their normal mode stability by a method similar to the standard Evans function method [8–10]. Unlike usual applications, the stability equations do not tend to constant coefficient differential equations away from the beam, but instead they tend to a system of Airy equations. We have used the Airy functions to develop a modification to the Evans function method and have applied it in a search for stability eigenvalues of the self-bending solitons.

In Sec. II, we introduce the ordinary differential equation obtained from the partial differential equation by a similarity variable reduction and briefly describe the characteristic profiles for the two types of solutions: rectilinear and self-bending. The stability eigenvalue problem is presented in Sec. III, where we prove the stability of the rectilinear beams using the *Vakhitov-Kolokolov* criterion. Sections IV and V are devoted to the Evans function method. First, we find the internal modes of the diffusionless case applying the standard version of the method. Then we define a suitable Evans function for the diffusive case. Its application confirms the stability and gives the internal modes of the self-bending solutions. Finally, in Sec. VI, we present the results of numerical integration of the full evolution equation, which are in agreement with the normal mode stability analysis.

II. MODEL AND LOCALIZED SOLUTIONS

Using the band transport model of the photorefractive effect by Kukhtarev and Vinetskii [11,12] to evaluate the space-charge field E_{sc} and considering the change of refractive index $\Delta n = n^3 r_{\text{eff}} E_{sc}$, we arrive at the following equation describing the evolution of the optical field [4,5]:

$$iq_z + q_{xx} - \frac{q}{1+|q|^2} + \gamma \frac{(|q|^2)_x q}{1+|q|^2} = 0, \tag{1}$$

where q, z, x, and γ are normalized versions of the complex beam envelope, propagation distance, transverse spatial coordinate, and diffusion parameter, respectively.

The above equation admits self-similar solutions having $\eta = x - 2Vz + az^2$ as a similarity variable (with V and a constants) [7]. Thus, introducing the ansatz $q(z,x) = \exp[i\theta(z,\eta)]F(\eta)$ into Eq. (1), with F and θ real, and requiring that $F \to 0$ as $\eta \to \pm\infty$, we obtain

$$F'' + \left[B + a\eta - \frac{1}{1+F^2} + \gamma \frac{2FF'}{1+F^2} \right] F = 0 \tag{2}$$

and

*Electronic address: M.M.Resende-Viera-Facao@sms.ed.ac.uk
†Electronic address: D.F.Parker@ed.ac.uk

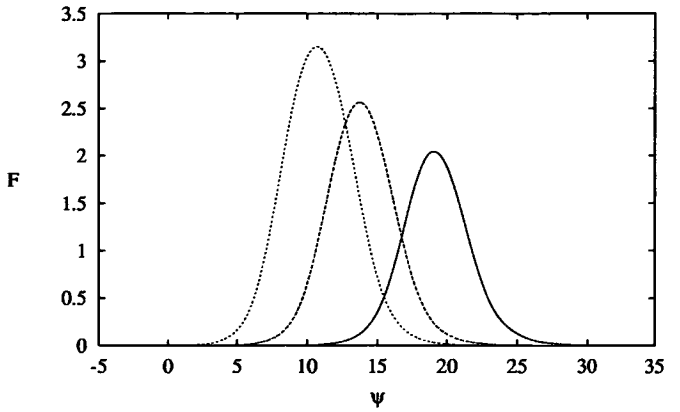

FIG. 1. Three beam profiles for $\gamma=0.1$, corresponding to points marked ○ in Fig. 2.

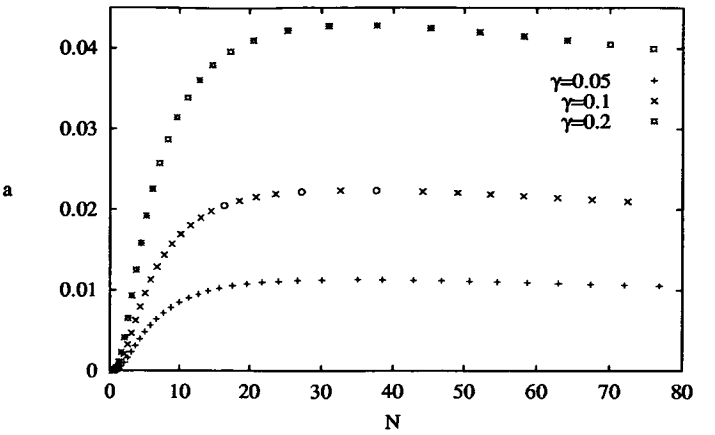

FIG. 2. Dependence of the curvature parameter a on the beam power N, for three values of γ.

$$\theta(z,\eta)=(V-az)\eta+\tfrac{1}{3}a^2z^3-aVz^2+(V^2-B)z+C, \tag{3}$$

where B and C are arbitrary parameters. For $\gamma=0$, the curvature parameter a should be equal to 0 and for each B, there then exists a family of solutions having peak amplitude μ related to B, through $B=\ln(1+\mu^2)/\mu^2$. They are symmetrical about the peak position $\eta=\eta_0$ [3,4]. In the diffusive case, $\gamma\neq 0$, the curvature parameter is necessarily nonzero. The beam profiles result from the numerical integration of Eq. (2), using a shooting method [6,7]. The method uses estimates obtained from a perturbation procedure based upon the diffusionless profiles ($\gamma=0$). The initial conditions for F and F' may be taken from the Airy functions in a way already used by Aleshkevich *et al.* [13] to treat the diffusive case of photorefractive solitons, but when the nonlinearity was of the Kerr type.

In the diffusive case, we transform Eq. (2) using $a\psi=a\eta+B-1$ so as to obtain an ordinary differential equation (ODE) without the parameter B as follows:

$$F''+\left[a\psi-\frac{F^2}{1+F^2}+\gamma\frac{2FF'}{1+F^2}\right]F=0. \tag{4}$$

In fact, in the tail region where $F\simeq 0$, Eq. (4) transforms to the Airy equation $F''-zF=0$ by the change of variable $z(\psi)=-a^{1/3}\psi$. The only solutions that decay as $z\to+\infty$ ($\psi\to-\infty$) are multiples of $\mathrm{Ai}(z)$. At the other extreme, both $\mathrm{Ai}(z)$ and $\mathrm{Bi}(z)$ decay algebraically and oscillatorily. Nevertheless, numerics on Eq. (4) give us beam profiles with rapid decay at either side. This suggests that the right tail of F is still in a region of positive z and is picking up the exponential behavior of $\mathrm{Bi}(z)$ for $z>0$. The algebraically decaying oscillations should appear in the right tail only when $|F|$ is already very small. Hence, the initial conditions for numerical integration of Eq. (4) are chosen as

$$F(\psi_1)=c_1\mathrm{Ai}[z(\psi_1)]=\epsilon,$$

$$F'(\psi_1)=-c_1a^{1/3}\mathrm{Ai}'[z(\psi_1)],$$

where ψ_1 is an estimate of the left tail position used in the shooting method. We were able, by adjusting ψ_1, to obtain localized solutions for γ up to 0.2 over a wide range of beam power $N=\int_{-\infty}^{\infty}F^2d\psi$. Figure 1 shows three of these beam profiles with different peak amplitudes $F_{\max}$, for $\gamma=0.1$. For fixed γ, the solutions may be parametrized by the curvature parameter a or by the beam power N. The dependence of a on N is not monotonic but exhibits a maximum (see Fig. 2). For larger γ, beam profiles have also been computed, but for $\gamma=0.3$, 0.4, and 0.5 the numerical procedure fails to find profiles for increasingly wide intervals of N.

III. NORMAL MODE STABILITY

In order to perform linear stability analysis, we consider a total solution of the form $q(z,\eta)=\exp[i\theta(z,\eta)][F(\eta)+w(z,\eta)]$, where $F(\eta)$ is the real beam profile obtained from Eq. (2) and $w(z,\eta)$ is a small complex perturbation term. Inserting the above form into Eq. (1), and seeking solutions in the form $w(\eta,z)=u(\eta)e^{i\lambda z}+v^*(\eta)e^{-i\lambda^* z}$, we obtain the following eigenvalue problem:

$$L\begin{pmatrix}u\\v\end{pmatrix}=\lambda\begin{pmatrix}u\\v\end{pmatrix}, \tag{5}$$

where the operator L is given by

$$L=\begin{pmatrix}\partial_{\eta\eta}+B+a\eta+\gamma\dfrac{F^2}{1+F^2}\partial_\eta+r(\eta) & \gamma\dfrac{F^2}{1+F^2}\partial_\eta+s(\eta)\\ -\gamma\dfrac{F^2}{1+F^2}\partial_\eta-s(\eta) & -\partial_{\eta\eta}-B-a\eta-\gamma\dfrac{F^2}{1+F^2}\partial_\eta-r(\eta)\end{pmatrix}$$

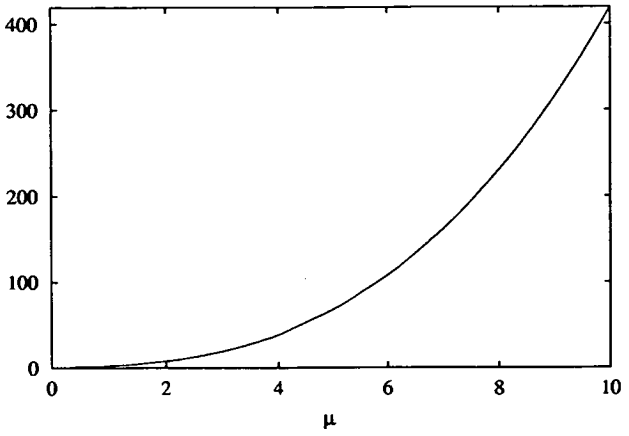

FIG. 3. Dependence of beam power N on the peak amplitude μ.

and r and s are functions of η defined in terms of F and F' as

$$r(\eta)=\frac{-1+3\gamma FF'+\gamma F^3F'}{(1+F^2)^2},$$

$$s(\eta)=\frac{F^2-\gamma F^3F'+\gamma FF'}{(1+F^2)^2}.$$

The stability of the diffusionless case ($\gamma=0$ and $a=0$) may be investigated by the well-known *Vakhitov-Kolokolov* criterion [14], which in this case predicts normal mode stability if $\partial N/\partial B<0$. This condition may be rewritten in the form $N'(\mu)/B'(\mu)<0$, where $N(\mu)$ is easily evaluated as the definite integral,

$$N(\mu)=\int_0^{\mu}\frac{\mu G^2dG}{\sqrt{\mu^2\ln(1+G^2)-\ln(1+\mu^2)G^2}}.$$

The derivative $B'(\mu)$ is negative for all positive μ and $N(\mu)$ is found through the numerical integration to increase monotonically for μ in the range (0,40). Results up to $\mu=10$ are shown in Fig. 3. Therefore, $\partial N/\partial B<0$ and, according to the *Vakhitov-Kolokolov* criterion, all rectilinear screening solitons are stable.

IV. THE EVANS FUNCTION METHOD APPLIED TO RECTILINEAR PROPAGATION

The stability problem for $\gamma=0$ and $a=0$ may also be treated using the Evans function method. We briefly introduce an approach to the standard Evans function method applied to this case. Stability system (5) for $\gamma=0$ and $a=0$ may be written as a system of first-order differential equations given by

$$\frac{dY}{d\eta}=A(\eta,\lambda)Y, \tag{6}$$

where $Y=(u\ u_\eta\ v\ v_\eta)^T$ and

$$A(\eta,\lambda)=\begin{pmatrix}0 & 1 & 0 & 0\\ -B-r(\eta)+\lambda & 0 & -s(\eta) & 0\\ 0 & 0 & 0 & 1\\ -s(\eta) & 0 & -B-r(\eta)-\lambda & 0\end{pmatrix}.$$

As $\eta\to\pm\infty$, $r(\eta)\to-1$, and $s(\eta)\to0$, thus the matrix operator tends to a constant matrix $A_\infty(\lambda)$. Hence, the asymptotic system has solutions of the form

$$Y_i^{\infty}(\eta,\lambda)=y_i(\lambda)\exp[\rho_i(\lambda)\eta],\quad i=1,\ldots,4,$$

where $\rho_i(\lambda)$ are the eigenvalues of $A_\infty(\lambda)$ given by $\pm\sqrt{\omega\pm\lambda}$, with $\omega=1-B$, and $y_i(\lambda)$ are the corresponding eigenvectors. Full problem (6) has four solutions Y_i^- for which the behavior as $\eta\to-\infty$ satisfies $Y_i^-(\eta,\lambda)\sim Y_i^{\infty}$ and has also four solutions Y_i^+ for which the behavior as $\eta\to+\infty$ satisfies $Y_i^+(\eta,\lambda)\sim Y_i^{\infty}$. Either set of solutions forms a basis for the solution space to Eq. (6). Whenever λ belongs to the set $S=\{\lambda\in\mathbb{R}:|\lambda|>\omega\}$ two of the values $\rho_i(\lambda)$ are purely imaginary and the remaining two are real and of opposite sign. For $\lambda\in S$ there is necessarily an intersection between the subspace spanned by the three solutions bounded at $+\infty$ and the subspace spanned by the three solutions bounded at $-\infty$. This set of eigenfunctions corresponds to the continuous spectrum. There are also isolated eigenvalues occurring in $\mathbb{C}\backslash S$, for which the eigenfunctions decay exponentially in both directions. One example is $\lambda=0$, which is always an eigenvalue of algebraic multiplicity equal to 4. This fact is related to the four invariances of evolution equation (1), namely, translations in z and in x, Galilean transformation and constant change of phase. For $\lambda\in\mathbb{C}\backslash S$, there are always two values of $\rho_i(\lambda)$ whose real part is positive. Let us denote them by $\rho_j(\lambda)$ $(j=1,2)$. The other two, which we denote by $\rho_k(\lambda)$ $(k=3,4)$, have negative real part. An eigenfunction corresponding to an isolated eigenvalue must be a linear combination of $Y_1^-(\eta,\lambda)$ and $Y_2^-(\eta,\lambda)$ and simultaneously a linear combination of $Y_3^+(\eta,\lambda)$ and $Y_4^+(\eta,\lambda)$. In other words, the two pairs of functions should be linearly dependent, that is,

$$a_1Y_1^-(\eta,\lambda)+a_2Y_2^-(\eta,\lambda)=a_3Y_3^+(\eta,\lambda)+a_4Y_4^+(\eta,\lambda). \tag{7}$$

Here we define the Evans function as the determinant whose columns are Y_j^- and Y_k^+ evaluated, for instance, at the peak location of F, which, by the translational invariance of the corresponding ODE [i.e., Eq. (2) with $a=0$, $\gamma=0$], may be chosen as $\eta=0$. Thus, the following determinant

$$D(\lambda)=\left|\begin{matrix}\vdots & \vdots & \vdots & \vdots\\ Y_1^- & Y_2^- & Y_3^+ & Y_4^+\\ \vdots & \vdots & \vdots & \vdots\end{matrix}\right|_{(0,\lambda)} \tag{8}$$

is an analytic function in λ, which is equal to 0 if and only if Eq. (7) is satisfied, that is, if and only if λ is an eigenvalue of Eq. (5). Moreover, the multiplicity of its 0's coincides with the algebraic multiplicity of the eigenvalues. One important

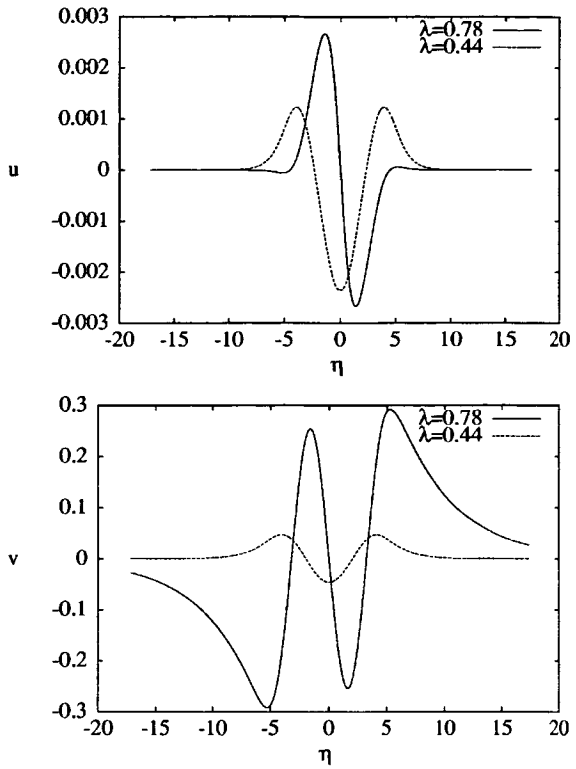

FIG. 4. Perturbations u and v that constitute the eigenfunctions corresponding to $\lambda=0.44$ and $\lambda=0.78$ for a solution $F(\eta)$ of amplitude $\mu=4.0$.

advantage of this method is based on the analyticity of $D(\lambda)$, which permits the use of the argument principle for counting the 0's of $D(\lambda)$ inside a certain region only by determining the change of $\arg D(\lambda)$, as $D(\lambda)$ is evaluated while λ moves around the boundary of such a region.

The application of the Evans function method to the symmetric beams, up to an amplitude of $\mu=6.0$, has confirmed their stability. All the eigenvalues lie on the real axis within the gap of the continuous spectrum. For small amplitudes, up to $\mu=1.2$, only the zero eigenvalue exists with the expected algebraic multiplicity equal to 4. Between $\mu=1.2$ and $\mu=1.3$, one pair of symmetrically placed eigenvalues emerges from the continuous spectrum and an increase in amplitude makes these eigenvalues move towards the origin. For higher amplitudes, further pairs of real eigenvalues were observed. For instance, for $\mu=4.0$ there are two nonzero pairs and for $\mu=6.0$ there are three nonzero pairs. These nonzero real eigenvalues are characteristic of nonintegrable generalized nonlinear Schrödinger (NLS) models and are usually called *internal modes* [15–17]. The eigenfunctions of the nonzero eigenvalues for $\mu=4.0$ are shown in Fig. 4. The eigenfunction corresponding to the pair of eigenvalues lower in magnitude is symmetric, while the other is antisymmetric.

V. THE EVANS FUNCTION METHOD APPLIED TO SELF-BENDING BEAMS

The normal mode stability for the diffusive case is less standard than for the diffusionless case. The numerically obtained profiles for $F(\psi)$ show rapid decay to 0 in both directions. Thus, the asymptotic form of eigenvalue problem (5) for the variable ψ takes the form of two Airy equations for which the independent variables depend on the eigenvalue λ. They read

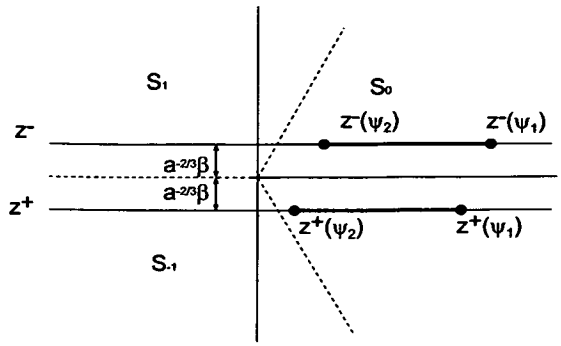

FIG. 5. $z^{\pm}$ lines and profile domains $[z^{\pm}(\psi_2),z^{\pm}(\psi_1)]$ for $\lambda=\alpha-\beta i$.

$$(\partial_{z^+z^+}-z^+)u=0, \quad (\partial_{z^-z^-}-z^-)v=0,$$

where $z^{\pm}=a^{-2/3}(-a\psi\pm\lambda)$. The variables z^+ and z^- are complex, since λ may be complex. For fixed λ, the domain of real ψ transforms into two parallel lines in the complex plane of $z^{\pm}$ (see Fig. 5). The lines lie in opposite half-planes being at equal distance from the real axis. Changing the real part of λ translates z^+ and z^- along the same line and, consequently, relocates the profile in the $z^{\pm}$ domains. Changing the imaginary part of λ translates each line vertically.

For all real λ, the two lines lie within the real axis. The portions corresponding to $[z^{\pm}(\psi_2),z^{\pm}(\psi_1)]$ will be called the profile domains. The profile locations in the z^+ and z^- domains coincide for $\lambda=0$ and are on the positive semiaxis, but as the modulus of λ increases they move apart in opposite directions. We define two important sets of real λ.

(1) $S_1=\{\lambda\in\mathbb{R}:0<|\lambda|<\lambda_1\}$. For $\lambda\in S_1$, both profile domains remain on the positive semiaxis and only solutions having rapid decay in both directions are the candidates as solutions of eigenvalue problem (5). They should match the behavior of $\mathrm{Ai}(z)$ to the left ($\psi-\psi^*<0$, where ψ^* is the peak position) and the behavior of $\mathrm{Bi}(z)$ to the right ($\psi-\psi^*>0$). Note that, although $\mathrm{Ai}(z)$ is also a bounded function (with algebraic decay) as $z\to-\infty$ ($\psi\to+\infty$), within and near the profile location it still grows to the left. Hence, we may assert that in S_1 the eigenvalues are discrete.

(2) $S_2=\{\lambda\in\mathbb{R}:|\lambda|>\lambda_1>0\}$. For $\lambda\in S_2$, one of the profile domains lies on the positive semiaxis and the other one has one or both limits on the negative semiaxis. Here, there exists an extra possible matching Airy function, which is $\mathrm{Ai}(z)$ to the left of the domain that lies in negative z. Hence, for any $\lambda\in S_2$, there exists a bounded solution to Eq. (5) and we may identify S_2 as the continuous spectrum. We still may divide the set S_2 in two subsets, namely, $S_{2a}=\{\lambda_1<|\lambda|<\lambda_2\}$ and $S_{2b}=\{|\lambda|>\lambda_2\}$. They correspond to the cases of the profile domain on the left being either only partially or totally on the negative semiaxis, respectively. The division embodies the fact that only for $\lambda\in S_{2b}$ are the solutions simi-

lar to the solutions in the continuous spectrum of the nondiffusive case and of other similar systems; that is, they are similar to radiation modes.

In order that an eigenvalue may have nonzero imaginary part, the corresponding solution of Eq. (5) should be bounded and should decay exponentially in both directions. This is possible if the solution matches the exponentially decaying Airy functions in each direction. Standard theory [18] involves three Airy functions $\mathrm{Ai}_0(z)$ and $\mathrm{Ai}_{\pm 1}(z)$, each of which decays exponentially in a 120° sector of the z plane. In such a sector it is said to be *recessive*. For certain regions of the λ plane, each of the loci $z^+(\psi)$ and $z^-(\psi)$ as $\psi \to \pm\infty$ remains in a fixed sector as λ varies. One such region is the lower half-plane, which we shall be treating later. Thus, numerical integration of the eigenvalue problem made within such regions needs to involve only a fixed choice of appropriate recessive Airy functions. In the lower half-plane, they are $\mathrm{Ai}_{-1}(z^+)$ as $z^+ \to -\infty$, $\mathrm{Ai}_0(z^+)$ as $z^+ \to +\infty$, $\mathrm{Ai}_1(z^-)$ as $z^- \to -\infty$, and $\mathrm{Ai}_0(z^-)$ as $z^- \to +\infty$.

From the above observations, let us define a modified Evans function. The stability system may also be written as a system of first-order differential equations as

$$\frac{dY}{d\psi} = A(\psi,\lambda)Y, \tag{9}$$

where $Y=(u\ u_\psi\ v\ v_\psi)^T$ and

$$A(\psi,\lambda)=\begin{pmatrix} 0 & 1 & 0 & 0 \\ -a\psi-1-r+\lambda & -\gamma F^2/(1+F^2) & -s & -\gamma F^2/(1+F^2) \\ 0 & 0 & 0 & 1 \\ -s & -\gamma F^2/(1+F^2) & -a\psi-1-r-\lambda & -\gamma F^2/(1+F^2) \end{pmatrix}. \tag{10}$$

For $\lambda \in \{\lambda:\lambda=\alpha+\beta i,\ \beta<0\}$, solutions to the asymptotic system include the following:

$$\begin{aligned} Y_1^\infty(\psi,\lambda) &= (\mathrm{Ai}_{-1}(z^+) \quad -a^{1/3}\mathrm{Ai}'_{-1}(z^+) \quad 0\ 0)^T, \\ Y_2^\infty(\psi,\lambda) &= (0\ 0\ \mathrm{Ai}_1(z^-) \quad -a^{1/3}\mathrm{Ai}'_1(z^-))^T, \\ Y_3^\infty(\psi,\lambda) &= (\mathrm{Ai}_0(z^+) \quad -a^{1/3}\mathrm{Ai}'_0(z^+) \quad 0\ 0)^T, \\ Y_4^\infty(\psi,\lambda) &= (0\ 0 \quad \mathrm{Ai}_0(z^-) \quad -a^{1/3}\mathrm{Ai}'_0(z^-))^T. \end{aligned} \tag{11}$$

As for the standard Evans function method described earlier, we construct two bases of solutions to the full problem, one set $\{Y_k^+\}$ whose behavior at $+\infty$ satisfies $Y_k^+(\psi,\lambda) \sim Y_k^\infty$ and the other set $\{Y_k^-\}$ whose behavior at $-\infty$ satisfies $Y_k^-(\psi,\lambda) \sim Y_k^\infty$. A localized solution exists for λ belonging to the lower half-plane if and only if the determinant

$$D_{ai}(\lambda)=\begin{vmatrix} \vdots & \vdots & \vdots & \vdots \\ Y_1^+ & Y_2^+ & Y_3^- & Y_4^- \\ \vdots & \vdots & \vdots & \vdots \end{vmatrix}_{(\psi^*,\lambda)} \tag{12}$$

is equal to 0. Note that the functions are evaluated at the peak location, here denoted by ψ^*. $D_{ai}(\lambda)$ is our modified version of the Evans function and for this to be used as $D(\lambda)$ we need to prove its analyticity in λ. The Airy functions are entire functions, i.e., functions that are analytic everywhere in $\mathbb{C}$, and the variables $z^\pm$ are analytic functions of λ. The initial conditions for numerical integration from ψ_1 and ψ_2 to ψ^* are based upon the asymptotic solutions Y_k^∞, thus they are analytic. Consequently, the solutions Y_i^+ $(i=1,2)$ and Y_j^- $(j=3,4)$ are also analytic in λ. The determinant is an algebraic operation; therefore, $D_{ai}(\lambda)$ is analytic in λ.

To prove stability, we need to evaluate $D_{ai}(\lambda)$ along a closed path enclosing all the lower half-plane of λ [or equivalently the upper half-plane, since the symmetry of Eq. (5) only allows sets of eigenvalues of the kind $\{\lambda,-\lambda,\lambda^*,-\lambda^*\}$]. However, in practice, we have chosen the contour as a semicircle of large radius (typically ~ 10) closed by a line parallel to the real axis but very close to it (at distance $\sim 5\times 10^{-5}$). Numerical limitations are that $D_{ai}(\lambda)$ appears chaotic for large values of $|\lambda|$. The number of 0's of $D_{ai}(\lambda)$ inside the semicircle was determined by the argument principle. For all profiles studied, the result was that no 0's were found, so confirming the stability of the self-bending solitons.

The defined Evans function was also useful for finding the quasilocalized solutions of Eq. (5), for real λ. One trivial example of those solutions is the profile $F(\psi)$, which is the eigenfunction corresponding to the eigenvalue $\lambda=0$. The zero eigenvalue is confirmed to have algebraic multiplicity equal to 4 as happens in the diffusionless case. Other solutions for $\lambda \neq 0$, if present, are the counterpart of internal modes of the diffusionless case. We have sought for them for λ on the real axis. As λ is real, $z^\pm$ is also real and we may replace Ai_{-1} and Ai_1 in Eq. (11) by the real function Bi. As anticipated, whenever such eigenfunctions exist, they correspond to $\lambda \in S_1$. For γ small, such solutions do exist for peak amplitudes greater than ~ 1.3, as in the diffusionless case. As γ increases and the peak amplitude is maintained, those localized solutions cease to exist. The explanation is that S_1 is narrowing as γ increases. The latter was confirmed by evaluating the value of λ that makes $z^\pm(\psi_2)=0$ where

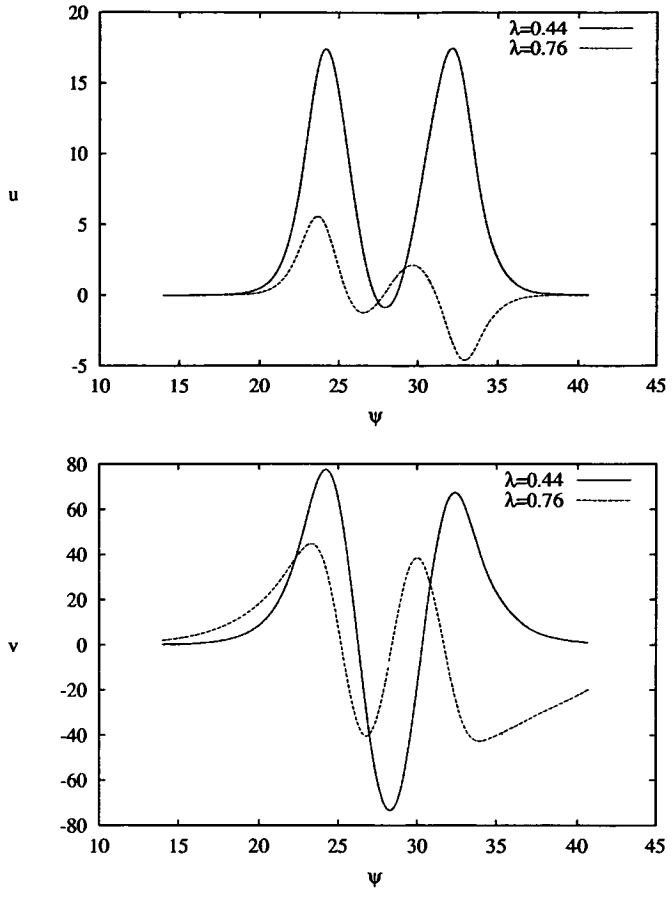

FIG. 6. Eigenfunctions corresponding to $\lambda=0.76$ and $\lambda=0.44$ for a beam profile with amplitude $F_{max}=4.0$ and $\gamma=0.03$.

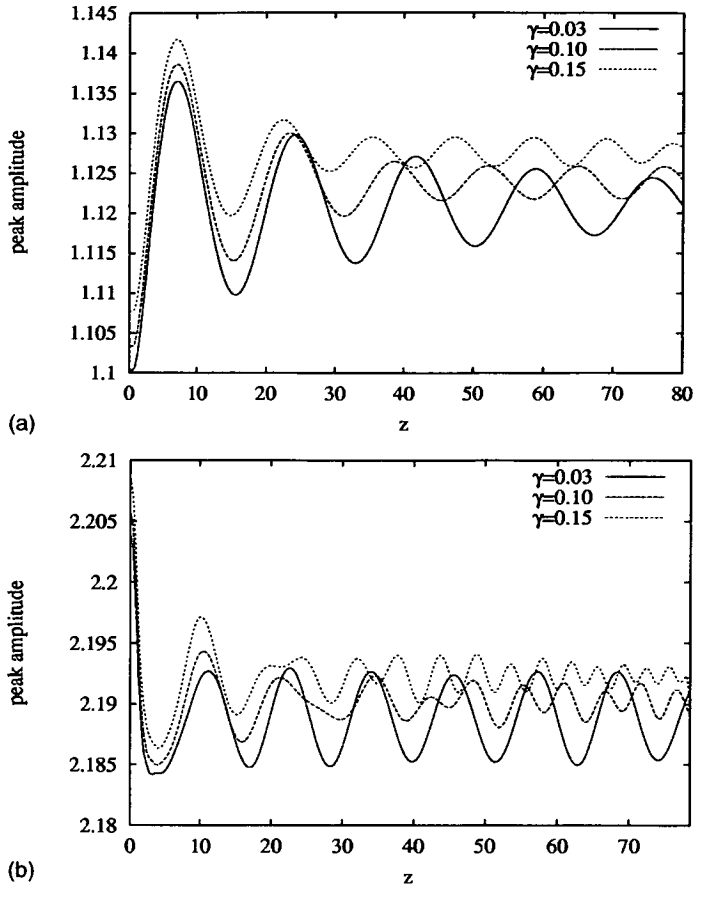

FIG. 7. Peak amplitude evolution for beams scaled by 10% concerning $\gamma=0.03, 0.10, 0.15$ and (a) $F_{max}\sim1.0$, (b) $F_{max}\sim2.0$.

ψ_2 is in the right tail of the peak. Moreover, S_1 tends to the continuous spectrum gap $(-\omega,\omega)$ of the diffusionless case as γ tends to 0.

Figure 6 shows the localized eigenfunctions found for a beam profile with $F_{max}=4.0$ and $\gamma=0.03$. They are qualitatively similar to those presented in Fig. 4 for the rectilinear beams, but with noticeable asymmetry. Increasing γ but maintaining F_{max} causes the eigenfunction corresponding to $\lambda=0.76$ to cease to exist. For even larger γ, we were unable to find a solution for the ODE defining F, suggesting that there is no localized self-similar solution.

VI. NUMERICAL SIMULATION OF THE PARTIAL DIFFERENTIAL EQUATION

To complement our stability analysis we used the computed beam profiles as initial conditions for numerical integration of evolution equation (1). We used a pseudospectral method based on Fornberg and Whitham [19].

The numerical simulations for $\gamma=0$ confirmed the stability of the symmetric beams. An initial condition consisting of a self-similar profile plus a small perturbation causes readjustment to a nearby beam shape with some emission of radiation. However, as is typical for other nonintegrable generalized NLS models [15,20], the consequent propagation exhibits persistent amplitude oscillations whenever the underlying self-similar beam possesses an internal mode.

The numerical simulations also confirmed the stability of the self-bending beams. We have used the corresponding beam profiles as initial conditions in a way that spans the studied ranges of γ and peak amplitude. In all cases, we have observed steady propagation along the predicted parabolic trajectory. Moreover, stable propagation arises even when initial conditions differ from those of a self-similar profile by small perturbations of three types: a sinusoid multiplying the profile, a multiple of the profile, and a multiple of its first derivative.

Analogously to the diffusionless case, the propagation of perturbed beams reveals the existence or absence of localized modes in their stability spectrum. Thus, we may observe large persistent oscillations in the propagation of beams whose spectrum admits localized modes and smaller decaying oscillations otherwise. The frequency of the decaying oscillations is, in this case, coincident with the limit λ_2 of S_{2b}. As regards the characteristic features of solutions to Eq. (5) for $\lambda\in S_{2b}$ given above, we may assert also that, when perturbed, the self-bending beams without *internal modes* relax with amplitude oscillations whose frequency is equal to the lowest frequency of their radiationlike modes. Figure 7(a) shows the peak amplitude evolution of solutions of Eq. (4) having $F_{max}\sim1.0$ but scaled by 1.1, for various values of

γ. We recall that these profiles have no localized modes except that corresponding to $\lambda=0$. The frequency of the amplitude oscillations increases with γ as also does λ_2. In fact, λ_2 is estimated in a way similar to λ_1, that is, by evaluation of the value of λ that makes $z^{\pm}(\psi_1)=0$, where ψ_1 is in the left tail of the peak. Furthermore, λ_2 also tends to ω as γ tends to 0. Figure 7(a) also shows a noticeable decrease in the amplitude of the oscillation with increasing γ. The case $\gamma=0.03$ of Fig. 7(b) shows the long-lived oscillation whose frequency coincides with the eigenvalue of the localized mode. However, the beams of similar peak amplitude but corresponding to larger diffusion parameter evolve accompanied by decaying oscillations. We have confirmed that the average beams of those latter cases have no localized modes. The frequency of the oscillations is again increasing with γ.

VII. CONCLUSION

We have proved linear stability for the rectilinear screening solitons and obtained their internal modes. We give a contribution to the stability analysis of the self-bending solitons, including a discussion of their internal modes. This is based on a modified Evans function that deals with asymptotic systems given by Airy equations, instead of constant coefficient differential equations. The modified Evans function procedure may be applied to similar stability problems, as is currently being done.

ACKNOWLEDGMENTS

M. Facão acknowledges the support of Fundação para a Ciência e a Tecnologia, Portugal.

[1] M. Segev, B. Crosignani, A. Yariv, and B. Fischer, Phys. Rev. Lett. **68**, 923 (1992).
[2] G. Duree, J.L. Shultz, G. Salamo, M. Segev, A. Yariv, B. Crosignani, P. DiPorto, E. Sharp, and R.R. Neurgaonkar, Phys. Rev. Lett. **71**, 533 (1993).
[3] M. Segev, G.C. Valley, B. Crosignani, P. DiPorto, and A. Yariv, Phys. Rev. Lett. **73**, 3211 (1994).
[4] D.N. Christodoulides and M.I. Carvalho, J. Opt. Soc. Am. B **12**, 1628 (1995).
[5] M.I. Carvalho, S.R. Singh, and D.N. Christodoulides, Opt. Commun. **120**, 311 (1995).
[6] W. Krolikowski, N. Akhmediev, B. Luther-Davies, and M. Cronin-Golomb, Phys. Rev. E **54**, 5761 (1996).
[7] D.F. Parker, C. Sophocleous, and C. Radha, J. Phys. A **35**, 1283 (2002).
[8] J.W. Evans, Indiana Univ. Math. J. **24**, 1169 (1975).
[9] J. Alexander, R. Gardner, and C. Jones, J. Reine Angew. Math. **410**, 167 (1990).
[10] R.L. Pego and M.I. Weinstein, Philos. Trans. R. Soc. London, Ser. A **340**, 47 (1992).
[11] V.L. Vinetskii and N.V. Kukhtarev, Sov. Phys. Solid State **16**, 2414 (1975).
[12] N. Kukhtarev, V.B. Markov, S.G. Odulov, M.S. Soskin, and V.L. Vinetskii, Ferroelectrics **22**, 949 (1979).
[13] V. Aleshkevich, Y. Kartashov, and V. Vysloukh, Phys. Rev. E **63**, 016603 (2000).
[14] M.G. Vakhitov and A.A. Kolokolov, Radiophys. Quantum Electron. **16**, 783 (1973).
[15] C. Etrich, U. Peschel, F. Lederer, B.A. Malomed, and Y.S. Kivshar, Phys. Rev. E **54**, 4321 (1996).
[16] D.E. Pelinovsky, Y.S. Kivshar, and V.V. Afanasjev, Physica D **116**, 121 (1998).
[17] Y.S. Kivshar, D.E. Pelinovsky, T. Cretegny, and M. Peyrard, Phys. Rev. Lett. **80**, 5032 (1998).
[18] F.W.J. Olver, *Asymptotics and Special Functions* (A.K. Peters, Wellesley, 1997).
[19] B. Fornberg and G.B. Whitham, Philos. Trans. R. Soc. London, Ser. A **289**, 373 (1978).
[20] V.V. Afanasjev, P.L. Chu, and Y.S. Kivshar, Opt. Lett. **22**, 1388 (1997).